CHEMICAL SCALE INVESTIGATIONS OF THE GATING MECHANISM OF ION CHANNELS

Thesis by

Lori WaiHang Lee

In Partial Fulfillment of the Requirements for the

Degree of

Doctor of Philosophy

CALIFORNIA INSTITUTE OF TECHNOLOGY

Pasadena, California

2007

(Defended December 18, 2006)

In memory of

Dan Vu Nguyen

ACKNOWLEDGEMENTS

I owe many thanks for my experience at Caltech. First, I thank the people along the path leading to my arrival at Caltech. In particular, I would like to thank Jerry Sawitz, Joel Galanda, Roberta Wang, Dr. Deborah Charych, Prof. Angelica Stacy, Prof. Bradley Moore, and Prof. Carolyn Bertozzi. Their commitment to education and their enthusiasm for learning made them significant influences in my life.

A great deal of thanks and appreciation goes to my advisor, Prof. Dennis Dougherty. His enthusiasm for science and his astuteness in scientific reasoning never cease to amaze me. I have been very fortunate to benefit from his commitment to the education of his students. Dennis also shows a genuine interest in the personal lives of his students and is always understanding and encouraging. One could not ask for anything more from an advisor.

I also owe a great deal of gratitude to Prof. Henry Lester for his mentorship. He has always made himself available for discussions, and I greatly admire his commitment to scientific education. Additionally, I have had the pleasure of collaborating with Prof. Douglas Rees whose excitement for science is contagious. In addition to Dennis, Henry, and Doug, I also thank the remaining members of my thesis committee, Prof. Peter Dervan and Prof. William Goddard. I am thankful for their time and commitment to my education. Their advice and support have been invaluable to me during my graduate career.

Members of the Dougherty group, past and present, have always been a great pleasure to work with. Donald Elmore and Joshua Maurer were very enjoyable to work with and I really appreciate the time and patience they took in training me. I also enjoyed all the discussions and debates about science and life with them. Niki Zacharias and Sarah May are very caring

people and they helped make my transition to the Dougherty group smooth. Gabriel Brandt was an amazing source of information, and it always seemed like he had the answer to just about every scientific question. Darren Beene was a pleasure to work with and I appreciate his humor and insight. James Petersson always found the time to help and answer questions no matter how many things he had on his plate. Tingwei Mu was always very nice and I thank him for all the help with my postdoc applications. Amanda Cashin, another "free agent" to go to the Dougherty group, always has a smile on her face and her positive attitude made her a great source of encouragement and support. I also really enjoyed my conversations and discussions with Steve Spronk and I look forward to seeing him in Michigan. Amy Eastwood is always quick to lend a hand, and I continue to be amazed by all the things she accomplishes. I have enjoyed getting to know her over the past years and hope she enjoys the 60 gallons of water and fish. Erik Rodriguez has a great attention for detail and is always willing to offer help. Joanne Xiu is always very friendly and fun to talk to. Jinti Wang cranks out data like no other, and I have enjoyed having a desk next to her. Katie McMenimen's love of science is apparent to all, and I am glad she appreciated the jelly beans. Ariele Hanek never fails to supply the lab with the most delicious homemade goods. Kristin Rule has an endless amount of energy, and I admire her pursuit to learn. Kiowa Bower always offers a unique perspective on things, and I thank him for all the interesting discussions. Mike Torrice has been a great friend and office mate. He has the ability to make me laugh with his great sense of humor and to make me extremely incensed with his daily "current blunders of the government." I thank him for the "shadowy figure" and for all the discussions (scientific and personal). Sean Kedrowski, Angela Blum, Jai Shanata, and Kay Limapichat are the new "rooks" to the group and I have enjoyed the brief time that I have known them. The discussions and debates have

all been of great value to me and I am thankful for them. I also greatly appreciate the opportunity to collaborate with Sarah Lummis from the University of Cambridge. She was a great pleasure to work with.

Caltech provides a very unique and collaborative environment to conduct research, and I have many people to thank for all the support during my graduate career. There are more people to thank than I have space, which is a testament to the supportive and collegial environment that Caltech provides. I owe much appreciation to the founding members of the Hsieh-Wilson group—Sarah Tully, Raymond Doss, Nelly Khidekel, Nathan Lamarre-Vincent, Katherine Poulin, Sherry Tsai, and Cristal Gama. Cristal Gama was a great pleasure to work with and share a bay with. I also thank the Stoltz group and the Grubbs group for their help and experimental support. In particular, I owe thanks to Eric Ferreira, Dan Caspi, Jeremy May, Ryan McFadden, and Diego Benitez. Many thanks are also due to Dr. Scott Ross, Dr. Mike Day, and Larry Henling for all their help in the characterization of compounds. Their enthusiasm for science is refreshing, and I am thankful for their eagerness to share their knowledge. I am also thankful for Linda Syme, Rick Gerhart, Mike Roy, Tom Dunn, Paul Carroad, Chris Smith, Anne Penney, Steve Gould, Lillian Kremar, Moses Renteria, Joe Drew and Terry James. I am also indebted to Dian Buchness for her commitment to the graduate students. She always made an effort to get to know the students personally.

My time at Caltech has also been greatly enriched by friends outside of the Dougherty group. I am amazed by the number of people who have passions outside of their research *and* actually made the time to do them despite the demands of graduate school. I am thankful for the opportunities that I have had to share in these interests. Jon Feenstra was one of the first

people I met on campus through TAing a class, and I am thankful we met up again years after the teaching was over. His passion for learning continues to inspire me and his birdwatching skills are amazing. I had never met anyone who could confidently identify a species of bird on a treetop while driving in a car at 80 mph. His friendship has been invaluable to me, and I appreciate his honesty, support, and eagerness for adventure. William Wehbi has been a constant friend through thick and thin, and for that I am eternally grateful. I am thankful for all the time we have spent together, whether it be discussing issues in science or life, or simply enjoying a good meal or going for a run. He is very much an older brother to me and spending time with him is like getting a taste of "home." Through the years, he continues to be someone I can depend on. Jordan Schooler is a very caring friend and I admire his candor and his courage to seek and ask questions. Julian Revie is the master of storytelling, and he is always very caring and willing to go out on a limb for his friends. Patrick Dondl's love of food and cooking are much appreciated. I am thankful for his generosity and kindness.

You know you have a good friend when they are willing to tell you the truth without the sugar coating—if you want to "hear it like it is," the eating club is the perfect place to go. Since its humble beginning one night at a salsa class, when we asked an old man for our money back, the eating club has evolved through many stages…all of which involve overeating. There is nothing like sharing a good meal with close friends. Uttam Tambar, Melanie Pribisko, and Anusha Narayan have all made the eating club a meeting that I look forward to every week and will surely miss when I move on from here (although I am certain my waistline will not). I have learned so much from all three of these amazing friends. They are the most genuine people one can encounter. I am thankful for their honesty, generosity, concern for others, and great sense of humor. I am most appreciative for the opportunity to get to know them and be

part of their lives. Their friendship has meant so much to me and I am always encouraged and inspired after spending time with them. Knowing them has made me truly believe that if you have good friends and good food, you have a good life.

I have also been blessed to know Amy Abrams, Barbara Keeler, and Eileen Anderson. Their support has meant so much to me and I have really enjoyed the time I have spent with them out on the Caltech lawns with our dogs and at teatime. Having them as friends is like having your own personal cheering squad. They are an inspiring group of independent women in my life and I will always cherish their friendships. Sid Chand has also been very encouraging, and I have learned a great deal from our conversations.

I also owe a special thanks to Dr. John H. Phillips. I thank him for the endless encouragement, patience, generosity, and energy. I greatly admire his natural curiosity and enthusiasm for learning. I am very blessed to be part of his life and look forward to the adventure.

Lastly (but certainly not the least), I thank my parents and siblings for their continued love and support. It was a great blessing to have my parents a car ride away for the past six years. My parents never cease to amaze me in all that they do and have been a constant source of encouragement and inspiration. I will be more than content if I achieve just half of what they have done. I appreciate all the support that they have given me over the past years and have greatly enjoyed the weekend dim sum outings. Debbie, Serena, and Irvin have all been very supportive and I have enjoyed all the conversations over the past 6 years as we have "grown up." My family continues to be a source of encouragement and inspiration, and for that I am very grateful.

ABSTRACT

The studies contained in this dissertation are aimed at utilizing chemistry to understand neurobiology and neuronal communication. Chapters 2 and 3 both address the gating of ion channels, describing structure-function studies to shed light on the gating mechanisms of two classes of ion channels. Chapter 2 studies the gating mechanism of the mechanosensitive channel of small conductance (MscS), which is voltage modulated. Elucidating the mechanism of voltage sensation in MscS may provide insight into how voltage-gated channels translate a change in membrane potential to channel gating. The research discussed in Chapter 2 is aimed at elucidating the role of two arginine residues, in the TM1 and TM2 of MscS, in voltage sensing. We generated two MscS mutants, Arg46Ala and Arg74Ala, to evaluate the effects of "neutralizing" the charged side chain on the voltage sensing ability of the channel. The mutants were evaluated using single channel analysis in *E. coli* spheroplasts. Our preliminary results indicated a potentially significant role for Arg46 in the voltage sensitivity of MscS, however this data set is not extensive due to inconsistency in the spheroplasts preparation.

In Chapter 3, we utilized nonsense suppression to incorporate unnatural amino acids to study the gating of the cation-selective Cys-loop family of ion channel receptors. Specifically, it describes work aimed at elucidating the role of *cis-trans* isomerization of a conserved proline residue in the gating mechanism of the serotonin-gated 5-hydroxy-tryptamine receptor 3A (5-HT_{3A}R) and the nicotinic acetylcholine receptor (nAChR). A series of proline analogues, of varying *cis* preference were incorporated at proline 308 in the M2-M3 loop of the 5-HT_{3A} receptor using *in vivo* nonsense suppression methodology in a *Xenopus* oocyte expression system. Electrophysiological analysis of the mutant channels revealed a linear relationship

between the *cis* preference of the proline analog and the EC_{50} of the mutant channel—suggesting that proline 308 may serve as a hinge during the gating of the 5-HT_{3A} receptor. From these data, we proposed a model of gating for the 5-HT_{3A} receptor. Initial results from similar studies in nAChR suggest that the analogous proline does not play a role in its gating. These results suggest that while the 5-HT_{3A} receptor and the nACh receptor are highly homologous and are members of the same superfamily of channels, they have evolved to utilize different mechanisms of gating.

Lastly, Chapter 4 addresses the role of fucose-galactose carbohydrates in learning and memory. It aims to identify lectins to fucose-α(1-2)-galactose as well as identify the corresponding glycoproteins bearing fucose-α(1-2)-galactose. Chemical probes were synthesized and used to study fucose-α(1-2)-galactose binding proteins. One of the probes was used to demonstrate the existence of fucose-α(1-2)-galactose binding proteins in hippocampal neurons. Furthermore, initial results from experiments with a photoreactive probe suggested that the design of our probe is sufficient to isolate fucose-α(1-2)-galactose binding proteins from the brain. Additionally, we were able to use antibodies specific to fucose-α(1-2)-galactose epitopes to examine fucose-α(1-2)-galactose bearing glycoproteins in the brain. Overall, results from both studies utilizing chemical probes and molecular probes strongly suggest that the modifications of proteins with fucose-α(1-2)-galactose epitopes and the expression of fucose-α(1-2)-galactose binding proteins are developmentally regulated.

TABLE OF CONTENTS

FIGURES AND TABLES

Chapter 1

Chapter 2

Chapter 3

Chapter 4

CHAPTER 1: INTRODUCTION

1.1 Introduction

1.1.1 Chemistry and the brain

The brain is the most complex organ of a vertebrate's body. It is the central command center that governs our perceptions, thoughts, feelings, movements and memory. The human brain weighs approximately 1.4 kg and contains roughly one hundred billion neurons.[1] Each neuron makes an estimated ten thousand connections, or synapses, with other neurons, forming a communication network of staggering complexity that has been the focus of intense study. Each neuron has one axon and many dendrites. Signaling between neurons occurs between the axon of one cell and a dendrite of another at a gap called the synapse cleft

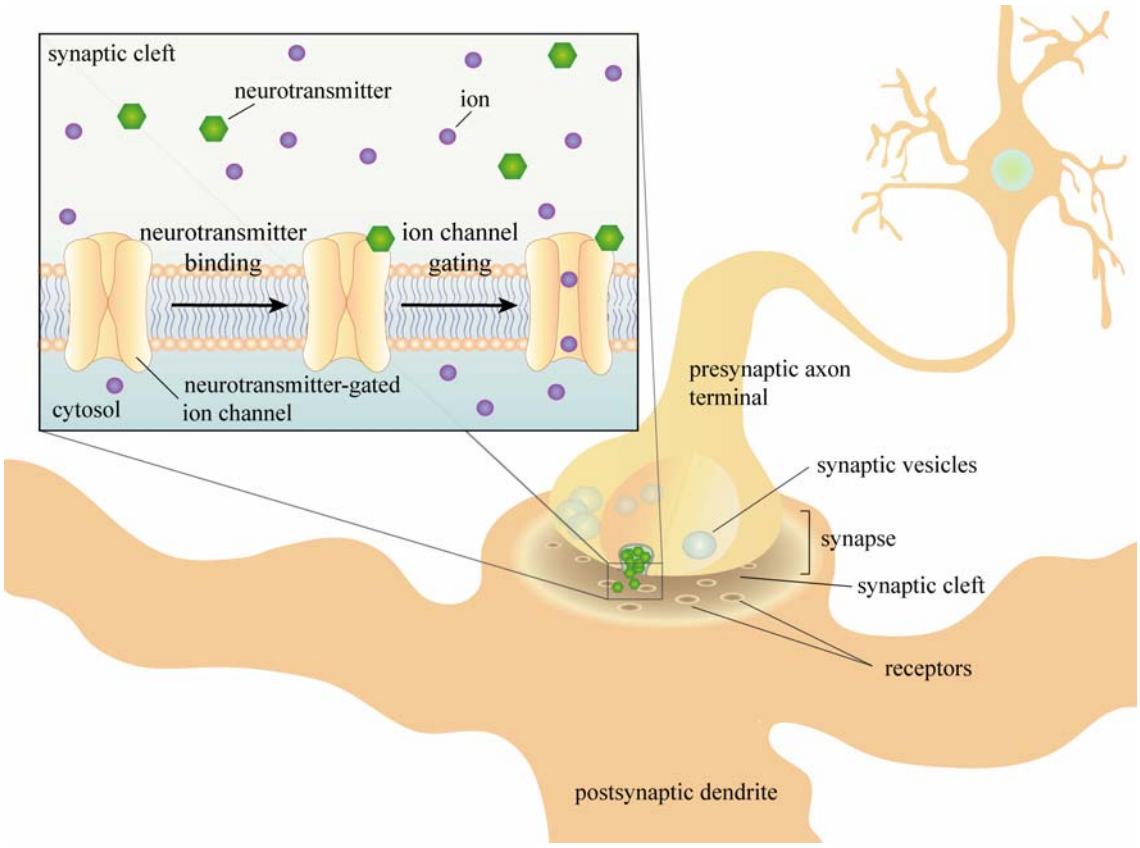

Figure 1.1. Synaptic transmission between neurons. Neurotransmitters are released from the presynaptic axon terminal into the synaptic cleft. The neurotransmitters bind to ion channels embedded in the membrane of the postsynaptic dendrite of a neighboring neuron. The ion channel is activated and gated, allowing for ions to flow, thus generating an electrical current.

(figure 1.1). Synaptic transmission is initiated when the presynaptic axon terminal releases small molecules called "neurotransmitters" from synaptic vesicles. These neurotransmitters are released at the synapse where they diffuse across the synaptic cleft to the postsynaptic dendrite of a neighboring neuron. The neurotransmitters bind to receptors embedded in the membrane of this dendrite, causing activation of the receptor, conveying the synaptic signal across the cell membrane.

Ion channels are a specialized class of receptors that form a pore across the membrane. They undergo an opening and closing process, known as gating, in response to stimuli such as neurotransmitter binding, voltage, or mechanical stress. During synaptic transmission, neurotransmitters bind to their partner ion channels which results in the gating of these ion channels (figure 1.1, inset). Ions pass through the pore of the channel constituting an electrical current, thus converting a chemical signal into an electrical signal. This electrical signal can then effect other changes in the neuron resulting in release of neurotransmitters. In this manner a signal is propagated from neuron to neuron via a sequence of chemical signals and electrical signals.

1.2 Chemical methodologies aimed at understanding protein function

1.2.1 Unnatural amino acid incorporation

Understanding protein function is at the heart of experimental biology. This endeavor frequently requires the generation of proteins that are modified to contain chemical probes or proteins that are homogeneous in naturally occurring posttranslational modifications, such as glycosylation or phosphorylation. The generation of these modified proteins is not available via standard ribosomal synthesis. Two methodologies have emerged as powerful methods to

generate modified proteins—native chemical ligation/expressed protein ligation and nonsense suppression. Developed by the Kent laboratory in 1994, native chemical ligation involves the reaction of two fully unprotected synthetic fragments under aqueous conditions, at physiological pH, resulting in the formation of a native peptide bond at the ligation site.[2] Expressed protein ligation is an extension of native chemical ligation where a synthetic or recombinant peptide fragment is chemoselectively ligated to a recombinantly expressed protein.[3, 4] This methodology allows for the generation of larger quantities of modified proteins than nonsense suppression; however, it does not allow for *in vivo* biochemical studies. Furthermore, the application of native chemical ligation/expressed protein ligation in the synthesis of membrane proteins has been limited due to several major technical challenges. While nonsense suppression may not afford the quantities needed for some biochemical studies, it does allow for the *in vivo* modification of proteins for biological studies.

For over a decade, the use of nonsense (stop codon) suppression methodology to incorporate unnatural amino acids, *in vitro* and *in vivo*, has expanded our ability to manipulate protein structure. Modification of proteins by conventional mutagenesis is limited by the twenty natural amino acids, whereas the incorporation of unnatural amino acids is limited by our synthetic ability. Consequently, precise changes can be made to the chemical properties of a specific amino acid enabling one to study electrostatic and steric effects (e.g., hydrogen bonding, cation-π, polarity, size, nucleophilicity, and redox potential). Furthermore, this methodology has been used to site-specifically introduce spectroscopic probes, posttranslational modifications, photoaffinity labels, and other chemical moieties in a protein of interest.[5-10] It has also been used to introduce "chemical handles" with orthogonal

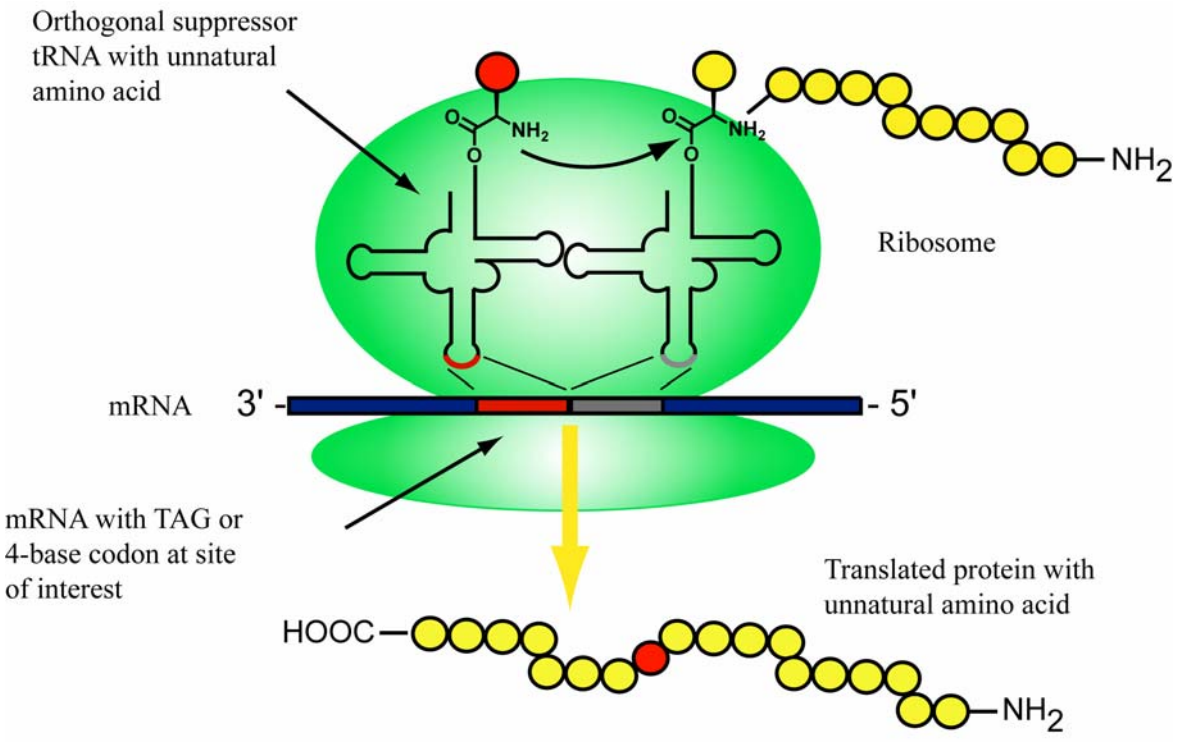

Figure 1.2. Nonsense suppression methodology.

chemical reactivities such that a native protein can be selectively modified under mild conditions with a variety of reagents without protecting groups.[9]

In 1989, Schultz et al. first introduced the biosynthetic incorporation of an unnatural amino acid using nonsense suppression and an *in vitro* translation system.[11-13] The fundamental approach to unnatural amino acid incorporation through nonsense suppression is shown in Figure 1.2. This methodology utilizes a noncoding or "nonsense codon"—typically a stop codon—to replace the codon for the amino acid of interest within a particular gene. This is achieved through conventional site-directed mutagenesis. Subsequently, a tRNA against this "nonsense codon" is chemically acylated with the desired unnatural amino acid and provided to the translational machinery with the modified gene of interest.[14] The translational machinery proceeds with protein translation, site-specifically incorporating the

desired unnatural amino acid within the desired gene; thus producing the full length modified protein. This methodology has been extended for *in vivo* systems and has been demonstrated in a variety of biological systems including *E. coli*,[15] yeast,[16] mammalian cells,[17] and *Xenopus laevis* oocytes.[18] Additionally, the evolution of specific aminoacyl-tRNA synthetases has allowed for the *in vivo* acylation of the suppressor tRNA with intracellular levels of the unnatural amino acid in *E. coli*.[8]

1.2.1.1 Nonsense suppression in Xenopus laevis oocytes for the expression of ion channels

The extension of nonsense suppression methodology to incorporate unnatural amino acids to living cells was first demonstrated in 1995.[19] The basic methodology is shown in Figure 1.3. First, site-directed mutagenesis is used to replace the amino acid codon of interest with the amber stop codon TAG in the desired gene. *In vitro* transcription is then used to generate the corresponding mRNA with the appropriately placed UAG. A suppressor tRNA, containing the anticodon CUA, is then chemically acylated with the desired unnatural amino acid. The mRNA and the amino-acylated tRNA are subsequently co-injected into *Xenopus laevis* oocytes. The oocytes are incubated for a period ranging from 24 to 72 hours during which protein synthesis, transport and surface assembly occurs. The result is the generation of the desired protein with the unnatural amino acid incorporated at the site of interest. The channel can then be characterized by electrophysiology. A limitation of this methodology is that the quantity of the modified protein is determined by the amount of aminoacylated tRNA that is injected since the tRNA is not reacylated once it has been used in protein translation. Therefore, the amount of modified protein is stoichiometric to the amount of tRNA injected. This limitation is minimized by the use of electrophysiology for

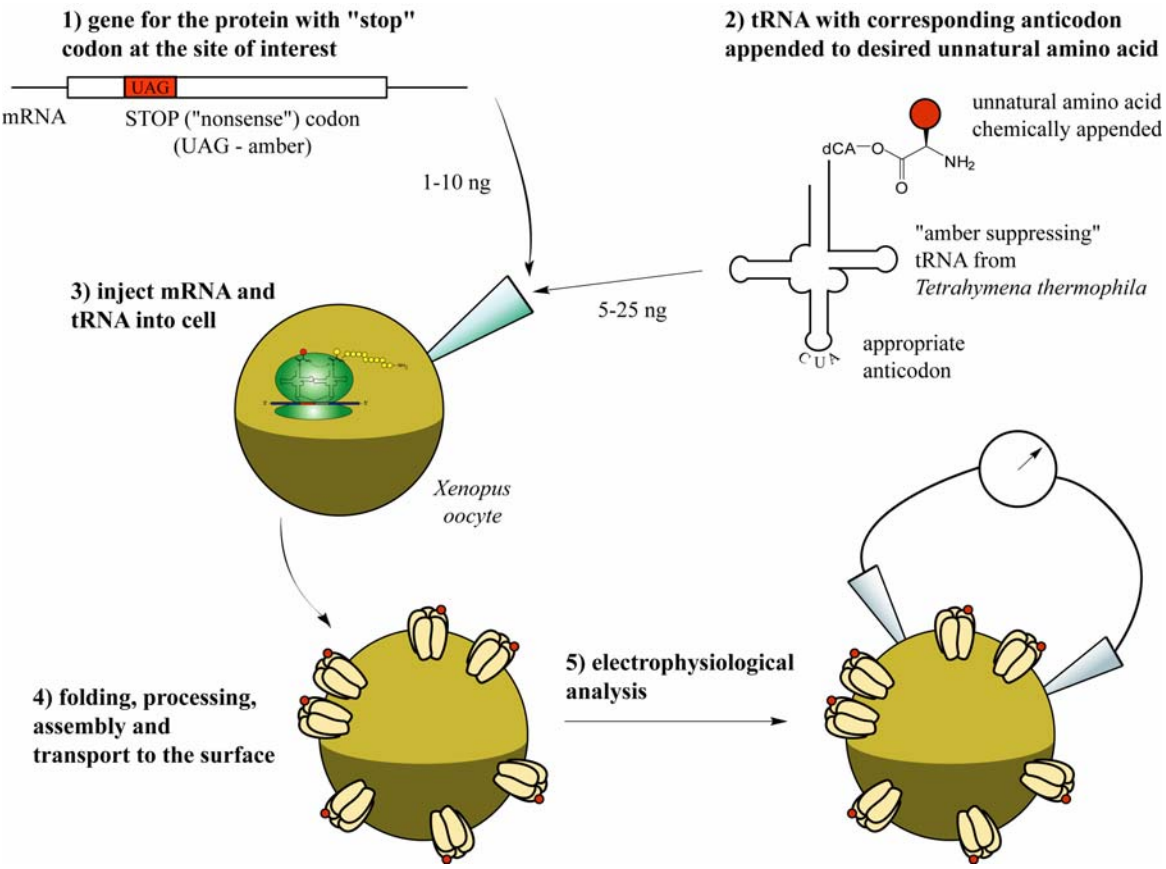

Figure 1.3. Schematic of *in vivo* nonsense suppression methodology using *Xenopus* oocytes for structure-function studies of ion channels.

the analysis of ion channels. Electrophysiology is a highly sensitive technique, allowing for functional characterization with very small amounts of expression ion channels.

The use of nonsense suppression for unnatural amino acid incorporation in *Xenopus laveis* oocytes requires the generation of an activated precursor—namely the aminoacyl suppressor tRNA (figure 1.4). This process begins with the synthesis of the desired unnatural amino acid. The free amino acid is amino protected, typically with a protecting group that can be removed with photolysis, such as a nitroveratryloxycarbonyl (NVOC) group. Conversion of the carboxylic acid to a cyanomethyl ester activates the amino acid for coupling to the dinucleotide dCA. Coupling of the unnatural amino acid is achieved via

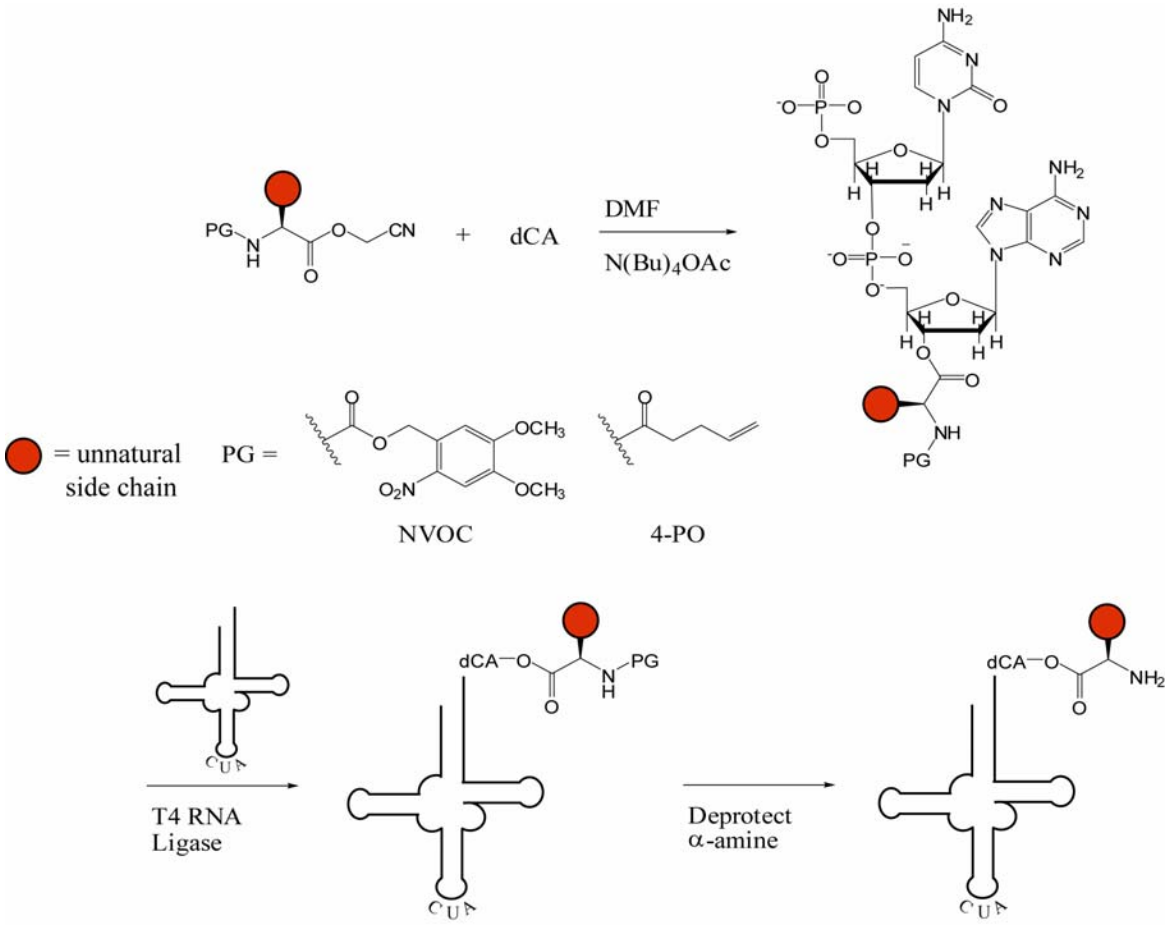

Figure 1.4. Chemical acylation of tRNA to append unnatural amino acids.

treatment with *tert*-butyl ammonium in the presence of dCA in dimethyl formamide (DMF). The dCA amino acid is enzymatically ligated to expressed 74-mer tRNA to produce the desired full length 76-base-pair aminoacyl tRNA. Immediately prior to injection of the charged tRNA, the amino-protecting group of the unnatural amino acid is removed by photolysis.

To date, over one hundred unnatural amino acids have been incorporated into proteins for *in vivo* biological studies in *Xenopus laevis* oocytes (figure 1.5). Nonsense suppression

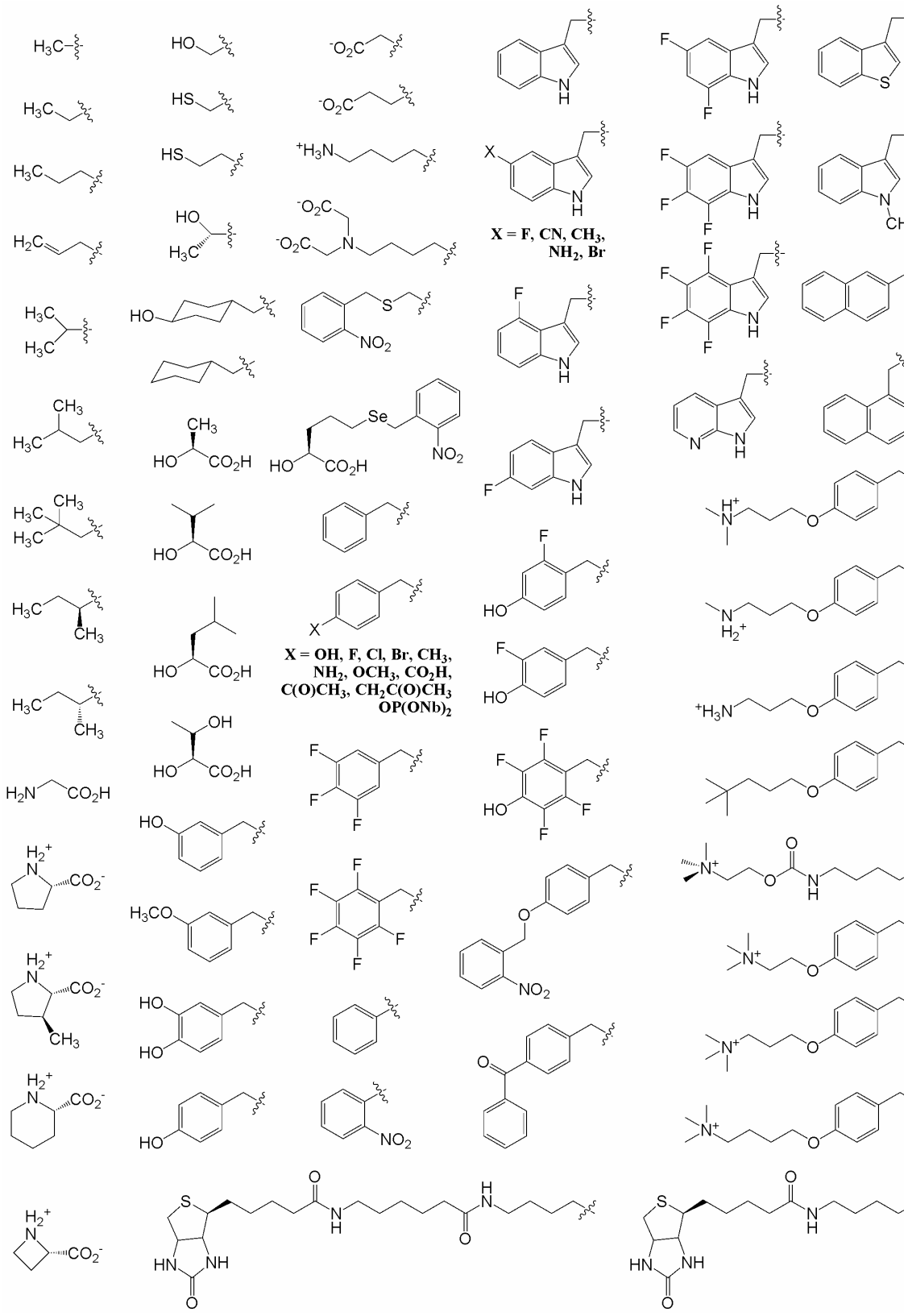

Figure 1.5. Representative unnatural amino acids that have been incorporated into membrane proteins using *in vivo* nonsense suppression in *Xenopus* oocytes.

has been used to study a variety of chemical interactions such as cation-pi interactions and hydrogen bonding in ion channels. It has also been used to incorporate backbone mutations as well as biophysical probes and fluorophores. Recently, multiple unnatural amino acids were site-specifically incorporated into proteins expressed in *Xenopus* oocytes using a combination of nonsense suppression and frameshift suppression.[20] This advancement should allow for greater structure-functions studies and FRET studies in ion channels.

1.2.2 Photoaffinity probes

The specific recognition of a bioactive ligand by its binding partners is a major event in biological processes; therefore the elucidation of the binding partners often provides invaluable information in the understanding of biological processes. The identification of binding partners may also facilitate the development of therapeutics. A variety of biological techniques have been developed aimed at identifying binding partners of a specific interaction; however the identification of binding partners is often hampered by low binding affinities due to the dynamic nature of these interactions. Photoaffinity labeling has emerged as a powerful technique to identify binding partners/proteins as well as to study how these binding partners interact.[21] This method overcomes low binding affinities by photochemically introducing a covalent bond between the ligand and binding partner.

Three photoreactive groups are commonly used in photoaffinity labeling—phenylazide, phenyldiazirine, and benzophenone (figure 1.6). Phenylazides are the mostly widely used photoaffinity label and upon photolysis at 300 nm they generate a highly reactive nitrene intermediate that forms nitrogen-carbon bonds or a more labile nitrogen-heteroatom bond. A drawback to the use of phenylazides is that the singlet phenylnitrenes

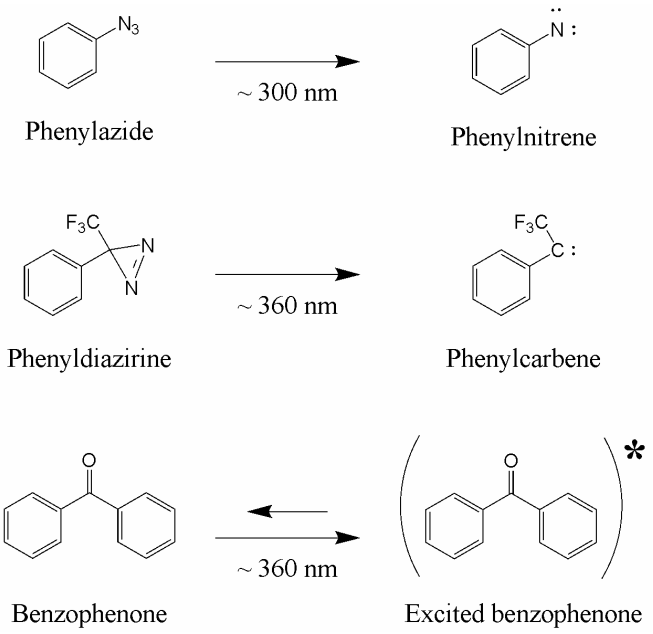

Figure 1.6. Three main classes of photoreactive reagents.

are short lived and rapidly rearrange into long-lived electrophiles, ketenimines, which are unreactive to nonactivated C-H bonds.[22] This can lead to nonspecific labeling. Furthermore, the lower wavelength of activation for azides of 300 nm can cause damage to proteins which is not seen with photoreactive groups with an activation wavelength of 360 nm. Phenyldiazirines form a carbene intermediate when photolyzed at 360 nm. The carbine is considered to be more reactive than a typical nitrene.[23] Similar to phenylazides, photolysis of phenyldiazirines also leads to long-lived electrophiles, diazo-isomers, which lead to nonspecific labeling. The formation of long-lived electrophiles in the case of both phenylazides and phenyldiazirines has been eliminated with the use of electron-withdrawing fluorine. Fluorination of the phenyl ring in phenylazides was shown to prevent the formation of ketenimines during photolysis.[24, 25] For phenyldiazirines, the trifluoromethyl substitution was shown to stabilize the diazo-functionality as shown by Brunner et al. with 3-trifluoromethyl-3-phenyldiazirine.[26] Benzophenone is part of the "carbonyl" photoreactive group and is unique from other photoreactive agents in that photo-dissociation does not occur. Excitation of benzophenone at 360 nm generates a reactive triplet state of the carbonyl that can undergo C-H bond

insertion. The excited state of the carbonyl relaxes to the ground state if C-H bond insertion does not occur; consequently, a higher cross-linking yield often can be achieved with repeated excitation.[27]

1.2.2.2 Applications of photoaffinity reagents in biological studies

The aforementioned photoaffinity probes have all been used in a variety of biological applications. They have been used to generate photoreactive DNA, photoreactive proteins, and photoreactive small molecules that act as probes. Both phenylazides and benzophenone derivatives have been extensively used for biological studies due to the ease of accessibility. Phenylazide derivatives are easily synthesized or are commercially available. Benzophenone derivatives are also commercially available. The use of phenyldiazirines in biological studies has been limited since the synthesis of phenyldiazirines is difficult and few are commercially available.

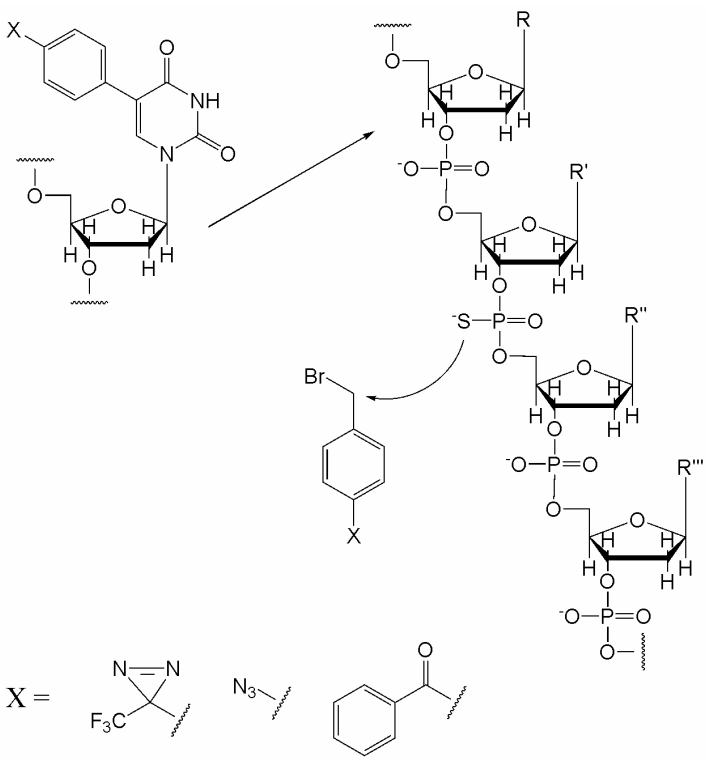

Figure 1.7. Two methods of generating photoreactive DNA.

The incorporation of photoreactive moieties into DNA has been used extensively to study interactions between nucleotides and proteins. Photoreactive nucleobases, in which the photoreactive bases

are substituted for normal bases, have been used to study transcriptional complexes,[28, 29] chromatin remodeling complexes[30, 31] and chromatin structure.[32] Photoreactive moieties have also been incorporated into DNA via the phosphate backbone in which one more of the desired phosphodiesters have been replaced with phosphorothioates. The sulfur undergoes nucleophilic deplacement of a bromide derivative of the photoreactive moiety, thus attaching the photoreactive moiety at the desired site (figure 1.7). This method of generating photoreactive DNA has been used to study binding interactions in transcriptional complexes and of transcriptional regulators.[33-36]

The use of photoaffinity reagents has also contributed extensively to the study of protein-protein interactions.[37-42] They have been incorporated into peptides and proteins to determine contact regions between binding partners. For example, this methodology has been used to determine the inner-strand contact region of β-amyloid peptide.[43] Typically photoreactive amino acids are incorporated into peptides using standard solid-phase synthesis or solution-phase synthesis (figure 1.8).[37-42, 44, 45] For larger proteins, photoreactive moieties have been incorporated using three main methods: 1) chemoselective incorporation via reaction of the bromide reagent with cysteine residues within the protein,[46-48] 2) with the use of a cell-free translation system,[49-54] and 3) *in vivo* using nonsense suppression

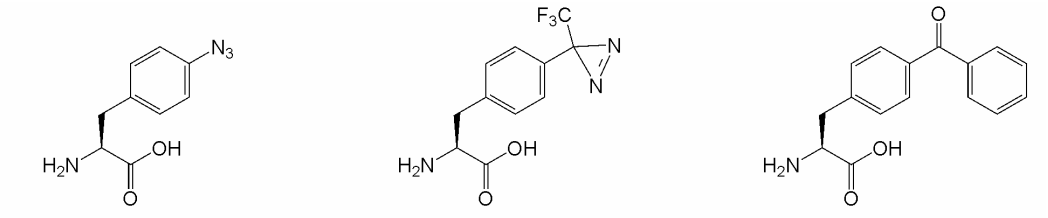

p-azido-L-phenylalanine

L-4'-(3-(trifluoromethyl)-3*H*-diazirine-3-yl)phenylalanine

p-benzoyl-L-phenylalanine

Figure 1.8. Photoreactive amino acids.

methodology.[5, 6, 55] The last methodology was used to incorporate *p*-benzoyl-L-phenylalanine site-specifically into human Grb2 protein in mammalian Chinese hamster ovary cells.[56] Irradiation of the cells resulted in the cross-linking of human Grb2 with its known binding partner, epidermal growth factor (EGF).

An extension of photoaffinity labeling is the generation of multifunctional probes for the identification and isolation of binding partners to proteins and ligands. This methodology utilizes the photoaffinity reagent to overcome weak binding affinities that often hamper conventional methods of isolating and identifying ligand/protein-protein binding partners and couples this reactivity to a purification handle, such as biotin, to allow for the facile isolation of the cross-linked complex. The isolated complex can then be analyzed using mass spectrometry to identify binding partners. A variety of biotinylated photoreactive probes has been synthesized and successfully used to study and isolate protein-substrates. Probes ranging from biotinylated photoactivated γ-secretase[57] inhibitors to bis-mannose photolabels to study glucose transporter isoform 4 (GLUT4)[58] have been synthesized. This methodology is particularly promising in the area of carbohydrate research in which lectins often exhibit low binding affinities.

1.3 Dissertation work

The studies contained in this dissertation are aimed at utilizing chemistry to understand neurobiology and neuronal communication. Chapters 2 and 3 both address the gating of ion channels, describing structure-function studies to shed light on the gating mechanisms of two classes of ion channels. Chapter 2 studies the gating mechanism of the mechanosensitive channel of small conductance (MscS). MscS is voltage modulated and

Chapter 2 describes studies to elucidate the role of arginine residues in the voltage sensitivity of MscS. In Chapter 3, we utilized nonsense suppression to incorporate unnatural amino acids to study the gating of the cation-selective Cys-loop family of ion channel receptors. Specifically, it describes work aimed at elucidating the role of *cis-trans* isomerization of a proline residue in the gating mechanism of the serotonin-gated 5-hydroxy-tryptamine receptor 3A ($5\text{-}HT_{3A}$) and the nicotinic acetylcholine receptor. Lastly, Chapter 4 addresses the role of fucose-galactose carbohydrates in learning and memory. It aims to identify lectins to fucose-α(1-2)-galactose as well as identify the corresponding glycoproteins bearing fucose-α(1-2)-galactose.

1.4 References

1. Blinkov, S. M. i.; Glezer, I. i. a. I., *The human brain in figures and tables; a quantitative handbook*. Basic Books: [New York], 1968; p xxxii, 482 p.
2. Dawson, P. E.; Muir, T. W.; Clark-Lewis, I.; Kent, S. B., Synthesis of proteins by native chemical ligation. *Science* **1994,** 266, (5186), 776-9.
3. Muir, T. W.; Sondhi, D.; Cole, P. A., Expressed protein ligation: a general method for protein engineering. *Proc Natl Acad Sci U S A* **1998,** 95, (12), 6705-10.
4. Severinov, K.; Muir, T. W., Expressed protein ligation, a novel method for studying protein-protein interactions in transcription. *J Biol Chem* **1998,** 273, (26), 16205-9.
5. Chin, J. W.; Martin, A. B.; King, D. S.; Wang, L.; Schultz, P. G., Addition of a photocrosslinking amino acid to the genetic code of Escherichiacoli. *Proc Natl Acad Sci U S A* **2002,** 99, (17), 11020-4.
6. Chin, J. W.; Santoro, S. W.; Martin, A. B.; King, D. S.; Wang, L.; Schultz, P. G., Addition of p-azido-L-phenylalanine to the genetic code of Escherichia coli. *J Am Chem Soc* **2002,** 124, (31), 9026-7.
7. Chin, J. W.; Schultz, P. G., In vivo photocrosslinking with unnatural amino Acid mutagenesis. *Chembiochem* **2002,** 3, (11), 1135-7.
8. Wang, L.; Xie, J.; Schultz, P. G., Expanding the genetic code. *Annu Rev Biophys Biomol Struct* **2006,** 35, 225-49.
9. Wang, L.; Zhang, Z.; Brock, A.; Schultz, P. G., Addition of the keto functional group to the genetic code of Escherichia coli. *Proc Natl Acad Sci U S A* **2003,** 100, (1), 56-61.
10. Zhang, Z.; Gildersleeve, J.; Yang, Y. Y.; Xu, R.; Loo, J. A.; Uryu, S.; Wong, C. H.; Schultz, P. G., A new strategy for the synthesis of glycoproteins. *Science* **2004,** 303, (5656), 371-3.
11. Noren, C. J.; Anthony-Cahill, S. J.; Griffith, M. C.; Schultz, P. G., A general method for site-specific incorporation of unnatural amino acids into proteins. *Science* **1989,** 244, (4901), 182-8.
12. Cornish, V. W.; Mendel, D.; Schultz, P. G., Probing Protein-Structure and Function with an Expanded Genetic-Code. *Angewandte Chemie-International Edition in English* **1995,** 34, (6), 621-633.
13. Cornish, V. W.; Benson, D. R.; Altenbach, C. A.; Hideg, K.; Hubbell, W. L.; Schultz, P. G., Site-specific incorporation of biophysical probes into proteins. *Proc Natl Acad Sci U S A* **1994,** 91, (8), 2910-4.
14. Nowak, M. W.; Gallivan, J. P.; Silverman, S. K.; Labarca, C. G.; Dougherty, D. A.; Lester, H. A., In vivo incorporation of unnatural amino acids into ion channels in Xenopus oocyte expression system. *Ion Channels, Pt B* **1998,** 293, 504-529.
15. Ryu, Y.; Schultz, P. G., Efficient incorporation of unnatural amino acids into proteins in Escherichia coli. *Nat Methods* **2006,** 3, (4), 263-5.
16. Chin, J. W.; Cropp, T. A.; Anderson, J. C.; Mukherji, M.; Zhang, Z.; Schultz, P. G., An expanded eukaryotic genetic code. *Science* **2003,** 301, (5635), 964-7.
17. Monahan, S. L.; Lester, H. A.; Dougherty, D. A., Site-specific incorporation of unnatural amino acids into receptors expressed in Mammalian cells. *Chem Biol* **2003,** 10, (6), 573-80.
18. Beene, D. L.; Dougherty, D. A.; Lester, H. A., Unnatural amino acid mutagenesis in mapping ion channel function. *Curr Opin Neurobiol* **2003,** 13, (3), 264-70.

19. Nowak, M. W.; Kearney, P. C.; Sampson, J. R.; Saks, M. E.; Labarca, C. G.; Silverman, S. K.; Zhong, W.; Thorson, J.; Abelson, J. N.; Davidson, N.; Schultz, P. G.; Dougherty, D. A.; Lester, H. A., Nicotinic Receptor-Binding Site Probed with Unnatural Amino-Acid-Incorporation in Intact-Cells. *Science* **1995,** 268, (5209), 439-442.
20. Rodriguez, E. A.; Lester, H. A.; Dougherty, D. A., In vivo incorporation of multiple unnatural amino acids through nonsense and frameshift suppression. *Proc Natl Acad Sci U S A* **2006,** 103, (23), 8650-5.
21. Brunner, J., New photolabeling and crosslinking methods. *Annu Rev Biochem* **1993,** 62, 483-514.
22. Li, Y. Z.; Kirby, J.; George, M.; Poliakoff, M.; Schuster, G. B., Photochemistry of Aryl Azides - Formation and Reactivity of Dehydroazepines. *Abstracts of Papers of the American Chemical Society* **1988,** 196, 322-ORGN.
23. Smith, R. A.; Knowles, J. R., Letter: Aryldiazirines. Potential reagents for photolabeling of biological receptor sites. *J Am Chem Soc* **1973,** 95, (15), 5072-3.
24. Chehade, K. A.; Spielmann, H. P., Facile and efficient synthesis of 4-azidotetrafluoroaniline: a new photoaffinity reagent. *J Org Chem* **2000,** 65, (16), 4949-53.
25. Karney, W. L.; Borden, W. T., Why does o-fluorine substitution raise the barrier to ring expansion of phenylnitrene? *Journal of the American Chemical Society* **1997,** 119, (14), 3347-3350.
26. Brunner, J.; Senn, H.; Richards, F. M., 3-Trifluoromethyl-3-phenyldiazirine. A new carbene generating group for photolabeling reagents. *J Biol Chem* **1980,** 255, (8), 3313-8.
27. Galardy, R. E.; Craig, L. C.; Printz, M. P., Benzophenone triplet: a new photochemical probe of biological ligand-receptor interactions. *Nat New Biol* **1973,** 242, (117), 127-8.
28. Forget, D.; Langelier, M. F.; Therien, C.; Trinh, V.; Coulombe, B., Photo-cross-linking of a purified preinitiation complex reveals central roles for the RNA polymerase II mobile clamp and TFIIE in initiation mechanisms. *Mol Cell Biol* **2004,** 24, (3), 1122-31.
29. Tate, J. J.; Persinger, J.; Bartholomew, B., Survey of four different photoreactive moieties for DNA photoaffinity labeling of yeast RNA polymerase III transcription complexes. *Nucleic Acids Res* **1998,** 26, (6), 1421-6.
30. Sengupta, S. M.; Persinger, J.; Bartholomew, B.; Peterson, C. L., Use of DNA photoaffinity labeling to study nucleosome remodeling by SWI/SNF. *Methods* **1999,** 19, (3), 434-46.
31. Sengupta, S. M.; VanKanegan, M.; Persinger, J.; Logie, C.; Cairns, B. R.; Peterson, C. L.; Bartholomew, B., The interactions of yeast SWI/SNF and RSC with the nucleosome before and after chromatin remodeling. *J Biol Chem* **2001,** 276, (16), 12636-44.
32. Pruss, D.; Bartholomew, B.; Persinger, J.; Hayes, J.; Arents, G.; Moudrianakis, E. N.; Wolffe, A. P., An asymmetric model for the nucleosome: a binding site for linker histones inside the DNA gyres. *Science* **1996,** 274, (5287), 614-7.
33. Mayer, A. N.; Barany, F., Photoaffinity cross-linking of TaqI restriction endonuclease using an aryl azide linked to the phosphate backbone. *Gene* **1995,** 153, (1), 1-8.
34. Musier-Forsyth, K.; Schimmel, P., Acceptor helix interactions in a class II tRNA synthetase: photoaffinity cross-linking of an RNA miniduplex substrate. *Biochemistry* **1994,** 33, (3), 773-9.

35. Westerheide, S. D.; Boss, J. M., Orientation and positional mapping of the subunits of the multicomponent transcription factors RFX and X2BP to the major histocompatibility complex class II transcriptional enhancer. *Nucleic Acids Res* **1999,** 27, (7), 1635-41.
36. Yang, S. W.; Nash, H. A., Specific photocrosslinking of DNA-protein complexes: identification of contacts between integration host factor and its target DNA. *Proc Natl Acad Sci U S A* **1994,** 91, (25), 12183-7.
37. Escher, E.; Schwyzer, R., p-Nitrophenylalanine, p-azidophenylalanine, m-azidophenylalanine, and o-nitro-p-azido-phenylalanine as photoaffinity labels. *FEBS Lett* **1974,** 46, (1), 347-50.
38. Fischli, W.; Caviezel, M.; Eberle, A.; Escher, E.; Schwyzer, R., [The synthesis of 4'-azido-3',5'-ditritio-l-phenylalanine peptides as "photo-affinity probes" for ligand-receptor interaction (author's transl)]. *Helv Chim Acta* **1976,** 59, (3), 878-9.
39. Kauer, J. C.; Erickson-Viitanen, S.; Wolfe, H. R., Jr.; DeGrado, W. F., p-Benzoyl-L-phenylalanine, a new photoreactive amino acid. Photolabeling of calmodulin with a synthetic calmodulin-binding peptide. *J Biol Chem* **1986,** 261, (23), 10695-700.
40. Nassal, M., 4'-(1-Azi-2,2,2-Trifluoroethyl)Phenylalanine, a Photolabile Carbene-Generating Analog of Phenylalanine. *Journal of the American Chemical Society* **1984,** 106, (24), 7540-7545.
41. Schwyzer, R.; Caviezel, M., p-Azido-L-phenylalanine: a photo-affinity 'probe' related to tyrosine. *Helv Chim Acta* **1971,** 54, (5), 1395-400.
42. Shih, L. B.; Bayley, H., A carbene-yielding amino acid for incorporation into peptide photoaffinity reagents. *Anal Biochem* **1985,** 144, (1), 132-41.
43. Egnaczyk, G. F.; Greis, K. D.; Stimson, E. R.; Maggio, J. E., Photoaffinity cross-linking of Alzheimer's disease amyloid fibrils reveals interstrand contact regions between assembled beta-amyloid peptide subunits. *Biochemistry* **2001,** 40, (39), 11706-14.
44. Escher, E. H.; Nguyen, T. M.; Robert, H.; St-Pierre, S. A.; Regoli, D. C., Photoaffinity labeling of the angiotensin II receptor. 1. Synthesis and biological activities of the labeling peptides. *J Med Chem* **1978,** 21, (9), 860-4.
45. O'Neil, K. T.; Erickson-Viitanen, S.; DeGrado, W. F., Photolabeling of calmodulin with basic, amphiphilic alpha-helical peptides containing p-benzoylphenylalanine. *J Biol Chem* **1989,** 264, (24), 14571-8.
46. Hixson, S. H.; Hixson, S. S., P-Azidophenacyl bromide, a versatile photolabile bifunctional reagent. Reaction with glyceraldehyde-3-phosphate dehydrogenase. *Biochemistry* **1975,** 14, (19), 4251-4.
47. Kaneda, M.; Sadakane, Y.; Hatanaka, Y., A novel approach for affinity-based screening of target specific ligands: application of photoreactive D-glyceraldehyde-3-phosphate dehydrogenase. *Bioconjug Chem* **2003,** 14, (5), 849-52.
48. Kenyon, G. L.; Bruice, T. W., Novel sulfhydryl reagents. *Methods Enzymol* **1977,** 47, 407-30.
49. Driessen, A. J.; Manting, E. H.; van der Does, C., The structural basis of protein targeting and translocation in bacteria. *Nat Struct Biol* **2001,** 8, (6), 492-8.
50. High, S.; Martoglio, B.; Gorlich, D.; Andersen, S. S.; Ashford, A. J.; Giner, A.; Hartmann, E.; Prehn, S.; Rapoport, T. A.; Dobberstein, B.; et al., Site-specific photocross-linking reveals that Sec61p and TRAM contact different regions of a membrane-inserted signal sequence. *J Biol Chem* **1993,** 268, (35), 26745-51.

51. Hohsaka, T.; Ashizuka, Y.; Taira, H.; Murakami, H.; Sisido, M., Incorporation of nonnatural amino acids into proteins by using various four-base codons in an Escherichia coli in vitro translation system. *Biochemistry* **2001,** 40, (37), 11060-4.
52. Hohsaka, T.; Sisido, M., Incorporation of non-natural amino acids into proteins. *Curr Opin Chem Biol* **2002,** 6, (6), 809-15.
53. Samuelson, J. C.; Chen, M.; Jiang, F.; Moller, I.; Wiedmann, M.; Kuhn, A.; Phillips, G. J.; Dalbey, R. E., YidC mediates membrane protein insertion in bacteria. *Nature* **2000,** 406, (6796), 637-41.
54. Scotti, P. A.; Urbanus, M. L.; Brunner, J.; de Gier, J. W.; von Heijne, G.; van der Does, C.; Driessen, A. J.; Oudega, B.; Luirink, J., YidC, the Escherichia coli homologue of mitochondrial Oxa1p, is a component of the Sec translocase. *Embo J* **2000,** 19, (4), 542-9.
55. Wang, L.; Brock, A.; Herberich, B.; Schultz, P. G., Expanding the genetic code of Escherichia coli. *Science* **2001,** 292, (5516), 498-500.
56. Hino, N.; Okazaki, Y.; Kobayashi, T.; Hayashi, A.; Sakamoto, K.; Yokoyama, S., Protein photo-cross-linking in mammalian cells by site-specific incorporation of a photoreactive amino acid. *Nat Methods* **2005,** 2, (3), 201-6.
57. Li, Y.-M., Photoactivatable gamma-secretase inhibitors directed to the active site covalently label presenilin 1. *Nature* **2000,** 405, 689-694.
58. Koumanov, F., Cell-surface Biotinylation of GLUT4 Using bis-Mannose Photolabels. *Biochemical Journal* **1998,** 330, 1209-1215.

CHAPTER 2: PUTATIVE VOLTAGE SENSING ARGININES IN THE MECHANOSENSITIVE CHANNEL OF SMALL CONDUCTANCE (MSCS)

2.1 Introduction

2.1.1 Mechanosensitive channels are ubiquitous across species

The ability of a cell to detect changes in its mechanical environment underlies a myriad of physiological processes including touch and pain sensation,[1-3] gravity detection, blood pressure control,[4] hearing and vestibular function,[5-7] tissue growth,[8] cell volume control,[9-11] and osmoregulation.[12] Additionally, mechanosensors have been suggested to play roles in neuronal development and plasticity as well as stress and inflammation. Given the vast roles of mechanosensitive mechanisms in physiological processes, it is not surprising that the disruption of these mechanosensitive mechanisms have been suggested to contribute to a variety of maladies such as neuronal and muscular degeneration,[13, 14] cardiac arrhythmias,[15-17] and hypertension,[18] arteriosclerosis,[19] and glaucoma.[20] In the past several decades, the molecular mechanisms underlying specific mechanosensitive processes have been identified. They include mechanosensitive channels,[21-23] mechanosensitive receptors,[24, 25] enzymes,[26, 27] and transmitter release.[28]

Mechanosensitive channels are integral membrane proteins that open and close in response to mechanical stress applied directly to the cell membrane or through indirect means via cytoskeletal components.[29-31] Mechanosensitive channels transduce a mechanical signal into an electrochemical response, thus allowing a cell to respond to stimuli such as sound, touch, gravity and pressure. They have been found in all branches of the phyllogenetic tree—*Eubacteria*, *Eukaya*, and *Archaea* and exhibit vast diversity both physiologically and structurally.[32] Eukaryotic mechanosensitive channels include the transient receptor potential vanilloid (TRPV) subclass of the Transient Receptor Potential

(TRP) channel family,[33] the TREK-1 and TRAKK members of the potassium channel family K_{2p},[34, 35] and the DEG/ENaC superfamily.[36, 37]

Given the role of mechanosensitive channels in a variety of biological processes, it is of interest to understand how these channels function. Unfortunately, eukaryotic mechanosensitive systems tend to be complex, involving multiple components, and as such they have yet to be well characterized biochemically. Prokaryotic mechanosensitive channels, on the other hand, can be relatively simple and tend to be intrinsically mechanosensitive, making them attractive model systems for studies on mechanosensation. Furthermore, prokaryotic mechanosensitive systems are significantly more amenable to genetic manipulations; hence more facile for biochemical and biophysical characterization. As a result, a wealth of information has been obtained through the study of prokaryotic mechanosensitive channels which might be relevant to the more complex eukaryotic mechanosensitive systems.

2.1.2 Prokaryotic mechanosensitive channels

First discovered in giant spheroplasts of bacteria, prokaryotic mechanosensitive channels are thought to function in the maintenance of cell turgor, acting as "emergency release valves" in the event of a sudden increase in external osmolarity.[38-42] There are three mechanosensitive proteins known to be associated with the mechanosensative channel activities of *E. coli*—the mechanosensitive channel of mini conductance (MscM),[43] the mechanosensitive channel of small conductance (MscS),[38, 43] and the mechanosensitive channel of large conductance (MscL).[44] These channels were characterized by their conductance and sensitivity to applied pressure with *in situ* and *in vitro* recordings

demonstrating that increased conductance correlated to a higher activation pressure. The conductance of MscL was shown to be between 2.5 and 3 nS whereas MscS has a conductance of 1 nS.[45, 46] Under osmotic stress, MscM opens first in attempts to maintain cell turgor followed by the opening of MscS should the gating of MscM not be sufficient. MscL acts as a last resort in response to sudden changes in external osmotic stress. MscL has been proposed to share an evolutionary origin with the sensor module of the eukaryotic, voltage-gated TRP channels as well as polycystin channels. Electrophysiological analysis of MscS activity was later shown to be the sum of the two channels KefA and YggB; however, reconstitution of YggB alone exhibited MscS conductance.[47, 48] Therefore, YggB became known as MscS and KefA was renamed MscK due to its interaction with K^+.[49] MscS and MscK share homology with each other and both have been proposed to be distantly related to MscL, although neither show strong homology with MscL.[50]

2.1.2.1 The mechanosensitive channel of small conductance

The mechanosensitive channel of small conductance (MscS) is characterized by a conductance of 1 nS and is opened with moderate pressure. The pressure threshold of opening for MscS was shown to be approximately 50% that of MscL.[22, 51] When first analyzed by electrophysiological analysis, MscS activity in *E. coli* was attributed to the sum of two channels, KefA and YggB. Booth and co-workers identified the protein YggB, which is 286 amino acids in length, as being necessary for MscS activity whereas deletion of the KefA gene appeared to be without a phenotype.[52] KefA was subsequently renamed MscK. KefA contains a domain highly homologous to YggB at the C-terminal tail of the protein and encodes a channel that displays MscS-like activity. Once the gene responsible for MscS was

discovered, it allowed for searches of genomic databases for homologous channels. The result of sequence homology searches has suggested that the MscS family is much larger and variable in size and sequence than the MscL family. MscS homologues appear to be prevelant in *Archaea* as well as eukaryotes.

Unlike MscL, MscS is not only mechanosensitive but it is also voltage modulated. The open probability of MscS increases *e*-fold for each +15 mV increase in membrane depolarization.[38] This is equivalent to the movement of 1.7 charges across the membrane during a gating event. MscS also shows a slight anion preference, although it is largely nonselective.[48, 50, 53] Mutational analysis suggests that MscS will tolerate minor mutations to the N-terminal region, however the C-terminal domain appears to be critical for its stability.[54]

2.1.2.2 Crystal structure of E. coli mechanosensitive channel of small conductance (MscS)

In 2002, the Rees group successfully obtained a crystal structure of *E. coli* MscS at 3.9 Å resolution.[55] The crystal structure represents the first structural look at a voltage-modulated ion channel. The 3.9 Å structure established that the channel assembled as a homoheptamer and could be divided into two regions—an extramembrane and transmembrane region (Figure 2.1). It is likely that the extramembrane region is cytoplasmic and the N-terminal region of MscS is periplasmic. The extramembrane region can be further divided into two domains that Bass *et al.* describe as the middle-beta domain and the carboxy-terminal domain. The channel spans approximately 120 Å in the direction parallel to the sevenfold axis with the extramembrane domain contributing 70 Å in length and the transmembrane domain contributing approximately 50 Å. The width of the channel in the direction perpendicular to the sevenfold axis spans approximately 80 Å.

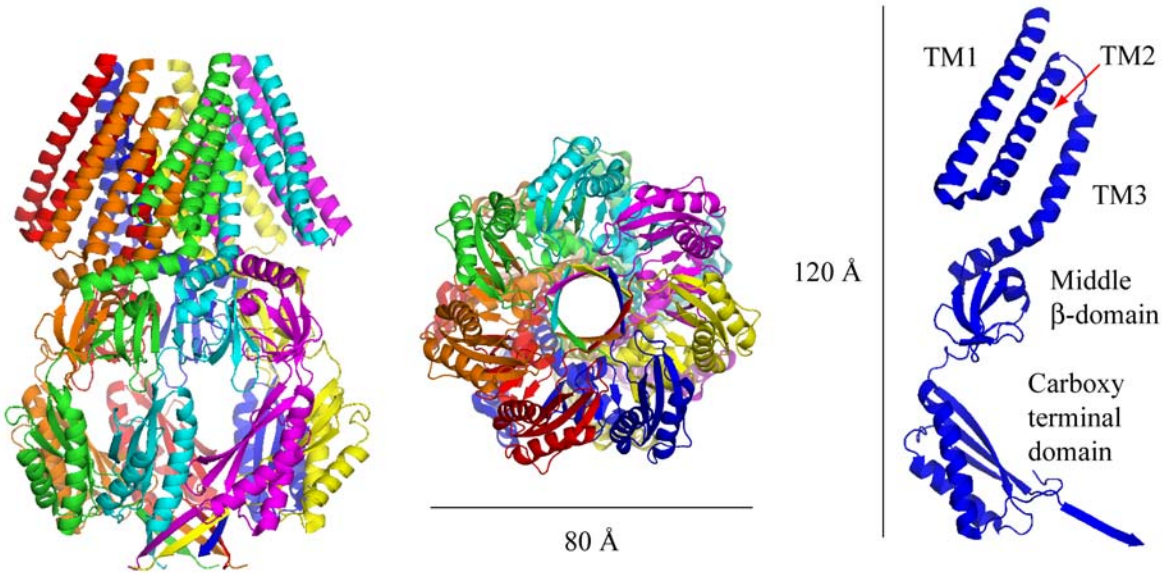

Figure 2.1. Crystal structure of MscS.

A channel is formed from helices from the membrane spanning region of each subunit that opens into a 40 Å chamber formed by the extramembrane regions. Interestingly, this chamber is connected to the cytoplasm through eight openings in between the middle-beta and carboxy-terminal domains of each subunit—seven openings on the sides of the chamber and a single opening at the bottom of the channel. The structural arrangement of MscS bares no resemblance to that of MscL or any other structural characterized channels.

Examination of each individual subunit that forms MscS reveals the transmembrane domain is comprised of three helices, TM1, TM2, and TM3. TM1 contains amino acids 29 to 57, TM2 is made of residues 68 to 91 and TM3 consists of residues 96 to 127. A prominent kink is present at glycine 113 within the TM3 region, presumably marking the membrane boundary of MscS. The pore of the channel is predominantly formed from the residues prior to this kink (residues 96 to 113) of TM3. The middle-beta domain, consisting

of residues 132 to 177, contains five beta-strands. The beta-strands of one subunit pack with those from other subunits to form a beta barrel like structure around the protein. The carboxy-terminal end of the protein exhibits a mixed alpha/beta structure and forms seven of the openings with the middle-beta domain, each with a diameter of approximately 14 Å. Because the structure reveals a permeation pathway that resembles a tapered cylinder with a diameter of 10 Å at the narrowest point, Bass *et al.*, propose that the crystal structure is most likely that of the open state of MscS.

2.1.2.3 Putative arginines in the voltage sensing mechanism of E. coli mechanosensitive channel of small conductance (MscS)

The crystal structure of MscS has several implications for the gating of MscS. In particular, the mechanism by which MscS is voltage modulated may be relevant to other voltage sensitive channels. The voltage sensitivity of K_v channels is conferred by a series of positively charged residues dispersed along the S4 helix. Most of these charged residues are arginines. The crystal structure of MscS reveals three arginines that may be appropriately positioned such that they could act as the voltage sensor in the voltage modulated gating of MscS (Figure 2.2). Arginine 46 and arginine 74 are located in TM1 and TM2 of MscS; TM1 and TM2 are adjacent to the permeation pathway and Bass *et al.* suggest they are likely candidates as mediators of the conformation change that occurs in MscS in response to applied tension or membrane depolarization. Therefore, the positions of Arg46 and Arg74 are such that their movement in response to changes in membrane potential could be translated into the opening and closing of the permeation pathway.

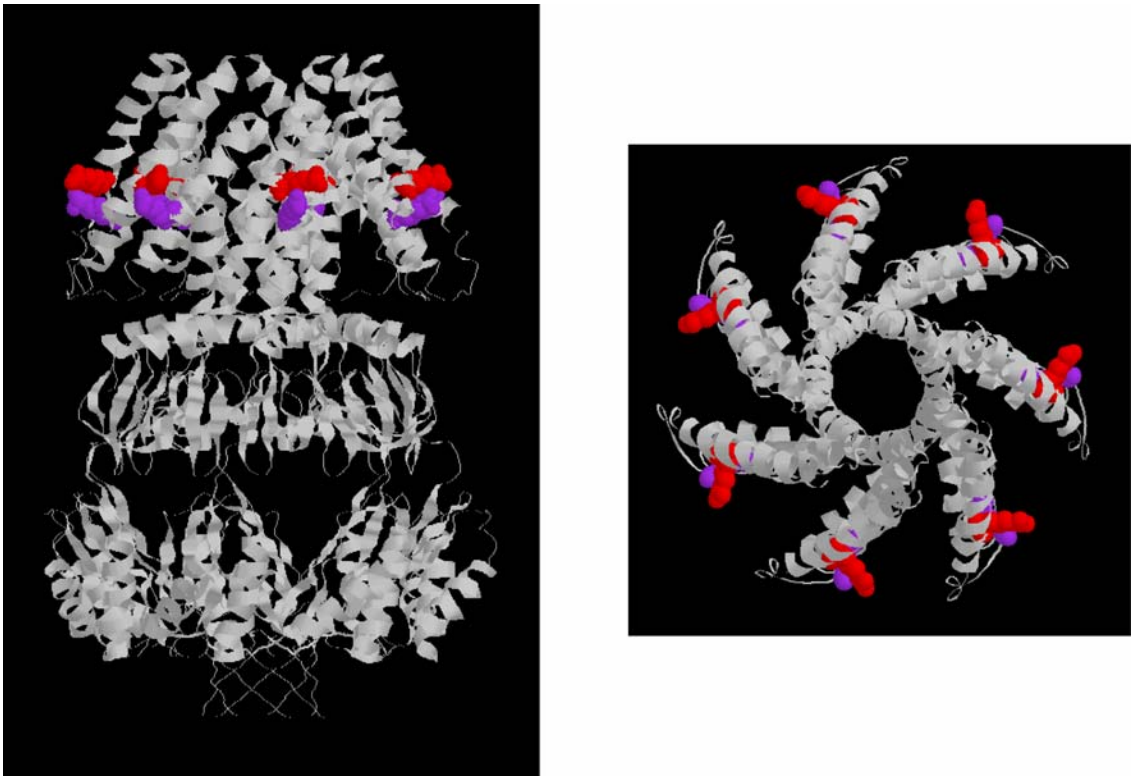

Figure 2.2. Putative voltage sensing arginines in MscS. Arg46 is shown in red and Arg 74 is shown in purple.

2.1.3 Voltage-gated ion channels

Electricity has a ubiquitous role in biology. The flow of ions through an ion channel and thus across a membrane constitutes an electrical current which results in a voltage difference across the membrane. All living cell have evolved the ability to exploit transmembrane electrical potentials in a myriad of biological processes through the use of voltage-gated ion channels. In particular, the group of "excitable cells" that includes neurons, muscle cells and endocrine cells extensively utilizes voltage-gated ion channels for fast electrical signaling. In neurons, electrical impulses result from action potentials, which are spike like changes in voltage across the membrane. They are millisecond long and are

capable of propagating at a rate of meters per second along a nerve fiber. Action potentials arise from the flow of various ions out of or into cells via membrane spanning ion channels that are voltage dependent. The ability to sense and respond to voltage is the key feature of voltage-gated ion channels that allow for the propagation of electrical signals in the nervous system and thus allows for the vast variety of firing patterns that are required for the processing of sensory information and generating motor outputs.

Hodgkin and Huxley were first to demonstrate the presence of voltage-activated sodium and potassium ion channels in the axon of a giant squid.[56-62] They showed that action potentials were made possible by a feedback process in which the direct action of voltage on ion channels resulted in channel gating and thus flow of ions. Sodium channels opened (activated) in response to a positive voltage, serving as the positive feedback segment. This is followed by the activation of potassium channels which serves as the negative feedback element. In essence, they demonstrated that there had to be charges or charge dipoles in the membrane that move in response to changes in voltage across the membrane thus turning the sodium and potassium ion channels on and off.

Voltage-gated channels share three defining features: 1) a pore forming domain that contains the permeation pathway and channel gates that control the flow of ions through the pore, 2) a voltage-sensing domain that contains the structural element that has the ability to respond to changes in transmembrane potential; also known as the voltage sensor and 3) a coupling element that links the voltage-sensing domain to the gates of the pore such that a change in transmembrane potential, and thus a response by the voltage-sensing domain, results in movement of the channel gates allowing ions to permeate the channel.

Since Hodgkin and Huxley's first voltage-clamp experiments were performed in 1952, an enormous effort has been put forth attempting to elucidate how voltage-gated ion channels work—both in how voltage causes the opening and closing of the channel and the coupling mechanism between the voltage sensor and the gate of the channel.

2.1.3.2 Voltage-gated potassium (K_v) ion channels

Much of what is known regarding the mechanism of gating for voltage-gated ion channels has come from the studies of the family of voltage-gated potassium channels (K_v). Voltage-gated potassium channels (K_v) channels are the prototypical voltage-gated channels and, as with voltage-gated Na^+ and Ca^{+2} channels, there is an enormous variety within its family. The K_v channel family is made up of over twenty-two different genes in mammals, with greater variations occurring from alternative splicing and heteromultimerization.

The basic channel architecture of the prototypical K_v channel is depicted in Figure 2.3.[63-65] They are typically tetrameric channels with each subunit containing a voltage sensor and a pore lining domain to contribute to the channel pore. A standard K_v channel subunit consists of six transmembrane domains (S1-S6) with both the amino- and carboxy-termini residing on the intracellular side of the membrane. The S5 and S6 segments comprise the pore forming domain. The narrowest part of the pore, the selectively filter, is formed by a loop between S5 and S6. The S4 domain contains multiple positively charged residues and contains the voltage sensor. K_v channels exhibit extremely high selectivity for the ions that are allowed to permeate, yet have transport rates that are close to the aqueous diffusion limit. High speed of ion transport and selectivity are critical in allowing these channels to accurately produce the rapid voltage changes necessary for action potentials in neurons

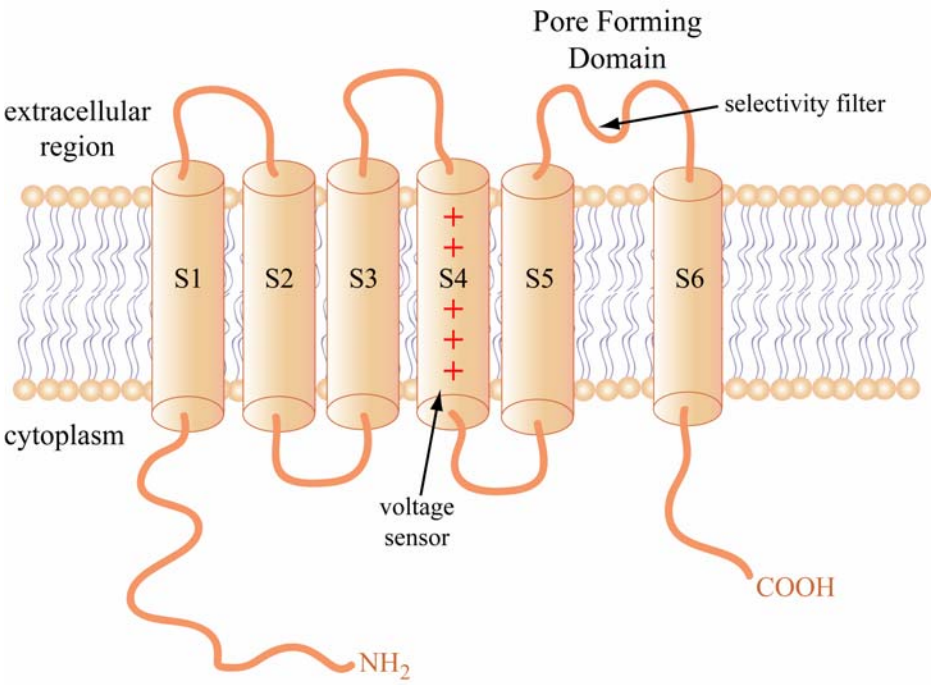

Figure 2.3. Schematic of a K_v channel subunit.

without the use of millions of proteins. The structural features that allow for a high speed of ion transport and ion selectivity have been well characterized.[66-69] The selectivity filter architecture will not be discussed here, however a number of reviews have been published that include discussion of the selectivity filter of K_v channels.[70-74]

2.1.3.3 Mechanisms of gating of voltage-gated potassium channels

While much is known about the architectural features that contribute to the high selectivity and rate of ion permeation of K_v channels, less is known about the mechanisms that govern the gating of K_v channels. A great deal of interest lies in understanding how a voltage-gated ion channel translates a change in membrane potential into a conformational change that results in channel gating. Understanding the gating mechanism involves three elements—1) the conformational change around the pore that occurs during its opening and

closing, 2) the movement of the voltage sensor in response to a change in membrane potential, and 3) the coupling between the voltage sensor and then pore that translate movement of the voltage sensor into conformational changes of the pore such that the pore opens or closes.

2.1.3.4 Mechanisms of pore closing in K_v channels

There are three proposed mechanisms by which the pore of voltage-gated K^+ channels close. Two mechanisms involve conformational changes such that a constriction occurs in the permeation pathway and the other involves obstruction of the pore by an inhibitory portion of the channel protein. The first mechanism of pore closing involves a "pinching" of the pore via movement of the S6 bundle, in which the S6 bundle moves such that it obstructs entrance to the water filled cavity via movement of the bottom ends (intracellular) of the S6 helices to form a "bundle crossing." This mechanism is supported by the interaction of ion channel blockers with the pore and the trapping of ion channel blockers within a cavity.[75, 76] It is also supported by high sequence conservation of the S6 transmembrane and intracellular portion among the principle families of voltage-gated K^+ channels—in particular, a highly conserved proline sequence (PxP or PxG) that may serve as a hinge.[77-79]

The second mechanism of inactivation is known as N-type inactivation, or the ball-and-chain mechanism, and does not involve pore constriction. Rather a physical obstruction of the pore by the N-terminus of one of the channel subunits is involded. N-type inactivation can be disrupted by enzymatic cleavage or by genetic removal of the N-terminus of the channel and can be restored by the addition of a soluble peptide derived from the N-terminus from an N-type inactivating channel.[80-83] It should be noted that there is little sequence

consensus among N-terminal portions that are capable of N-type inactivation, however it appears as though positive charge and hydrophobic character are important for the interaction of the N-terminus with the open pore of the channel.[82, 84]

The third mechanism by which the pore of a K_v channel can close involves the pinching of the selectivity filter itself, known as C-type inactivation. This type of interaction was observed in Shaker K^+ channels that had the N-terminal blocking peptide removed. This type of mechanism has been supported by various studies.[85-89] In particular, Yellen *et al.,* showed that once this type of inactivation occurred, it could be locked shut by a metal ion bridging cysteines that had been introduced into each subunit.[88] Furthermore this type of inactivation can be prevented by locking the selectivity filter open with the addition of extracellular tetrabutylammonium ion.[90]

2.1.3.5 Mechanisms of voltage-sensation and translation into pore gating

An area of enormous interest has been in understanding the movement of the voltage sensor and how its movement is coupled to the gating of the pore.[91-94] Fifty years of biophysical studies supported two main models—the helical screw model and the transporter model (figure 2.4(A) and 2.4(B)). The helical screw model posits that the S4 segment of each subunit rotates upon depolarization.[95-99] As the S4 segment rotates on its axis, it also translates perpendicular to the membrane such that it is exposed to the extracellular solution, thus moving the intracellular charges. This movement effectively translocates 4 e_0 per subunit across the membrane. In the transporter model, the translocation of charges is achieved by the tilt and rotation of the S4 segment. In the closed state, the charges occupy a water crevice exposed to the intracellular solution. The tilt and rotation of the S4 segments

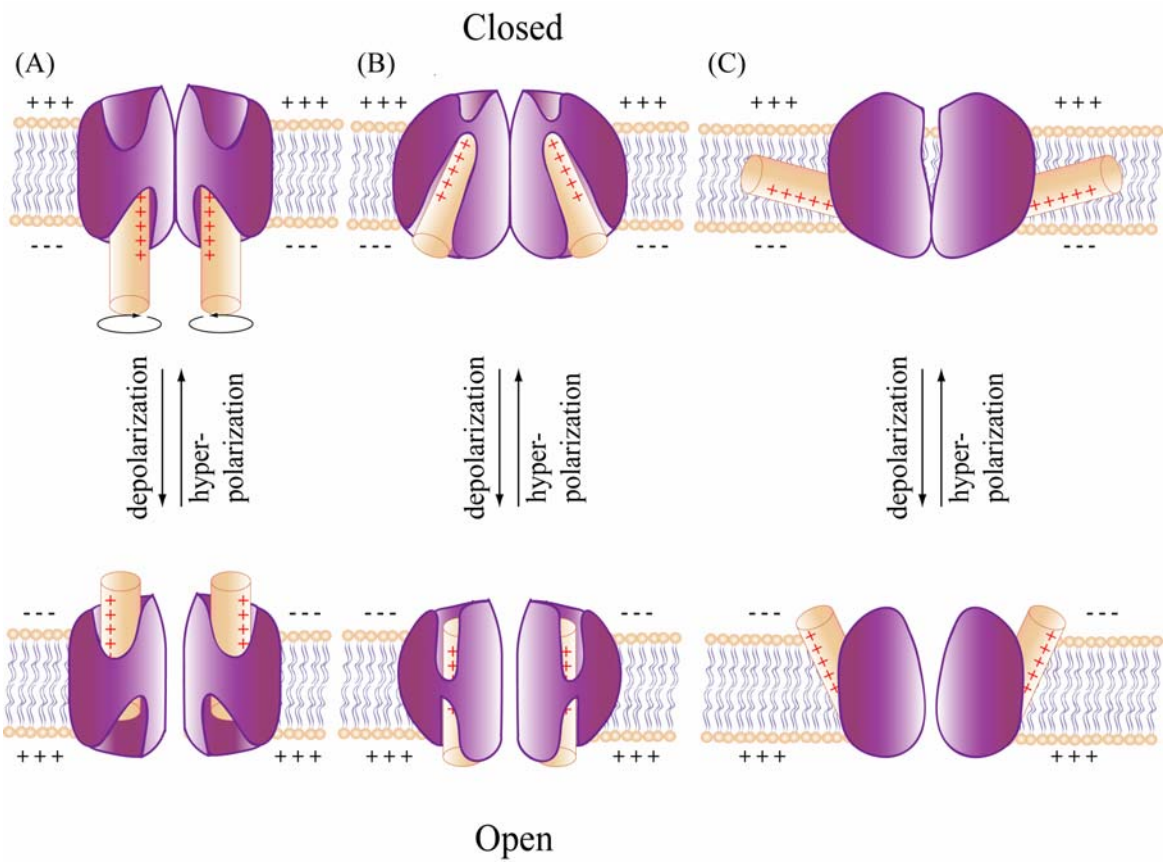

Figure 2.4. Three models of voltage sensing in voltage-gated ion channels. (A) Helical screw model, (B) transporter model, (C) paddle model.

to the open position results in the charges occupying another water crevice that exposes them to the extracellular solution.[92, 100]

In 2003, the MacKinnon group introduced a model that is dramatically different from the helical-screw and transporter models.[101, 102] The crystal structure of K_vAP coupled with data from biotin and streptavidin "scanning" experiments support a "paddle" model in which the S4 segment is located in the periphery of the channel with the charges embedded in the membrane bilayer (figure 2.4(C)). Depolarization results in a large translation of the S4 segment such that the charges go from being embedded in the bilayer in the closed state to

being exposed to the extracellular solution in the open state. This model has raised many questions given its stark difference to the helical-screw and transporter models.[103, 104]

2.2 Experimental design

The focus of the research described herein was to elucidate the role of arginine 46 and arginine 74 in the voltage sensitivity of MscS. The method to elucidate the role of these putative arginines in voltage sensation is relatively straightforward. Conventional mutagenesis was used to separately mutate each arginine amino acid to alanine residues, effectively removing the putative contribution of that particular arginine to the voltage sensitivity of MscS. The mutant channel was then expressed in *E. coli*. The cultures were used to generate giant *E. coli* spheroplasts for single channel analysis by cell-detached patch clamp electrophysiology. If either or both arginines contribute to the voltage sensitivity of MscS then we expect the dependence of the open probability of the mutant MscS on membrane depolarization to be diminished.

2.3 Results

2.3.1 Spheroplasts preparation

E. coli spheroplasts were generated using a standard established procedure with slight modifications.[45, 105] Spheroplasts allow for the use of bacterial systems for patch clamp. Bacteria are typically 1 μm in diameter, which is the approximate size of the electrode tip; therefore bacteria cannot be used to form a patch for electrophysiological analysis. Spheroplasts range in diameter from 6 to 10 μm and are the appropriate size for patch formation.

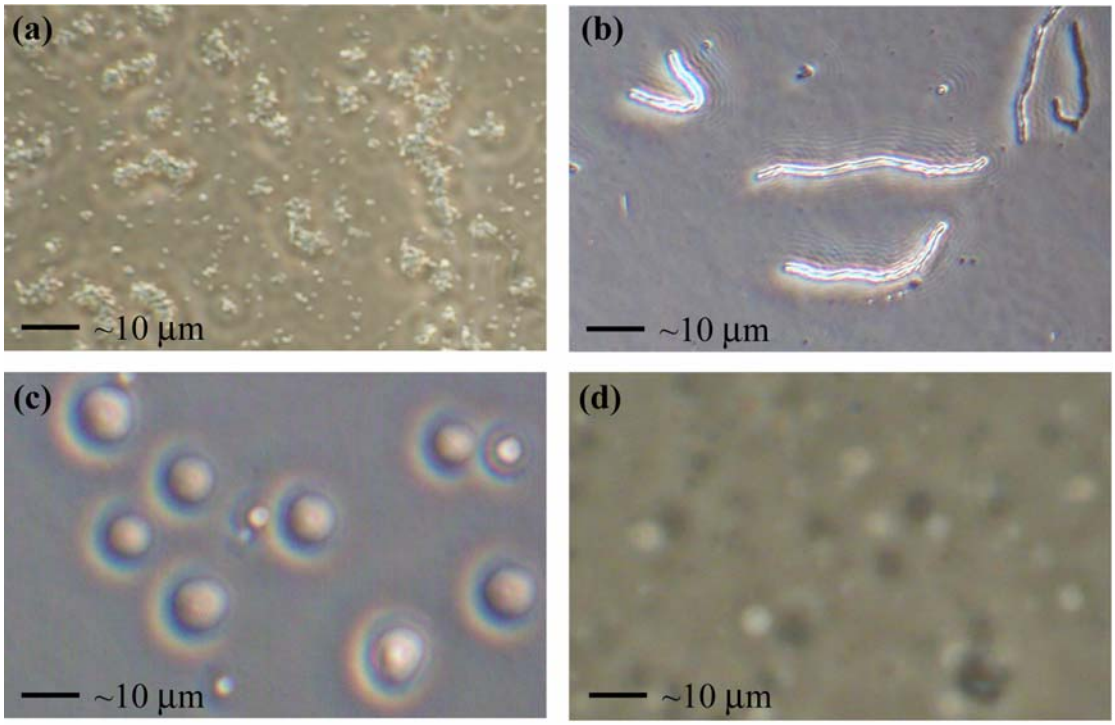

Figure 2.5. Generation of giant spheroplasts from *E. coli*. (A) *E. coli* culture, (B) "snakes" formed from cephalexin treatment, (C) healthy spheroplasts (D) unhealthy spheroplasts.

To generate spheroplasts, *E. coli* were cultured to an OD_{600} = 0.65 and then treated with cephalexin, an antibiotic that prevents septation but not the growth of the bacteria. The result is the formation of snake like strands of bacteria that are up to 100 µm in length (figure 2.5). Protein expression was induced in the snakes with the addition of isopropyl-β-D-thiogalactopyranoside (IPTG) and then the snakes were harvested and treated with lysozyme to digest the outer peptidoglycan layer of the snakes. Digestion with lysozyme forms the spheroplasts (Figure 2.5 (c)).

Spheroplast formation was highly inconsistent, such that less than 10% of the preparations yielded spheroplasts that were suitable for patch formation. More often than not, the preparations yielded collapsed spheroplasts or very weak spheroplasts that could not withstand the pressure needed to form a proper gigaohm seal (figure 2.5(d)). Numerous

attempts to optimize the protocol were not successful and did not appear to increase the rate of success for spheroplasts formation. The parameters that were varied in the optimization were the cephalexin incubation time, IPTG induction time, lysozyme induction time, amount of lysozyme, and the sucrose composition of the sucrose in the filtering solution. The shaking speed during the formation of snakes was also varied.

We speculate that the triple null strain MscL/MscS/MscK used in these experiments results in compromised *E. coli* membranes making them less durable to the demands of the spheroplast preparation. Because of the difficulty encountered in the generation of the spheroplasts, the data set for the wildtype and Arg46Ala mutant MscS channels is not extensive.

2.3.2 Electrophysiological characterization of wildtype MscS

Initial efforts were aimed at characterizing wildtype MscS using patch electrophysiology. The MscS channel was overexpressed in *E. coli* and characterized by cell detached inside out patch clamp electrophysiology. Expression was carried out in the MJF465 strain which has the three mechanosensitive channels MscL, MscS, and MscK knocked out. This was to ensure that any mechanosensitive channel activity would be due to the expressed gene product of the transformed MscS plasmid. *E. coli* that had been transformed with the expression plasmid containing the gene encoding MscS were used to generate spheroplasts using established protocols with some modifications.

Spheroplasts expressing MscS were evaluated using cell detached inside out patch clamp electrophysiology under symmetric buffer conditions with a total salt concentration of 300 mM. Initially, patches were held at a constant membrane potential of 20 mV and

pressure was gradually applied using suction until channel activity was observed. It should be noted that the amount of suction, and therefore pressure, needed to elicit a response from the expressed wildtype MscS channel varied from patch to patch due to differences in patch formation and membrane integrity. Once the minimum amount of pressure needed to elicit a response was determined for a particular patch, the patch was subjected to a developed voltage protocol. A schematic of this protocol is shown in figure 2.6. The determined pressure minimum was applied and held constant for each voltage jump while the membrane potential was increased in intervals of 10 mV. The pressure and desired membrane potential were applied for a 10 s period followed by a 50 s "rest" interval followed by another application of pressure with the next increment of membrane potential.

The wildtype MscS channel produced a single channel conductance of 1.5 nS under the aforementioned patch clamp recording conditions. The wildtype MscS channel also

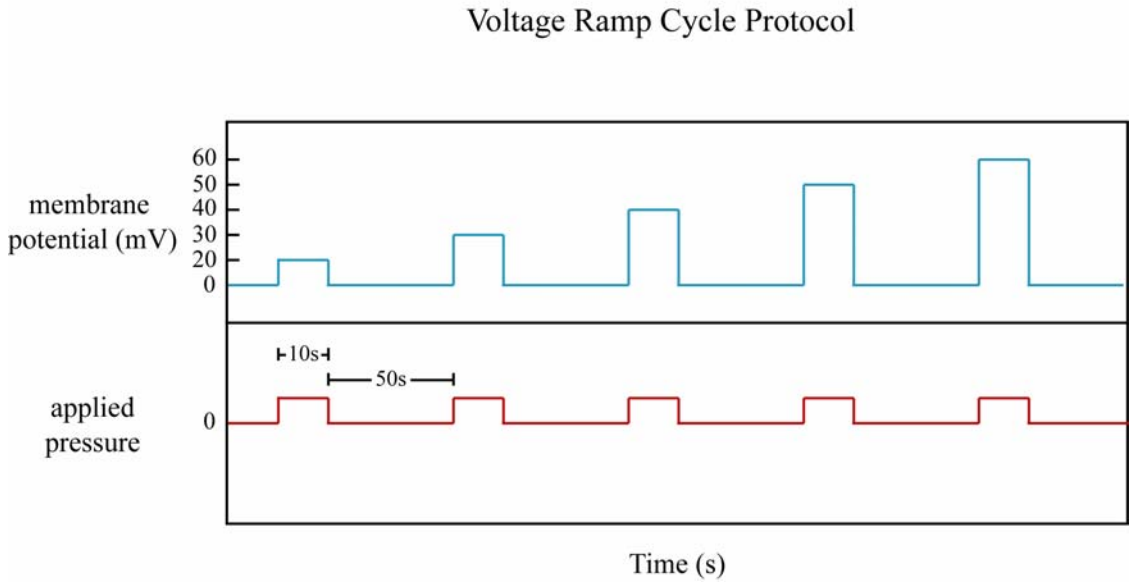

Figure 2.6. Schematic of voltage step protocol used for electrophysiological analysis of wildtype and mutant MscS.

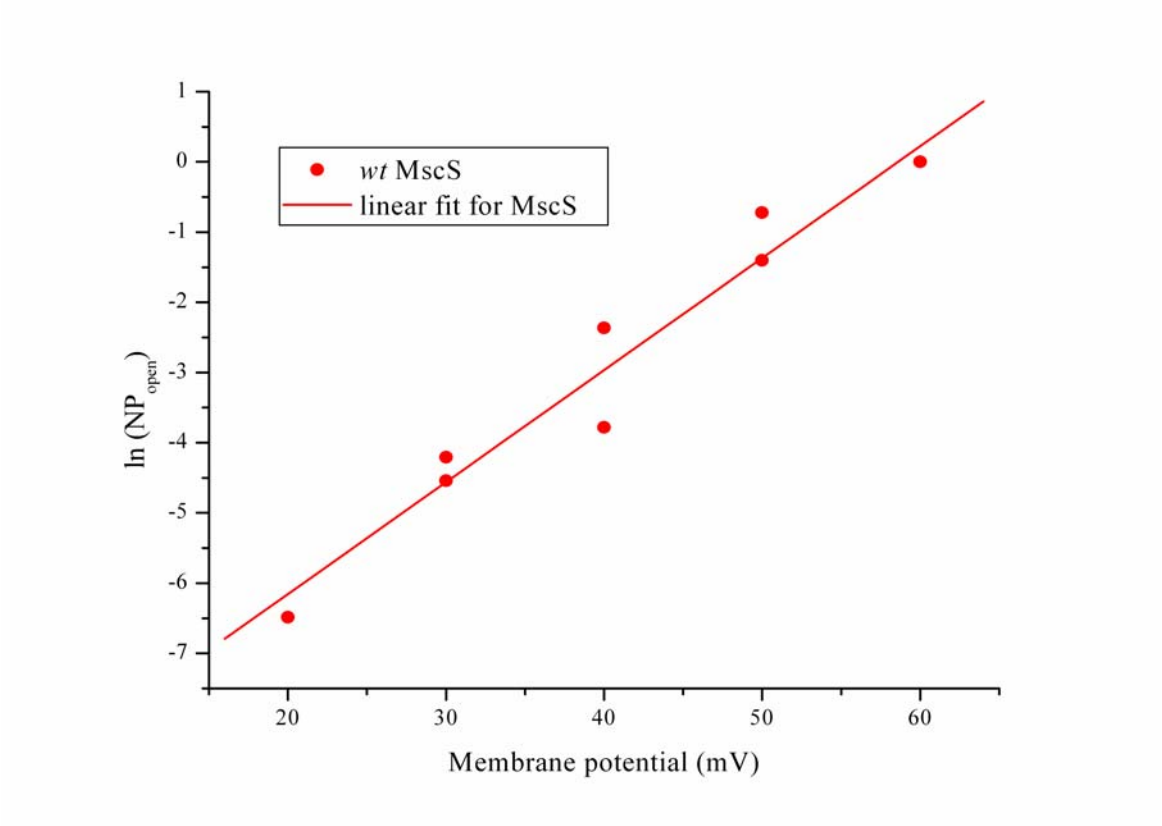

Figure 2.7. ln (NP_{open}) vs. membrane potential for *wildtype* MscS.

showed a strong dependence on voltage (figure 2.7) as observed by the open probability at various applied membrane potentials. At a constant applied pressure of 124 torr, the open probability, measured as $Np_{(open)}$, showed a linear log relationship with voltage (or applied membrane potential). Based on these initial measurements, an *e*-fold change in open probability occurs for every 6.44 mV change in voltage.

Interestingly, the activity of the wildtype MscS channels exhibited an unanticipated inactivation behavior. A successfully formed patch could only be evaluated with a single series of voltage steps before a significant loss of detected signal (figure 2.8). Application of multiple cycles of the voltage step protocol showed that the largest decrease in signal occurs after the first cycle and subsequent cycles show a much lower rate of signal decrease.

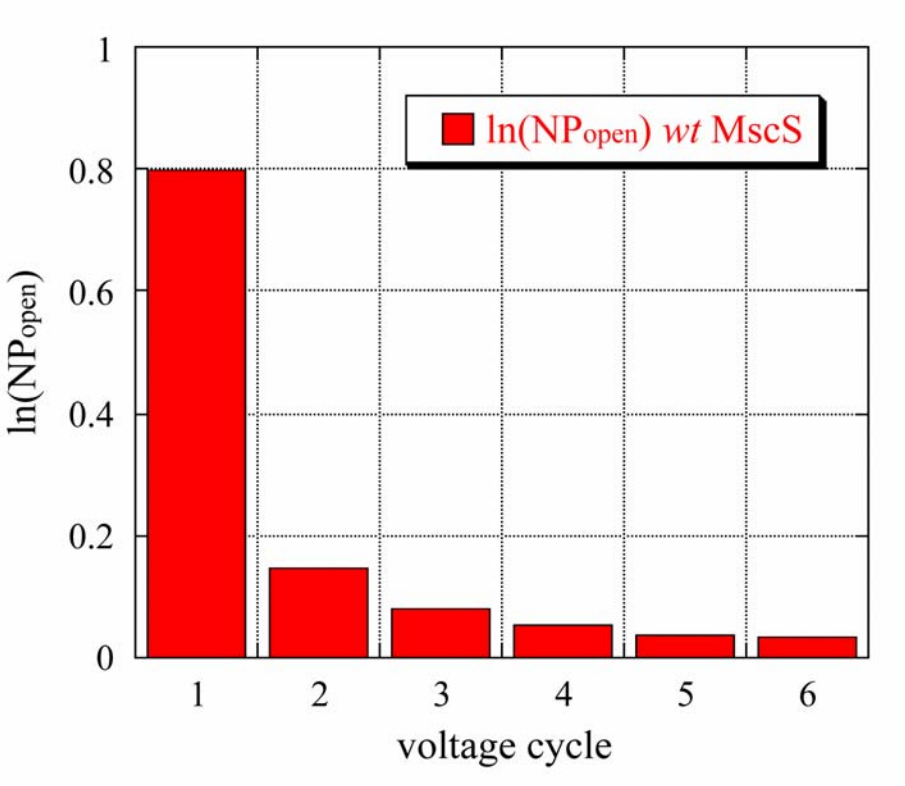

Figure 2.8. Wildtype MscS exhibits diminished activity after one cycle of the voltage step protocol.

2.3.3 Electrophysiological characterization of Arg46Ala mutant MscS

Arginine 46 in MscS was mutated to an alanine residue to determine the importance of arginine 46 in the voltage modulation of MscS. If arginine 46 is part of the voltage sensor of MscS, then neutralizing it should effectively remove or diminish the voltage sensitivity of the channel. Conventional site directed mutagenesis was used to generate the Arg46Ala mutant MscS which was then transformed into the MJF465 *E. coli* strain (Yan Poon, Rees Laboratory). Spheroplasts were generated using the transformed strain similar to the wildtype and subjected to electrophysiological analysis using patch clamp techniques. Successful patches containing the Arg46Ala mutant channels were subject to the same

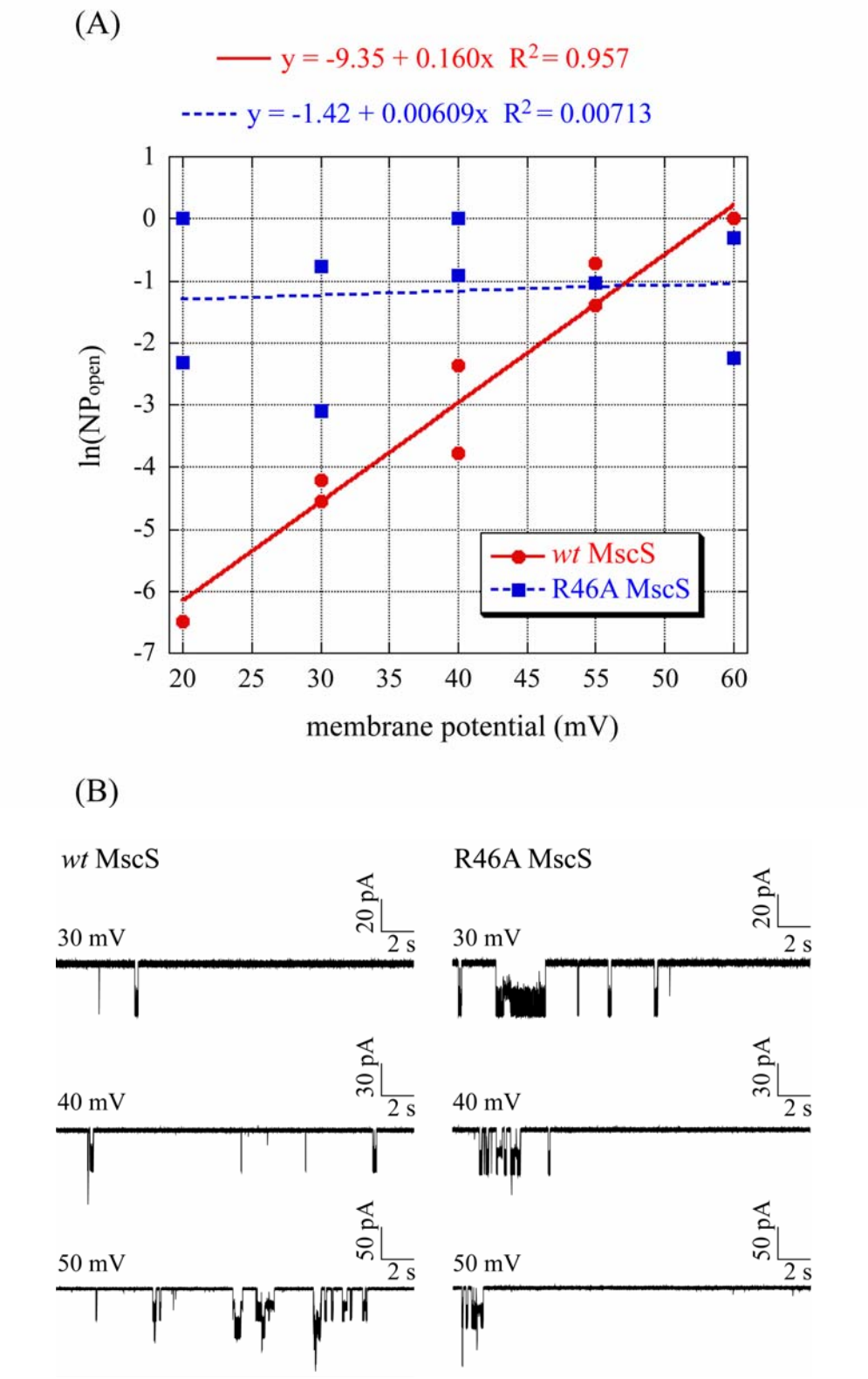

Figure 2.9. Comparison of $\ln(NP_{open})$ of wildtype MscS and Arg46Ala mutant MscS.

voltage protocol as the patches containing wildtype MscS channels, under the same bath conditions.

As seen in Figure 2.9, initial single channel recordings show no clear linear relationship between Np(open) and voltage for the Arg46Ala mutant MscS channel. The overall variation in Np(open) was significantly smaller than that of the wildtype. An attempted log fit of the data results in a very poor fit compared to that of the wildtype and the resulting slope is much less than for the wildtype. The mutant also differed from the wildtype MscS in several other interesting ways. The minimum pressure required to open the mutant channel at a membrane potential of +20 mV was 50% higher (186 torr) than that of the wildtype channel. Furthermore, the mutant channel did not exhibit the same drastic decrease in signal after the first series of voltage steps. A given successful patch containing Arg46Ala mutant MscS channels could be subjected to multiple cycles of the voltage step protocol without any significant decrease in channel signal (data not shown).

2.3.4. Characterization of Arg74Ala mutant MscS

Arginine 74 was mutated to an alanine residue and subjected the same analysis as the wildtype and Arg46Ala mutant MscS channels using patch clamp electrophysiology. Viable patches were formed from healthy spheroplasts, however all patches that were formed exhibited no channel activity. A substantial number of viable patches were tested, none of which exhibited channel activity. To ensure the channel was still properly expressed with the mutation at position 74, Western blot analysis of the membrane fraction was performed. As shown in Figure 2.10, both the Arg74Ala and Arg46Ala mutant MscS channels showed expression levels comparable to that of the wildtype.

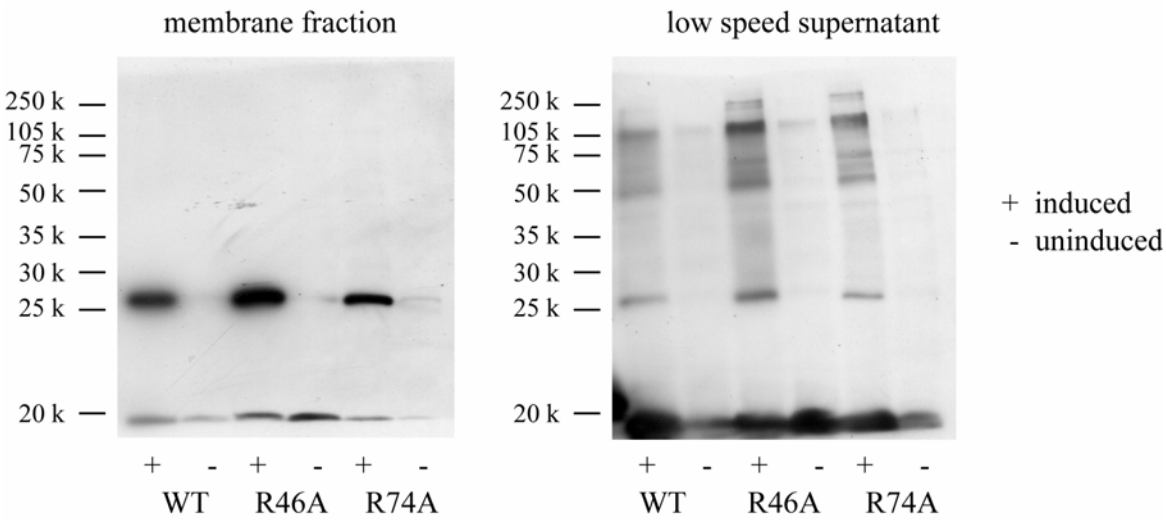

Figure 2.10. Western blot analysis of *wildtype* and mutant MscS expression levels from the membrane fraction (left) and the supernatant recovered after low speed centrifugation (right).

2.4 Discussion

Voltage-gated ion channels have been of great interest for biophysical studies since they were first detected by Hodgkin and Huxley. Decades of biophysical studies resulted in the proposed "helical screw" model for the mechanism of gating for voltage-gated ion channels. The controversial "paddle" model was proposed by MacKinnon *et al.* with the structure of K_vAP in 2003. This model differs considerably from the helical screw model and as such, intense interest continues to surround the field of voltage-gated ion channels. While MscS is not a typical voltage-gated ion channel, it shares some features that make it an attractive system to study that may lead to some insight into the mechanism of gating of voltage-gated ion channels. In particular, two arginine residues at position 46 and 74, located in TM1 and TM2 respectively, point out into the lipid membrane making them ideally placed to serve as voltage sensors during the gating process. Consequently the focus of the described work was aimed at elucidating the role of these arginines in the voltage-modulated

gating of MscS using single channel analysis with patch clamp electrophysiology in *E. coli* spheroplasts.

Our preliminary data indicated a strong voltage dependence for the wildtype MscS channel as compared to the R46A mutant MscS channel, which showed no apparent dependence on voltage. These results suggested that Arg46 plays a critical role in the voltage sensitivity of MscS since neutralization of this residue, by mutation to an alanine, removed or significantly reduced the voltage sensitivity. Additionally, computational work done by Spronk *et al.*, suggests that Arg46 and Arg74 are important for channel function.[106] Furthermore, this mutant channel also required a 50% higher minimum applied pressure to achieve comparable open probabilities to the wildtype. We also observed an inactivation behavior for the wildtype which was not seen with the R46A mutant channel. Based on these preliminary data, the wildtype channel indicated an *e*-fold change in Np(open) for every 6.44 mV change of transmembrane potential. Earlier work by Martinac *et al.*, suggested an *e*-fold change for every 15 mV change. The Arg74Ala mutant MscS channel exhibited no apparent channel activity despite healthy spheroplast and viable patch formation. Western blot analysis suggested the lack of channel activity was not due to lack of expression of the mutant channel.

These studies were greatly hampered by the inconsistent yield for the spheroplasts preparation. Less than 10% of the preparations yielded healthy spheroplasts that could form viable patches for electrophysiological analysis. Furthermore, the unanticipated inactivation behavior observed for the wildtype MscS channel also established another obstacle in obtaining a more extensive data set. It should also be noted that similar work performed by

Dr. Daniel A. Clayton yielded varying results in which the Arg46Ala mutant exhibited no apparent voltage dependence.

2.5 Conclusions

The research discussed herein was aimed at elucidating the role of two arginine residues in the TM1 and TM2 of MscS, a mechanosensitive ion channel that is also voltage-modulated. The MscS crystal structure reveals that these two arginines are appropriately positioned, pointing into the membrane, such that they could act as voltage sensors during gating. We generated two MscS mutants, Arg46Ala and Arg74Ala, to evaluate the effects of "neutralizing" the charged side chain on the voltage sensing ability of the channel. Using cell detached inside out patch clamp electrophysiology in *E. coli* spheroplasts, we evaluated the mutant channels and compared them to the wildtype MscS. Our preliminary results indicated a potentially significant role for Arg46 in the voltage sensitivity of MscS.

2.6 Experimental methods and materials

2.6.1 General

Unless otherwise stated, all reagents were purchased from commercial sources and used as is. MJF465 cells were received as a generous gift from Ian Booth. Site directed mutagenesis was performed by Yan Poon (Rees Laboratory) to generate the MscS mutants.

2.6.2 Electroporation of MJF465 cells with pB10b vector containing MscS

1 μL of mini-prep DNA expression plasmid was mixed with a 40 μL aliquot of MJF465 cells (MscL/MscS/MscK null *E. coli* strain). The MJF465 cells were thawed on ice

for 10 min prior to use. The cells and DNA mixture were mixed by gentle pipetting and then loaded into a 0.1 cm electroporation cuvette. The cuvettes were stored at –20 °C until needed. The cell and DNA mixture was then electroporated at 1800 V. A time constant in the range of 4.2 to 5.0 typically yielded efficiently transformed colonies. The cells were "rescued" with the addition of 0.5 mL of SOC media that had been warmed to 37 °C. The cells were mixed by gentle pipeting followed by transfer to a falcon culture tube. The culture was then incubated at 37 °C with shaking (300 rpm) for 15 to 20 min. The rescued culture was then plated on to LB-agar supplemented with ampicillin. 50 mL to 100 mL of culture was used per plate. Plates were incubated upside down at 37 °C for 10 h or until distinct colonies were observed. Colonies were then picked when needed to inoculate cultures.

2.6.3 Spheroplasts Preparation

A single colony or a perma-culture of a desired transformed *E. coli* strain was used to inoculate a 2 mL LB culture supplemented with ampicillin (0.1 μg/mL) (LB amp (+)) which was incubated at 37 °C with shaking at 300 rpm overnight (10 to 14 h) to produce a saturated culture. An aliquot (100 μL) of the saturated culture was removed and used to inoculate a 25 mL LB amp (+) culture. The culture was incubated at 37 °C and 300 rpm until the OD_{600} = 0.65, as measured by UV-vis spectroscopy. Subsequently, 5 mL of the 25 mL culture was added to a 50 mL LB amp (+) culture. To this culture was added 5.4 mg of cephalexin which was then incubated at 37 °C with shaking at 300 rpm for 1.5 h. Protein expression was induced by the addition of 0.5 mL of 100 mM IPTG and incubation was continued at 37 °C, 300 rpm for 15 min. The resulting snakes were aliquoted in 1 mL portions in eppendorfs and then harvested by centrifugation at 1500 x g for 15 min. at 4 °C. The supernatant was

decanted and the cell pellets were kept on ice during all subsequent steps unless otherwise noted. A 0.8 M sucrose solution (1 mL) was gently layered over each cell pellet without disturbing the pellet. The pellet was incubated on ice for 1 min. The sucrose solution was then gently removed and a fresh portion of 0.8 M sucrose (1 mL) was added. The pellet was gently resuspended by shaking. Vortexing was avoided. The resuspension was transferred to a glass test tube (10 x 75 mm). To each resuspension was added, in the following order with agitation: 1 M Tris-HCl, pH 7.8 (62.5 μL), 5 mg/mL lysozyme solution (60 μL) or lysonase (1 μL), 10 mg/mL DNAse (7.5 μL), and 0.5 M EDTA, pH 8.0 (18.75 μL). The reaction was incubated at room temperature with agitation (shake with hands) for 2-5 min. Reactions were monitored using light microscopy. Digestion reactions were terminated by the dropwise (with agitation) addition of 0.5 mL of "stop solution" (0.7 M sucrose, 20 mM $MgCl_2$, 10 mM Tris, pH 7.8). The terminated reaction was carefully layered on 10 mL of "filtering solution" (0.8 M sucrose, 10 mM $MgCl_2$, 10 mM Tris-HCl, pH 8.0) and subsequently centrifuged at 800 x g at 4 °C for 3 min. Each layer and partition was examined by microscropy to determine the presence of properly formed spheroplasts. The layers containing spheroplasts were harvested and aliquoted. Aliquots were promptly stored at -20 °C. When needed aliquots were thawed on ice.

During attempts to optimize this protocol the following parameters were varied: the cephalexin incubation time, IPTG induction time, lysozyme reaction time, lysonase amounts and reaction times, sucrose concentration in filtering solution, as well as the shaking speed during cephalexin incubation.

2.6.4 Electrophysiological characterization of MscS

The MscS channel was characterized by electrophysiology using the inside-out cell-detached patch clamp method. *E. coli* strain MJF465 ($MscL^-MscS^-MscK^-$) was used for all analysis. Spheroplasts expressing MscS were generated using an established protocol, and the channels were evaluated under symmetric buffer conditions (200 mM KCl, 90 mM $MgCl_2$, 100 mM $CaCl_2$, 15 mM HEPES, pH 7.5). Electrodes were pulled from borosilicate capillary tubes (World Precision Instruments, Sarasota, FL) using a micropipette puller (Model P-80/PC, Sutter Instruments, Novato CA). They were subsequently fire polished (MF-83, Narishige Scientific Instrument Lab, Tokyo, Japan) to give a pipette resistance of ~6 GΩ in recording solution. Negative pressure was applied through a syringe and measured by a calibrated pressure transducer (Omega Engineering, Stamford, CT). Currents were acquired with an AxoPatch 1-D amplifier (Axon Instruments) at a sampling rate of 25 kHz, filtered at 5 kHz and analyzed using pCLAMP9.0 software (Axon Instruments). All measurements were acquired from at least two spheroplasts preparations.

2.6.5 Membrane fraction isolation

An *E. coli* colony of the desired transformed strain was used to inoculate a 2 mL LB culture supplemented with ampicillin (0.1 μg/mL**)** (LB-amp +). The 2 mL culture was incubated overnight at 37 °C with shaking at (300 rpm) for 12 to 14 h to produce a saturated culture. 200 mL of the saturated culture was used to inoculate 50 mL of LB-amp (+) culture which was then incubated at 37 °C with shaking (300 rpm) until the OD_{600} = 0.6 to 0.8. Cephalexin (5.4 mg) was added to the culture which was then incubated for 1.5 hours to generate "snakes." Subsequently, 500 μL of 100 mM IPTG was added to induce protein

expression. Induction was allowed to proceed for 2 h at 37 °C with shaking (300 rpm). The resulting "snakes" were harvested by centrifugation, in pre-weighed centrifugation vessels, at 2000 x g for 10 min at 4 °C. The supernatant was decanted and the weight of the cell pellet was determined. Lysis buffer (5 mM EDTA, 50 mM Tris pH 7.5, 200 mM NaCl) was then added at the ratio of 200 mL of lysis buffer for every 25 g of cell pellet. Prior to resuspension and lysis, protease inhibitors (10 μg/mL), DNAse (1 mM), and lysozyme were added (5 μg/mL). $MgCl_2$ was added to a final concentration of 2 mM (add 2 μL of 1M $MgCl_2$ per 1 mL lysis buffer). The mixture was then sonicated to resuspend and the cell pellet. A probe sonicator with a microtip was used and sonication was performed on ice for a total of 15 s in 1 s sonication intervals with 10 s rest intervals to prevent overheating of the samples. The cell lysate was then centrifuged at 11,000 x g for 20 min at 4 °C. The low-speed supernatant was removed and saved and the pellet was resuspended in a volume of buffer equivalent to the volume of low-speed supernatant recovered (i.e., if there was 3 mL of supernatant, pellet was resuspended in 3 mL of buffer). This was done to normalize the volumes to allow for a direct comparison of Western blot analysis. A small portion (10 μL) of the low speed supernatant was reserved for Western blot analysis and then the remaining low speed supernatant was centrifuged at 150,000 x g for 1 hr. at 4 ºC to pellet the membranes. The high-speed supernatant was removed and saved and the resulting pellet was resuspended using normalizing volumes as before. The low-speed supernatant, high-speed supernatant, and pellet fraction were then subject to resolution by SDS-PAGE followed by Western blot analysis.

2.7 *References*

1. Tavernarakis, N.; Driscoll, M., Molecular modeling of mechanotransduction in the nematode Caenorhabditis elegans. *Annu Rev Physiol* **1997,** 59, 659-89.
2. Nakamura, F.; Strittmatter, S. M., P2Y1 purinergic receptors in sensory neurons: contribution to touch-induced impulse generation. *Proc Natl Acad Sci U S A* **1996,** 93, (19), 10465-70.
3. Burnstock, G.; Wood, J. N., Purinergic receptors: their role in nociception and primary afferent neurotransmission. *Curr Opin Neurobiol* **1996,** 6, (4), 526-32.
4. Burnstock, G., Release of vasoactive substances from endothelial cells by shear stress and purinergic mechanosensory transduction. *J Anat* **1999,** 194 (Pt 3), 335-42.
5. Howard, J.; Roberts, W. M.; Hudspeth, A. J., Mechanoelectrical transduction by hair cells. *Annu Rev Biophys Biophys Chem* **1988,** 17, 99-124.
6. Hackney, C. M.; Furness, D. N.; Benos, D. J.; Woodley, J. F.; Barratt, J., Putative immunolocalization of the mechanoelectrical transduction channels in mammalian cochlear hair cells. *Proc Biol Sci* **1992,** 248, (1323), 215-21.
7. Hackney, C. M.; Furness, D. N., Mechanotransduction in vertebrate hair cells: structure and function of the stereociliary bundle. *Am J Physiol* **1995,** 268, (1 Pt 1), C1-13.
8. Duncan, R. L.; Turner, C. H., Mechanotransduction and the functional response of bone to mechanical strain. *Calcif Tissue Int* **1995,** 57, (5), 344-58.
9. Wang, Y.; Roman, R.; Lidofsky, S. D.; Fitz, J. G., Autocrine signaling through ATP release represents a novel mechanism for cell volume regulation. *Proc Natl Acad Sci U S A* **1996,** 93, (21), 12020-5.
10. Okada, Y., Volume expansion-sensing outward-rectifier Cl- channel: fresh start to the molecular identity and volume sensor. *Am J Physiol* **1997,** 273, (3 Pt 1), C755-89.
11. Nilius, B.; Eggermont, J.; Voets, T.; Buyse, G.; Manolopoulos, V.; Droogmans, G., Properties of volume-regulated anion channels in mammalian cells. *Prog Biophys Mol Biol* **1997,** 68, (1), 69-119.
12. Gustin, M. C.; Zhou, X. L.; Martinac, B.; Kung, C., A mechanosensitive ion channel in the yeast plasma membrane. *Science* **1988,** 242, (4879), 762-5.
13. Franco, A., Jr.; Lansman, J. B., Calcium entry through stretch-inactivated ion channels in mdx myotubes. *Nature* **1990,** 344, (6267), 670-3.
14. Driscoll, M.; Chalfie, M., The mec-4 gene is a member of a family of Caenorhabditis elegans genes that can mutate to induce neuronal degeneration. *Nature* **1991,** 349, (6310), 588-93.
15. Hansen, D. E.; Craig, C. S.; Hondeghem, L. M., Stretch-induced arrhythmias in the isolated canine ventricle. Evidence for the importance of mechanoelectrical feedback. *Circulation* **1990,** 81, (3), 1094-105.
16. Franz, M. R.; Cima, R.; Wang, D.; Profitt, D.; Kurz, R., Electrophysiological effects of myocardial stretch and mechanical determinants of stretch-activated arrhythmias. *Circulation* **1992,** 86, (3), 968-78.
17. Dean, J. W.; Lab, M. J., Arrhythmia in heart failure: role of mechanically induced changes in electrophysiology. *Lancet* **1989,** 1, (8650), 1309-12.
18. Kohler, R.; Distler, A.; Hoyer, J., Increased mechanosensitive currents in aortic endothelial cells from genetically hypertensive rats. *J Hypertens* **1999,** 17, (3), 365-71.

19. Dimmeler, S.; Hermann, C.; Zeiher, A. M., Apoptosis of endothelial cells. Contribution to the pathophysiology of atherosclerosis? *Eur Cytokine Netw* **1998,** 9, (4), 697-8.
20. Mitchell, C. H.; Carre, D. A.; McGlinn, A. M.; Stone, R. A.; Civan, M. M., A release mechanism for stored ATP in ocular ciliary epithelial cells. *Proc Natl Acad Sci U S A* **1998,** 95, (12), 7174-8.
21. Morris, C. E., Mechanosensitive ion channels. *J Membr Biol* **1990,** 113, (2), 93-107.
22. Sukharev, S. I.; Blount, P.; Martinac, B.; Kung, C., Mechanosensitive channels of Escherichia coli: the MscL gene, protein, and activities. *Annu Rev Physiol* **1997,** 59, 633-57.
23. Martinac, B., Mechanosensitive channels in prokaryotes. *Cell Physiol Biochem* **2001,** 11, (2), 61-76.
24. Casado, M.; Ascher, P., Opposite modulation of NMDA receptors by lysophospholipids and arachidonic acid: common features with mechanosensitivity. *J Physiol* **1998,** 513 (Pt 2), 317-30.
25. Paoletti, P.; Ascher, P., Mechanosensitivity of NMDA receptors in cultured mouse central neurons. *Neuron* **1994,** 13, (3), 645-55.
26. Lehtonen, J. Y.; Kinnunen, P. K., Phospholipase A2 as a mechanosensor. *Biophys J* **1995,** 68, (5), 1888-94.
27. Matsumoto, H.; Baron, C. B.; Coburn, R. F., Smooth muscle stretch-activated phospholipase C activity. *Am J Physiol* **1995,** 268, (2 Pt 1), C458-65.
28. Chen, B. M.; Grinnell, A. D., Kinetics, Ca2+ dependence, and biophysical properties of integrin-mediated mechanical modulation of transmitter release from frog motor nerve terminals. *J Neurosci* **1997,** 17, (3), 904-16.
29. Gillespie, P. G.; Walker, R. G., Molecular basis of mechanosensory transduction. *Nature* **2001,** 413, (6852), 194-202.
30. Hamill, O. P.; Martinac, B., Molecular basis of mechanotransduction in living cells. *Physiol Rev* **2001,** 81, (2), 685-740.
31. Society of General Physiologists. Symposium (50th : 1996 Woods Hole Mass.); Froehner, S. C.; Bennett, V., *Cytoskeletal regulation of membrane function : Society of General Physiologists 50th annual symposium, Marine Biological Laboratory, Woods Hole, Massachusetts, 5-7 September 1996*. Rockefeller University Press: New York, 1997; p vii, 280 p.
32. Pivetti, C. D.; Yen, M. R.; Miller, S.; Busch, W.; Tseng, Y. H.; Booth, I. R.; Saier, M. H., Jr., Two families of mechanosensitive channel proteins. *Microbiol Mol Biol Rev* **2003,** 67, (1), 66-85, table of contents.
33. Clapham, D. E.; Runnels, L. W.; Strubing, C., The TRP ion channel family. *Nat Rev Neurosci* **2001,** 2, (6), 387-96.
34. Maingret, F.; Fosset, M.; Lesage, F.; Lazdunski, M.; Honore, E., TRAAK is a mammalian neuronal mechano-gated K+ channel. *J Biol Chem* **1999,** 274, (3), 1381-7.
35. Maingret, F.; Patel, A. J.; Lesage, F.; Lazdunski, M.; Honore, E., Mechano- or acid stimulation, two interactive modes of activation of the TREK-1 potassium channel. *J Biol Chem* **1999,** 274, (38), 26691-6.
36. Welsh, M. J.; Price, M. P.; Xie, J., Biochemical basis of touch perception: mechanosensory function of degenerin/epithelial Na+ channels. *J Biol Chem* **2002,** 277, (4), 2369-72.

37. Tavernarakis, N.; Driscoll, M., Mechanotransduction in Caenorhabditis elegans: the role of DEG/ENaC ion channels. *Cell Biochem Biophys* **2001,** 35, (1), 1-18.
38. Martinac, B.; Buechner, M.; Delcour, A. H.; Adler, J.; Kung, C., Pressure-sensitive ion channel in Escherichia coli. *Proc Natl Acad Sci U S A* **1987,** 84, (8), 2297-301.
39. Szabo, I.; Petronilli, V.; Zoratti, M., A patch-clamp investigation of the Streptococcus faecalis cell membrane. *J Membr Biol* **1993,** 131, (3), 203-18.
40. Zoratti, M.; Petronilli, V.; Szabo, I., Stretch-activated composite ion channels in Bacillus subtilis. *Biochem Biophys Res Commun* **1990,** 168, (2), 443-50.
41. Delcour, A. H.; Martinac, B.; Adler, J.; Kung, C., Voltage-sensitive ion channel of Escherichia coli. *J Membr Biol* **1989,** 112, (3), 267-75.
42. Le Dain, A. C.; Saint, N.; Kloda, A.; Ghazi, A.; Martinac, B., Mechanosensitive ion channels of the archaeon Haloferax volcanii. *J Biol Chem* **1998,** 273, (20), 12116-9.
43. Berrier, C.; Coulombe, A.; Houssin, C.; Ghazi, A., A patch-clamp study of ion channels of inner and outer membranes and of contact zones of E. coli, fused into giant liposomes. Pressure-activated channels are localized in the inner membrane. *FEBS Lett* **1989,** 259, (1), 27-32.
44. Sukharev, S. I.; Blount, P.; Martinac, B.; Blattner, F. R.; Kung, C., A large-conductance mechanosensitive channel in E. coli encoded by mscL alone. *Nature* **1994,** 368, (6468), 265-8.
45. Blount, P.; Sukharev, S. I.; Moe, P. C.; Martinac, B.; Kung, C., Mechanosensitive channels of bacteria. *Methods Enzymol* **1999,** 294, 458-82.
46. Sukharev, S., Mechanosensitive channels in bacteria as membrane tension reporters. *Faseb J* **1999,** 13 Suppl, S55-61.
47. Okada, K.; Moe, P. C.; Blount, P., Functional design of bacterial mechanosensitive channels. Comparisons and contrasts illuminated by random mutagenesis. *J Biol Chem* **2002,** 277, (31), 27682-8.
48. Sukharev, S., Purification of the small mechanosensitive channel of Escherichia coli (MscS): the subunit structure, conduction, and gating characteristics in liposomes. *Biophys J* **2002,** 83, (1), 290-8.
49. Li, Y.; Moe, P. C.; Chandrasekaran, S.; Booth, I. R.; Blount, P., Ionic regulation of MscK, a mechanosensitive channel from Escherichia coli. *Embo J* **2002,** 21, (20), 5323-30.
50. Kloda, A.; Martinac, B., Mechanosensitive channels of bacteria and archaea share a common ancestral origin. *Eur Biophys J* **2002,** 31, (1), 14-25.
51. Blount, P.; Moe, P. C., Bacterial mechanosensitive channels: integrating physiology, structure and function. *Trends Microbiol* **1999,** 7, (10), 420-4.
52. Levina, N.; Totemeyer, S.; Stokes, N. R.; Louis, P.; Jones, M. A.; Booth, I. R., Protection of Escherichia coli cells against extreme turgor by activation of MscS and MscL mechanosensitive channels: identification of genes required for MscS activity. *Embo J* **1999,** 18, (7), 1730-7.
53. Kloda, A.; Martinac, B., Common evolutionary origins of mechanosensitive ion channels in Archaea, Bacteria and cell-walled Eukarya. *Archaea* **2002,** 1, (1), 35-44.
54. Miller, S.; Bartlett, W.; Chandrasekaran, S.; Simpson, S.; Edwards, M.; Booth, I. R., Domain organization of the MscS mechanosensitive channel of Escherichia coli. *Embo J* **2003,** 22, (1), 36-46.

55. Bass, R. B.; Strop, P.; Barclay, M.; Rees, D. C., Crystal structure of Escherichia coli MscS, a voltage-modulated and mechanosensitive channel. *Science* **2002,** 298, (5598), 1582-7.
56. Hodgkin, A. L.; Huxley, A. F., Propagation of electrical signals along giant nerve fibers. *Proc R Soc Lond B Biol Sci* **1952,** 140, (899), 177-83.
57. Hodgkin, A. L.; Huxley, A. F., A quantitative description of membrane current and its application to conduction and excitation in nerve. *J Physiol* **1952,** 117, (4), 500-44.
58. Hodgkin, A. L.; Huxley, A. F., The dual effect of membrane potential on sodium conductance in the giant axon of Loligo. *J Physiol* **1952,** 116, (4), 497-506.
59. Hodgkin, A. L.; Huxley, A. F., The components of membrane conductance in the giant axon of Loligo. *J Physiol* **1952,** 116, (4), 473-96.
60. Hodgkin, A. L.; Huxley, A. F., Currents carried by sodium and potassium ions through the membrane of the giant axon of Loligo. *J Physiol* **1952,** 116, (4), 449-72.
61. Hodgkin, A. L.; Huxley, A. F., Movement of sodium and potassium ions during nervous activity. *Cold Spring Harb Symp Quant Biol* **1952,** 17, 43-52.
62. Hodgkin, A. L.; Huxley, A. F.; Katz, B., Measurement of current-voltage relations in the membrane of the giant axon of Loligo. *J Physiol* **1952,** 116, (4), 424-48.
63. Agnew, W. S.; Levinson, S. R.; Brabson, J. S.; Raftery, M. A., Purification of the tetrodotoxin-binding component associated with the voltage-sensitive sodium channel from Electrophorus electricus electroplax membranes. *Proc Natl Acad Sci U S A* **1978,** 75, (6), 2606-10.
64. Noda, M.; Shimizu, S.; Tanabe, T.; Takai, T.; Kayano, T.; Ikeda, T.; Takahashi, H.; Nakayama, H.; Kanaoka, Y.; Minamino, N.; et al., Primary structure of Electrophorus electricus sodium channel deduced from cDNA sequence. *Nature* **1984,** 312, (5990), 121-7.
65. Tempel, B. L.; Papazian, D. M.; Schwarz, T. L.; Jan, Y. N.; Jan, L. Y., Sequence of a probable potassium channel component encoded at Shaker locus of Drosophila. *Science* **1987,** 237, (4816), 770-5.
66. Doyle, D. A.; Morais Cabral, J.; Pfuetzner, R. A.; Kuo, A.; Gulbis, J. M.; Cohen, S. L.; Chait, B. T.; MacKinnon, R., The structure of the potassium channel: molecular basis of K+ conduction and selectivity. *Science* **1998,** 280, (5360), 69-77.
67. Zhou, Y.; Morais-Cabral, J. H.; Kaufman, A.; MacKinnon, R., Chemistry of ion coordination and hydration revealed by a K+ channel-Fab complex at 2.0 A resolution. *Nature* **2001,** 414, (6859), 43-8.
68. Morais-Cabral, J. H.; Zhou, Y.; MacKinnon, R., Energetic optimization of ion conduction rate by the K+ selectivity filter. *Nature* **2001,** 414, (6859), 37-42.
69. Berneche, S.; Roux, B., Energetics of ion conduction through the K+ channel. *Nature* **2001,** 414, (6859), 73-7.
70. Choe, S., Potassium channel structures. *Nat Rev Neurosci* **2002,** 3, (2), 115-21.
71. Sansom, M. S.; Shrivastava, I. H.; Bright, J. N.; Tate, J.; Capener, C. E.; Biggin, P. C., Potassium channels: structures, models, simulations. *Biochim Biophys Acta* **2002,** 1565, (2), 294-307.
72. Yellen, G., Permeation in potassium channels: implications for channel structure. *Annu Rev Biophys Biophys Chem* **1987,** 16, 227-46.
73. Corry, B.; Chung, S. H., Mechanisms of valence selectivity in biological ion channels. *Cell Mol Life Sci* **2006,** 63, (3), 301-15.

74. Kurata, H. T.; Fedida, D., A structural interpretation of voltage-gated potassium channel inactivation. *Prog Biophys Mol Biol* **2006,** 92, (2), 185-208.
75. Armstrong, C. M., Interaction of tetraethylammonium ion derivatives with the potassium channels of giant axons. *J Gen Physiol* **1971,** 58, (4), 413-37.
76. Holmgren, M.; Smith, P. L.; Yellen, G., Trapping of organic blockers by closing of voltage-dependent K+ channels: evidence for a trap door mechanism of activation gating. *J Gen Physiol* **1997,** 109, (5), 527-35.
77. Holmgren, M.; Shin, K. S.; Yellen, G., The activation gate of a voltage-gated K+ channel can be trapped in the open state by an intersubunit metal bridge. *Neuron* **1998,** 21, (3), 617-21.
78. del Camino, D.; Holmgren, M.; Liu, Y.; Yellen, G., Blocker protection in the pore of a voltage-gated K+ channel and its structural implications. *Nature* **2000,** 403, (6767), 321-5.
79. del Camino, D.; Yellen, G., Tight steric closure at the intracellular activation gate of a voltage-gated K(+) channel. *Neuron* **2001,** 32, (4), 649-56.
80. Antz, C.; Bauer, T.; Kalbacher, H.; Frank, R.; Covarrubias, M.; Kalbitzer, H. R.; Ruppersberg, J. P.; Baukrowitz, T.; Fakler, B., Control of K+ channel gating by protein phosphorylation: structural switches of the inactivation gate. *Nat Struct Biol* **1999,** 6, (2), 146-50.
81. Murrell-Lagnado, R. D.; Aldrich, R. W., Energetics of Shaker K channels block by inactivation peptides. *J Gen Physiol* **1993,** 102, (6), 977-1003.
82. Murrell-Lagnado, R. D.; Aldrich, R. W., Interactions of amino terminal domains of Shaker K channels with a pore blocking site studied with synthetic peptides. *J Gen Physiol* **1993,** 102, (6), 949-75.
83. Zagotta, W. N.; Hoshi, T.; Aldrich, R. W., Restoration of inactivation in mutants of Shaker potassium channels by a peptide derived from ShB. *Science* **1990,** 250, (4980), 568-71.
84. Aldrich, R. W., Fifty years of inactivation. *Nature* **2001,** 411, (6838), 643-4.
85. Hoshi, T.; Zagotta, W. N.; Aldrich, R. W., Two types of inactivation in Shaker K+ channels: effects of alterations in the carboxy-terminal region. *Neuron* **1991,** 7, (4), 547-56.
86. Liu, Y.; Jurman, M. E.; Yellen, G., Dynamic rearrangement of the outer mouth of a K+ channel during gating. *Neuron* **1996,** 16, (4), 859-67.
87. Ruppersberg, J. P.; Stocker, M.; Pongs, O.; Heinemann, S. H.; Frank, R.; Koenen, M., Regulation of fast inactivation of cloned mammalian IK(A) channels by cysteine oxidation. *Nature* **1991,** 352, (6337), 711-4.
88. Yellen, G.; Sodickson, D.; Chen, T. Y.; Jurman, M. E., An engineered cysteine in the external mouth of a K+ channel allows inactivation to be modulated by metal binding. *Biophys J* **1994,** 66, (4), 1068-75.
89. Hoshi, T.; Zagotta, W. N.; Aldrich, R. W., Biophysical and molecular mechanisms of Shaker potassium channel inactivation. *Science* **1990,** 250, (4980), 533-8.
90. Choi, K. L.; Aldrich, R. W.; Yellen, G., Tetraethylammonium blockade distinguishes two inactivation mechanisms in voltage-activated K+ channels. *Proc Natl Acad Sci U S A* **1991,** 88, (12), 5092-5.
91. Tombola, F.; Pathak, M. M.; Isacoff, E. Y., How Does Voltage Open an Ion Channel? *Annu Rev Cell Dev Biol* **2006,** 22, 23-52.
92. Bezanilla, F., Voltage sensor movements. *J Gen Physiol* **2002,** 120, (4), 465-73.

93. Bezanilla, F., Voltage-gated ion channels. *IEEE Trans Nanobioscience* **2005,** 4, (1), 34-48.
94. Bezanilla, F.; Perozo, E., Structural biology. Force and voltage sensors in one structure. *Science* **2002,** 298, (5598), 1562-3.
95. Durell, S. R.; Guy, H. R., Atomic scale structure and functional models of voltage-gated potassium channels. *Biophys J* **1992,** 62, (1), 238-47; discussion 247-50.
96. Gandhi, C. S.; Isacoff, E. Y., Molecular models of voltage sensing. *J Gen Physiol* **2002,** 120, (4), 455-63.
97. Durell, S. R.; Shrivastava, I. H.; Guy, H. R., Models of the structure and voltage-gating mechanism of the shaker K+ channel. *Biophys J* **2004,** 87, (4), 2116-30.
98. Catterall, W. A., Molecular properties of voltage-sensitive sodium channels. *Annu Rev Biochem* **1986,** 55, 953-85.
99. Ahern, C. A.; Horn, R., Specificity of charge-carrying residues in the voltage sensor of potassium channels. *J Gen Physiol* **2004,** 123, (3), 205-16.
100. Starace, D. M.; Bezanilla, F., A proton pore in a potassium channel voltage sensor reveals a focused electric field. *Nature* **2004,** 427, (6974), 548-53.
101. Jiang, Y.; Lee, A.; Chen, J.; Ruta, V.; Cadene, M.; Chait, B. T.; MacKinnon, R., X-ray structure of a voltage-dependent K+ channel. *Nature* **2003,** 423, (6935), 33-41.
102. Jiang, Y.; Ruta, V.; Chen, J.; Lee, A.; MacKinnon, R., The principle of gating charge movement in a voltage-dependent K+ channel. *Nature* **2003,** 423, (6935), 42-8.
103. Cohen, B. E.; Grabe, M.; Jan, L. Y., Answers and questions from the KvAP structures. *Neuron* **2003,** 39, (3), 395-400.
104. Miller, C., A charged view of voltage-gated ion channels. *Nat Struct Biol* **2003,** 10, (6), 422-4.
105. Ruthe, H. J.; Adler, J., Fusion of bacterial spheroplasts by electric fields. *Biochim Biophys Acta* **1985,** 819, (1), 105-13.
106. Spronk, S. A.; Elmore, D. E.; Dougherty, D. A., Voltage-dependent hydration and conduction properties of the hydrophobic pore of the mechanosensitive channel of small conductance. *Biophys J* **2006,** 90, (10), 3555-69.

CHAPTER 3: *CIS-TRANS* ISOMERIZATION AT A CONSERVED PROLINE DURING GATING OF A CYS-LOOP RECEPTOR

3.1 Introduction

3.1.1 Ligand-gated ion channels

As discussed in Chapter 1, synaptic transmission is initiated when the presynaptic axon terminal releases neurotransmitters into the synaptic cleft. The neurotransmitters diffuse across the synaptic cleft and bind to receptors embedded in the membrane of a post-synaptic dendrite of a neighboring neuron. Binding of the neurotransmitter activates the receptor, eliciting cellular events in the postsynaptic neuron, thus modulating its activity. There are a variety of neurotransmitters and neuroreceptors. There are two main categories of neuroreceptors—1) metabotropic and 2) ionotropic receptors. Metabotropic receptors are responsible for slow synaptic transmission and act through second messenger pathways. Binding of neurotransmitter initiates cascades that can result in gating of ion channels or other cellular effects. Metabotropic receptors include the G-protein coupled receptor family.

Ionotropic receptors are also known as ligand-gated ion channels (LGICs) and are responsible for fast synaptic transmission. Binding of the neurotransmitter to a LGIC causes a conformational change of the entire channel, resulting in gating of the channel and the flow of ions. LGICs are highly selective, allowing for the transport of specific ions. This selectivity allows for the modulation of action potentials in a postsynaptic neuron. Whether or not a postsynaptic neuron fires an action potential is determined by whether or not the activated LGIC is excitatory (cation selective) or inhibitory (anion selective). The balance of excitatory and inhibitory activity through the activation of LGICs influences information processing in our brain. Not surprisingly, aberrations of this balance can result in disease states and/or abnormal activity including anxiety, epilepsy and neuronal death.[1-15] Furthermore, LGICs are therapeutic targets for numerous maladies including Alzheimer's

disease, Parkinson's disease, learning and attention disorders, and depression and drug addiction.[16]

The class of LGICs is comprised of four superfamilies: the glutamate receptors, the transient receptor potential (TRP) channels, the ATP-gated channels, and the Cys-loop receptor superfamily. The glutamate receptors include the N-methyl-D-aspartate (NMDA) receptors, the α-amino-3-hydroxy-5-methyl-4-isoxalepropionic acid (AMPA) receptors and kainite receptors. The Cys-loop receptor superfamily consists of both cationic and anionic ligand-gated ion channels.

3.1.2 Cys-loop receptors

As mentioned before, the Cys-loop receptor superfamily can be divided further into two classes based on their ion permeation properties. The cationic selective class of Cys-loop receptors includes the nicotinic acetylcholine receptors (nAChR) and the serotonin gated 5-hydroxytryptamine-3 (5-HT_3) receptors.[17-22] The anion selective class of receptors includes the γ-aminobutyric acid (GABA) receptors and the glycine receptors.[23, 24] Cys-loop receptors perform important physiological functions, and mutations in these channels can result in a myriad of pathological states, or channelopathies, such as epilepsy, hyperekplexia, and Angelman's syndrome. Cys-loop receptors are also therapeutic targets for Alzeheimer's disease,[25] Parkinson's disease,[26] anxiety, learning and attention disorders,[27, 28] as well as targets of analgesics, anti-emetics, and anesthesia.[16, 29-37]

Members of the Cys-loop superfamily are thought to share similar architecture. Each receptor is comprised of a pentameric structure with five subunits assembled to construct a ring structure forming the pore.[38, 39] Some subunits can form a homogeneous receptor, while

other receptors are formed by a heterogeneous composition of receptor subunits.[40-43] Each subunit consists of four transmembrane domains (M1-M4), a large extracellular N-terminal domain and an extracellular C-terminal domain (Figure 3.1A).[44-47] The large N-terminal domain contains the ligand binding site as well as a characteristic Cys-loop, for which the family is named, formed by a cysteine disulfide bond. The sequence alignment of known Cys-loop subunits shows a fair amount of homology, with roughly 25% to 30% identity. Each subunit is arranged in a pentameric array with the M2 region of each subunit lining the pore (figure 1B). It should be noted that for each receptor in the family, there exists a variety of subunit isoforms that combine in different compositions to form distinct receptor subtypes.[48, 49] For many of these receptors, the exact composition of subunit isoforms is unknown.

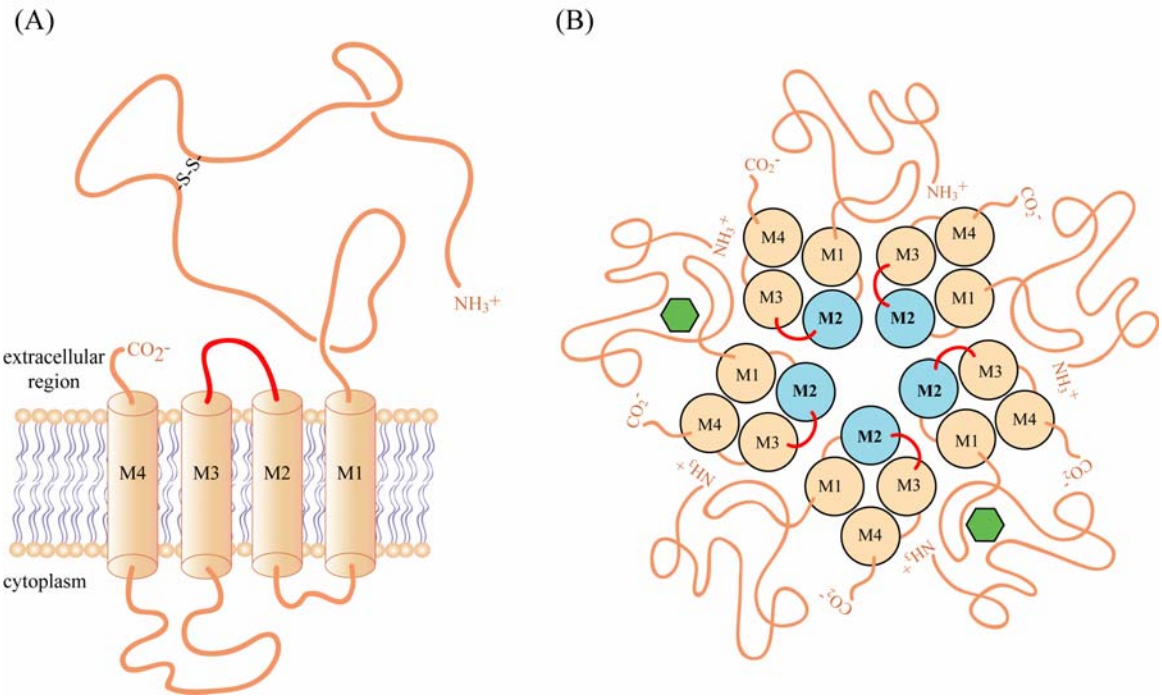

Figure 3.1. A) Schematic for one subunit of a Cys-loop receptor. B) Subunits arrange to form a pentameric array with a central pore lined by the M2 helices.

3.1.3 Gating model for Cys-loop receptors

Given the role of Cys-loop receptors in a variety of neurological processes and as therapeutic targets for numerous pathologies, it is of great interest to gain a greater functional understanding of these channels. Specifically, it is of interest to elucidate the mechanism by which binding of an agonist initiates a series of conformational changes that ultimately results in the opening of an ion channel. The agonist binding site and channel gate are separated by 50 Å and 100 amino acids of the protein's primary sequence; the process of gating represents an elegant feat achieved by a sequence of steric and noncovalent interactions. The amazing nature of this process is further appreciated when one considers the size of an ion channel relative to typical organic molecules. Despite advances in both experimental and theoretical methods, the molecular details of the mechanism of ion channel gating are still poorly understood.

As integral membrane proteins, ion channels have been resistant to crystallographic analysis and as such, there are limited structural data for Cys-loop receptors. The lack of structural data has made it difficult to attribute functional changes in structure-function studies to specific structural changes during gating. In 2001, the crystal structure of the acetylcholine binding protein (AChBP) was obtained. AChBP is a small soluble protein that is homologous to the extracellular N-terminal domain of the nicotinic acetylcholine receptor. Since the discovery of the crystal structure of AChBP, several members of the Cys-loop family have been modeled onto the crystal structure to predict their quaternary structures. The resulting models were consistent with 40 years of biochemical studies that accurately predicted the formation of the ligand-binding domains at the interfaces between subunits.

In 1995, Unwin provided the first evidence of a dynamic structure for a Cys-loop receptor.[50] Using freeze trapping methods and cyro-electron microscopy, 9 Å resolution images were obtained for the nicotinic acetylcholine receptor. The freeze trapping method allowed for images to be created for the open and closed states of the nAChR. From these cryo-electron microscopic data, Unwin proposed a gating model for nAChR and therefore, by extension all ligand-gated ion channels (figure 3.2). In 2003, cyro-electron microscropic images were extended to a resolution of 4 Å.[51, 52]

In Unwin's proposed model, binding of a ligand results in a 15 degree rotation of the α subunits. The rotation of these subunits causes movement of valine 44 of the α-subunit, which resides at the apex of the extracellular β1-β2 loop (loop 2). Valine 44 of the α-subunit makes contact with the M2-M3 loop through a hydrophobic interaction. The model proposes that α-valine 44 docks into a hydrophobic pocket formed by residues serine 269 to proline 272. Movement of α-valine 44, causes movement of the M2-M3 loop resulting in rotation of the M2 helix. This movement destabilizes the hydrophobic "girdle" that forms the gate, thus resulting in a widening of the pore that permits ions to pass.

3.1.4 M2-M3 loop movement in the mechanism of channel gating

In Unwin's "pin-and-socket" model, the M2-M3 loop is proposed to play a major role in channel gating by acting as a direct physical link that enables the propagation of a conformational change at the binding site to the channel gate (figure 3.2). Rotation of the inner sheets of the α-subunit is translated to a rotation of the M2 helix via the M2-M3 loop with the M2-M3 loop acting as a pivot point. Biochemical studies also support a prominent role for the M2-M3 loop in channel gating.[53-65] Substituted cysteine accessibility studies

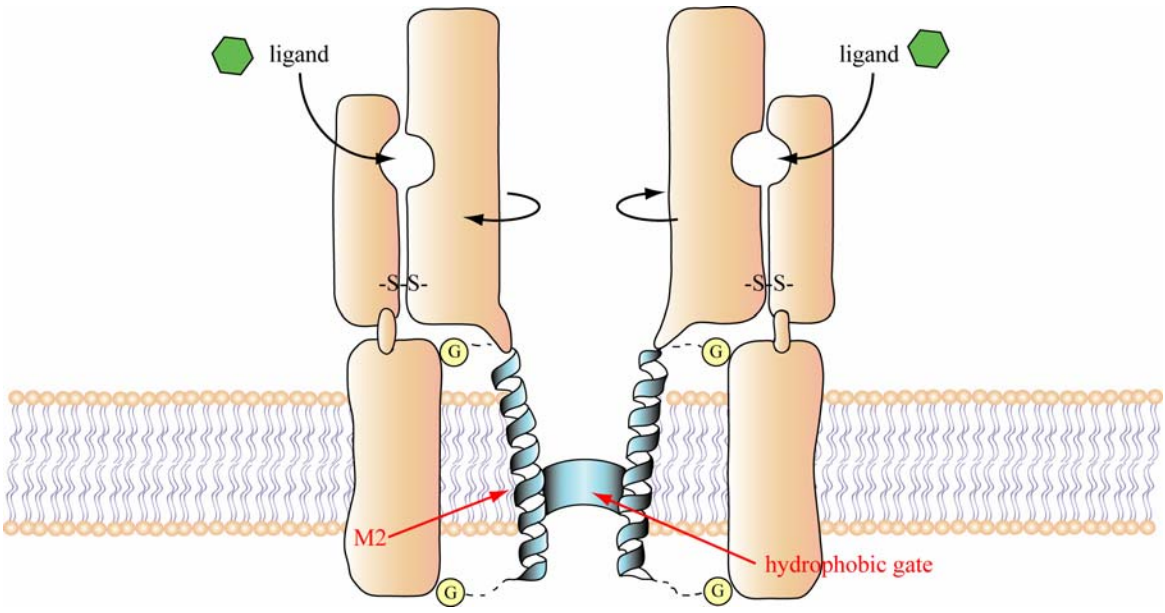

Figure 3.2. Unwin's pin-and-socket mechanism of gating for LGICs.

have suggested that the surface accessibility of the M2-M3 loop increases upon gating in the glycine receptor, implying movement of the M2-M3 loop during gating.[66] Similar studies in the $GABA_A$ receptor yielded similar conclusions.[64] Furthermore, mutational analysis of the glycine receptor and the nAChR supports a model where the M2-M3 loop acts as a coupling between the binding site and the channel gate. Mutations of critical residues in the M2-M3 loop resulted in the decoupling of ligand binding and channel gating.

Additional mutational analysis of the M2-M3 region, using single channel analysis, indicated that the M2-M3 loop in nAChR serves as a linker whose hydrophobicity influences channel gating.[67] Substitution of residues near the middle of the loop in the α-subunit with hydrophobic residues appeared to enhance channel gating whereas hydrophilic mutations showed no apparent effect. Another important result of these studies was that mutations in this region had little effect on the agonist affinity for the opened and closed state but had an

effect on the gating equilibrium. Recently, similar mutational studies done in the M2-M3 loop of a chimeric α7-5-HT_{3A} receptor further supported a functional role for the M2-M3 loop as a control element in gating.[68] Mutational analysis of the chimeric receptor also yielded receptors with altered channel gating without altered agonist binding affinity.

A growing body of evidence suggests a prominent role for the M2-M3 loop during channel gating and recently, biophysical studies have provided evidence for a direct interaction between the M2-M3 loop and the Cys-loop. Kash *et al.* performed mutational analysis in the $GABA_A$ receptor in which two charged residues, one located in the M2-M3 loop and the other in the Cys-loop were reversed.[65] They were able to demonstrate the presence of an electrostatic interaction between a lysine in the M2-M3 loop and an asparagine residue in the Cys-loop. It should be noted that this lysine is not conserved in the nAChR and in the 5-HT_{3A} receptor nor did analogous studies in the glycine receptor yield similar results. However, it is possible that variations exist among receptors in how the M2-M3 loop interacts with the Cys-loop. Furthermore, Unwin's cryo-electron microscopic images and biochemical studies also suggest an interaction of M2-M3 loop with the Cys-loop and the extracellular β1-β2 loop (loop 2). Therefore, it is likely that the interactions with *both* the Cys-loop and β1-β2 loop are important for the coupling of ligand binding to channel gating. Nonetheless, despite the ambiguity for the exact nature of the M2-M3 loop's role in channel gating, results of these studies all support a prominent functional role for it in the gating mechanism.

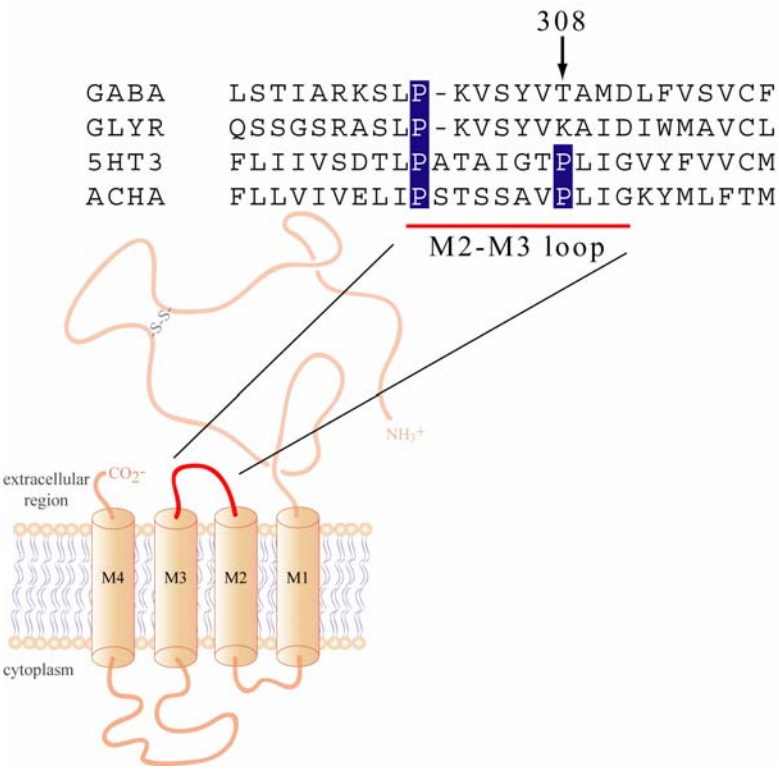

Figure 3.3. M2-M3 loop sequence alignment for the Cys-loop family of ligand gated ion channels.

3.1.5 Conserved prolines in the M2-M3 loop of the cation-selective Cys-loop receptors

Examination of the M2 helix and M2-M3 loop sequences for the Cys-loop receptors reveals two conserved prolines in the cation-selective Cys-loop receptors, the 5-HT_{3A} receptor and the nAChR (figure 3.3). Proline 301 in the 5-HT_{3A} receptor (corresponding to proline 265 in nAChR) is conserved among all Cys-loop receptors and proline 308 (corresponding to proline 272 in nAChR) is conserved among the cation-selective Cys-loop receptors. Proline 301 is located two helical turns below the C-terminal end of the M2 helix. Proline 308 is located near the C-terminal end of the M2 helix and resides in the M2-M3 loop. It is analogous to proline 272 in nAChR which is proposed to form the hydrophobic pocket in which the valine residue of the β1-β2 loops docks. Given the unique role of

proline in biological processes, the conserved prolines may play key roles in the function of M2-M3 loop during channel gating.

3.1.6 Proline in biological processes

Of the twenty natural amino acids, proline is unique in that it lacks a primary amine due to the covalent bonding of the three carbon side chain to the nitrogen atom of the peptide backbone. Therefore proline has no amide hydrogen to act as a hydrogen bond donor. Furthermore, the distinctive five-membered ring, formed by the side-chain forming a covalent bond with the backbone, imparts a greater rigidity on the backbone and restricts the backbone conformation of neighboring amino acids.[69, 70] As a result, proline is considered the classic helix breaker and is used by nature in a variety of irregular structures.[70-72]

Proline is also unique in that it is the only natural amino acid in which the *cis* conformation is readily accessible (figure 3.4). All other peptide bonds occur predominantly in the *trans* conformation due to an energy barrier of approximately 20 kcal/mol between the *trans* and *cis* conformation. This results in a scarcity of *cis* peptide bonds occurring in proteins.[73] However, in the case of the Xaa-Pro peptide bond (where Xaa is any amino acid), the difference in energy between the conformers is only about 0.5 kcal/mol. Thus a survey of the protein data base reveals a significant proportion (about 5-6%) of the Xaa-Pro peptide

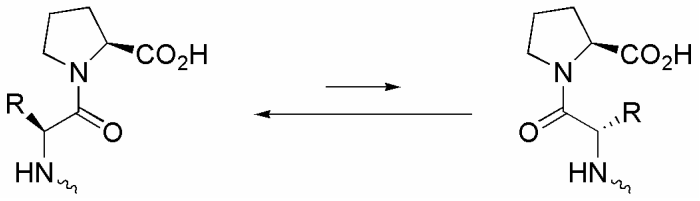

Figure 3.4. Proline is a unique amino acid in that the *cis*-conformation is readily accessible.

bonds adopting the *cis* conformation compared to only 0.03-0.05 percent of Xaa-nonPro peptide bonds occurring in the *cis* conformation.[74-77]

The ability of proline to adopt the *cis* conformation distinguishes it from the other natural amino acids. Proline *cis-trans* isomerization has been implicated in the regulation of biological activity in proteins/peptides containing this amino acid, by acting as a molecular switch.[78] Evidence suggests it also plays a role in protein folding and stability.[79-85] Interestingly, evidence suggests that local structural changes caused by *cis-trans* isomerization are minimal; however there is amplification of these small structural changes through the peptide backbone, allowing for structural changes in areas removed from the immediate proline locale.[86]

A variety of studies highlight the importance of the proline conformation in biological recognition. For example, biochemical assays and structural studies suggested that a *cis* conformation around a tyrosine-proline amide bond is necessary for the biological activity of morphiceptin, a tetrapeptide.[87-89] A *cis* conformation was found to be necessary for the μ-receptor binding and selectivity of morphiceptin. Furthermore, a *cis* conformation has also been shown to be required for the activity of the muscle selective μ-conotoxins GIIIB, which act a blocker of voltage-sensitive sodium channels.[90] A *cis* conformation is also necessary for the interaction of interleukin-3 with its receptor.[91]

Proline *cis-trans* isomerization may also play a role in regulating the agonist/antagonist activity of peptides. Studies by Halab *et al*., suggests that oxytoxin with a *cis* proline acts as an antagonist to its receptor while a *trans*-conformation is critical for agonist activity.[92, 93] Evidence also implicates proline *cis-trans* isomerization in T-cell signaling through conformer-specific recognition of the ligand.[94]

3.2 Experimental design

The research described herein is a continuation of work spearheaded by Dr. Darren L. Beene and done in collaboration with Dr. Sarah C.R. Lummis (Cambridge). It was aimed at studying the role of two conserved prolines in the M2-M3 loop region of the cation selective Cys-loop receptor—the serotonin gated 5-hydroxytryptamine$_{3A}$ receptor (5-HT$_{3A}$) and the nicotinic acetylcholine receptor (nAChR). The *cis-trans* isomerization of proline has been suggested to play a role in biological processes. As such, this research was aimed at studying the role of the *cis-trans* isomerization in the gating of Cys-loop receptors. Using *in vivo* nonsense suppression methodology in *Xenopus* oocytes, a series of proline analogues of

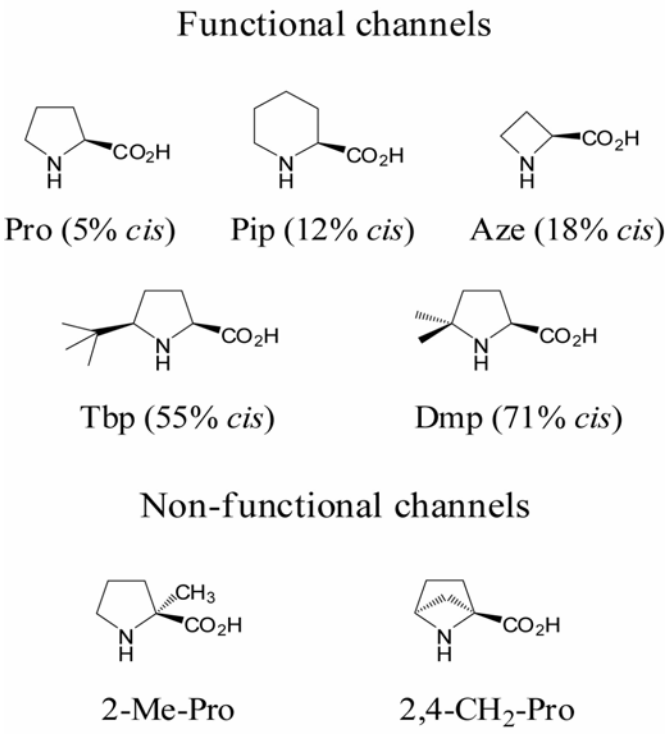

Figure 3.5. Structures of proline analogues that were incorporated into cation selective Cys-loop receptors using nonsense suppression methodology. Proline analogues with a greater *cis* preference than native proline produced functional channels. Percentage *cis* preference is shown in parentheses.

varying *cis* preference were incorporated at the 1* (301) and 8* (308) proline site in the M2-M3 loop of the 5-HT_{3A} receptor (Figure 3.5). The mutant channels were then functionally evaluated using two-electrode voltage clamp electrophysiology. If the *cis-trans* isomerization of either proline plays a role in the gating mechanism of the channel, then we anticipate changes in the gating of the channel with the replacement of the native proline with the synthesized proline analogues. This chapter also describes initial work examining the role of *cis-trans* isomerization at the analogous prolines (265 and 272) in nAChR.

3.3 Results

3.3.1 Introduction

We aimed to examine the role of *cis-trans* isomerization of two conserved proline residues, at site 301 and 308 in the gating of the 5-HT_{3A} receptor. A series of proline analogs were incorporated at these sites to examine the role of these prolines in receptor function. Previous studies done by Dr. Darren L. Beene and Dr. Sarah C. R. Lummis showed that site 301 tolerated a variety of mutations without loss of receptor function. Experimental data strongly suggest that proline 301 is not critical for receptor function in 5-HT_{3A}. Experimental data strongly suggested a critical role for proline 308 in receptor function. Substitution of proline 308 with glycine, alanine, cysteine, valine, lysine or asparagine resulted in receptors that were non-functional but were properly trafficked to the membrane and displayed wild type binding properties for a radiolabeled agonist. This indicated that these mutations affected the gating of the receptor and not ligand binding or assembly of the receptor. These data strongly suggested that an intrinsic characteristic of proline was required for the proper gating of this receptor.

A series of unnatural proline analogs were substituted at site 308 using nonsense suppression in *Xenopus* oocytes, and experimental results suggest it was neither the cyclic nature of proline nor the lack of hydrogen bonding ability that was critical for proper receptor function. However, substitution with 2,4-CH_2-Pro and 2-Me-Pro, which show a reduced *cis* preference relative to proline, produced non-functional receptors although these receptors did reach the cell surface. Furthermore, incorporation of azetidine, pipecolic acid, and 5,5-dimethylproline which have varying *cis* preferences appeared to support a model of gating in which proline 308 serves as a hinge during gating. The research described herein is a continuation of the work done by Dr. Darren L. Beene and Dr. Sarah C. R. Lummis and involves the incorporation of *cis*-5-*tert*-butyl-L-proline, which has a *cis* preference that is between that of Aze and Dmp. As a result a crucial data point that was intermediate between those for pipecolic acid and 5,5-dimethylproline was obtained for a plot of the *cis*-*trans* energy gap versus receptor activation. *Cis*-5-*tert*-butylproline is not commercially available and as such, the continuation of these studies began with the chemical synthesis of *cis*-5-*tert*-butyl-L-proline.

3.3.2 Synthesis of cis-5-tert-butyl-Lproline

The synthesis of *cis*-5-*tert*-butyl-L-proline was achieved using previous reported methods with minor modifications (figure 3.6).[95] Glutamic acid gamma-methyl ester **1** was amino-protected with a phenylfluorenyl protecting group using triethylamine and 9-bromo-9-phenylfluorene.[96] Acylation of the phenylfluorenyl protected glutamic acid gamma-methylester **2** was performed by first generating the enolate using lithium bis(trimethylsilyl)amide (LiHMDS) in tetrahydrofuran. The enolate was subsequently

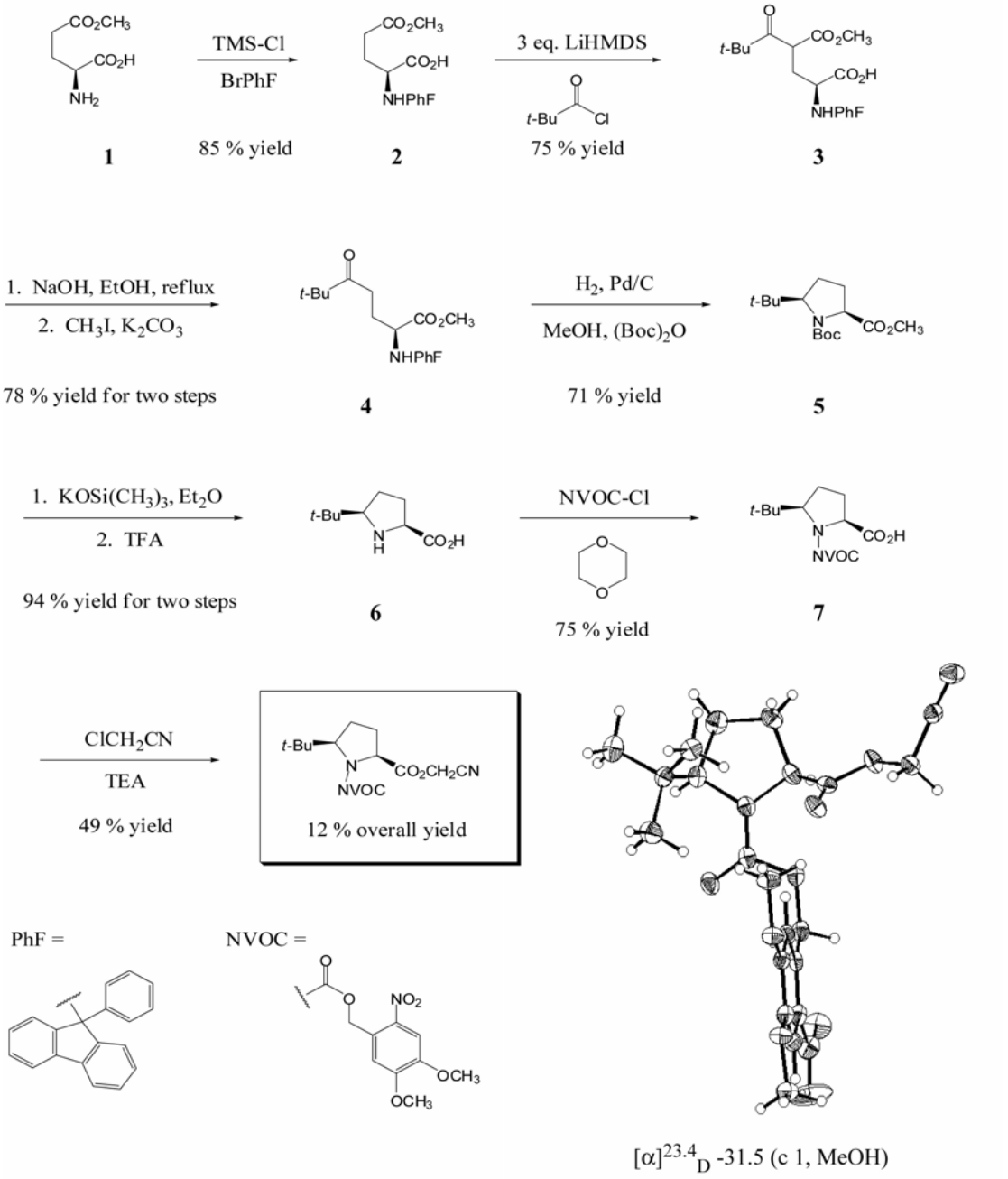

Figure 3.6. Synthesis of *cis*-5-*tert*-butyl-L-proline.

treated with pivaloyl choride to yield the beta-keto ester **3** as a mixture of diastereomers. Hydrolysis and decarboxylation using sodium hydroxide followed by esterification cleanly converted **3** to the heptanoate **4** in a 78% yield for both steps. Treatment of heptanoate **4**

with 10% palladium on carbon in the presence of hydrogen gas results in a three step—one pot reaction. This proceeds by cleavage of the phenylfluorenyl group, cyclization via reductive amination, followed by BOC protection and hydrogen addition to yield the BOC protected *cis*-5-*tert*-butyl-L-proline methyl ester in 71% yield. At this stage the relative stereochemistry was confirmed to be *cis* using polarimetry. Saponification of methyl ester **5** was achieved using potassium trimethylsilanolate in diethyl ether. Removal of the BOC protecting group with trifluoroacetic acid in dichloromethane yielded the free amino acid which was then NVOC-protected and converted to the cyanomethyl ester in preparation for dCA coupling for tRNA ligation. Prior to coupling to dCA, X-ray crystallography and polarimetry were used to establish the stereochemistry of the *tert*-butyl moiety as *cis* relative to the carboxylic acid functionality.

3.3.3 Incorporation of cis-5-tert-butyl-L-proline into Pro 8 of the M2-M3 loop of 5-HT$_{3A}$ receptor using nonsense suppression*

Cis-5-*tert*-butyl-L-proline was incorporated into the 5-HT$_{3A}$ receptor using nonsense suppression methodology. First, c*is*-5-*tert*-butyl-L-proline was chemically coupled to dCA and then enzymatically ligated to tRNA in preparation for use for nonsense suppression. Prior to use, the NVOC-protecting group was photolyzed using an arc lamp. mRNA was translated from DNA encoding for 5-HT$_{3A}$ subunit with the TAG mutation inserted at position 308 (corresponding to the 8* proline in the M2-M3 loop). Subsequently, the charged tRNA bearing c*is*-5-*tert*-butyl-L-proline was co-injected with the corresponding mRNA into *Xenopus* oocytes. The oocytes were then incubated to allow for the processing, assembly and surface transport of the expressed mutant channel.

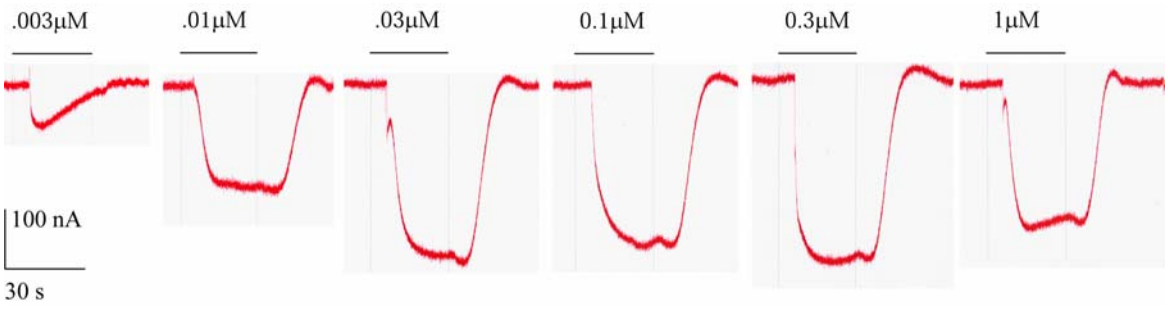

Figure 3.7. Representative traces for mutant 5-HT_{3A} receptors containing Tbp at site 308 (8*). Bars represent application of 5-HT.

3.3.4 Electrophysiological analysis using two voltage clamp electrophysiology

Xenopus oocytes expressing 5-HT_{3A} receptor with *cis*-5-*tert*-butyl-L-proline (Tbp) at site 308 were evaluated using two-electrode voltage clamp electrophysiology. Oocytes were perfused with varying concentrations of serotonin (5-HT) to generate dose-response curves. It should be noted that expression of Tbp mutant receptors was poor relative to that of the wild type recovery receptors in which Pro was inserted using the same nonsense suppression methodology. Expression levels seen for Tbp were roughly 5-10% of that seen for the Pro insertion by the same technique. Diminished expression levels of mutant receptor were previously seen for the other proline analogs (Pip, Aze, and Dmp). For

Residue	Per cent *cis**	EC_{50} (μM)†	$\Delta\Delta G(c\text{-}t)$ (kcal/mol)‡	$\Delta\Delta G(c\text{-}t)$ (kcal/EC_{50})§
Pro	5	1.29 ± 0.07	0	0
Pip	12	0.75 ± 0.06	-0.54	-0.32
Aze	18	0.42 ± 0.03	-0.85	-0.66
Tbp	55	0.030 ± 0.024	-1.86	-1.73
Dmp	71	0.021 ± 0.009	-2.28	-2.47

*Determined from studies of model peptide systems reported previously. Because variations are seen dependingon methodology and exact model system, all values are referenced to the *cis-trans* ratio seen for Pro in the same study, and Pro is set to 5%, the value obtained from statistical surveys of protein structures.
†Values are in ±s.e.m.
‡Values are relative to proline.
§ Equals -RTln(EC_{50}(mutant)/EC_{50}(Pro)).

Table 3.1 Influence of proline isomerism on receptor function.

Tbp traces, the waveforms seen were similar to that seen for the wild type receptor (figure 3.7). The EC_{50} value for 5-HT_{3A} receptor containing Tbp at site 308 was determined to be 0.030 μM ± 0.024, a 40-fold decrease in EC_{50} value compared to the wild type receptor. Table 3.1 shows a summary of EC_{50} values for proline analogs of varying *cis* preference as well as percent *cis* for each analog. The relationship between the *cis-trans* energy gap and that of receptor activation is shown in Figure 3.8. A linear relationship is observed between the the *cis-trans* energy gap and that of receptor activation with a slope of nearly one.

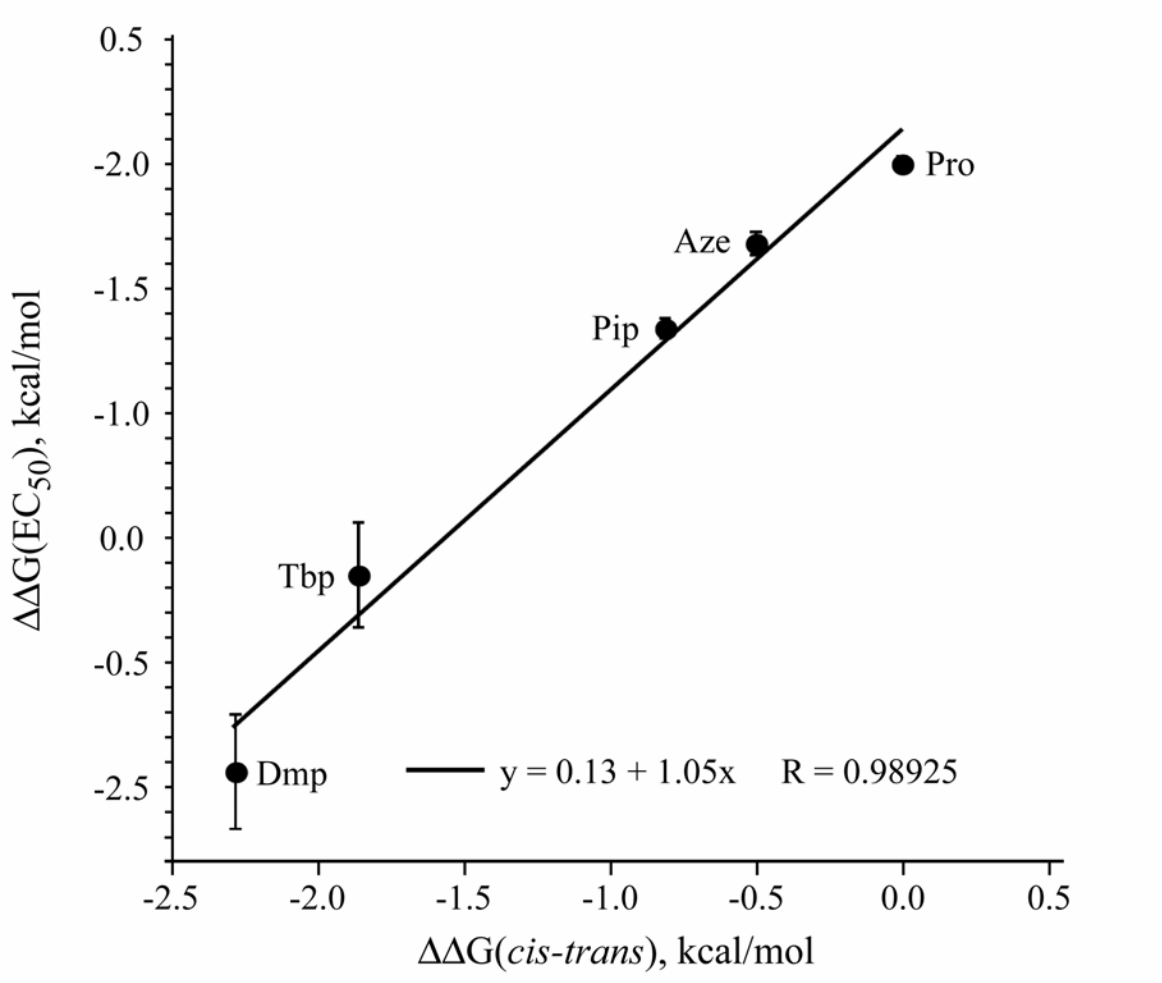

Figure 3.8. Linear free energy correlation between *cis-trans* isomerization and receptor activation.

3.3.5 Schild plot analysis for representative proline analogues in the 5-HT$_{3A}$ receptor

It should be appreciated that our functional analysis produces an EC_{50} value which reflects the combination of binding and gating events. Schild analysis was performed to validate that the changes in EC_{50} values upon substitution of Pro 308 with proline analogs was due to a change in gating and not antagonist binding affinity. Schild plots were generated using the competitive antagonist MDL72222 (figure 3.9(A)) in wild type 5-HT$_{3A}$ and in mutant 5-HT$_{3A}$ channels where Pro 308 was substituted with either pipecolic acid (Pip) or 5,5-dimethyl-L-proline (Dmp). The choice of proline analogs was such that it represents a range of *cis* preference (< 0.1% to 71%). Figure 3.9(B) shows a dose response curve of serotonin, in the presence of increasing concentrations of MDL722222 for the wild type 5-HT$_{3A}$. EC_{50} values (in nM units) determined at each concentration of MDL72222

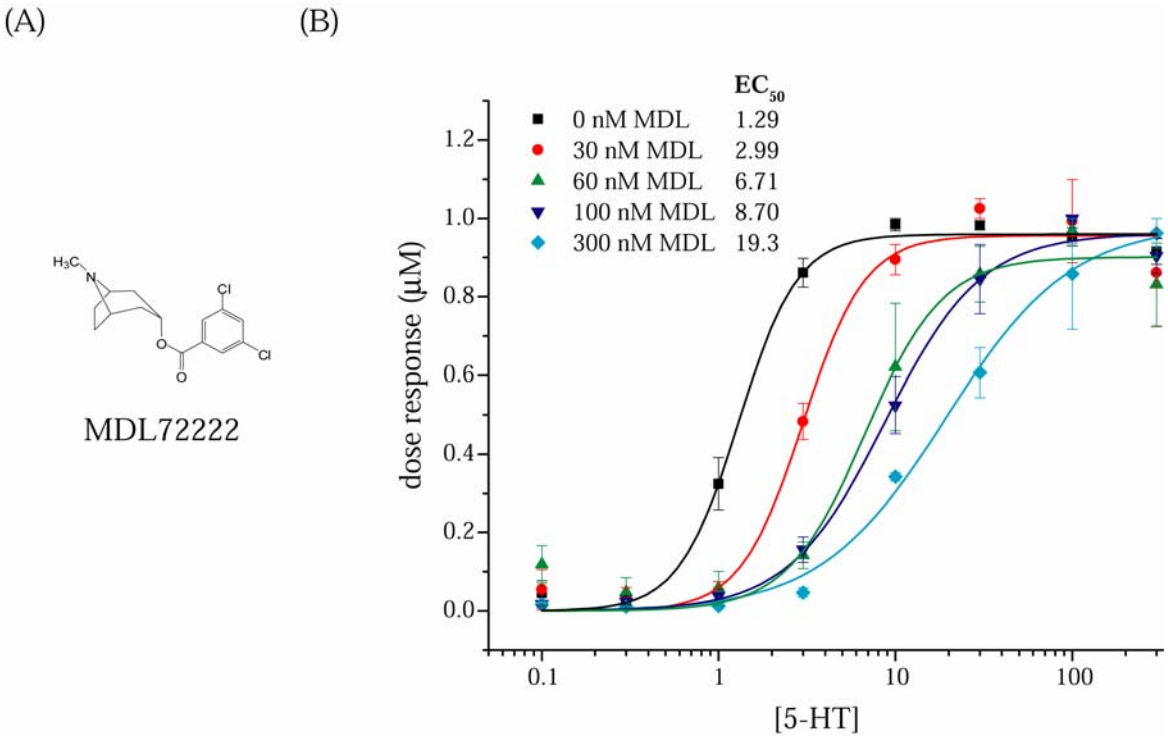

Figure 3.9. (A) Chemical structure of MDL72222, a 5-HT$_{3A}$ receptor antagonist. (B) Dose response curves for wild type 5-HT$_{3A}$ receptor at varying concentrations of MDL72222.

were: 1.29 ± 0.08 (0 nM of MDL72222), 2.99 ± 0.33 (30 nM of MDL72222), 6.70 ± 1.21 (60 nM), 8.69 ± 0.86 (100 nM), and 19.29 ± 2.21 (300 nM). Similar dose response data were generated for receptors containing Pip substituted at Pro 308. EC_{50} values for receptors containing Pip were: 0.64 ± 0.20 (0 nM of MDL72222), 1.07 ± 0.19 (30 nM of MDL72222), 2.59 ± 0.08 (60 nM of MDL72222), 3.18 ± 0.31 (100 nM of MDL72222), and 5.77 ± 1.3 (300 nM of MDL72222).

The dose response data were used to generate Schild plots (figure 3.10), both of which showed slopes not significantly different from 1. Similar K_d values for MDL72222

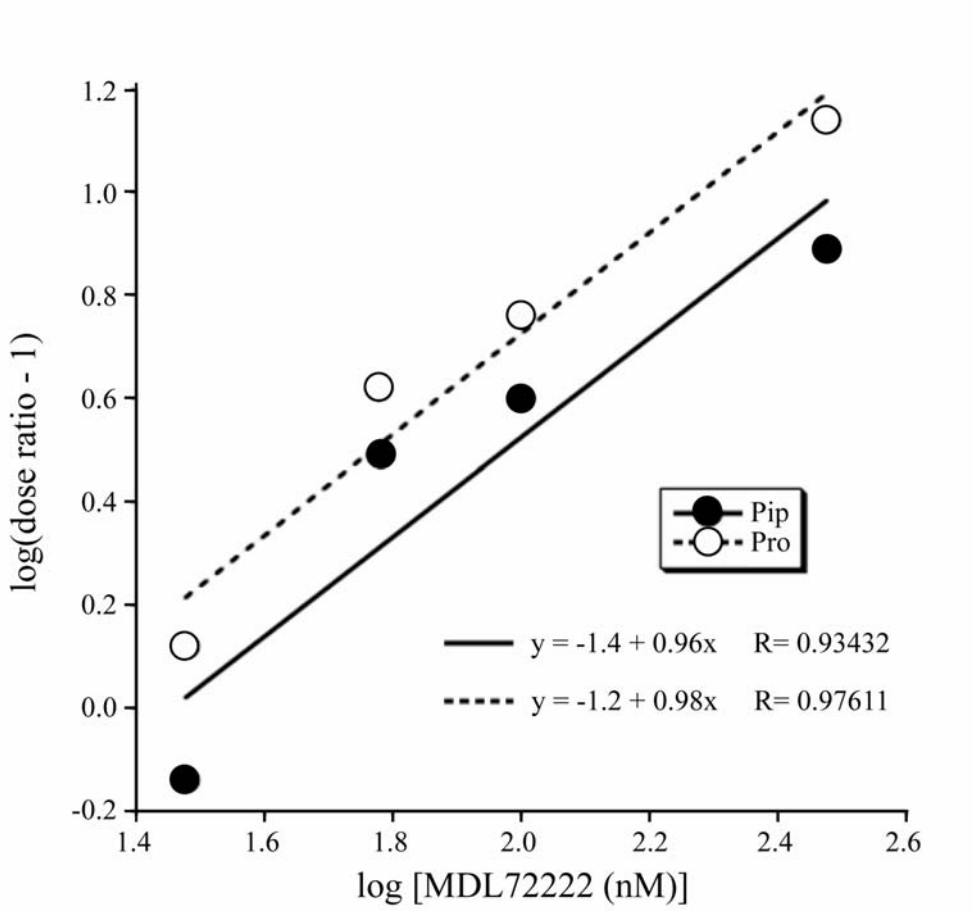

Figure 3.10. Schild Plots for mutant 5-HT_{3A}receptor containing Pip and wild type 5-HT_{3A}receptor.

were obtained for both the wildtype receptor and receptors containing Pip. K_d values were calculated from the *x*-intercepts to be 18.1 nM for the wild type and 28.9 nM for Pip. MDL72222 IC_{50} values were obtained for the wild type receptor, the Pip containing receptor, and the Dmp containing receptor at their respective EC_{50} values (obtained with serotonin). MDL72222 IC_{50} values determined for the wild type and Pip containing receptors were similar to the obtained MDL72222 K_d values. The MDL72222 IC_{50} values were determined to be 25.9 nM for the wild type receptor and 20.6 nM for the Pip containing channel. The determined IC_{50} value for Dmp, at its EC_{50} value, was also similar to that of the wild type and was determined to be 44.7 nM. The plot of the pIC_{50} at the respective EC_{50}, against the –log (EC_{50}) showed a slope that does not deviate significantly from zero (figure 3.11).

3.3.6 Electrophysiological analysis for substitution of at site 265 and site 272 of the alpha subunit of the nicotinic acetylcholine receptor

Conventional mutagenesis was used to generate mutants in which the proline at either site 265 or site 272 of the alpha subunit of the nicotinic acetylcholine receptor was substituted to glycine, alanine or valine. Sites 265 and 272 are analogous to proline 301 and 308, respectively of the 5-HT_{3A} receptor. Corresponding messenger RNA was transcribed and subsequently injected into *Xenopus* oocytes for functional analysis using two-electrode voltage clamp electrophysiology. Conventional mutants were used initially to determine if either proline is necessary to produce functional channels.

Interestingly, substitutions at site 265 in the alpha subunit of the nicotinic acetylcholine receptor were not tolerated and none of the three mutant receptors showed channel activity. This result was unanticipated since the analogous site in the 5-HT_{3A}

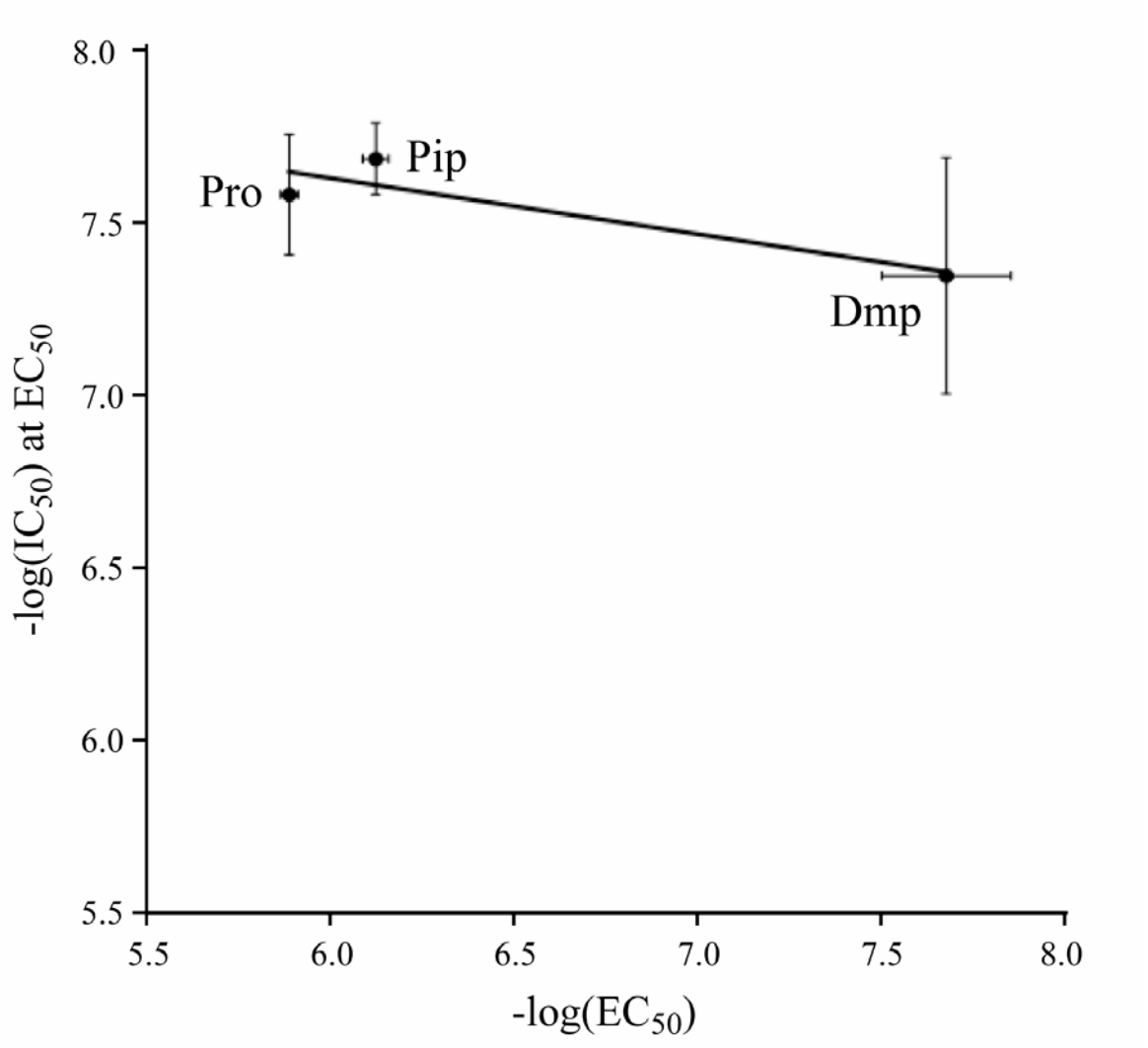

Figure 3.11. pIC50 values (at the respective EC50) plotted against –log (EC_{50}) for Schild Plot for wild type 5-HT_{3A}receptor and mutant 5-HT_{3A}receptors containing Pip or Dmp.

receptor (Pro 301) was shown to be promiscuous and a variety of substitutions produced functional receptors. Conversely, substitutions at site 272 (analogous to Pro 308 of the 5-HT_{3A} receptor) appear to be well tolerated. EC_{50} values for the alanine and glycine mutant receptors showed no significant difference from that obtained for the wild type receptor.

3.4 Discussion

3.4.1 Cis-trans isomerization of Proline 308 in the gating of 5-HT$_{3A}$ receptor

A series of proline analogs were substituted at site 308 of the 5-HT$_{3A}$ receptor using nonsense suppression methodology in a *Xenopus* oocyte expression system. Functional analysis was performed using two-electrode voltage clamp electrophysiology. Analogs that had a reduced *cis* preference relative to proline, namely 2,4-CH$_2$-Pro and 2-Me-Pro, produced receptors that were transported to the cell surface, but were nonfunctional. C-4F-Pro and t-4F-Pro, which show similar intrinsic *cis-trans* preferences to proline, produced EC$_{50}$ values similar to that of the wild-type receptor.

Analysis of EC$_{50}$ values obtained for proline analogs with a range of *cis-trans* preferences strongly supports a role for *cis-trans* isomerization of proline 308 in the gating of the 5-HT$_{3A}$ receptor. A linear free energy relationship was observed between the intrinsic *cis-trans* energy gap of the proline analog and activation of the receptor. Because EC$_{50}$ values represent a combination of ligand binding and gating events, Schild analysis was performed to establish that substitutions at site 308 affected gating and not ligand binding affinity. Experimental results from Schild analysis using the competitive antagonist MDL72222 indicate that substitution with amino acids with a range of *cis* preferences does not perturb the binding site. We therefore conclude that the changes in EC$_{50}$ values, upon substitution at site 308, are due to changes in receptor gating, not binding. Specifically, our experimental data strongly suggest a link between the *cis-trans* isomerization at site 308 (Pro 8*) and the gating of the 5-HT$_{3A}$ receptor.

From these data, we propose a model of gating for the 5-HT$_{3A}$ receptor (figure 3.12). In the closed state of the channel, proline 308 is in the *trans* conformation. Upon ligand

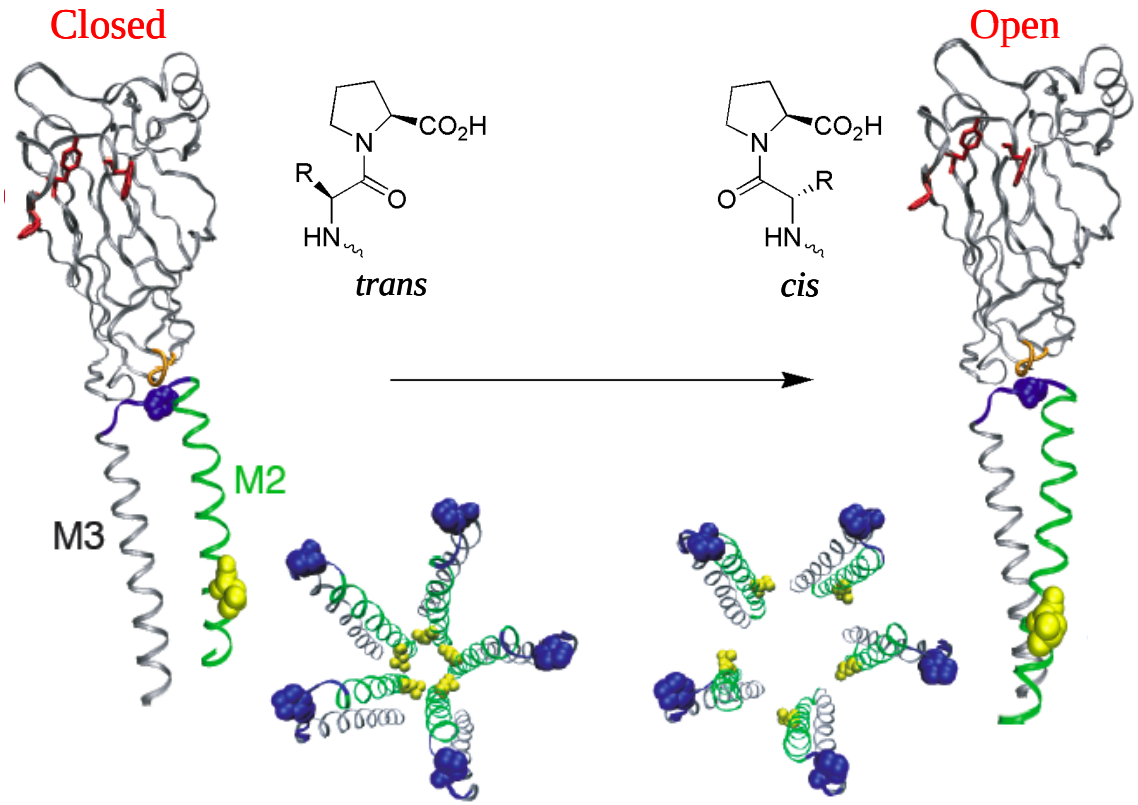

Figure 3.12. Proposed model for the gating mechanism of the 5-HT_{3A} receptor.

binding, a series of conformational changes occurs that results in the isomerization of proline 308 to the *cis* conformation. Proline 308 serves as a hinge point in the M2-M3 loop; isomerization to the *cis* conformation causes a reorientation of the M2 transmembrane helix which opens the channel. Proline 308 is positioned at the apex of the M2-M3 loop and is in close proximity to the extracellular β1-β2 loop and the Cys-loop (loops 2 and 7, respectively). As such, it may serve as the link between the ligand binding site and the channel gate. Previous models have proposed that loops 2 and 7 conformationally restrict the M2 helix in the closed state. We expand on this model by proposing that loop 2 and 7 act as "calipers" to hold proline 308 in the *trans* conformation in the closed state. Ligand binding

results in the movement of tryptophan 183, a key tryptophan in the binding site; this movement is propagated such that it releases the clamp on proline 308, which can then undergo *cis-trans* isomerization, gating the channel.

We recognize that the time scale of gating for the 5-HT_{3A} receptor is on the order 10-100 s^{-1} while the intrinsic rate for the *cis-trans* isomerization of proline has been reported to be roughly ten times slower. This timescale difference can be reconciled if we consider the possibility that structural features of the receptor may accelerate the isomerization rate. Proline *cis-trans* isomerization is widely accepted as the rate limiting step in protein folding, and these processes can be significantly accelerated by protein prolyl isomerases. Furthermore, it has been demonstrated that a hydrogen bond to the proline amide nitrogen can accelerate the isomerization rate roughly 260-fold. Therefore, it is possible that the 5-HT_{3A} receptor utilizes structural features to accelerate the isomerization of proline 308.

3.4.2 Studies of proline 1 and 8* of the alpha subunit of nAChR*

We extended our studies to the nicotinic acetylcholine receptor to examine if the *cis-trans* isomerization of the analogous proline plays a role in channel gating. Functional analysis of mutant receptors of Proline 265 (Pro 1*), in the alpha subunit of the nicotinic acetylcholine receptor, containing glycine, alanine or valine suggested that mutations at this site are not tolerated. None of the mutant receptors showed channel activity. These results are in contrast to those found with substitutions at the analogous proline site (site 301) in the 5-HT_{3A} receptor, which appeared to be well tolerated.

Replacement of proline 272, which is analogous to proline 265 in the 5-HT_{3A} receptor, with glycine or alanine produced receptors that showed channel activity similar to

wild type activity (data not shown). EC_{50} values for the mutant receptors did not deviate significantly from that obtained for the wild type receptor. This was an unanticipated result since comparable mutations in the analogous site in the 5-HT_{3A} receptor produced non-functional channels. Our initial results suggest that proline 272 of the nicotinic acetylcholine receptor does not play a significant role in channel gating. This is interesting because it suggests that these channels have evolved to utilize different mechanisms of gating despite being highly homologous and being members of the same superfamily. This work was done in the muscle type nicotinic receptor which exhibits faster kinetics than that of the neuronal subtype receptor, which may account for the differences in experimental observations. Similar studies in a neuronal subtype of the nicotinic acetylcholine receptor are now underway.

3.5 Conclusions

A series of proline analgues, of varying *cis* preference were incorporated at proline 308 in the M2-M3 loop of the 5-HT_{3A} receptor to examine the possible role of *cis-trans* isomerization in the gating of the channel. *In vivo* nonsense suppression methodology was used to incorporate these proline analogs in a *Xenopus* oocyte expression system. Electrophysiological analysis of the mutant channels was used to generate dose-response curves and determine an EC_{50} for each mutant channel. Data show a linear relationship between the *cis* preference of the proline analog and the EC_{50} of the mutant channel—suggesting that proline 308 may serve as a hinge during the gating 5-HT_{3A}. Schild plots were generated to validate that the shifts in EC_{50} were due to changes in channel gating and not

changes in agonist binding affinity. From these data, we proposed a model of gating for the 5-HT_{3A} receptor.

Initial studies were also done on the analogous prolines in the nicotinic acetylcholine receptor to examine if these prolines are critical for channel function. Conventional mutagenesis was performed on prolines 265 and 272 to generate glycine, valine and alanine mutants. Mutations of proline 272 (analogous to proline 308 in 5-HT_{3A}R) of the alpha subunit of nAChR produced functional channels. Furthermore, incorporation of Aze and Pip using nonsense suppression at proline 272 yielded EC_{50} values on the same order of magnitude as wildtype channels. Interestingly, mutations at proline 265 of nAChR were not tolerated and yielded no channel activity. Proline 301 of 5-HT_{3A} was previously shown to tolerate mutations. Our initial data suggest that while proline 8* is involved in gating of 5-HT_{3A} receptors, it does not play the same role in nAChR; however, proline 1* in the alpha subunit of nAChR may play a critical role in gating although the equivalent proline does not appear to play a role in 5-HT_{3A} gating. These data are interesting because they suggest that these two channels have evolved to utilize different gating mechanisms despite being highly homologous and part of the same superfamily. The observed difference may also be due to the kinetics of the muscle type nAChR since the initial studies were done in the mouse muscle type receptor. To address this issue, these studies are being continued by Joanne Xiu in a neuronal nACh receptor.

3.6 Experimental method and materials

3.6.1 General synthetic information

Unless otherwise stated, all reactions were performed in flame-dried glassware under an atmosphere of nitrogen gas or argon gas. Reagents were obtained from commercial sources and used as received. Thin-layer chromatography (TLC) was performed using E. Merck silica gel 60 F254 precoated plates (0.25 mm). Visualization of the developed chromatogram was performed by fluorescence quenching, cerium ammonium molybdate stain, ninhydrin stain, or basic potassium permanganate stain. Chromatography (flash) was performed using ICN Silica gel (0.032-0.063 mm) or Fluka alumina oxide type 507 C neutral (0.05-0.15 mm). ^{1}H-NMR and ^{13}C-NMR were recorded on a Varian Mercury 300 (300 MHz for ^{1}H-NMR and 74.5 MHz for ^{13}C-NMR) at room temperature. Infrared (IR) spectra were obtained using a Perkin Elmer Paragon spectrometer and are reported in terms of frequency of absorption (cm^{-1}). UV (vis) spectra were recorded on a Unikon Spectrophotometer 930 and are reported in terms of wavelength of maximum absorbance (λ_{max}). Mass spectra were obtained from the Protein/Peptide MicroAnalytical Laboratory at the California Institute of Technology, Pasadena, California.

3.6.2 Synthesis of (2S,5R)-5-tert-Butylproline

*3.6.2.1 N-(9-(9-Phenylfluorenyl))glutamic Acid γ-Methyl Ester (**2**)*

To a suspension of glutamic acid γ-methyl ester **1** (4.06 g, 25.2 mmol) in freshly distilled chloroform (50.4 mL) was added chlorotrimethylsilane (TMS-Cl) (2.88 g, 3.36 mL) via syringe at room temperature. The reaction mixture was heated at reflux for 2 h. and cooled to room temperature. Freshly distilled triethylamine (7.39 mL) was added followed

by lead nitrate (5.01 g, 15.13 mmol) and 9-bromo-9-phenylfluorene (9.71 g, 30.23 mmol) in chloroform (50.4 mL). The resulting mixture was stirred for 87 h. at room temperature, after which dry methanol (16.8 mL) was added and the reaction was stirred for another 15 minutes. The solution was filtered by vacuum filtration and the filtrate was concentrated *in vacuo*. The resulting residue was dissolved in 5% citric acid (84 mL) and extracted three times with ethyl acetate (3 x 84 mL). The combined organic layers were dried with anhydrous sodium sulfate (granular), filtered and concentrated *in vacuo*. Column chromatography on silica gel (gradient 1:1 EtOAc: Hexanes to 2:1 EtOAc: Hexanes) yielded a yellow residue (85 % yield). ^{1}H NMR (300 MHz, $CDCl_3$) δ = 1.58-1.81 (2H, m), 2.31 (2H, t, J = 6.9), 2.56 (1H, dd, J = 4.8, J = 7.5), 3.58 (3H, s), 6.00 (1H, bs), 7.10-7.61 (13H, m). ^{13}C NMR (300 MHz, $CDCl_3$) δ = 28.11, 30.49, 52.07, 55.55, 73.05, 74.06, 120.30, 120.42, 125.34, 126.17, 126.29, 127.76, 128.05, 128.33, 128.73, 128.99, 129.14, 140.59, 141.20, 143.66, 147.44, 151.08, 159.78, 174.61, 177.98. MS Calcd for $C_{25}H_{23}NO_4$ = 401.16. Found: (ESI^+) 402.2 $[M + H]^+$, 424.0 $[M + Na]^+$

*3.6.2.2 (2S, 4RS)-6,6-dimethyl-5-oxo-4-[(methyloxy)carbonyl]-2-[(N-(PhF)amino] hepantoic acid (**3**)*

To a -78 °C solution of 1 M lithium bis(trimethylsilyl)amide (12.35 mL), is added dropwise **2** (1.5 g, 3.74 mmol) dissolved in dry tetrahydrofuran (THF) (4.78 mL) that has been cooled to -78 °C. The reaction mixture is stirred at -78 °C for 2 h. to generate the enolate. To the enolate is added dropwise a -78 ºC solution of trimethylacetylchloride (pivaloyl chloride) (1.29 mL) in dry tetrahydrofuran (THF) (0.875mL). The reaction mixture is stirred at -78 ºC for 1 h, after which 1 M sodium dihydrogen phosphate (NaH_2PO_4) is

added. The reaction is allowed to come to room temperature with stirring. The reaction is then extracted with ethyl acetate (4 x 7.3 mL), and the combined organic layers are washed with cold water (3 x 2.9 mL) and brine (2 x 4.35 mL), dried with anhydrous sodium sulfate (granular), filtered and concentrated *in vacuo* to yield an orange residue (75% yield). The residue is used without further purification in the next reaction.

3.6.2.3 (2S)-6,6-dimethyl-5-oxo-2-[N-(PhF)amino heptanoic acid

Crude β-keto ester **3** (diastereomers, 1.36 g, 2.81 mmol scale) from the previous reaction was dissolved in 200 proof ethanol (18.2 mL) and treated with 2N NaOH (18.2 mL) and stirred under reflux for 48 h. The reaction was cooled to room temperature and the pH was adjusted to 5 using 10% aqueous HCl. The solution was extracted with ethyl acetate (three times), dried with anhydrous sodium sulfate (granular), filtered, and concentrated *in vacuo* to yield a light yellow residue. The product did not require further purification and was used in the next reaction. ^{1}H NMR (300 MHz, $CDCl_3$) δ = 1.12 (9H, s), 1.61-184 (2H, m), 2.51 (2H, m), 2.61 (1H, dd, *J* = 5.1, *J* = 6.6), 7.23-7.73 (13H, m). MS Calcd for $C_{28}H_{29}NO_3$ = 427.53. Found: (ESI^+) 428.2 $[M + H]^+$.

*3.6.2.4 (2S)-methyl 6,6-dimethyl-5-oxo-2-[N-(PhF)amino heptanoic acid (**4**)*

Crude acid (2S)-6,6-dimethyl-5-oxo-2-[N-(PhF)amino heptanoic acid (from previous reaction) was dissolved in dry acetonitrile (2.77 mL) and to that was added K_2CO_3 (0.947 g, and methyl iodide (0.728 mL) and stirred at room temperature for 19 h. Brine was added to the reaction mixture and then the reaction mixture was extracted with ethyl acetate (3 x 15 mL). The combined organic phases were washed with 0.65M sodium thiosulfate (29.1 mL)

and then brine. It was then dried with anhydrous sodium sulfate (granular), filtered and concentrated *in vacuo*. Column chromatography on silica gel (1:9 ethyl acetate:hexanes) yielded a white powder (78% for two steps). ^{1}H NMR (300 MHz, $CDCl_3$) δ = 1.11 (9H, s), 1.62 (2H, m), 2.31 (1H, ddd, *J* = 6.0, *J* = 9.3, *J* = 18), 2.53 (1H, dd, *J* = 5.4, *J* = 7.5), 2.72 (1H, ddd, *J* = 5.7, *J* = 9.5, *J* = 18), 3.00 (1H, bs), 3.27 (3H, s), 7.16 – 7.70 (13H, m). ^{13}C NMR (300 MHz, $CDCl_3$) δ = 14.41, 26.75, 29.31, 33.29, 44.21, 51.74, 55.21, 120.11, 120.26, 125.50, 126.25, 126.47, 127.46, 127.53, 127.96, 128.52, 128.59, 140.33, 141.31, 144.63, 148.75, 149.28, 176.77. MS Calcd for $C_{29}H_{31}NO_3$ = 441.56. Found: (ESI^+) 442.2 $[M + H]^+$, 464.0 $[M + Na]^+$, 480.0 $[M + K]^+$.

*3.6.2.5 (2S,5R)-N-(BOC)-5-tert-Butylproline Methyl Ester (**5**)*

A solution of **4** (1.30 g, 2.94 mmol) and di-*tert*-butyldicarbonate (1.77 g, 8.11 mmol) in anhydrous methanol (89.4 mL) was treated with 10% palladium-on-carbon (239.6 mg) and stirred under 4 atm (58 psi) of hydrogen using a par hydrogenator for 48 h. The mixture was filtered through Celite and washed with methanol and the filtrate was concentrated *in vacuo*. Column chromatography on silica (0 to 25% EtOAc in Hexanes) yielded a white crystalline solid (71% yield). ^{1}H NMR (300 MHz, $CDCl_3$) δ = 0.95 (9H, s), 1.43 (9H, s), 1.95 (3H, m), 2.27 (1H, m), 3.70 (3H, s), 3.77 (1H, d, *J* = 8.1), 4.27 (1H, m). ^{13}C NMR (300 MHz, $CDCl_3$) δ = 26.85, 27.63, 28.43, 29.82, 36.55, 52.00, 61.70, 66.82, 80.13, 155.90, 173.70. MS Calcd for $C_{15}H_{27}NO_4$ = 285.38. Found: (ESI^+) 286.2 $[M + H]^+$, 308.1 $[M + Na]^+$, 324.1 $[M + K]^+$ $[\alpha]^{23.4}_D$ -31.5 (*c* 1, MeOH).

3.6.2.6 (2S,5R)-N-(BOC)-5-tert-Butylproline (6)

Methyl ester *cis*-**5** (187 mg, 0.655 mmol) was dissolved in diethyl ether (4.6 mL) and treated with potassium trimethylsilanolate ($KOSiMe_3$) (93.5 mg, 0.729 mmol) and stirred at room temperature for 22 h after which another portion of potassium trimethylsilanolate (93.5 mg, 0.729 mmol) was added and the reaction was stirred for another 2 h. The reaction was concentrated *in vacuo* and the residue was redissolved in 5% citric acid (40 mL). The solution was extracted with ethyl acetate (3 x 25 mL). The combined organic layers were washed with brine, dried with anhydrous sodium sulfate (granular), filtered and concentrated *in vacuo* to yield the desired product (quant. yield). No further purification was necessary. ^{1}H NMR (300 MHz, $CDCl_3$) δ = 0.95 (9H, s), 1.43 (9H, s), 1.95 (3H, m), 2.28 (1H, m), 3.78 (1H, d, *J* = 7.8), 4.28 (1H, m). ^{13}C NMR (300 MHz, CD_3OD) δ = 27.71, 28.12, 28.71, 30.80, 37.38, 62.81, 68.32, 81.44, 158.00, 176.86. MS Calcd for $C_{14}H_{25}NO_4$ = 271.35. Found: (ESI$^+$) 272.1 $[M + H]^+$, 294.0 $[M + Na]^+$, 310.0 $[M + K]^+$, 316.0 $[M + 2Na - H]^+$, 332.0 $[M + K + Na - H]^+$.

*3.6.2.7 (2S,5R)-5-tert-Butylproline (**6**)*

A solution of (2S,5R)-N-(BOC)-5-*tert*-Butylproline **6** (189.58 mg, 0.699 mmol) in anhydrous CH_2Cl_2 (20 mL) was treated with trifluoroacetic acid (1 mL) and stirred at room temperature for 12 h. The reaction was concentrated *in vacuo* to yield (2S,5R)-5-*tert*-Butylproline trifluoroacetate salt. No purification was necessary and material was used in next reaction as is. ^{1}H NMR (300 MHz, $CDCl_3$) TFA salt δ = 1.08 (9H, s), 1.65 (1H, m), 2.05 (1H, m), 2.41 (2H, m), 3.52 (1H, m), 4.38 (1H, bs), 6.51 (1H, bs), 10.66 (1H, bs). ^{13}C NMR (300 MHz, $CDCl_3$) δ = 25.28, 26.16, 29.29, 32.27, 59.25, 72.40, 172.79. MS Calcd for $C_9H_{17}NO_2$ = 171.24. Found: (ESI$^+$) 172.0 $[M + H]^+$, 194.0 $[M + Na]^+$.

*3.6.2.8 (2S,5R)-N-(NVOC)-5-tert-Butylproline (**8**)*

(2S,5R)-5-*tert*-Butylproline **7** (53.7 mg, 0.314 mmol) was added to 10% sodium carbonate (1.20 mL). Another equivalent of Na_2CO_3 (120 mg) was added to account for the TFA. To this was added dioxane (0.91 mL) and the reaction was cooled to 0 ºC (ice bath). NVOC-Cl (90.9 mg, 0.330 mmol) was added slowly to the reaction at 0 ºC. The reaction mixture was removed from the ice bath and allowed to warm to room temperature and stirred at room temperature for 4 h. Subsequently, the reaction was poured over water then washed with diethyl ether (3 x). The aqueous layer was acidified to pH 2 with 6 N HCl. Upon acidification, the aqueous layer becomes opaque as product begins to precipitate. The aqueous layer is extracted with methylene chloride (3 x or until the aqueous layer is no longer orange). The combined organic layers were dried with anhydrous sodium sulfate (granular), filtered and concentrated *in vacuo* to yield an orange residue (75% yield). No further purification was necessary and residue was used in next reaction.

*3.6.2.9 (2S,5R)-N-(NVOC)-5-tert-Butylproline Cyano-Methyl Ester (**9**)*

(2S,5R)-N-(NVOC)-5-*tert*-Butylproline **8** (128.9 mg, 0.314 mmol) was dissolved in anhydrous chloroacetonitrile (1.19 g, 15.7 mmol, 0.993 mL) and to that was added freshly distilled triethylamine (95.4 mg, 0.942 mmol, 0.131 mL). The reaction was stirred at room temperature until reaction was complete as monitored by thin layer chromatography. The reaction was concentrated *in vacuo* to yield an orange residue. Column chromatography on silica gel (1:2 Ethyl acetate: Hexanes) yielded the desired product (49% yield). ^{1}H NMR (600 MHz, $CDCl_3$, 22 ºC) δ = 0.91 (9H, s), 1.93 (2H, m), 2.01 (1H, m), 2.36 (1H, m), 3.91

(3H, s), 3.92 (1H, m), 4.03 (3H, s), 4.50 (1H, t, *J* = 9, 9.6), 4.76 (2H, abx pattern*, *J* = 16.2, 15.6), 5.52 (2H, ab pattern, *J* = 15.3), 7.00 (1H, s), 7.68 (1H, s). ^{13}C NMR (300 MHz, $CDCl_3$) δ = 26.60, 27.45, 29.89, 36.51, 48.94, 56.52, 56.96, 60.81, 64.61, 67.99, 108.27, 109.69, 110.89, 114.19, 128.92, 139.32, 148.09, 154.18, 155.95, 171.86. MS Calcd for $C_9H_{17}NO_2$ = 449.45. Found: (ESI$^+$) 472.0 $[M + Na]^+$, 487.8 $[M + K]^+$.

*at -10 ºC: 4.745 (2H, abx, J_{AB} = 25.2, J_{BX} = 15.6, J_{AB} = 22.8, J_{AX} = 15.6)

CALIFORNIA INSTITUTE OF TECHNOLOGY

BECKMAN INSTITUTE

X-RAY CRYSTALLOGRAPHY LABORATORY

Date 15 December 2004

Crystal Structure Analysis of:

LWL01

(shown below)

For Investigator: Lori Lee ext. 6009

Advisor: D. A. Dougherty ext. 6089

Account Number: DAD.00007-1-NIH.000076

By Michael W. Day 116 Beckman ext. 2734

e-mail: mikeday@caltech.edu

Contents

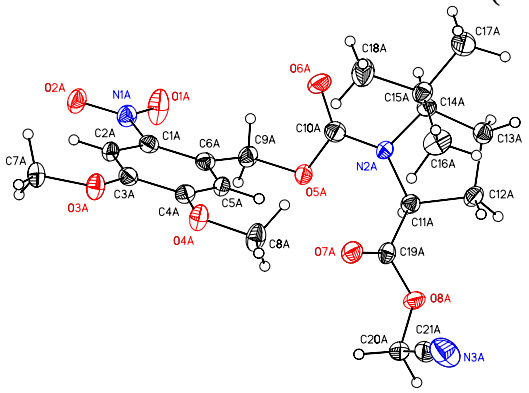

LWL01

Note: The crystallographic data have been deposited in the Cambridge Database (CCDC) and has been placed on hold pending further instructions from me. The deposition number is 258350. Ideally the CCDC would like the publication to contain a footnote of the type: "Crystallographic data have been deposited at the CCDC, 12 Union Road,

Cambridge CB2 1EZ, UK and copies can be obtained on request, free of charge, by quoting the publication citation and the deposition number 258350."

Table 3.2. Crystal data and structure refinement for LWL01 (CCDC 258350).

Empirical formula	$C_{21}H_{27}N_3O_8$
Formula weight	449.46
Crystallization Solvent	Ethylacetate
Crystal Habit	Block
Crystal size	0.30 x 0.28 x 0.26 mm^3
Crystal color	Yellow
Data Collection	
Type of diffractometer	Bruker SMART 1000
Wavelength	0.71073 Å MoKα
Data Collection Temperature	100(2) K
θ range for 12341 reflections used in lattice determination	2.24 to 27.04°
Unit cell dimensions	a = 8.6423(8) Å b = 26.431(2) Å β= 96.1050(10)° c = 9.7211(8) Å
Volume	2208.0(3) $Å^3$
Z	4
Crystal system	Monoclinic
Space group	$P2_1$
Density (calculated)	1.352 Mg/m^3
F(000)	952
Data collection program	Bruker SMART v5.630
θ range for data collection	1.54 to 28.46°
Completeness to θ = 28.46°	93.4 %
Index ranges	$-10 \le h \le 11$, $-34 \le k \le 35$, $-12 \le l \le 12$
Data collection scan type	ω scans at 5 ϕ settings
Data reduction program	Bruker SAINT v6.45A
Reflections collected	31693
Independent reflections	10131 [R_{int}= 0.0550]
Absorption coefficient	0.105 mm^{-1}
Absorption correction	None
Max. and min. transmission	0.9733 and 0.9693

Table 3.2 (cont.)

Structure solution and Refinement

Structure solution program	SHELXS-97 (Sheldrick, 1990)
Primary solution method	Direct methods
Secondary solution method	Difference Fourier map
Hydrogen placement	Difference Fourier map
Structure refinement program	SHELXL-97 (Sheldrick, 1997)
Refinement method	Full matrix least-squares on F^2
Data / restraints / parameters	10131 / 1 / 793
Treatment of hydrogen atoms	Unrestrained
Goodness-of-fit on F^2	1.101
Final R indices [$I>2\sigma(I)$, 7697 reflections]	R1 = 0.0373, *w*R2 = 0.0536
R indices (all data)	R1 = 0.0566, *w*R2 = 0.0564
Type of weighting scheme used	Sigma
Weighting scheme used	$w=1/\sigma^2(Fo^2)$
Max shift/error	0.002
Average shift/error	0.000
Absolute structure parameter	0.4(5) Can not be reliably determined for light atom structures.
Largest diff. peak and hole	0.185 and -0.179 e.Å^{-3}

Special Refinement Details

Refinement of F^2 against ALL reflections. The weighted R-factor (*w*R) and goodness of fit (S) are based on F^2, conventional R-factors (R) are based on F, with F set to zero for negative F^2. The threshold expression of $F^2 > 2\sigma(F^2)$ is used only for calculating R-factors(gt) etc. and is not relevant to the choice of reflections for refinement. R-factors based on F^2 are statistically about twice as large as those based on F, and R-factors based on ALL data will be even larger.

All esds (except the esd in the dihedral angle between two l.s. planes) are estimated using the full covariance matrix. The cell esds are taken into account individually in the estimation of esds in distances, angles and torsion angles; correlations between esds in cell parameters are only used when they are defined by crystal symmetry. An approximate (isotropic) treatment of cell esds is used for estimating esds involving l.s. planes.

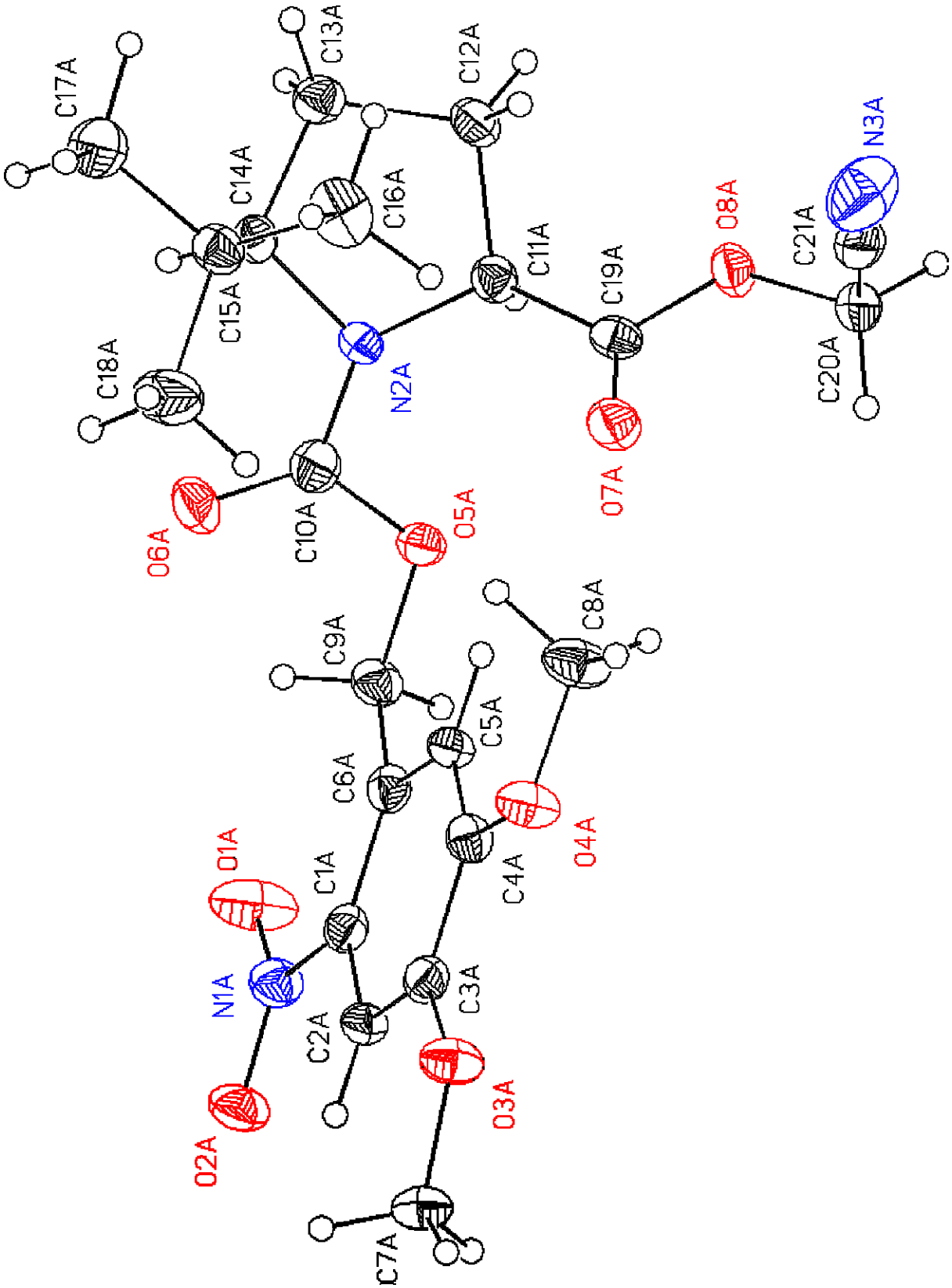
C17A
C13A
C12A
C14A
C16A
N3A
O8A
C21A
C15A
C11A
C19A
C18A
N2A
C20A
O6A
C10A
O5A
O7A
C9A
C8A
C5A
C6A
O1A
C1A
C4A
O4A
N1A
C2A
C3A
O2A
O3A
C7A

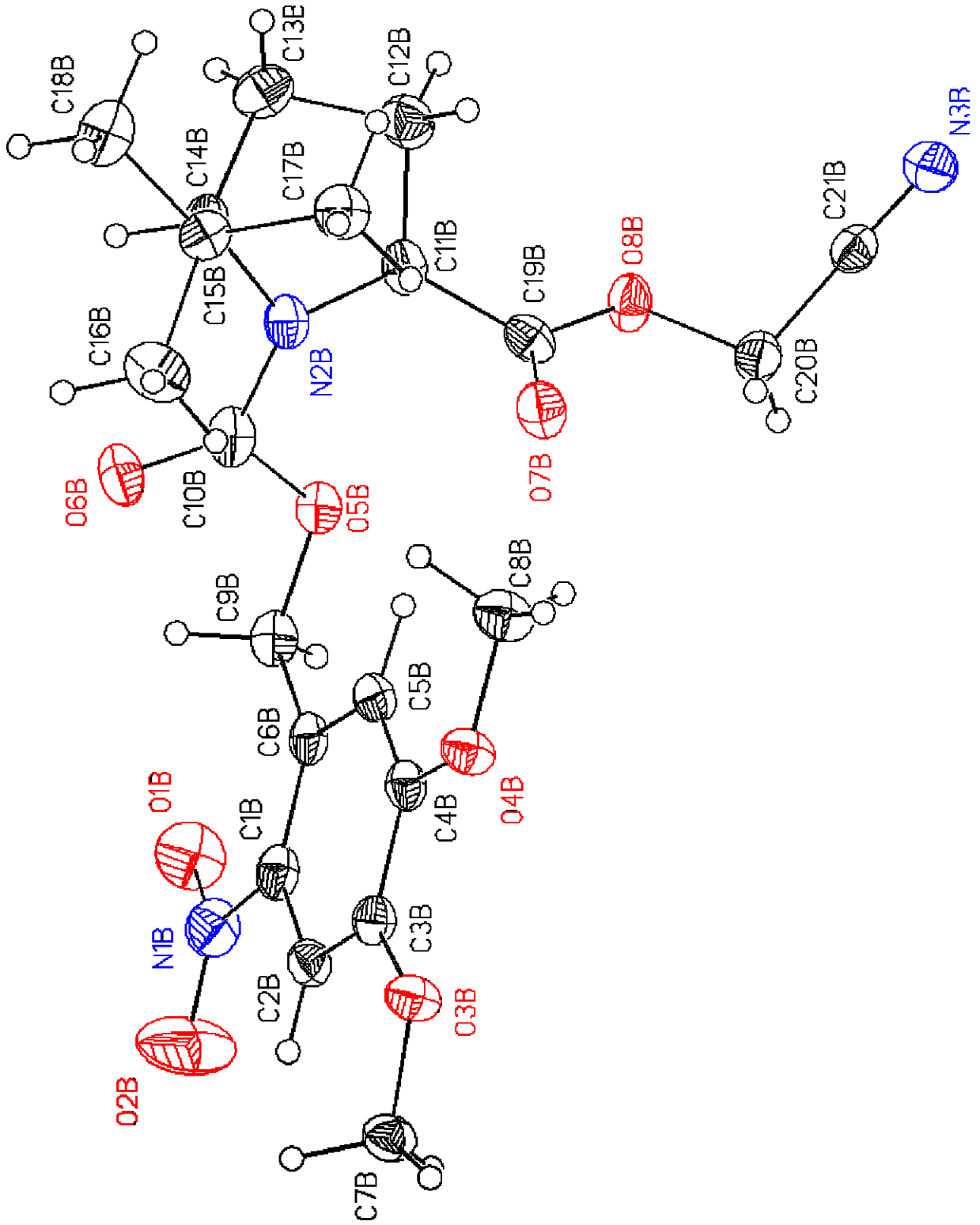
C18B
C13B
C12B
C14B
C17B
C11B
C15B
C19B
O8B
C21B
N3B
C16B
N2B
C20B
O6B
C10B
O5B
O7B
C8B
C9B
C5B
C6B
O1B
C1B
C4B
O4B
N1B
C3B
C2B
O3B
O2B
C7B

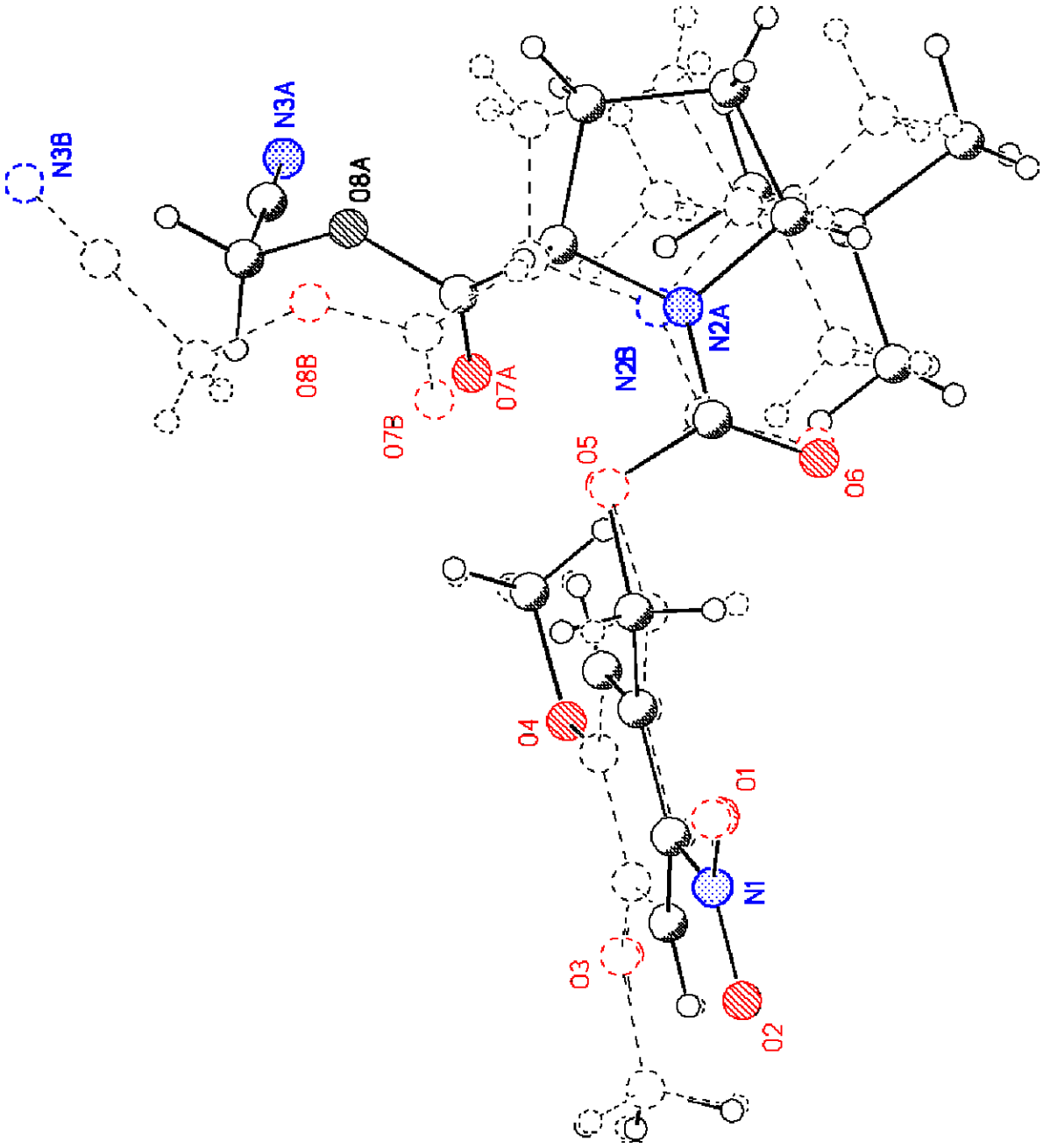
N3B
N3A
O8A
O8B
O7B
O7A
N2B
N2A
O5
O6
O4
O1
N1
O3
O2

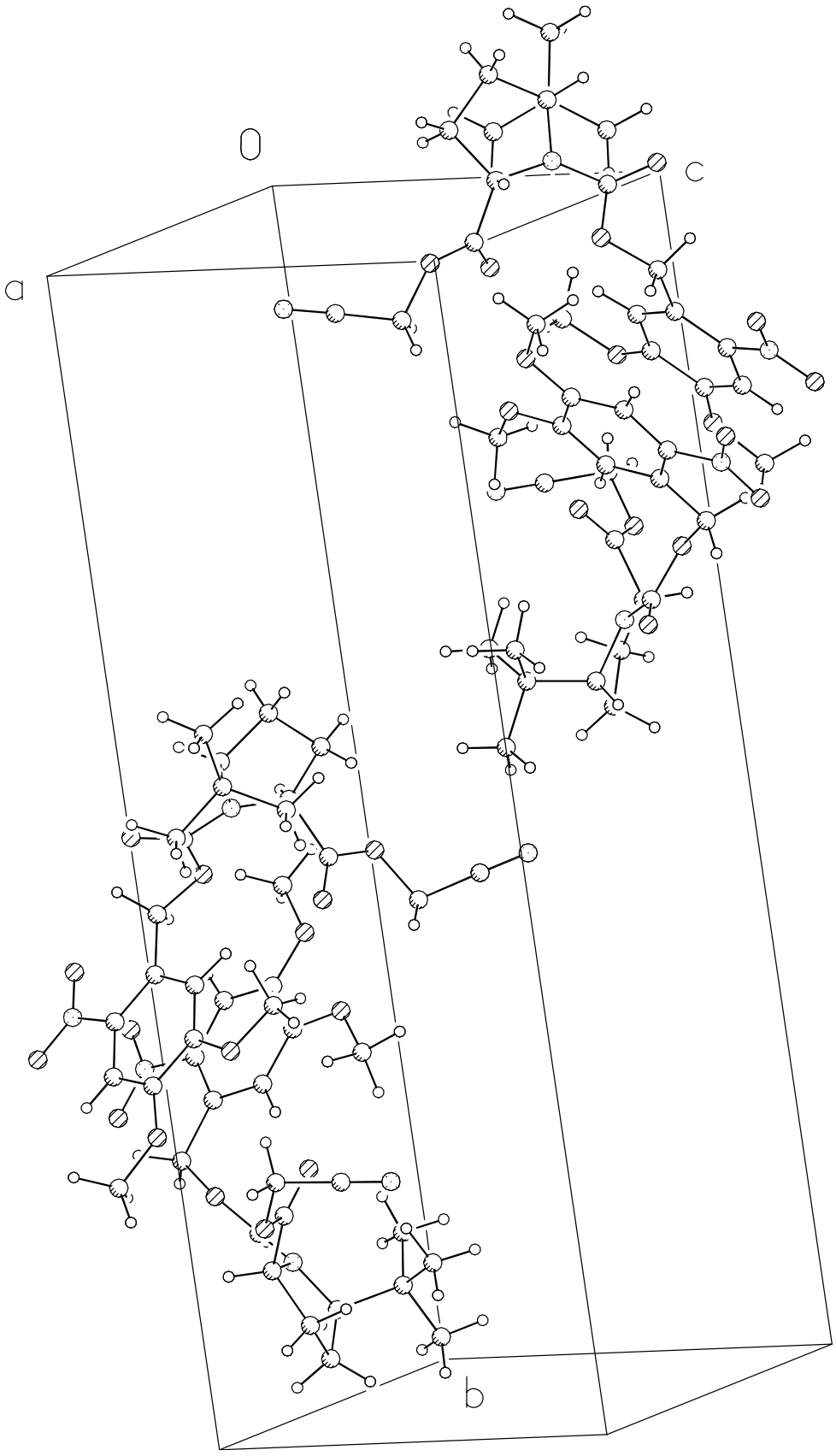
O
C
a
b

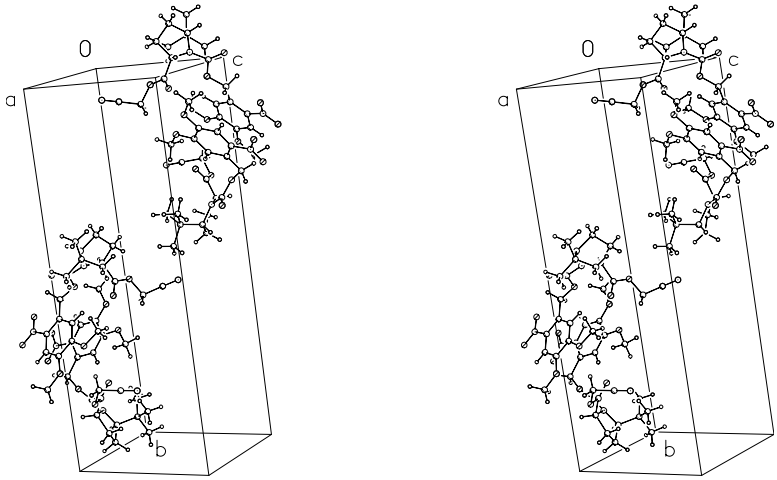
0
c
a
b
0
c
a
b

Table 3.3. Atomic coordinates (x 10^4) and equivalent isotropic displacement parameters ($Å^2$x 10^3) for LWL01 (CCDC 258350). U(eq) is defined as the trace of the orthogonalized U^{ij} tensor.

	x	y	z	U_{eq}
O(1A)	4696(2)	2483(1)	14230(1)	43(1)
O(2A)	6229(2)	1843(1)	14509(1)	31(1)
O(3A)	6527(2)	1098(1)	9861(1)	28(1)
O(4A)	4806(2)	1655(1)	8172(1)	28(1)
O(5A)	2405(1)	3022(1)	10632(1)	22(1)
O(6A)	4504(2)	3534(1)	10757(1)	36(1)
O(7A)	1379(2)	2747(1)	7496(1)	29(1)
O(8A)	-1036(1)	3073(1)	7370(1)	24(1)
N(1A)	5348(2)	2121(1)	13762(2)	25(1)
N(2A)	2583(2)	3616(1)	8993(1)	21(1)
N(3A)	-897(2)	2725(1)	4040(2)	50(1)
C(1A)	5116(2)	2018(1)	12283(2)	21(1)
C(2A)	5937(2)	1605(1)	11827(2)	21(1)
C(3A)	5811(2)	1490(1)	10439(2)	22(1)
C(4A)	4852(2)	1793(1)	9505(2)	21(1)
C(5A)	4049(2)	2196(1)	9991(2)	20(1)
C(6A)	4146(2)	2322(1)	11386(2)	20(1)
C(7A)	7386(3)	750(1)	10778(2)	28(1)
C(8A)	3820(3)	1945(1)	7183(2)	32(1)
C(9A)	3180(2)	2762(1)	11829(2)	24(1)
C(10A)	3267(2)	3406(1)	10174(2)	26(1)
C(11A)	919(2)	3566(1)	8532(2)	21(1)
C(12A)	560(2)	4016(1)	7542(2)	25(1)
C(13A)	1857(2)	4395(1)	7938(2)	24(1)
C(14A)	3288(2)	4079(1)	8461(2)	23(1)
C(15A)	4460(2)	3975(1)	7398(2)	25(1)
C(16A)	3680(3)	3743(1)	6074(2)	36(1)
C(17A)	5215(3)	4478(1)	7079(3)	35(1)
C(18A)	5748(3)	3618(1)	8005(3)	40(1)
C(19A)	512(2)	3076(1)	7771(2)	22(1)
C(20A)	-1614(3)	2645(1)	6559(2)	26(1)
C(21A)	-1201(2)	2691(1)	5135(2)	30(1)
O(1B)	7075(2)	6109(1)	-3713(1)	43(1)
O(2B)	8512(2)	6739(1)	-4103(2)	69(1)
O(3B)	11317(1)	7245(1)	387(1)	27(1)
O(4B)	10593(1)	6587(1)	2149(1)	25(1)
O(5B)	6898(1)	5335(1)	-150(1)	24(1)
O(6B)	8956(2)	4858(1)	-603(1)	31(1)
O(7B)	7178(2)	5569(1)	2991(1)	29(1)

O(8B)	4667(1)	5341(1)	2977(1)	28(1)
N(1B)	8061(2)	6424(1)	-3326(2)	32(1)
N(2B)	7731(2)	4726(1)	1332(2)	24(1)
N(3B)	2749(2)	5548(1)	5735(2)	36(1)
C(1B)	8687(2)	6432(1)	-1873(2)	24(1)
C(2B)	9725(2)	6827(1)	-1481(2)	25(1)
C(3B)	10325(2)	6874(1)	-136(2)	22(1)
C(4B)	9911(2)	6517(1)	837(2)	21(1)
C(5B)	8882(2)	6133(1)	432(2)	22(1)
C(6B)	8240(2)	6076(1)	-940(2)	22(1)
C(7B)	11695(3)	7632(1)	-556(2)	28(1)
C(8B)	10226(3)	6240(1)	3197(2)	29(1)
C(9B)	7139(2)	5642(1)	-1335(2)	25(1)
C(10B)	7953(2)	4959(1)	130(2)	26(1)
C(11B)	6272(2)	4772(1)	1955(2)	25(1)
C(12B)	6293(3)	4334(1)	2986(2)	32(1)
C(13B)	7443(3)	3953(1)	2469(2)	32(1)
C(14B)	8628(2)	4268(1)	1780(2)	25(1)
C(15B)	10175(2)	4373(1)	2686(2)	25(1)
C(16B)	11216(3)	4723(1)	1943(2)	35(1)
C(17B)	9912(3)	4610(1)	4072(2)	30(1)
C(18B)	11013(3)	3863(1)	2910(2)	34(1)
C(19B)	6143(2)	5280(1)	2673(2)	24(1)
C(20B)	4380(3)	5795(1)	3740(2)	28(1)
C(21B)	3462(2)	5651(1)	4858(2)	25(1)

Table 3.4. Bond lengths [Å] and angles [°] for LWL01 (CCDC 258350).

O(1A)-N(1A)	1.2222(19)	C(15A)-C(16A)	1.517(3)
O(2A)-N(1A)	1.2370(18)	C(15A)-C(17A)	1.528(3)
O(3A)-C(3A)	1.359(2)	C(15A)-C(18A)	1.529(3)
O(3A)-C(7A)	1.432(2)	C(16A)-H(16A)	0.981(19)
O(4A)-C(4A)	1.3439(19)	C(16A)-H(16B)	0.98(2)
O(4A)-C(8A)	1.436(2)	C(16A)-H(16C)	1.07(2)
O(5A)-C(10A)	1.362(2)	C(17A)-H(17A)	1.004(19)
O(5A)-C(9A)	1.452(2)	C(17A)-H(17B)	0.99(2)
O(6A)-C(10A)	1.204(2)	C(17A)-H(17C)	1.05(2)
O(7A)-C(19A)	1.195(2)	C(18A)-H(18A)	0.94(2)
O(8A)-C(19A)	1.353(2)	C(18A)-H(18B)	0.98(2)
O(8A)-C(20A)	1.438(2)	C(18A)-H(18C)	0.99(2)
N(1A)-C(1A)	1.456(2)	C(20A)-C(21A)	1.471(3)
N(2A)-C(10A)	1.353(2)	C(20A)-H(20A)	0.99(2)
N(2A)-C(11A)	1.466(2)	C(20A)-H(20B)	0.97(2)
N(2A)-C(14A)	1.486(2)	O(1B)-N(1B)	1.222(2)
N(3A)-C(21A)	1.128(2)	O(2B)-N(1B)	1.216(2)
C(1A)-C(6A)	1.397(2)	O(3B)-C(3B)	1.364(2)
C(1A)-C(2A)	1.400(2)	O(3B)-C(7B)	1.435(2)
C(2A)-C(3A)	1.376(3)	O(4B)-C(4B)	1.360(2)
C(2A)-H(2A)	0.924(17)	O(4B)-C(8B)	1.432(2)
C(3A)-C(4A)	1.412(2)	O(5B)-C(10B)	1.357(2)
C(4A)-C(5A)	1.380(2)	O(5B)-C(9B)	1.442(2)
C(5A)-C(6A)	1.390(2)	O(6B)-C(10B)	1.209(2)
C(5A)-H(5A)	0.933(18)	O(7B)-C(19B)	1.193(2)
C(6A)-C(9A)	1.519(3)	O(8B)-C(19B)	1.349(2)
C(7A)-H(7A)	1.01(2)	O(8B)-C(20B)	1.448(2)
C(7A)-H(7B)	0.96(2)	N(1B)-C(1B)	1.458(2)
C(7A)-H(7C)	1.010(19)	N(2B)-C(10B)	1.352(2)
C(8A)-H(8A)	1.04(2)	N(2B)-C(11B)	1.461(2)
C(8A)-H(8B)	1.03(2)	N(2B)-C(14B)	1.479(2)
C(8A)-H(8C)	1.012(18)	N(3B)-C(21B)	1.137(2)
C(9A)-H(9A)	1.023(17)	C(1B)-C(6B)	1.389(3)
C(9A)-H(9B)	0.955(16)	C(1B)-C(2B)	1.403(3)
C(11A)-C(19A)	1.514(3)	C(2B)-C(3B)	1.360(2)
C(11A)-C(12A)	1.542(3)	C(2B)-H(2B)	0.923(15)
C(11A)-H(11A)	0.961(15)	C(3B)-C(4B)	1.410(2)
C(12A)-C(13A)	1.521(3)	C(4B)-C(5B)	1.379(2)
C(12A)-H(12A)	1.006(17)	C(5B)-C(6B)	1.397(2)
C(12A)-H(12B)	0.972(18)	C(5B)-H(5B)	0.983(15)
C(13A)-C(14A)	1.532(3)	C(6B)-C(9B)	1.515(3)
C(13A)-H(13A)	1.003(18)	C(7B)-H(7D)	1.042(19)
C(13A)-H(13B)	1.008(19)	C(7B)-H(7E)	0.945(19)
C(14A)-C(15A)	1.547(3)	C(7B)-H(7F)	1.012(19)
C(14A)-H(14A)	1.007(15)	C(8B)-H(8D)	0.976(18)

C(8B)-H(8E)	1.043(19)
C(8B)-H(8F)	0.969(19)
C(9B)-H(9C)	0.903(17)
C(9B)-H(9D)	0.998(17)
C(11B)-C(19B)	1.523(3)
C(11B)-C(12B)	1.529(3)
C(11B)-H(11B)	0.998(16)
C(12B)-C(13B)	1.536(3)
C(12B)-H(12C)	1.003(19)
C(12B)-H(12D)	1.00(2)
C(13B)-C(14B)	1.528(3)
C(13B)-H(13C)	0.955(19)
C(13B)-H(13D)	0.974(19)
C(14B)-C(15B)	1.546(2)
C(14B)-H(14B)	0.969(15)
C(15B)-C(16B)	1.524(3)
C(15B)-C(17B)	1.525(3)
C(15B)-C(18B)	1.534(3)
C(16B)-H(16D)	0.99(2)
C(16B)-H(16E)	1.03(2)
C(16B)-H(16F)	0.97(2)
C(17B)-H(17D)	1.034(19)
C(17B)-H(17E)	0.972(19)
C(17B)-H(17F)	0.99(2)
C(18B)-H(18D)	1.02(2)
C(18B)-H(18E)	1.01(2)
C(18B)-H(18F)	0.929(18)
C(20B)-C(21B)	1.463(3)
C(20B)-H(20C)	1.009(17)
C(20B)-H(20D)	0.929(18)

C(3A)-O(3A)-C(7A)	117.47(14)
C(4A)-O(4A)-C(8A)	117.07(14)
C(10A)-O(5A)-C(9A)	113.15(14)
C(19A)-O(8A)-C(20A)	115.89(14)
O(1A)-N(1A)-O(2A)	121.68(15)
O(1A)-N(1A)-C(1A)	119.54(15)
O(2A)-N(1A)-C(1A)	118.76(15)
C(10A)-N(2A)-C(11A)	123.26(15)
C(10A)-N(2A)-C(14A)	118.35(14)
C(11A)-N(2A)-C(14A)	113.13(14)
C(6A)-C(1A)-C(2A)	122.79(16)
C(6A)-C(1A)-N(1A)	121.31(15)
C(2A)-C(1A)-N(1A)	115.89(16)
C(3A)-C(2A)-C(1A)	119.51(18)
C(3A)-C(2A)-H(2A)	124.4(10)
C(1A)-C(2A)-H(2A)	116.1(10)
O(3A)-C(3A)-C(2A)	125.56(17)
O(3A)-C(3A)-C(4A)	115.44(15)
C(2A)-C(3A)-C(4A)	119.00(17)
O(4A)-C(4A)-C(5A)	125.16(16)
O(4A)-C(4A)-C(3A)	114.87(15)
C(5A)-C(4A)-C(3A)	119.97(16)
C(4A)-C(5A)-C(6A)	122.62(17)
C(4A)-C(5A)-H(5A)	120.1(11)
C(6A)-C(5A)-H(5A)	117.2(11)
C(5A)-C(6A)-C(1A)	116.11(16)
C(5A)-C(6A)-C(9A)	118.85(15)
C(1A)-C(6A)-C(9A)	125.02(15)
O(3A)-C(7A)-H(7A)	107.0(11)
O(3A)-C(7A)-H(7B)	112.0(12)
H(7A)-C(7A)-H(7B)	112.5(16)
O(3A)-C(7A)-H(7C)	113.2(10)
H(7A)-C(7A)-H(7C)	108.5(14)
H(7B)-C(7A)-H(7C)	103.8(15)
O(4A)-C(8A)-H(8A)	106.2(10)
O(4A)-C(8A)-H(8B)	111.7(11)
H(8A)-C(8A)-H(8B)	105.6(15)
O(4A)-C(8A)-H(8C)	110.1(10)
H(8A)-C(8A)-H(8C)	113.5(15)
H(8B)-C(8A)-H(8C)	109.7(15)
O(5A)-C(9A)-C(6A)	110.80(14)
O(5A)-C(9A)-H(9A)	105.5(9)
C(6A)-C(9A)-H(9A)	111.7(9)
O(5A)-C(9A)-H(9B)	108.7(9)
C(6A)-C(9A)-H(9B)	110.3(10)
H(9A)-C(9A)-H(9B)	109.7(13)
O(6A)-C(10A)-N(2A)	124.79(17)
O(6A)-C(10A)-O(5A)	123.02(17)
N(2A)-C(10A)-O(5A)	112.18(16)
N(2A)-C(11A)-C(19A)	113.30(15)
N(2A)-C(11A)-C(12A)	104.27(15)
C(19A)-C(11A)-C(12A)	109.55(14)
N(2A)-C(11A)-H(11A)	110.3(9)
C(19A)-C(11A)-H(11A)	105.2(9)
C(12A)-C(11A)-H(11A)	114.5(9)
C(13A)-C(12A)-C(11A)	104.85(15)
C(13A)-C(12A)-H(12A)	112.4(10)
C(11A)-C(12A)-H(12A)	108.2(10)
C(13A)-C(12A)-H(12B)	114.1(10)
C(11A)-C(12A)-H(12B)	112.2(10)
H(12A)-C(12A)-H(12B)	105.0(13)

C(12A)-C(13A)-C(14A)	105.86(16)	C(3B)-O(3B)-C(7B)	116.86(14)
C(12A)-C(13A)-H(13A)	111.7(10)	C(4B)-O(4B)-C(8B)	118.23(14)
C(14A)-C(13A)-H(13A)	112.0(10)	C(10B)-O(5B)-C(9B)	114.93(15)
C(12A)-C(13A)-H(13B)	108.9(11)	C(19B)-O(8B)-C(20B)	115.40(14)
C(14A)-C(13A)-H(13B)	108.2(11)	O(2B)-N(1B)-O(1B)	122.31(16)
H(13A)-C(13A)-H(13B)	110.0(14)	O(2B)-N(1B)-C(1B)	118.76(17)
N(2A)-C(14A)-C(13A)	102.60(15)	O(1B)-N(1B)-C(1B)	118.91(17)
N(2A)-C(14A)-C(15A)	113.98(15)	C(10B)-N(2B)-C(11B)	121.96(15)
C(13A)-C(14A)-C(15A)	116.00(15)	C(10B)-N(2B)-C(14B)	120.59(15)
N(2A)-C(14A)-H(14A)	105.7(8)	C(11B)-N(2B)-C(14B)	113.22(15)
C(13A)-C(14A)-H(14A)	110.2(8)	C(6B)-C(1B)-C(2B)	122.72(16)
C(15A)-C(14A)-H(14A)	107.9(8)	C(6B)-C(1B)-N(1B)	121.46(17)
C(16A)-C(15A)-C(17A)	109.93(17)	C(2B)-C(1B)-N(1B)	115.79(17)
C(16A)-C(15A)-C(18A)	108.58(19)	C(3B)-C(2B)-C(1B)	119.78(18)
C(17A)-C(15A)-C(18A)	107.81(17)	C(3B)-C(2B)-H(2B)	118.8(10)
C(16A)-C(15A)-C(14A)	112.04(16)	C(1B)-C(2B)-H(2B)	121.4(10)
C(17A)-C(15A)-C(14A)	107.65(16)	C(2B)-C(3B)-O(3B)	125.75(17)
C(18A)-C(15A)-C(14A)	110.73(16)	C(2B)-C(3B)-C(4B)	119.09(17)
C(15A)-C(16A)-H(16A)	108.9(11)	O(3B)-C(3B)-C(4B)	115.17(14)
C(15A)-C(16A)-H(16B)	113.0(12)	O(4B)-C(4B)-C(5B)	124.76(16)
H(16A)-C(16A)-H(16B)	104.2(16)	O(4B)-C(4B)-C(3B)	114.99(15)
C(15A)-C(16A)-H(16C)	112.8(11)	C(5B)-C(4B)-C(3B)	120.25(15)
H(16A)-C(16A)-H(16C)	112.6(16)	C(4B)-C(5B)-C(6B)	121.93(18)
H(16B)-C(16A)-H(16C)	104.9(17)	C(4B)-C(5B)-H(5B)	119.8(9)
C(15A)-C(17A)-H(17A)	108.6(11)	C(6B)-C(5B)-H(5B)	118.2(9)
C(15A)-C(17A)-H(17B)	109.0(11)	C(1B)-C(6B)-C(5B)	116.22(17)
H(17A)-C(17A)-H(17B)	104.7(15)	C(1B)-C(6B)-C(9B)	123.96(15)
C(15A)-C(17A)-H(17C)	110.4(11)	C(5B)-C(6B)-C(9B)	119.82(16)
H(17A)-C(17A)-H(17C)	111.4(15)	O(3B)-C(7B)-H(7D)	104.1(10)
H(17B)-C(17A)-H(17C)	112.5(16)	O(3B)-C(7B)-H(7E)	108.4(11)
C(15A)-C(18A)-H(18A)	107.4(11)	H(7D)-C(7B)-H(7E)	113.1(15)
C(15A)-C(18A)-H(18B)	110.5(12)	O(3B)-C(7B)-H(7F)	111.9(10)
H(18A)-C(18A)-H(18B)	103.2(17)	H(7D)-C(7B)-H(7F)	111.7(14)
C(15A)-C(18A)-H(18C)	113.0(12)	H(7E)-C(7B)-H(7F)	107.7(14)
H(18A)-C(18A)-H(18C)	113.1(17)	O(4B)-C(8B)-H(8D)	105.0(10)
H(18B)-C(18A)-H(18C)	109.2(17)	O(4B)-C(8B)-H(8E)	110.2(9)
O(7A)-C(19A)-O(8A)	123.81(17)	H(8D)-C(8B)-H(8E)	108.9(14)
O(7A)-C(19A)-C(11A)	127.71(17)	O(4B)-C(8B)-H(8F)	106.3(10)
O(8A)-C(19A)-C(11A)	108.41(15)	H(8D)-C(8B)-H(8F)	114.3(14)
O(8A)-C(20A)-C(21A)	110.22(16)	H(8E)-C(8B)-H(8F)	111.8(14)
O(8A)-C(20A)-H(20A)	106.6(11)	O(5B)-C(9B)-C(6B)	111.39(15)
C(21A)-C(20A)-H(20A)	106.4(11)	O(5B)-C(9B)-H(9C)	104.7(11)
O(8A)-C(20A)-H(20B)	111.4(11)	C(6B)-C(9B)-H(9C)	111.7(11)
C(21A)-C(20A)-H(20B)	107.6(11)	O(5B)-C(9B)-H(9D)	107.2(9)
H(20A)-C(20A)-H(20B)	114.6(16)	C(6B)-C(9B)-H(9D)	111.8(9)
N(3A)-C(21A)-C(20A)	179.4(2)	H(9C)-C(9B)-H(9D)	109.8(14)

O(6B)-C(10B)-N(2B)	125.92(17)
O(6B)-C(10B)-O(5B)	123.44(17)
N(2B)-C(10B)-O(5B)	110.64(16)
N(2B)-C(11B)-C(19B)	111.82(15)
N(2B)-C(11B)-C(12B)	104.98(15)
C(19B)-C(11B)-C(12B)	111.33(15)
N(2B)-C(11B)-H(11B)	109.3(9)
C(19B)-C(11B)-H(11B)	107.6(10)
C(12B)-C(11B)-H(11B)	111.8(10)
C(11B)-C(12B)-C(13B)	104.15(16)
C(11B)-C(12B)-H(12C)	110.1(10)
C(13B)-C(12B)-H(12C)	110.4(10)
C(11B)-C(12B)-H(12D)	111.7(11)
C(13B)-C(12B)-H(12D)	112.0(11)
H(12C)-C(12B)-H(12D)	108.5(15)
C(14B)-C(13B)-C(12B)	105.92(17)
C(14B)-C(13B)-H(13C)	107.9(11)
C(12B)-C(13B)-H(13C)	107.5(11)
C(14B)-C(13B)-H(13D)	112.8(11)
C(12B)-C(13B)-H(13D)	109.6(11)
H(13C)-C(13B)-H(13D)	112.8(17)
N(2B)-C(14B)-C(13B)	102.68(15)
N(2B)-C(14B)-C(15B)	114.51(15)
C(13B)-C(14B)-C(15B)	115.33(17)
N(2B)-C(14B)-H(14B)	105.8(9)
C(13B)-C(14B)-H(14B)	112.4(9)
C(15B)-C(14B)-H(14B)	105.8(9)
C(16B)-C(15B)-C(17B)	108.71(17)
C(16B)-C(15B)-C(18B)	107.83(18)
C(17B)-C(15B)-C(18B)	110.37(17)
C(16B)-C(15B)-C(14B)	110.95(16)
C(17B)-C(15B)-C(14B)	112.09(16)
C(18B)-C(15B)-C(14B)	106.80(15)
C(15B)-C(16B)-H(16D)	110.1(11)
C(15B)-C(16B)-H(16E)	113.1(11)
H(16D)-C(16B)-H(16E)	107.2(15)
C(15B)-C(16B)-H(16F)	112.0(11)
H(16D)-C(16B)-H(16F)	109.3(16)
H(16E)-C(16B)-H(16F)	104.9(15)
C(15B)-C(17B)-H(17D)	111.4(10)
C(15B)-C(17B)-H(17E)	110.1(10)
H(17D)-C(17B)-H(17E)	107.1(15)
C(15B)-C(17B)-H(17F)	113.3(11)
H(17D)-C(17B)-H(17F)	107.5(15)
H(17E)-C(17B)-H(17F)	107.2(15)
C(15B)-C(18B)-H(18D)	107.9(11)
C(15B)-C(18B)-H(18E)	109.0(12)
H(18D)-C(18B)-H(18E)	114.3(15)
C(15B)-C(18B)-H(18F)	111.3(11)
H(18D)-C(18B)-H(18F)	103.6(15)
H(18E)-C(18B)-H(18F)	110.6(15)
O(7B)-C(19B)-O(8B)	124.56(18)
O(7B)-C(19B)-C(11B)	126.50(17)
O(8B)-C(19B)-C(11B)	108.82(15)
O(8B)-C(20B)-C(21B)	107.46(16)
O(8B)-C(20B)-H(20C)	108.8(9)
C(21B)-C(20B)-H(20C)	108.8(9)
O(8B)-C(20B)-H(20D)	107.2(10)
C(21B)-C(20B)-H(20D)	109.5(11)
H(20C)-C(20B)-H(20D)	114.8(15)
N(3B)-C(21B)-C(20B)	178.6(2)

Table 3.5. Anisotropic displacement parameters ($Å^2 x 10^4$) for LWL01 (CCDC 258350). The anisotropic displacement factor exponent takes the form: $-2\pi^2 [h^2 a^{*2} U^{11} + ... + 2 h k a^* b^* U^{12}]$

	U^{11}	U^{22}	U^{33}	U^{23}	U^{13}	U^{12}
O(1A)	671(11)	400(9)	223(7)	-19(7)	10(7)	268(8)
O(2A)	374(8)	300(8)	221(7)	28(6)	-71(6)	61(6)
O(3A)	333(8)	267(8)	224(7)	11(6)	32(6)	110(6)
O(4A)	356(8)	280(7)	204(7)	-7(6)	-5(6)	120(6)
O(5A)	244(7)	202(7)	212(6)	15(6)	-23(5)	25(6)
O(6A)	311(8)	430(9)	317(8)	113(7)	-128(6)	-114(7)
O(7A)	273(7)	236(7)	343(7)	-68(6)	-36(6)	63(6)
O(8A)	197(7)	241(7)	280(7)	-65(6)	-32(6)	1(6)
N(1A)	292(9)	254(9)	198(8)	8(7)	0(7)	14(8)
N(2A)	216(8)	205(8)	180(8)	18(7)	-43(6)	-3(7)
N(3A)	780(16)	392(11)	315(11)	-48(9)	46(10)	-129(11)
C(1A)	230(10)	207(10)	191(10)	4(8)	19(8)	-40(8)
C(2A)	214(10)	220(10)	201(10)	52(8)	-8(8)	-2(8)
C(3A)	204(10)	184(10)	259(10)	-6(8)	29(8)	-5(8)
C(4A)	220(10)	236(11)	170(10)	-15(8)	17(8)	-6(8)
C(5A)	199(10)	197(10)	195(10)	25(8)	-2(8)	25(8)
C(6A)	210(10)	217(10)	181(9)	7(8)	26(8)	-34(8)
C(7A)	305(13)	234(12)	304(12)	52(10)	34(10)	80(10)
C(8A)	413(14)	319(13)	202(11)	-18(9)	-9(10)	136(11)
C(9A)	276(11)	265(11)	166(10)	9(9)	-15(9)	11(9)
C(10A)	270(11)	241(11)	261(10)	-24(8)	13(9)	-1(9)
C(11A)	213(10)	217(10)	203(9)	-14(8)	7(8)	6(8)
C(12A)	213(11)	265(11)	257(11)	-13(9)	-36(8)	38(9)
C(13A)	276(11)	209(11)	245(11)	-22(9)	14(9)	28(9)
C(14A)	252(11)	218(11)	196(10)	-5(8)	-27(8)	-33(8)
C(15A)	207(10)	280(11)	253(10)	17(9)	30(8)	21(9)
C(16A)	314(13)	467(15)	302(12)	-67(11)	82(11)	27(12)
C(17A)	306(13)	363(13)	384(13)	52(11)	57(11)	-16(11)
C(18A)	291(13)	416(16)	488(16)	113(13)	83(12)	96(12)
C(19A)	238(10)	243(11)	162(9)	45(8)	17(8)	26(9)
C(20A)	267(12)	217(11)	275(11)	-16(9)	-46(9)	-14(9)
C(21A)	374(13)	206(11)	283(12)	-28(9)	-58(10)	-24(9)
O(1B)	439(9)	522(10)	287(8)	-43(7)	-98(7)	-86(8)
O(2B)	1186(17)	607(12)	236(9)	98(8)	-117(9)	-357(11)
O(3B)	305(8)	286(8)	227(7)	18(6)	18(6)	-78(6)
O(4B)	294(7)	282(7)	174(7)	0(6)	-6(5)	-71(6)
O(5B)	208(7)	267(7)	227(7)	-24(6)	-3(5)	21(6)
O(6B)	286(8)	421(9)	217(7)	-14(6)	47(6)	93(7)
O(7B)	227(8)	326(8)	313(7)	-86(6)	52(6)	-76(6)

O(8B)	209(7)	284(8)	369(8)	-116(6)	82(6)	-45(6)
N(1B)	396(10)	340(11)	222(9)	-26(8)	-20(8)	33(9)
N(2B)	213(9)	282(9)	208(8)	-43(7)	1(7)	17(7)
N(3B)	494(12)	287(10)	309(10)	0(8)	113(9)	-28(9)
C(1B)	254(10)	281(11)	191(10)	-36(8)	-13(8)	79(9)
C(2B)	291(11)	264(11)	199(10)	21(9)	58(8)	49(9)
C(3B)	215(10)	236(10)	217(10)	-34(8)	9(8)	0(9)
C(4B)	219(10)	255(11)	164(9)	-28(8)	9(8)	30(9)
C(5B)	192(10)	264(11)	209(10)	-9(9)	32(8)	14(9)
C(6B)	186(10)	258(11)	208(10)	-35(8)	14(8)	60(8)
C(7B)	340(13)	286(12)	214(11)	32(9)	28(10)	-25(10)
C(8B)	340(14)	355(14)	171(11)	15(9)	-51(10)	-71(10)
C(9B)	212(11)	306(12)	223(11)	-32(9)	-25(9)	41(9)
C(10B)	202(11)	339(12)	228(10)	-75(9)	-43(9)	15(9)
C(11B)	204(10)	301(11)	235(10)	-63(9)	15(8)	-19(9)
C(12B)	300(12)	329(13)	337(13)	-23(10)	78(10)	-60(10)
C(13B)	309(12)	267(12)	382(13)	-32(10)	-15(10)	-67(10)
C(14B)	239(11)	265(12)	225(10)	-70(8)	2(9)	4(9)
C(15B)	235(11)	245(10)	247(10)	-9(8)	-30(8)	-14(9)
C(16B)	220(12)	483(15)	320(13)	43(11)	-36(10)	-50(11)
C(17B)	318(13)	328(13)	237(11)	-16(9)	-25(10)	-27(10)
C(18B)	295(14)	374(14)	336(13)	-76(11)	-71(11)	32(11)
C(19B)	223(11)	317(12)	180(10)	6(8)	9(8)	-48(9)
C(20B)	267(12)	251(11)	318(12)	-33(9)	67(10)	2(9)
C(21B)	282(11)	200(11)	250(11)	-24(9)	11(9)	8(8)

Table 3.6. Hydrogen coordinates (x 10^4) and isotropic displacement parameters ($Å^2$x 10^3) for LWL01 (CCDC 258350).

	x	y	z	U_{iso}
H(2A)	6510(20)	1420(6)	12506(18)	17(5)
H(5A)	3400(20)	2392(7)	9379(18)	27(5)
H(7A)	7840(20)	488(7)	10182(19)	34(5)
H(7B)	6750(20)	602(8)	11430(20)	37(6)
H(7C)	8260(20)	915(7)	11385(18)	26(5)
H(8A)	3960(20)	1791(7)	6220(20)	40(6)
H(8B)	4190(20)	2314(8)	7138(19)	39(6)
H(8C)	2710(20)	1936(6)	7422(17)	21(5)
H(9A)	2310(20)	2641(6)	12384(17)	18(5)
H(9B)	3828(18)	2998(6)	12364(16)	12(4)
H(11A)	327(18)	3562(6)	9315(16)	9(4)
H(12A)	563(19)	3890(7)	6566(18)	21(5)
H(12B)	-480(20)	4150(6)	7589(16)	17(5)
H(13A)	2060(20)	4615(7)	7136(18)	27(5)
H(13B)	1560(20)	4609(7)	8730(20)	35(5)
H(14A)	3870(17)	4246(5)	9291(15)	7(4)
H(16A)	4460(20)	3697(7)	5421(18)	31(5)
H(16B)	2890(30)	3965(8)	5580(20)	48(6)
H(16C)	3070(20)	3400(8)	6250(20)	46(6)
H(17A)	6070(20)	4410(7)	6478(18)	29(5)
H(17B)	5760(20)	4619(7)	7950(20)	42(6)
H(17C)	4380(20)	4727(8)	6600(20)	43(6)
H(18A)	6430(20)	3567(7)	7320(19)	31(5)
H(18B)	5330(20)	3278(9)	8140(20)	42(6)
H(18C)	6280(20)	3740(8)	8890(20)	42(6)
H(20A)	-2760(20)	2662(7)	6498(19)	33(5)
H(20B)	-1170(20)	2332(8)	6937(19)	35(6)
H(2B)	10007(17)	7060(6)	-2117(16)	7(4)
H(5B)	8530(17)	5902(6)	1130(16)	10(4)
H(7D)	12410(20)	7880(7)	58(18)	30(5)
H(7E)	10760(20)	7785(7)	-945(18)	26(5)
H(7F)	12240(20)	7490(7)	-1341(19)	24(5)
H(8D)	10850(20)	6350(6)	4038(18)	18(4)
H(8E)	10560(20)	5874(7)	2953(17)	26(5)
H(8F)	9110(20)	6264(6)	3237(17)	23(5)
H(9C)	6180(20)	5753(6)	-1655(17)	15(5)
H(9D)	7545(18)	5414(6)	-2032(17)	18(5)
H(11B)	5380(19)	4745(6)	1218(17)	22(5)
H(12C)	6680(20)	4455(7)	3940(20)	29(5)
H(12D)	5240(20)	4184(7)	3012(19)	42(6)

H(13C)	6880(20)	3751(7)	1770(19)	31(5)
H(13D)	7920(20)	3753(7)	3240(20)	35(6)
H(14B)	8915(17)	4112(5)	941(16)	4(4)
H(16D)	10680(20)	5049(8)	1727(19)	36(6)
H(16E)	11510(20)	4575(7)	1030(20)	39(6)
H(16F)	12200(20)	4785(7)	2487(19)	39(6)
H(17D)	9330(20)	4951(8)	3939(18)	34(5)
H(17E)	10900(20)	4679(6)	4607(18)	24(5)
H(17F)	9310(20)	4391(8)	4650(20)	37(6)
H(18D)	11070(20)	3702(7)	1960(20)	39(6)
H(18E)	10460(20)	3653(8)	3560(20)	43(6)
H(18F)	12050(20)	3907(6)	3250(17)	20(5)
H(20C)	5410(20)	5937(6)	4158(16)	16(4)
H(20D)	3800(20)	6012(7)	3133(17)	21(5)

3.6.2 Electrophysiology and molecular biology general:

Unless otherwise stated, chemicals and molecular biology reagents were purchased from commercial sources and used as is. *Xenopus laevis* were purchased from Xenopus Express (Plant City, FL) and Xenopus One (Dexter, MI).

3.6.2.1 Site-directed mutagenesis of subunits of nAChR

Mutagenetic primers were custom ordered from Integrated DNA Technology (IDT) Inc. (San Diego, CA) in 25 nmole amounts with standard desalting. These primers had the following properties: length: 25-45 bases, $T_m \geq 78$ °C, CG content 40%-50 %, and terminates with one or more C/G at the 3' end. Quickchange kits from Qiagen (Valencia, CA) were used.

To a PCR tube was added 10 x polymerase buffer (5 μL), 5-50 ng of circular DNA (2 μL volume), 125 ng of mutagenic primer #1 (125 μL), 125 ng of mutagenic primer #2 (125 μL), 25 mM dNTP mix (1 μL) and RNase free water (38.5 μL) for total volume of 49 μL. The reaction was mixed by gentle pipetting. Polymerase (1 μL) was added to the reaction mixture and it was mixed. The reaction mixture was subject to the following cycling parameters:

Cycle 1 (1 cycle): 95 °C for 30 s.

Cycle 2 (18 cycles): Step 1 – 95 °C for 30 s.

Step 2 – 55 to 61 °C for 1 min.

Step 3 – 68 °C for 10 min.

Cycle 3 (1 cycle): 68 °C for 7 min.

Hold at 4 °C until digestion with Dpn I.

The Quickchange reactions were screened by electrophoresis through 1 % agarose gel. 10 μL of each Quickchange reaction mixture was removed and mixed with 2 μL 6 x DNA gel-loading buffer (0.25 % bromophenol blue, 0.25 % xylene cyanol FF, 30 % glycerol in Millipore water) and resolved on a 1 % agarose gel for 1 hr, followed by visualization with ethidium bromide. 1 μL of Dpn I was then added to each reaction and the reaction was incubated at 37 °C for 1 h. Only reactions that showed amplification were transformed into Top10 cells.

3.6.2.2 Transformation of Quickchange reactions

1 μL of a Quickchange reaction was added to 40 μL of Blue Top10 cells that had been thawed on ice. The cells were mixed by gentle pipetting. The mixture was electroporated at 1800 V using a chilled 0.1 mm cuvette. 500 μL of SOC media at 37 °C was added mixed with the cells. The mixture was removed and placed in a 5 mL Falcon tube. The recovered bacteria were incubated at 37 °C with shaking (300 rpm) for 20 min. Each culture was then plated on LB-agar supplemented with ampicillin. The plates were incubated upside down at 37 °C for 10-12 h. Distinct colonies were picked and used to inoculate cultures for minipreps. The miniprepped DNA was sequenced to select for the correct mutant.

The primers used to make the mutations were (mutation site shown in red):

Alpha subunit nAChR:

Pro272TAG

5’-CCACCTCCAGCGCTGTGTAGCTGATCGGGAAGTATATG-3’

Pro272TAG Reverse complement

5’-CATATACTTCCCGATCAGCTACACAGCGCTGGAGGTGG-3’

Pro272Ala

5’-CCACCTCCAGCGCTGTGGCCCTGATCGGGAAGTATATG-3’

Pro272Ala reverse complement

5’-CATATACTTCCCGATCAGGGCCACAGCGCTGGAGGTGG-3’

Pro272Gly

5’-CCACCTCCAGCGCTGTGGGCCTGATCGGGAAGTATATG-3’

Pro272Gly reverse complement

5’-CATATACTTCCCGATCAGGCCCACAGCGCTGGAGGTGG-3’

Pro272Val

5’-CCACCTCCAGCGCTGTGGTCCTGATCGGGAAGTATATG-3’

Pro272Val reverse complement

5’-CATATACTTCCCGATCAGGACCACAGCGCTGGAGGTGG-3’

Pro265TAG

5’-GGTCATTGTGGAGCTAATCTAGTCCACCTCCAGCGC-3’

Pro265TAG reverse complement

5’-GCGCTGGAGGTGGACTAGATTAGCTCCACAATGACC-3’

Pro265Val

5’-GGTCATTGTGGAGCTAATCGTTTCCACCTCCAGCGC-3’

Pro265Val reverse Complement

5’-GCGCTGGAGGTGGAAACGATTAGCTCCACAATGACC-3’

Pro265Gly

5’-GGTCATTGTGGAGCTAATCGGTTCCACCTCCAGCGC-3’

Pro265Gly reverse complement

5’-GCGCTGGAGGTGGAACCGATTAGCTCCACAATGACC-3’

Pro265Ala

5’-GGTCATTGTGGAGCTAATCGCTTCCACCTCCAGCGC-3’

Pro265Ala reverse Complement

5’-GCGCTGGAGGTGGAAGCGATTAGCTCCACAATGACC-3’

3.6.2.3 mRNA Transcription from plasmid DNA

Plasmid DNA linearization: Plasmid DNA (5-10 μg, 30 μL) containing the desired subunit gene was mixed with 10 x Buffer (5 μL) and DEPC/nuclease free water (12 μL). To the mixture was added the appropriate restriction enzyme (3 μL). The reaction mixture was mixed by pipetting and incubated at 37 °C for 6 hours to overnight. A sample of the reaction mixture was then resolved on a 1 % agarose gel with ethidium bromide staining to ensure the plasmid DNA was completely linearized. If the plasmid DNA was not completely linearized, additional restriction enzyme (3 μL) was added, the reaction was incubated at 37 °C for another 4 hours, and followed by agarose gel analysis. Once the plasmid DNA was completely linearized, the reaction was heat inactivated for 20 min. at 65 °C.

Work up for Plasmid DNA linearization (follows Qiagen MinElute PCR Purification Kit protocol): Ethanol (96%–100 %) was added to Buffer PE before use (see bottle label for volume). All centrifugation steps were at 14,000 rpm in a tabletop micro-centrifuge. Five volumes of Buffer PB were added to 1 volume of linearization reaction and mixed by pipetting. A MinElute column was placed in a provided 2 mL collection tube. The reaction mix was applied to the MinElute column and centrifuged for 1 min. The flow-through was

discarded and the MinElute was placed back in the same 2 mL collection tube. The DNA was washed by an application of Buffer PE (750 µL) and centrifuged for 1 min. The flow-through was discarded and the MinELute was placed in the same collection tube. The column was centrifuged for an additional 1 min. to ensure all residual ethanol was removed from the column. The MinElute column was placed in a 1.5 mL collection tube. The DNA was eluted from the column by adding DEPC/nuclease free water (9 µL) directly to the center of the column membrane, incubating for 1 min. and then centrifuging for 1min. 8 µL was recovered, which was used directly in mRNA transcription reactions.

T7 mMessage Machine Transcription (Uses Ambion T7 mMessage Transcription Kit): 10x transcription buffer (2 µL), 2 x NTPs (10 µL), linearized plasmid DNA (4 µL), DEPC/nuclease free water (2 µL) were combined and mixed by pipetting. To the mixture was added T7 mMessage Machine Enzyme Mix (2 µL). Subsequently, the reaction was mixed by pipetting and incubated for 2 hours at 37 °C. The reaction was quenched by the addition of 1 µL of DNAse I, followed by incubating at 37 °C for 15 min.

mRNA Cleanup (uses Qiagen RNeasy Mini for RNA Cleanup Kit): 10 µL of β-ME was added per 1 mL Buffer RLT. For first time use, 4 volumes of ethanol (96%–100 %) was added to Buffer RPE (supplied as a concentrate), as indicated on the bottle, to obtain a working solution. The volume of the T7mMessage Machine Transcription reaction was adjusted to 100 µL with DEPC/nuclease free water. Buffer RLT (350 µL) was added and the reaction was mixed thoroughly by pipetting. To the diluted RNA, was added ethanol (96%–100 %, 250 µL). The mixture was mixed thoroughly and applied to an RNeasy mini column placed in a 2 ml collection tube. The tube was closed gently and centrifuged for 15 sec. The flow-through and collection tube were discarded. The column was placed in a new 2 mL

collection tube. Buffer RPE (500 μL) was pipetted into the column and the column was centrifuged for 15 sec. Another portion of Buffer RPE (500 μL) was added to the column and the column was centrifuged for 2 min. to ensure the RNeasy silica-gel membrane is completely dry. The flow-through and collection tube were discarded and the column was placed in a new 2 mL collection tube and centrifuged for 1 min. to remove all residual ethanol. The RNA was eluted from the column by transferring the RNeasy column to a new 1.5 ml collection tube. DEPC/nuclease free water (30–50 μL) was pipetted directly onto the RNeasy silica-gel membrane. The tube was closed and centrifuged for 1 min. to elute. The eluted solution was reapplied to the column and centrifuged for 1 min. to increase yield.

3.6.2.4 tRNA transcription from plasmid DNA

Plasmid DNA linearization: Plasmid DNA (50-60 μg, 180 μL) was mixed with Buffer 4 (60 μL) and DEPC/nuclease free water (342 μL). To the mixture was added the Fok I (18 μL). The reaction mixture was mixed by pipetting and incubated at 37 °C for 6 hours to overnight. A sample of the reaction mixture was then resolved on a 1 % agarose gel to ensure the plasmid DNA was completely linearized. If the plasmid DNA was not completely linearized, additional Fok I (6 μL) was added, the reaction was incubated at 37 °C for another 4 hours, and followed by agarose gel analysis. Once the plasmid DNA was completely linearized, the reaction was heat inactivated for 20 min. at 65 °C.

Linearization workup: All centrifugation steps are at 14,000 rpm. The reaction was split into 2 tubes. To each tube, PCI (300 μL) was added and mixture was vortexed for 1 min. followed by centrifugation for 2 min. The aqueous layer (top layer) was removed and saved. To the organic layer was added DEPC/nuclease free water (150 μL), which was then

vortexed for 1 min. and centrifuged for 2 min. The aqueous layer (top layer) was removed and saved. The saved aqueous layers were combined and vortexed briefly. CI (450 µL) was added to the combined aqueos layers and mixture was vortexed for 1 min., followed by centrifugation for 2 min. The aqueous layer (top layer) was removed. To the organic layer was added DEPC/nuclease free water (150 µL), which was then vortexed for 1 min. and centrifuged for 2 min. The aqueous layer (top layer) was removed and split into 2 tubes (300 µL each). To each tube was added: 1 µL seeDNA, 30 µL 5M NH_4OAc, and 900 µL EtOH. The tubes were stored at -20 °C for at least an hour (usually overnight) to precipitate. The tubes were centrifuged at 4 °C for 15 min. and the supernatant was removed. The pellets were dried under vacuum in a desiccator. All four pellets were redissolved in DEPC/nuclease free water (60 µL total). The linearized DNA was used directly in the transcription.

T7 MEGAshortscript transcription (uses Ambion T7 MEGAshortscript Transcription Kit): 10x transcription buffer (12 µL), 75 mM ATP (12 µL), 75 mM CTP (12 µL), 75 mM GTP (12 µL), 75 mM UTP (12 µL), linearized plasmid DNA (30 µL), DEPC/nuclease free water (18 µL) were combined and mixed by pipetting. To the mixture was added T7 MEGAshortscript Enzyme Mix (12 µL). Subsequently, the reaction was mixed by pipetting and incubated for 2 hours at 37 °C. The DNA was digested by the addition of 6 µL of DNAse I, followed by incubating at 37 °C for 15 min. The transcription reaction was quenched by the addition of DEPC/nuclease free water (414 µL) and NH_4OAc “Stopping Solution” (60 µL).

tRNA MEGAshortscript Transcription Workup: PCI (600 µL) was added to the quenched reaction. The mixture was vortexed for 1 min then centrifuged for 2 min. The

aqueous layer (top layer) was removed and saved. To the organic layer was added DEPC/nuclease free water (300 µL). It was then vortexed, centrifuged for 2 min. and the aqueous layer removed and saved. The aqueous layers were combined, vortexed briefly and then divided into two 450 µL portions. A CI extraction was performed on each tube by adding CI (450 µL), vortexing for 1 min, centrifuging for 2 min and then removing the aqueous layer (top layer). Isopropanol (450 µL) was added to each aqueous extract. The mixture was stored at -20 °C overnight to precipitate. The tubes are centrifuged for 15 min. at 4 °C and the supernatant was removed. The pellets were dried under vacuum in a dessicator and then both pellets were dissolved and combined in DEPC/nuclease free water (100 µL total).

Column purification of tRNA: 2 BD Bioscience CHROMA SPIN-30 DEPC-H_2O columns were equilibrated by spinning for 5 min. at 3000 rpm. (2 columns used to avoid overloading.) The flow-through was discarded and the columns were placed in new eppendorf tubes. The process was repeated until there was no more flow-through. The tRNA solution was divided in half (50 µL each portions) and each portion was applied to one equilibrated column. Each portion was applied carefully to avoid touching the sides of the tube. The tRNA solution was eluted from the CHROMA SPIN-30 columns by centrifuging for 5 min. at 3000 rpm. The eluted tRNA solution from both columns was combined, yielding 100 µL.

3.6.2.5 tRNA ligation to dCA-unnatural amino acid

Denature tRNA: 74-mer tRNA (30 µg) is brought to a volume of 45 µL using 10 mM HEPES, pH 7.5 (room temperature). It is placed in a beaker of boiling water and allowed to cool to 37 °C in air or in an ice bath.

2.5 x reaction mix: The following reagents were combined and mixed thoroughly to make the 2.5 x reaction mix used in ligations: 400 mM HEPES, pH 7.5 (25 µL), 100 mM DTT (10 µL), 200 mM $MgCl_2$ (25 µL), 10 mM ATP (thaw on ice, 4 µL), 5 mg/mL Ac-BSA (thaw on ice, 10 µL), DEPC/nuclease free water (25 µL), and RNAse Inhibitor (1 µL).

Ligation reaction: The following were combined: DEPC/nuclease free water (7.8 µL), 2.5 x Reaction mix (room temp, 48 µL), dCA-aa (3mM in DMSO, 12 µL), tRNA/HEPES mix (45 µL), and T4 RNA ligase (7.2 µL). The reaction was vortexed and incubated at 37 °C for 30 min. The reaction is quenched with the addition of 3.0 M NaOAc, pH 5.0 (12.5 µL) and DEPC water (17.5 µL).

tRNA Ligation Workup: PCI, pH 5.2 (150 µL) was added to the quenched reaction. The mixture was vortexed for 1 min then centrifuged for 2 min. The aqueous layer (top layer) was removed and saved. To the organic layer was added 3 M NaOAc (6.3 µL) and DEPC/nuclease free water (68.7 µL). It was then vortexed, centrifuged for 2 min. and the aqueous layer removed and saved. The aqueous layers were combined. A CI extraction was performed on each tube by adding CI (225 µL), vortexing for 1 min., centrifuging for 2 min. and then removing the aqueous layer (top layer). Ethanol (200 proof, 675 µL) was added to the aqueous extract. The mixture was stored at -20 °C overnight to precipitate. The tube was centrifuged for 15 min. at 4 °C and the supernatant was removed. The pellet was dried under vacuum in a dessicator and then redissolved in 1 mM NaOAc, pH 4.5 (room temp, 25 µL).

Column purification of tRNA ligation: A BD Bioscience CHROMA SPIN-30 DEPC-H_2O column was equilibrated by spinning for 5 min. at 3000 rpm. The flow-through was discarded and the column was placed in new eppendorf tubes. The process was repeated until there was no more flow-through. The tRNA ligation solution was applied carefully to avoid touching the sides of the tube. The tRNA ligation solution was eluted from the CHROMA SPIN-30 column by centrifuging for 5 min. at 3000 rpm. 25 µL was typically recovered.

MALDI Mass Spectrometry Analysis of tRNA Ligation: 3-HPA mix is made by combining 3-hydroxypicolinic acid (42 mg), picolinic acid (2 mg), and diammonium citrate (2 mg) in 9:1 water:CH_3CN (500 µL). This solution was stored at -20 °C and was thawed and sonicated for 2 min. before each use. For the cation exchange treatment, a 20-200 µL pipetman tip was cut at the bevel near the tip's end. The cut tip was used to place NH_4^+-loaded cation exchange bead slurry (5 µL) in an eppendorf. Using an uncut pipetman tip, the water was removed from the slurry, leaving the beads behind. Amino acid-tRNA solution (0.5 µL) was applied to the beads. To the amino acid-tRNA bead mixture was added 3-HPA mix (2.5 µL), followed by picofuging to get all the material at the bottom of the tube. The mixture was incubated at room temperature for 10 min. BSA calibration mix was made by combining α-CN matrix solution (2.2 µL, saturated α-cyanohydroxycinnamic acid in 2:1 water/CH_3CN) with PE Biosystems BSA calibrant (0.2 µL). The calibration mixture and tRNA matrix solution (0.5 µL) were each spotted on separate areas on the MALDI plate and allowed to dry completely. The plate was loaded with Plate ID: Plate #1. The system was allowed to pump down to ~ 3.0×10^{-7} torr. The Voyager Instrument Control Panel was set to the following:

Mode/Digitizer:

Instrument mode: Operation Mode: Linear, Extraction type: Delayed, Polarity type: Positive, Laser type: Internal, Laser rate type: Optimized

Linear Digitizer: Bin size: 0.5 ns, Vertical scale: 100 mV, Vertical offset: 0.0%, Input bandwidth: Full

Control Mode: Manual

Voltages: Voltage: 25,000 V, Grid voltage: 92.5 %, Guide wire: 0.15 %, Delay: 500 ns, Spectrum acquisition: 100 Shots/spectrum, Mass range: 20,000-35,000 Da; Low mass gate: 10,000 Da

For the BSA Calibration, the Laser power was set to 2000. The Calibration was set to α-CN default. The BSA calibration spot was blasted with 100 shot scans. Typically ten 100 shot scans were accumulated and averaged. The file was saved and then file was opened in Data Explorer. Manual Calibration was performed on +2 and +3 BSA peaks (+2: 33,216 Da; +3: 22,144 Da). (Selected peaks by right-clicking around them). Match peaks, Plot, Apply calibration and Export calibration file. Returning to Instrument Control, the newly generated calibration file was loaded as External File.

For the amino acid-tRNA samples, the Laser Power was set to 2500. The spots were blasted with 100 scan shot. Typically ten 100 shot scans were accumulated and averaged. The average scan was saved. To work up the data in Data Explorer, the mass range was set to 22,000-27,000. The Noise Filter was set to 1.0 and Gaussian Smoothing was set to 11 pts. Unligated 74-mer has a mass of 23,700 and hydrolyzed ligation product (76-mer) has a mass of 24,300.

3.6.2.6 Injection of Stage VI Xenopus laevis oocytes

Stage VI oocytes of *Xenopus laevis* were harvested according to approved protocol (Qi Huang and Purnima Deshpande, *Lester Laboratory*, California Institute of Technology, Pasadena, CA). Charged tRNA was deprotected immediately prior to injection into oocytes. Deprotection was performed by photolysis for 5 min. using an Arc Lamp (Oriel Corporation, Stratford, CT), powered to 400 W and filtered for 350 nm light. Typically, 25 ng of deprotected charged tRNA was injected along with 15 ng of mRNA in a total volume of 50 nL per oocyte. mRNA was prepared as previously described. Ligation of dCA coupled unnatural amino acid to 74-mer tRNA was performed as previously described.

Oocytes were injected using glass injection needles pulled from 10 μL sp1 8 inch Borosilicate capillaries (Item #3-000-210-G8, Drummond Scientific, Broomall, PA). Injection needles were pulled on a KOPF Vertical Pipette Puller set on 13.3 (David Kopf Instruments, Tujunga, CA). The tip of the injection needle was broken off using tweezers to a diameter of ~25 μm as visualized under a microscope (*under setting 2.0, one tick mark on eyepiece ruler equals 50* μm, Model S6E, Leica Microsystems, Wetzlar, Germany). The needle was filled with mineral oil and put on a 10 μL microdispenser (Drummond Digital Microdispenser, Drummond Scientific Co., Broomall, PA). The deprotected amino acid-tRNA with mRNA mixture was drawn into the injection needle and then used to inject each oocyte with 50 nL of the mixture. Oocytes were then incubated at 18 °C in ND96 with 5 % horse serum.

3.6.2.7 Two-electrode voltage clamp electrophysiological analysis

Recordings were made 36-72 h post-injection in two-electrode voltage cell clamp mode using an OpusXpress (Axon Instruments, now part of Molecular Devices, Novato, CA). Ooctyes were perfused with Ca^{+2} free ND96.

3.6.2.8 20 x Ca^{+2} free ND96

Mix together NaCl (56.10 g), KCl (1.49 g), $MgCl_2 \cdot 6H_20$ (2.03 g), and HEPES (11.92 g) in millipore water (~400 mL). Adjust the mixture to pH = 7.5 with NaOH. Add water to make a total volume of 500 mL. Filter through a 0.2 μm filter (Nalgene). Store at 4 °C. Dilute with Millipore water to make 1x Ca^{+2} free ND96. The osmolarity of the 1x Ca^{+2} free ND96 was checked to ensure that it is between 195 and 240.

3.6.2.9 20 x ND96

Mix together NaCl (56.10 g), KCl (1.49 g), $MgCl_2 \cdot 6H_20$ (2.03 g), $CaCl_2 \cdot 6H_20$ (2.65 g), and HEPES (11.92 g) in millipore water (~400 mL). Adjust the mixture to pH = 7.5 with NaOH. Add water to make a total volume of 500 mL. Filter through a 0.2 μm filter (Nalgene). Store at 4 °C.

3.6.2.10 1 x ND96

Dilute 20 x ND96 (25 mL) with Millipore water (450 mL). To the mixture add Na·Pyruvate (138 mg) and theophyllen (60 mg). The solution was then adjusted to pH 7.5 with NaOH and then filtered through a 0.2 μm filter (Nalgene). Gentamicin (500 μL) was added. The osmolarity was checked to ensure that it is between 195 and 240.

3.7 References

1. Baulac, S.; Huberfeld, G.; Gourfinkel-An, I.; Mitropoulou, G.; Beranger, A.; Prud'homme, J. F.; Baulac, M.; Brice, A.; Bruzzone, R.; LeGuern, E., First genetic evidence of GABA(A) receptor dysfunction in epilepsy: a mutation in the gamma2-subunit gene. *Nat Genet* **2001,** 28, (1), 46-8.
2. Brune, W.; Weber, R. G.; Saul, B.; von Knebel Doeberitz, M.; Grond-Ginsbach, C.; Kellerman, K.; Meinck, H. M.; Becker, C. M., A GLRA1 null mutation in recessive hyperekplexia challenges the functional role of glycine receptors. *Am J Hum Genet* **1996,** 58, (5), 989-97.
3. Buckwalter, M. S.; Cook, S. A.; Davisson, M. T.; White, W. F.; Camper, S. A., A frameshift mutation in the mouse alpha 1 glycine receptor gene (Glra1) results in progressive neurological symptoms and juvenile death. *Hum Mol Genet* **1994,** 3, (11), 2025-30.
4. De Fusco, M.; Becchetti, A.; Patrignani, A.; Annesi, G.; Gambardella, A.; Quattrone, A.; Ballabio, A.; Wanke, E.; Casari, G., The nicotinic receptor beta 2 subunit is mutant in nocturnal frontal lobe epilepsy. *Nat Genet* **2000,** 26, (3), 275-6.
5. Elmslie, F. V.; Hutchings, S. M.; Spencer, V.; Curtis, A.; Covanis, T.; Gardiner, R. M.; Rees, M., Analysis of GLRA1 in hereditary and sporadic hyperekplexia: a novel mutation in a family cosegregating for hyperekplexia and spastic paraparesis. *J Med Genet* **1996,** 33, (5), 435-6.
6. Gunther, U.; Benson, J.; Benke, D.; Fritschy, J. M.; Reyes, G.; Knoflach, F.; Crestani, F.; Aguzzi, A.; Arigoni, M.; Lang, Y.; et al., Benzodiazepine-insensitive mice generated by targeted disruption of the gamma 2 subunit gene of gamma-aminobutyric acid type A receptors. *Proc Natl Acad Sci U S A* **1995,** 92, (17), 7749-53.
7. Hirose, S.; Iwata, H.; Akiyoshi, H.; Kobayashi, K.; Ito, M.; Wada, K.; Kaneko, S.; Mitsudome, A., A novel mutation of CHRNA4 responsible for autosomal dominant nocturnal frontal lobe epilepsy. *Neurology* **1999,** 53, (8), 1749-53.
8. Phillips, H. A.; Favre, I.; Kirkpatrick, M.; Zuberi, S. M.; Goudie, D.; Heron, S. E.; Scheffer, I. E.; Sutherland, G. R.; Berkovic, S. F.; Bertrand, D.; Mulley, J. C., CHRNB2 is the second acetylcholine receptor subunit associated with autosomal dominant nocturnal frontal lobe epilepsy. *Am J Hum Genet* **2001,** 68, (1), 225-31.
9. Saenz, A.; Galan, J.; Caloustian, C.; Lorenzo, F.; Marquez, C.; Rodriguez, N.; Jimenez, M. D.; Poza, J. J.; Cobo, A. M.; Grid, D.; Prud'homme, J. F.; Lopez de Munain, A., Autosomal dominant nocturnal frontal lobe epilepsy in a Spanish family with a Ser252Phe mutation in the CHRNA4 gene. *Arch Neurol* **1999,** 56, (8), 1004-9.
10. Scheffer, I. E.; Bhatia, K. P.; Lopes-Cendes, I.; Fish, D. R.; Marsden, C. D.; Andermann, F.; Andermann, E.; Desbiens, R.; Cendes, F.; Manson, J. I.; et al., Autosomal dominant frontal epilepsy misdiagnosed as sleep disorder. *Lancet* **1994,** 343, (8896), 515-7.
11. Shiang, R.; Ryan, S. G.; Zhu, Y. Z.; Fielder, T. J.; Allen, R. J.; Fryer, A.; Yamashita, S.; O'Connell, P.; Wasmuth, J. J., Mutational analysis of familial and sporadic hyperekplexia. *Ann Neurol* **1995,** 38, (1), 85-91.
12. Shiang, R.; Ryan, S. G.; Zhu, Y. Z.; Hahn, A. F.; O'Connell, P.; Wasmuth, J. J., Mutations in the alpha 1 subunit of the inhibitory glycine receptor cause the dominant neurologic disorder, hyperekplexia. *Nat Genet* **1993,** 5, (4), 351-8.
13. Steinlein, O. K.; Magnusson, A.; Stoodt, J.; Bertrand, S.; Weiland, S.; Berkovic, S. F.; Nakken, K. O.; Propping, P.; Bertrand, D., An insertion mutation of the CHRNA4 gene in

a family with autosomal dominant nocturnal frontal lobe epilepsy. *Hum Mol Genet* **1997,** 6, (6), 943-7.
14. Steinlein, O. K.; Mulley, J. C.; Propping, P.; Wallace, R. H.; Phillips, H. A.; Sutherland, G. R.; Scheffer, I. E.; Berkovic, S. F., A missense mutation in the neuronal nicotinic acetylcholine receptor alpha 4 subunit is associated with autosomal dominant nocturnal frontal lobe epilepsy. *Nat Genet* **1995,** 11, (2), 201-3.
15. Kullmann, D. M., The neuronal channelopathies. *Brain* **2002,** 125, (Pt 6), 1177-95.
16. Ashcroft, F. M., *Ion channels and disease : channelopathies*. Academic Press: San Diego, 2000; p xxi, 481 p.
17. Yang, J., Ion permeation through 5-hydroxytryptamine-gated channels in neuroblastoma N18 cells. *J Gen Physiol* **1990,** 96, (6), 1177-98.
18. Yakel, J. L.; Shao, X. M.; Jackson, M. B., The selectivity of the channel coupled to the 5-HT3 receptor. *Brain Res* **1990,** 533, (1), 46-52.
19. Huang, L. Y.; Catterall, W. A.; Ehrenstein, G., Selectivity of cations and nonelectrolytes for acetylcholine-activated channels in cultured muscle cells. *J Gen Physiol* **1978,** 71, (4), 397-410.
20. Dwyer, T. M.; Adams, D. J.; Hille, B., The permeability of the endplate channel to organic cations in frog muscle. *J Gen Physiol* **1980,** 75, (5), 469-92.
21. Cohen, B. N.; Labarca, C.; Davidson, N.; Lester, H. A., Mutations in M2 alter the selectivity of the mouse nicotinic acetylcholine receptor for organic and alkali metal cations. *J Gen Physiol* **1992,** 100, (3), 373-400.
22. Bertrand, D.; Galzi, J. L.; Devillers-Thiery, A.; Bertrand, S.; Changeux, J. P., Mutations at two distinct sites within the channel domain M2 alter calcium permeability of neuronal alpha 7 nicotinic receptor. *Proc Natl Acad Sci U S A* **1993,** 90, (15), 6971-5.
23. Bormann, J.; Hamill, O. P.; Sakmann, B., Mechanism of anion permeation through channels gated by glycine and gamma-aminobutyric acid in mouse cultured spinal neurones. *J Physiol* **1987,** 385, 243-86.
24. Fatima-Shad, K.; Barry, P. H., Anion permeation in GABA- and glycine-gated channels of mammalian cultured hippocampal neurons. *Proc Biol Sci* **1993,** 253, (1336), 69-75.
25. Samochocki, M.; Hoffle, A.; Fehrenbacher, A.; Jostock, R.; Ludwig, J.; Christner, C.; Radina, M.; Zerlin, M.; Ullmer, C.; Pereira, E. F.; Lubbert, H.; Albuquerque, E. X.; Maelicke, A., Galantamine is an allosterically potentiating ligand of neuronal nicotinic but not of muscarinic acetylcholine receptors. *J Pharmacol Exp Ther* **2003,** 305, (3), 1024-36.
26. Tanner, C. M.; Goldman, S. M.; Aston, D. A.; Ottman, R.; Ellenberg, J.; Mayeux, R.; Langston, J. W., Smoking and Parkinson's disease in twins. *Neurology* **2002,** 58, (4), 581-8.
27. Levin, E. D.; Conners, C. K.; Silva, D.; Hinton, S. C.; Meck, W. H.; March, J.; Rose, J. E., Transdermal nicotine effects on attention. *Psychopharmacology (Berl)* **1998,** 140, (2), 135-41.
28. Shytle, R. D.; Silver, A. A.; Wilkinson, B. J.; Sanberg, P. R., A pilot controlled trial of transdermal nicotine in the treatment of attention deficit hyperactivity disorder. *World J Biol Psychiatry* **2002,** 3, (3), 150-5.
29. Bruss, M.; Eucker, T.; Gothert, M.; Bonisch, H., Exon-intron organization of the human 5-HT3A receptor gene. *Neuropharmacology* **2000,** 39, (2), 308-15.
30. Greenshaw, A. J., Behavioural pharmacology of 5-HT3 receptor antagonists: a critical update on therapeutic potential. *Trends Pharmacol Sci* **1993,** 14, (7), 265-70.

31. Gyermek, L., 5-HT3 receptors: pharmacologic and therapeutic aspects. *J Clin Pharmacol* **1995,** 35, (9), 845-55.
32. Barann, M.; Gothert, M.; Fink, K.; Bonisch, H., Inhibition by anaesthetics of 14C-guanidinium flux through the voltage-gated sodium channel and the cation channel of the 5-HT3 receptor of N1E-115 neuroblastoma cells. *Naunyn Schmiedebergs Arch Pharmacol* **1993,** 347, (2), 125-32.
33. Downie, D. L.; Hope, A. G.; Belelli, D.; Lambert, J. J.; Peters, J. A.; Bentley, K. R.; Steward, L. J.; Chen, C. Y.; Barnes, N. M., The interaction of trichloroethanol with murine recombinant 5-HT3 receptors. *Br J Pharmacol* **1995,** 114, (8), 1641-51.
34. Emerit, M. B.; Riad, M.; Fattaccini, C. M.; Hamon, M., Characteristics of [14C]guanidinium accumulation in NG 108-15 cells exposed to serotonin 5-HT3 receptor ligands and substance P. *J Neurochem* **1993,** 60, (6), 2059-67.
35. Machu, T. K.; Harris, R. A., Alcohols and anesthetics enhance the function of 5-hydroxytryptamine3 receptors expressed in Xenopus laevis oocytes. *J Pharmacol Exp Ther* **1994,** 271, (2), 898-905.
36. Peters, J. A.; Malone, H. M.; Lambert, J. J., Ketamine potentiates 5-HT3 receptor-mediated currents in rabbit nodose ganglion neurones. *Br J Pharmacol* **1991,** 103, (3), 1623-5.
37. White, P. F.; Way, W. L.; Trevor, A. J., Ketamine--its pharmacology and therapeutic uses. *Anesthesiology* **1982,** 56, (2), 119-36.
38. Karlin, A., Structure of nicotinic acetylcholine receptors. *Curr Opin Neurobiol* **1993,** 3, (3), 299-309.
39. Corringer, P. J.; Le Novere, N.; Changeux, J. P., Nicotinic receptors at the amino acid level. *Annu Rev Pharmacol Toxicol* **2000,** 40, 431-58.
40. Mishina, M.; Takai, T.; Imoto, K.; Noda, M.; Takahashi, T.; Numa, S.; Methfessel, C.; Sakmann, B., Molecular distinction between fetal and adult forms of muscle acetylcholine receptor. *Nature* **1986,** 321, (6068), 406-11.
41. Sakmann, B.; Methfessel, C.; Mishina, M.; Takahashi, T.; Takai, T.; Kurasaki, M.; Fukuda, K.; Numa, S., Role of acetylcholine receptor subunits in gating of the channel. *Nature* **1985,** 318, (6046), 538-43.
42. Anand, R.; Conroy, W. G.; Schoepfer, R.; Whiting, P.; Lindstrom, J., Neuronal nicotinic acetylcholine receptors expressed in Xenopus oocytes have a pentameric quaternary structure. *J Biol Chem* **1991,** 266, (17), 11192-8.
43. Lindstrom, J.; Schoepfer, R.; Conroy, W.; Whiting, P.; Das, M.; Saedi, M.; Anand, R., The nicotinic acetylcholine receptor gene family: structure of nicotinic receptors from muscle and neurons and neuronal alpha-bungarotoxin-binding proteins. *Adv Exp Med Biol* **1991,** 287, 255-78.
44. Claudio, T.; Ballivet, M.; Patrick, J.; Heinemann, S., Nucleotide and deduced amino acid sequences of Torpedo californica acetylcholine receptor gamma subunit. *Proc Natl Acad Sci U S A* **1983,** 80, (4), 1111-5.
45. Noda, M.; Furutani, Y.; Takahashi, H.; Toyosato, M.; Tanabe, T.; Shimizu, S.; Kikyotani, S.; Kayano, T.; Hirose, T.; Inayama, S.; et al., Cloning and sequence analysis of calf cDNA and human genomic DNA encoding alpha-subunit precursor of muscle acetylcholine receptor. *Nature* **1983,** 305, (5937), 818-23.
46. Smith, G. B.; Olsen, R. W., Functional domains of GABAA receptors. *Trends Pharmacol Sci* **1995,** 16, (5), 162-8.

47. Karlin, A., Emerging structure of the nicotinic acetylcholine receptors. *Nat Rev Neurosci* **2002,** 3, (2), 102-14.
48. Conti-Tronconi, B. M.; Raftery, M. A., The nicotinic cholinergic receptor: correlation of molecular structure with functional properties. *Annu Rev Biochem* **1982,** 51, 491-530.
49. Changeux, J. P.; Devillers-Thiery, A.; Chemouilli, P., Acetylcholine receptor: an allosteric protein. *Science* **1984,** 225, (4668), 1335-45.
50. Unwin, N., Acetylcholine receptor channel imaged in the open state. *Nature* **1995,** 373, (6509), 37-43.
51. Unwin, N., Structure and action of the nicotinic acetylcholine receptor explored by electron microscopy. *FEBS Lett* **2003,** 555, (1), 91-5.
52. Miyazawa, A.; Fujiyoshi, Y.; Unwin, N., Structure and gating mechanism of the acetylcholine receptor pore. *Nature* **2003,** 423, (6943), 949-55.
53. Sigel, E.; Buhr, A.; Baur, R., Role of the conserved lysine residue in the middle of the predicted extracellular loop between M2 and M3 in the GABA(A) receptor. *J Neurochem* **1999,** 73, (4), 1758-64.
54. Shan, Q.; Nevin, S. T.; Haddrill, J. L.; Lynch, J. W., Asymmetric contribution of alpha and beta subunits to the activation of alphabeta heteromeric glycine receptors. *J Neurochem* **2003,** 86, (2), 498-507.
55. Rovira, J. C.; Vicente-Agullo, F.; Campos-Caro, A.; Criado, M.; Sala, F.; Sala, S.; Ballesta, J. J., Gating of alpha3beta4 neuronal nicotinic receptor can be controlled by the loop M2-M3 of both alpha3 and beta4 subunits. *Pflugers Arch* **1999,** 439, (1-2), 86-92.
56. Rovira, J. C.; Ballesta, J. J.; Vicente-Agullo, F.; Campos-Caro, A.; Criado, M.; Sala, F.; Sala, S., A residue in the middle of the M2-M3 loop of the beta4 subunit specifically affects gating of neuronal nicotinic receptors. *FEBS Lett* **1998,** 433, (1-2), 89-92.
57. O'Shea, S. M.; Harrison, N. L., Arg-274 and Leu-277 of the gamma-aminobutyric acid type A receptor alpha 2 subunit define agonist efficacy and potency. *J Biol Chem* **2000,** 275, (30), 22764-8.
58. Lynch, J. W.; Rajendra, S.; Pierce, K. D.; Handford, C. A.; Barry, P. H.; Schofield, P. R., Identification of intracellular and extracellular domains mediating signal transduction in the inhibitory glycine receptor chloride channel. *Embo J* **1997,** 16, (1), 110-20.
59. Lewis, T. M.; Sivilotti, L. G.; Colquhoun, D.; Gardiner, R. M.; Schoepfer, R.; Rees, M., Properties of human glycine receptors containing the hyperekplexia mutation alpha1(K276E), expressed in Xenopus oocytes. *J Physiol* **1998,** 507 (Pt 1), 25-40.
60. Kusama, T.; Wang, J. B.; Spivak, C. E.; Uhl, G. R., Mutagenesis of the GABA rho 1 receptor alters agonist affinity and channel gating. *Neuroreport* **1994,** 5, (10), 1209-12.
61. Deane, C. M.; Lummis, S. C., The role and predicted propensity of conserved proline residues in the 5-HT3 receptor. *J Biol Chem* **2001,** 276, (41), 37962-6.
62. Davies, M.; Newell, J. G.; Dunn, S. M., Mutagenesis of the GABA(A) receptor alpha1 subunit reveals a domain that affects sensitivity to GABA and benzodiazepine-site ligands. *J Neurochem* **2001,** 79, (1), 55-62.
63. Campos-Caro, A.; Sala, S.; Ballesta, J. J.; Vicente-Agullo, F.; Criado, M.; Sala, F., A single residue in the M2-M3 loop is a major determinant of coupling between binding and gating in neuronal nicotinic receptors. *Proc Natl Acad Sci U S A* **1996,** 93, (12), 6118-23.
64. Bera, A. K.; Chatav, M.; Akabas, M. H., GABA(A) receptor M2-M3 loop secondary structure and changes in accessibility during channel gating. *J Biol Chem* **2002,** 277, (45), 43002-10.

65. Kash, T. L.; Jenkins, A.; Kelley, J. C.; Trudell, J. R.; Harrison, N. L., Coupling of agonist binding to channel gating in the GABA(A) receptor. *Nature* **2003,** 421, (6920), 272-5.
66. Lynch, J. W.; Han, N. L.; Haddrill, J.; Pierce, K. D.; Schofield, P. R., The surface accessibility of the glycine receptor M2-M3 loop is increased in the channel open state. *J Neurosci* **2001,** 21, (8), 2589-99.
67. Grosman, C.; Salamone, F. N.; Sine, S. M.; Auerbach, A., The extracellular linker of muscle acetylcholine receptor channels is a gating control element. *Journal of General Physiology* **2000,** 116, (3), 327-339.
68. Castillo, M.; Mulet, J.; Bernal, J. A.; Criado, M.; Sala, F.; Sala, S., Improved gating of a chimeric alpha7-5HT3A receptor upon mutations at the M2-M3 extracellular loop. *FEBS Lett* **2006,** 580, (1), 256-60.
69. Schimmel, P. R.; Flory, P. J., Conformational energies and configurational statistics of copolypeptides containing L-proline. *J Mol Biol* **1968,** 34, (1), 105-20.
70. MacArthur, M. W.; Thornton, J. M., Influence of proline residues on protein conformation. *J Mol Biol* **1991,** 218, (2), 397-412.
71. Chakrabarti, P.; Pal, D., The interrelationships of side-chain and main-chain conformations in proteins. *Prog Biophys Mol Biol* **2001,** 76, (1-2), 1-102.
72. Bhattacharyya, R.; Chakrabarti, P., Stereospecific interactions of proline residues in protein structures and complexes. *J Mol Biol* **2003,** 331, (4), 925-40.
73. Stewart, D. E.; Sarkar, A.; Wampler, J. E., Occurrence and role of cis peptide bonds in protein structures. *J Mol Biol* **1990,** 214, (1), 253-60.
74. Weiss, M. S.; Jabs, A.; Hilgenfeld, R., Peptide bonds revisited. *Nat Struct Biol* **1998,** 5, (8), 676.
75. Song, J.; Burrage, K.; Yuan, Z.; Huber, T., Prediction of cis/trans isomerization in proteins using PSI-BLAST profiles and secondary structure information. *BMC Bioinformatics* **2006,** 7, 124.
76. Pal, D.; Chakrabarti, P., Cis peptide bonds in proteins: residues involved, their conformations, interactions and locations. *J Mol Biol* **1999,** 294, (1), 271-88.
77. Jabs, A.; Weiss, M. S.; Hilgenfeld, R., Non-proline cis peptide bonds in proteins. *J Mol Biol* **1999,** 286, (1), 291-304.
78. Vanhoof, G.; Goossens, F.; De Meester, I.; Hendriks, D.; Scharpe, S., Proline motifs in peptides and their biological processing. *Faseb J* **1995,** 9, (9), 736-44.
79. Huang, G. C.; Zhou, J. M., The two slow refolding processes of creatine kinase are catalyzed by cyclophilin. *J Protein Chem* **2000,** 19, (4), 285-9.
80. Kamen, D. E.; Woody, R. W., Identification of proline residues responsible for the slow folding kinetics in pectate lyase C by mutagenesis. *Biochemistry* **2002,** 41, (14), 4724-32.
81. Kamen, D. E.; Woody, R. W., Folding kinetics of the protein pectate lyase C reveal fast-forming intermediates and slow proline isomerization. *Biochemistry* **2002,** 41, (14), 4713-23.
82. Kim, D. H.; Jang, D. S.; Nam, G. H.; Choi, K. Y., Folding mechanism of ketosteroid isomerase from Comamonas testosteroni. *Biochemistry* **2001,** 40, (16), 5011-7.
83. Slupsky, C. M.; Sykes, D. B.; Gay, G. L.; Sykes, B. D., The HoxB1 hexapeptide is a prefolded domain: implications for the Pbx1/Hox interaction. *Protein Sci* **2001,** 10, (6), 1244-53.

84. Stukenberg, P. T.; Kirschner, M. W., Pin1 acts catalytically to promote a conformational change in Cdc25. *Mol Cell* **2001,** 7, (5), 1071-83.
85. von Ahsen, O.; Lim, J. H.; Caspers, P.; Martin, F.; Schonfeld, H. J.; Rassow, J.; Pfanner, N., Cyclophilin-promoted folding of mouse dihydrofolate reductase does not include the slow conversion of the late-folding intermediate to the active enzyme. *J Mol Biol* **2000,** 297, (3), 809-18.
86. Reimer, U.; Fischer, G., Local structural changes caused by peptidyl-prolyl cis/trans isomerization in the native state of proteins. *Biophys Chem* **2002,** 96, (2-3), 203-12.
87. Keller, M.; Boissard, C.; Patiny, L.; Chung, N. N.; Lemieux, C.; Mutter, M.; Schiller, P. W., Pseudoproline-containing analogues of morphiceptin and endomorphin-2: evidence for a cis Tyr-Pro amide bond in the bioactive conformation. *J Med Chem* **2001,** 44, (23), 3896-903.
88. Mierke, D. F.; Nossner, G.; Schiller, P. W.; Goodman, M., Morphiceptin analogs containing 2-aminocyclopentane carboxylic acid as a peptidomimetic for proline. *Int J Pept Protein Res* **1990,** 35, (1), 35-45.
89. Yamazaki, T.; Probsti, A.; Schiller, P. W.; Goodman, M., Biological and conformational studies of [Val4]morphiceptin and [D-Val4]morphiceptin analogs incorporating cis-2-aminocyclopentane carboxylic acid as a peptidomimetic for proline. *Int J Pept Protein Res* **1991,** 37, (5), 364-81.
90. Nielsen, K. J.; Watson, M.; Adams, D. J.; Hammarstrom, A. K.; Gage, P. W.; Hill, J. M.; Craik, D. J.; Thomas, L.; Adams, D.; Alewood, P. F.; Lewis, R. J., Solution structure of mu-conotoxin PIIIA, a preferential inhibitor of persistent tetrodotoxin-sensitive sodium channels. *J Biol Chem* **2002,** 277, (30), 27247-55.
91. Feng, Y.; Hood, W. F.; Forgey, R. W.; Abegg, A. L.; Caparon, M. H.; Thiele, B. R.; Leimgruber, R. M.; McWherter, C. A., Multiple conformations of a human interleukin-3 variant. *Protein Sci* **1997,** 6, (8), 1777-82.
92. Halab, L.; Lubell, W. D., Use of Steric Interactions To Control Peptide Turn Geometry. Synthesis of Type VI beta-Turn Mimics with 5-tert-Butylproline. *J Org Chem* **1999,** 64, (9), 3312-3321.
93. Belec, L.; Slaninova, J.; Lubell, W. D., A study of the relationship between biological activity and prolyl amide isomer geometry in oxytocin using 5-tert-butylproline to augment the Cys(6)-Pro(7) amide cis-isomer population. *J Med Chem* **2000,** 43, (8), 1448-55.
94. Mallis, R. J.; Brazin, K. N.; Fulton, D. B.; Andreotti, A. H., Structural characterization of a proline-driven conformational switch within the Itk SH2 domain. *Nat Struct Biol* **2002,** 9, (12), 900-5.
95. Beausoleil, E.; LArcheveque, B.; Belec, L.; Atfani, M.; Lubell, W. D., 5-tert-butylproline. *Journal of Organic Chemistry* **1996,** 61, (26), 9447-9454.
96. Koskinen, A. M. P.; Rapoport, H., Synthesis of 4-Substituted Prolines as Conformationally Constrained Amino-Acid Analogs. *Journal of Organic Chemistry* **1989,** 54, (8), 1859-1866.

CHAPTER 4: FUCOSE-GALACTOSE IN LEARNING AND MEMORY

4.1 Introduction

4.1.1 Carbohydrates in neurological processes

Carbohydrates play important roles in numerous biological processes and recently, interest in identifying the biological functions of this class of biomolecule has intensified. Carbohydrates are ubiquitous in nature and structurally diverse, allowing for a broad range of biological functions. They facilitate proper protein localization as well as protein folding and stability.[1] Additionally they are critical to cell-cell communication events such as immune response,[2] microbial virulence,[3] and inflammation.[4] The surface of a cell is decorated with a variety of motifs that play a crucial role in mediating many biological processes—among these motifs are glycosylated lipids and proteins. These glycoconjugates serve as receptors and ligands, providing a structural link between a cell and its environment. The high complexity and heterogeneity of the adorning carbohydrates encode information, allowing cells to communicate.

Not surprisingly, extensive glycosylation has been found on the surface of nerve cells.[5, 6] Carbohydrates present at the synapse have various functions ranging from cell adhesion and axon pathfinding during brain development, to neurotransmitter reception and memory formation processes in mature synapses.[7] In particular, it has been shown that transmembrane glycoproteins containing sialyl or fucosyl epitopes play a role in neuronal processes.[6, 8] A well-studied example is neural cell adhesion molecule (NCAM), a member of the immunoglobulin superfamily which is glycosylated with polysialic acid (PSA) residues. NCAM is crucial in development and regeneration of the nervous system and is also involved in synaptic plasticity associated with learning and memory.[5, 8, 9] Interestingly, the PSA residues on NCAM greatly affect these neuronal processes. Enzymatic removal of

PSA on NCAM using endoneuraminidase (endo N), which selectively degrades PSA, perturbs neuron migration and axon outgrowth during development.[7, 10] Furthermore, injection of endo N into the hippocampus causes significant impairment of spatial memory and completely prevents induction of long term potentiation (LTP), a measure of learning and memory.[10]

4.1.2 Implications for fucosylation in learning and memory

Similar to sialyl epitopes, fucosyl epitopes have also been heavily implicated in neuronal processes such as development and learning and memory. Fucosylated glycoproteins are enriched in the central nervous system and account for as much as 85% of the protein-bound sugars in synaptic plasma membranes.[11] Altered fucosylation of brain glycoconjugates have been shown to play a role in the molecular mechanisms underlying long term memory formation and information processing. Studies have shown an increase in [^{3}H]-fucose incorporation into brain glycoproteins in rats during passive avoidance training tasks.[6, 12, 13] Increased fucose uptake into hippocampal and cortical glycoproteins has also been demonstrated in rats trained in a brightness discrimination task.[14, 15] Furthermore, increased fucosylation was associated with increased activity of fucokinase, an enzyme involved in fucose activation prior to the fucosylation step in a variety of species, including both rats and chicks.[16] Not only has an increase in fucosylation been seen during particular training tasks, but treatment with fucose has been shown to cause an increase in LTP, which is correlated with synaptic strength.[17, 18]

If fucosylation is necessary for the process of memory formation, then inhibition of fucosylation might be expected to disrupt this process. Indeed this is the case. Fucose plays

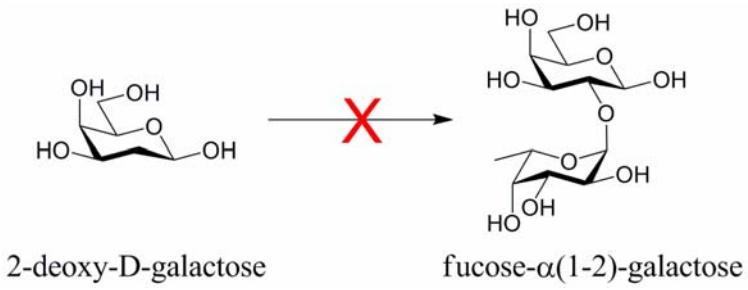

Figure 4.1. 2-Deoxy-D-galactose inhibits fucosylation by competition with galactose for incorporation into oligosaccharaides. The lack of a C-2 hydroxyl group prevents the formation of the α(1-2) glycosidic linkage.

a major role as a terminal sugar in glycoproteins and is often covalently linked to galactose by a 1-2 glycosidic linkage. If galactose is replaced by 2-deoxy-D-galactose, the 1-2 linkage cannot be formed, due to the lack of a C-2 hydroxyl, and fucosylation is inhibited (Figure 4.1). Intracerebral injection of 2-deoxy-D-galactose into the brains of rats and chicks exerts amnesic effects during passive avoidance training tasks—further implicating fucose in learning and memory.[19-22] 2-Deoxy-D-galactose has also been shown to decrease levels of [^{3}H]-fucose incorporation into neuronal glycoproteins.[22] In addition, blocking the fucose-α(1-2)-galactose epitope using an antibody against fucose-α(1-2)-galactose also results in loss of memory in rats.[23]

Taken together, evidence overwhelmingly implicates fucose in memory formation. Despite the evidence, the exact molecular role of fucose is not known and neuronal glycoproteins bearing this epitope have not been identified. Carbohydrate binding proteins (i.e. lectins) to fucose-α(1-2)-galactose epitopes in the brain also have not been identified. In summary, the molecular mechanisms surrounding the role of fucose have not been determined.

4.1.3 Challenges and chemical methodologies in carbohydrate research

Despite the overwhelming evidence demonstrating the involvement of carbohydrates in a vast number of biological systems and processes, elucidation of the molecular basis of their function has been slow relative to studies of proteins and nucleic acids. The study of carbohydrates in biological processes poses numerous challenges due to the high complexity and heterogeneity of carbohydrates found in biological systems. Furthermore, the biosynthesis of carbohydrates is not template driven nor under direct translational control, unlike other biopolymers; therefore, carbohydrates can be highly heterogeneous making it difficult to perform structure-function studies using conventional genetic manipulations. Adding to this complexity is the ability for carbohydrates to undergo further modifications such as sulfation. These modifications are also not directly encoded genetically. Consequently, it has proven to be very difficult to delineate the effects of these modifications on the overall biological function of the carbohydrate. Evidence suggests that minor changes in how the carbohydrate is presented (i.e., type of carbohydrate and sulfation pattern) on the protein have significant consequences to the biological activity of the glycosylated protein so it of great interest to develop methods for the structure-function studies of carbohydrates.

Another challenge in the study of carbohydrates arises from the fact that glycosyltransferases, enzymes that catalyze the transfer of a carbohydrate monomer unit to a protein or another carbohydrate molecule, are fairly promiscuous. The ability for glycosyltransferases to recognize multiple substrates further complicates their study since the removal of a glycosyltransferase by genetic knock out methods can result in lethality or deleterious effects to other biological processes within a system.

Despite the challenges in carbohydrate research, some progress has been made toward

novel methodologies that have allowed for the study of carbohydrates and their role in biological processes. While enzymatic and genetic methods have contributed considerably to functional studies of carbohydrates, chemical tools have proven to be invaluable to glycobiology. For biochemical studies, homogeneous populations of carbohydrates have been obtained using chemical and bioenzymatic synthesis.[24-28] While the chemical synthesis of carbohydrates, especially of larger oligosaccharides, is generally seen as extremely formidable, it affords greater flexibility than enzymatic means. It also allows one to obtain homogeneous carbohydrate samples of well-defined structure and modification.

Chemical methods have also been used in the development of other tools in glycobiology. For example, chemical strategies have been used to inhibit the synthesis or function of specific oligosaccharides and glycoconjugates.[29-34] The inhibition of the synthesis of specific glycoconjugates allows one to ascertain its biological role. Additionally, chemical methods have been used generate probes and scaffolds aimed at studying lectins that recognize glycoconjugates.[35-38] They have also been used in the development of unnatural metabolic substrates that allow for the biosynthetic engineering of cell surface glycoconjugates, termed metabolic oligosaccharide engineering. This particular method has been used to disrupt carbohydrate synthesis, probe metabolic pathways, and to identify lectins/glycoproteins.

Clearly, chemical tools have played and will continue to play a critical role in glycobiology. The coupling of developing chemical strategies with advancing biochemical and genetic methodologies will provide invaluable tools to address challenges in carbohydrate research.

4.2 Experimental design

4.2.1 Proposed models for fucose involvement in memory formation

We propose several models as to how fucose may be involved in memory formation. It is possible that fucose-α(1-2)-galactose serves to mediate protein-protein interactions between a fucose-α(1-2)-galactose lectin and the cognate glycoprotein at the cell surface (figure 4.2, mechanism A). Alternatively, the fucose-α(1-2)-galactose epitope may be acting to target proteins to specific subcellular compartments (figure 4.2, mechanism B). These two mechanisms could also be working in concert as a feedback loop to recruit more fucosyl glycoproteins to the cell surface. Finally, it is also possible that fucosyl lectins and/or glycoproteins act intracellularly in signaling pathways responsible for memory formation (figure 4.2, mechanism C).

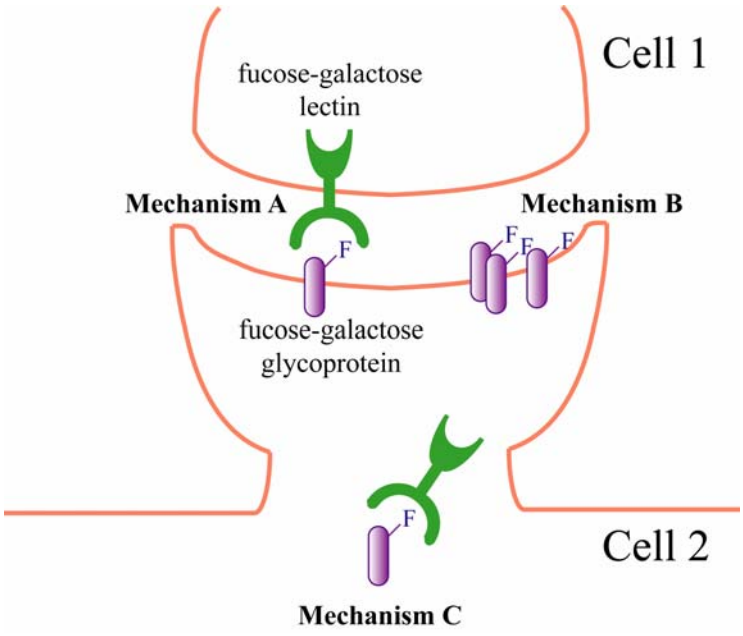

Figure 4.2. Model of how fucosyl saccharides may play a role in learning and memory. Mechanism A) Fucose-galactose glycoproteins are presented at the surface and mediate interactions through binding to a lectin. Mechanism B) Fucose-galactose glycoproteins act as a targeting element to recruit more fucosyl glycoproteins to the surface. Mechanism C) Fucose-galactose glycoproteins and their binding partners act intracellularly during memory formation.

Identification of the fucose-α(1-2)-galactose bearing glycoproteins as well as their binding counterpart proteins may provide new insights into the molecular mechanisms underlying memory formation. Furthermore, identification of these proteins would allow for more detailed study of the role of fucose in learning processes. This research describes efforts to isolate and identify fucose-α(1-2)-galactose bearing glycoproteins as well as fucose-α(1-2)-galactose binding proteins. Molecular techniques such as immunoprecipitation will be employed to isolate fucose-α(1-2)-galactose bearing glycoproteins, while chemical probes will be used to isolate fucose-α(1-2)-galactose binding proteins.

4.2.2 Identification of fucose-α(1-2)-galactose binding proteins with chemical probes

Chemical probes have emerged as a powerful tool to study protein-substrate interactions.[39] The modification of substrates to incorporate "tagging" groups allows for the visualization, tracking, or isolation of enzymes/proteins of interest. We have designed two chemical probes for the purpose of studying and identifying fucose-α(1-2)-galactose binding

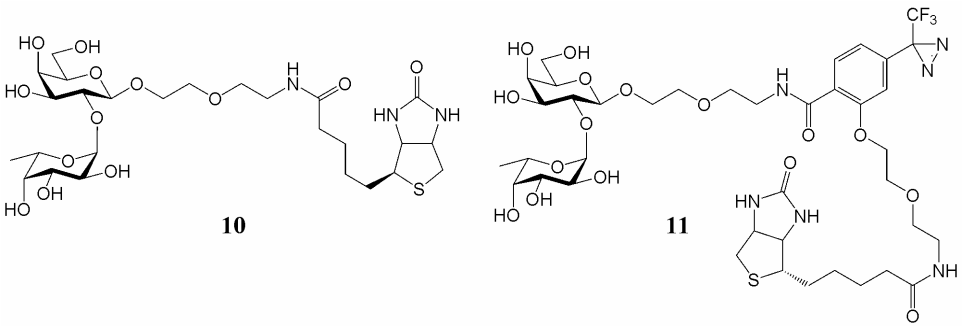

Figure 4.3. Probe **10** contains a fucose-α(1-2)-galactose recognition element and biotin moiety. Photoactivatible probe **11** also contains a photoreactive diazirine group for chemical crosslinking to target proteins.

proteins in the brain (figure 4.3). Probe **10** was synthesized to establish whether fucose-α(1-2)-galactose binding proteins exist in the brain. Probe **11** was synthesized to isolate fucose-α(1-2)-galactose binding proteins.

*4.2.2.1 Design of probe **10***

The design of the probe **10** incorporated two main features: (1) a fucose-α(1-2)-galactose epitope for protein binding, and (2) a biotin moiety for neuron imaging using dye-conjugated streptavidin (figure 4.3A). The two elements are connected via a hydrophilic linker to increase the solubility of the molecule under physiological conditions. The fucose-α(1-2)-galactose epitope was chosen as the recognition element over the monosaccharide and trisaccharide because evidence has strongly implicated the disaccharide and has not conclusively implicated the trisaccharide. The design of probe **10** is modular such that different linkers and reporter groups can be incorporated without major revisions to the overall synthesis.

*4.2.2.2 Design of photoreactive crosslinking probe **11***

Probe **11** was designed for the purpose of isolating fucose-α(1-2)-galactose binding proteins present in the brain (figure 4.3B). In addition to the fucose-α(1-2)-galactose epitope and biotin moiety found in **10**, probe **11** contains a 3-trifluoromethyl-3-phenyldiazirine (TPD) moiety, allowing for chemical crosslinking to capture the target protein(s). By forming a covalent linkage to the proteins of interest, the protein-probe complex can withstand rigorous washing in the purification process. Similar to probe **10**, the synthetic design is very modular such that different analogs can be readily made, if needed. For

example, the linker arm length or crosslinking moiety could easily be changed without the necessity of redesigning the overall synthesis. This convergent synthesis combines the power of photoaffinity crosslinking with the advantages of a biotin-avidin system.

Photoaffinity labeling is a well-established technique to elucidate ligand-biomolecule interactions. This technique has been used to successfully label enzymes, membranes, protein structures, neural receptors and RNA/DNA structures.[40-46] Typically, the substrate is modified to bear the photoreactive element, and radiolabels are incorporated to allow for the identification of the binding site. The covalently labeled enzyme/protein can also be visualized with a variety of other techniques such as spectroscopic analysis and fluorophore methods.[40]

Combining the power of photoaffinity labeling with the advantages of biotinylating substrates creates a chemical probe that allows for a covalent bond to be formed between the enzyme and the substrate, as well as a handle to isolate the complex with the use of immobilized avidin. The photoreactive element is anticipated to overcome weak binding affinities between the protein and substrate, which has been reported for a variety of lectins.[47] The biotin moiety also offers the advantage of sensitive, non-radioactive detection of labeled protein using streptavidin-conjugated-horseradish peroxidase (HRP). A variety of biotinylated photoreactive probes have been synthesized and successfully used to study and isolate protein-substrates. Probes ranging from biotinylated photoactivated γ-secretase[48] inhibitors to bis-mannose photolabels to study glucose transporter isoform 4 (GLUT4)[49] have been synthesized.

For the photoreactive crosslinking moiety, we selected the diazirine group over benzophenone, phenylazides and other photoaffinity labels for several reasons. First, unlike

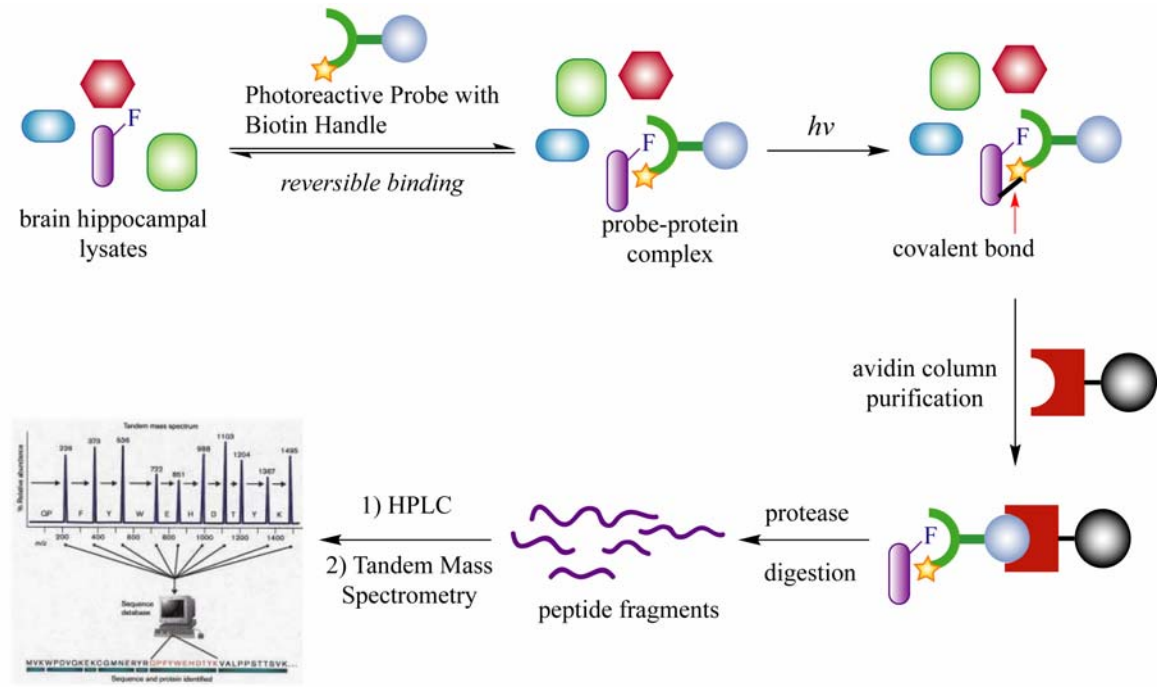

Figure 4.4. Schematic of how compound **11** can be used to isolate and identify fucose-α(1-2)-galactose binding proteins. Brain lysates would be incubated with photoreactive probe **11**. Photo-induced crosslinking results in the formation of a covalent bond between fucose-α(1-2)-galactose binding proteins and **11**. The biotin handle of **11** will allow for the purification of the crosslinked complexes using avidin-agarose. The recovered fucose-α(1-2)-galactose binding proteins can then be identified using tandem mass spectrometry.

phenyl azides, the activation of TPD occurs at 353 nm, which is out of range for protein damage. Photoactivation of diazirines at 353 nm generates a highly reactive triplet carbene species that has been shown to undergo efficient O-H and C-H insertion. The carbene intermediate of the TPD is also more reactive than the nitrene intermediate of phenyl azides. Second, while the activation of benzophenone is above 300 nm, the TPD is small and nonbulky. Furthermore, TPD has relative thermal stability as well as stability to moderately acidic (1N HCl) conditions and moderately basic conditions (1 N NaOH).[50] It has also been shown to be inert to reducing agents, whereas phenylazides are rapidly reduced by reducing agents such as DTT. Given the stability of TPD, it is expected to be stable to conditions

anticipated in biochemical labeling studies.[50]

The strategy for the isolation and identification of fucose-α(1-2)-galactose binding proteins, using photoreactive probe **11** is depicted in Figure 4.4. Rat hippocampal lysates would be incubated with **11** and irradiated with 353 nm light to activate the diazirine moiety for crosslinking to bound proteins. The crosslinked complex would then be isolated using immobilized streptavidin, followed by digestion with proteases and sequencing by tandem mass spectrometry.

4.2.3 Identification of fucose-α(1-2)-galactose bearing proteins with immunoprecipitation

The second portion of the described research was aimed at identifying glycoproteins bearing fucose-α(1-2)-galactose epitopes in neurons. The availability of antibodies specific towards fucose-α(1-2)-galactose carbohydrates allowed for the use of standard molecular biology techniques to detect fucose-α(1-2)-galactose glycoproteins in a variety of studies. The research herein describes preliminary efforts to study fucose-α(1-2)-galactose glycoproteins in neurons using antibodies.

4.3 Results

*4.3.1 Synthesis of Probe **10***

Synthesis of probe **10** began with construction of the disaccharide moiety (figure 4.5). Synthesis of the disaccharide was performed using methods reported by Wegmann, et al.,[51] with some modifications. The synthesis started with treatment of commercially available L-fucose **1** with acidic ion-exchange resin in refluxing methanol to form the methyl glycoside.[52] Benzylation[53, 54] followed by hydrolysis[55] gave **2**, which was then transformed

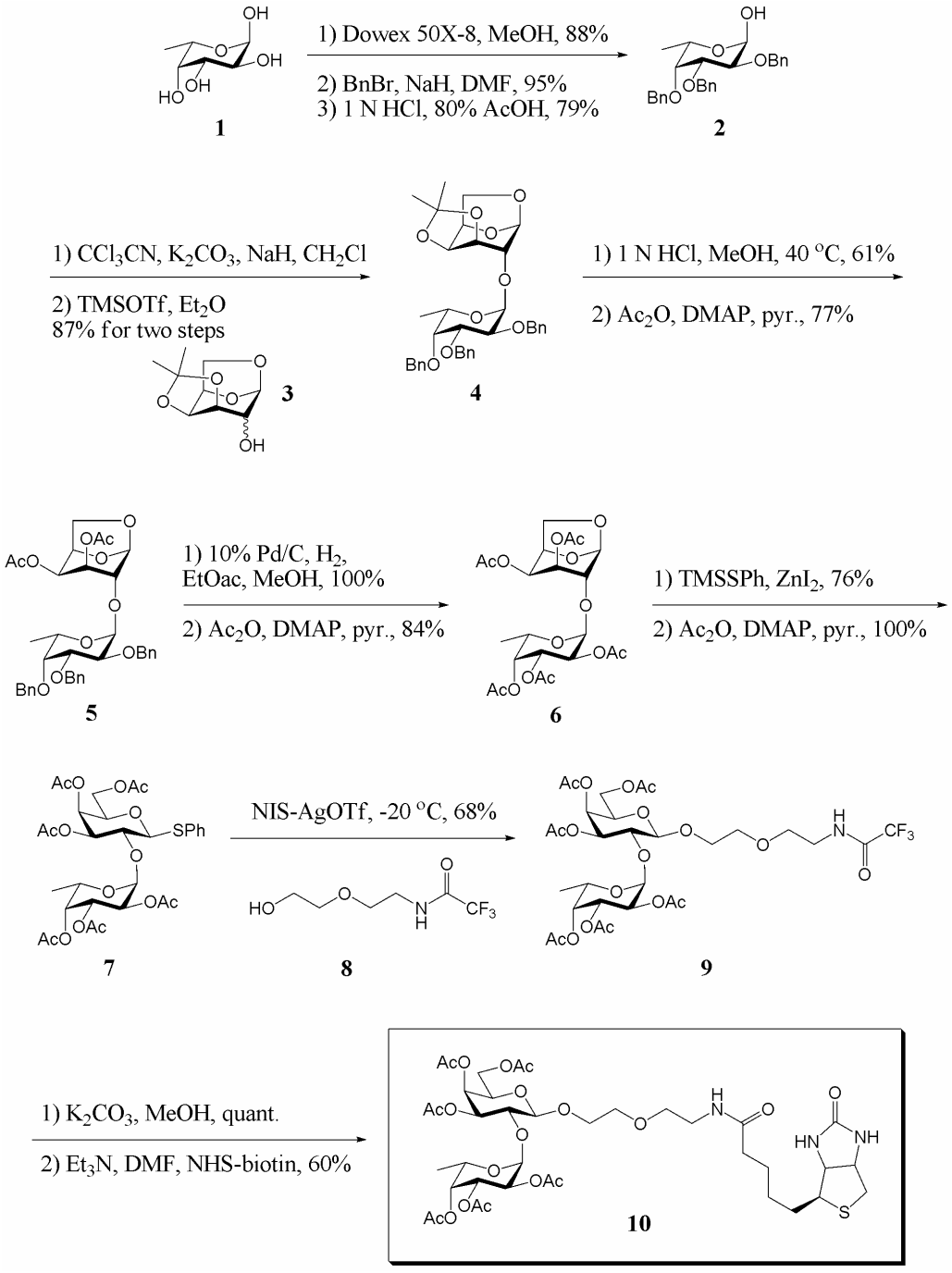

Figure 4.5. Synthesis of probe **10.**

to the corresponding imidate using sodium hydride and trichloroacetonitrile.[56] Attempts to isolate the imidate were unsuccessful due to its susceptibility to hydrolysis. Therefore, the crude product was used in subsequent reactions without further purification. Treatment of

the crude α-imidate and 1,6-anhydro-3,4-isopropylidene-β-D-galactose **3** with trimethylsilyl trifluoromethanesulfonate (TMSOTf) in diethyl ether afforded the disaccharide with the desired α(1-2) glycosidic linkage in 87% yield. At this stage, attempts to deprotect the acetonide group and debenzylate in one step, using standard hydrogenolysis conditions doped with palladium (II) chloride were unsuccessful. Consequently, **4** was treated with 1 N hydrochloric acid and gentle heating to remove the acetonide, and acetylated using acetic anhydride to yield **5**. Debenzylation of **5** followed by acetylation gave **6,** which was then transformed to the β-thioglycoside using the conditions of Motawia et al.[57] This involved treatment of **6** with (phenylthio)trimethylsilane and zinc iodide to open the anhydro ring to form the thioglycoside, followed by acetylation to afford **7**. With the peracetylated thioglycoside in hand, **9** was readily obtained by coupling **7** and **8** using *N*-iodosuccidimide (NIS) and silver triflate.[58] Complete deprotection of **9** using potassium carbonate[59] followed by addition of *N*-hydroxysuccinimide (NHS) biotin under basic conditions yielded the desired product **10**.

4.3.2 Biological studies using probe 10: Imaging hippocampal neurons

With probe **10** in hand, we began the first round of biological experiments to determine whether fucose-α(1-2)-galactose binding proteins were present in the brain. Probe **10** was used to image neurons to examine the subcellular localization of fucose-α(1-2)-galactose binding proteins. The biotin moiety allowed for fluorescence microscopy using streptavidin-dye conjugates (Molecular Probes). Fluorescence microscopy, done by Cristal Gama (Hsieh-Wilson Lab, California Institute of Technology, Pasadena, CA), of cultured neurons incubated with 10 mM solutions of **10** revealed fucose-α(1-2)-galactose binding

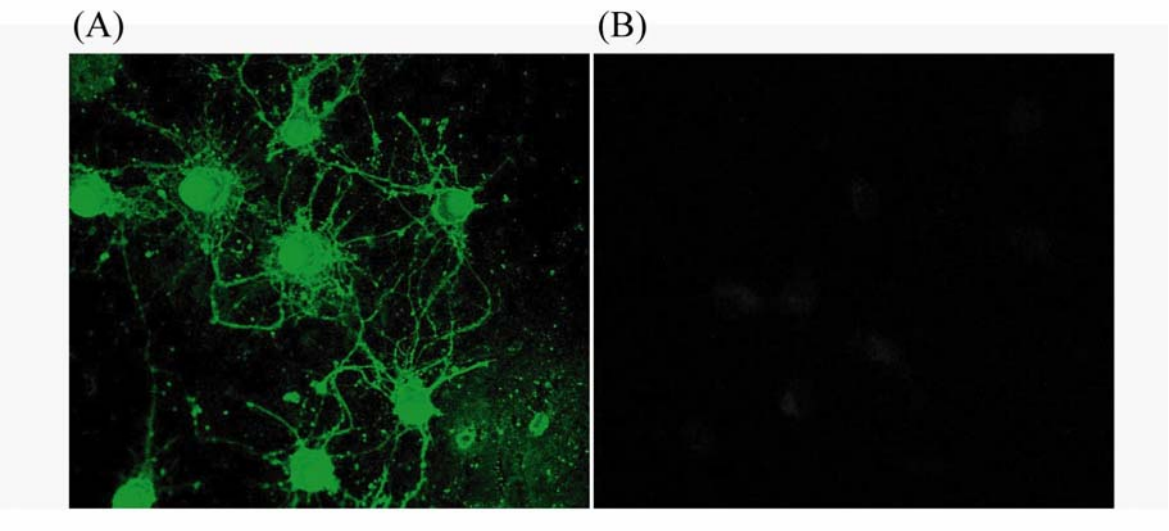

Figure 4.6. Probe **10** binds to cultured hippocampal neurons. A) Cultured embryonic rat hippocampal neurons incubated with probe **10** and treated with streptavidin-dye conjugate and imaged using confocal fluorescence microscopy. B) Cultured embryonic rat hippocampal neurons incubated with streptavidin-dye conjugate as a negative control. (Cristal Gama, Hsieh-Wilson Laboratory).

proteins on the surface of neurons (figure 4.6A). Neurons incubated with biotin and imaged with streptavidin dye-conjugate showed little to no staining, indicating that the binding of the probe was due to the fucose-α(1-2)-galactose epitope (figure 4.6B). These fluorescence microscopy images therefore strongly suggest the presence of fucose-α(1-2)-galactose binding proteins in the brain.

4.3.3 Synthesis of capture probe 11

Synthesis of the capture probe **11** was achieved using methods described by Hatanaka *et al* (figure 4.7).[60, 61] 3'-Bromoanisole was converted to the corresponding Grignard reagent and reacted with *N*-(trifluoroacetyl)piperidine[62] to afford **12**. Treatment of the trifluoroacetophenone with hydroxylamine hydrochloride yielded the oxime **13**, which was then transformed to the diaziridine with *p*-toluenesulfonyl chloride followed by treatment

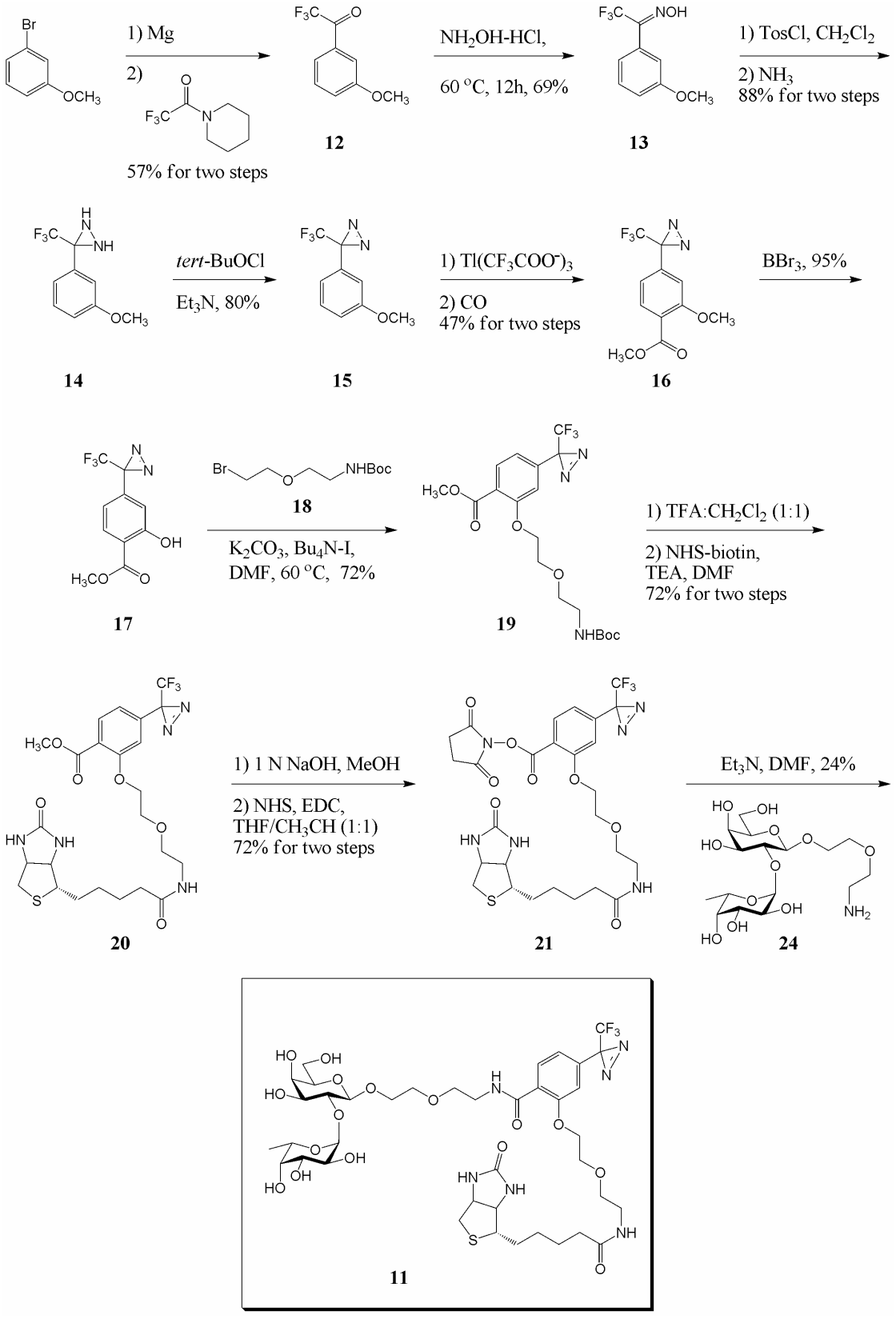

Figure 4.7. Synthesis of photoreactive probe **11.**

with liquid ammonia. The diazirine **15** was obtained with 80% yield via oxidation of **14** with *tert*-butyl hypochlorite.[63] UV spectrophotometry was used to monitor formation of the diazirine structure, which shows an absorption band at approximately 350 nm (whereas the diazo isomer absorbs at around 450 nm). Carboxylation of **15** was performed using conventional thallation conditions, using thallium (III) trifluoroacetate, followed by palladium-catalyzed carboxylation to afford **16**. Because thallium compounds are known to be very toxic, thallations were performed in a glove box with all necessary safety precautions to prevent exposure and contamination. Carboxylations with carbon monoxide were performed in a well-ventilated hood. Demethylation of **16** with boron tribromide afforded **17** in 95% yield. With **17** in hand, all the necessary components of the full probe were ready for the final couplings, using procedures reported by Hatanaka et al.[61]

Alkylation of **17** with linker arm, **18**, was performed using tetrabutylammonium iodide and potassium carbonate to afford **19**. The synthesis of **18** was adapted from previously reported procedures (figure 4.8).[61] Boc-deprotection of **19** with trifluoroacetic acid followed by amide bond coupling to NHS-biotin afforded **20**, which was readily converted to the NHS ester **21** via saponification and reaction with NHS and EDC. The desired capture probe was obtained using conventional amide bond coupling conditions between **21** and **24**. **24** was obtained from complete deprotection of **9** using potassium

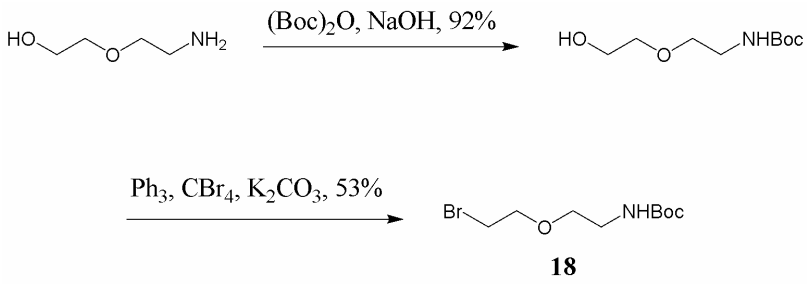

Figure 4.8. Synthesis of PEG linker **18**.

carbonate.

*4.3.4 Biological studies using capture probe **11***

4.3.4.1 General

Once probe **11** was synthesized, a series of experiments were performed to establish the potential of **11** as a suitable means to isolate fucose-α(1-2)-galactose binding proteins. Initial experiments were aimed at examining the binding potential of **11** to fucose-α(1-2)-galactose binding proteins in embryonic rat hippocampal neurons and adult rat hippocampal neurons. Subsequently, a series of experiments were performed to assess the ability for **11** to be used in the isolation of fucose-α(1-2)-galactose binding proteins from lysates. Lastly, competition experiments were performed to establish the binding specificity of **11** via its fucose-α(1-2)-galactose epitope.

*4.3.4.2 Binding potential of probe **11** to fucose-α(1-2)-galactose binding proteins in cultured embryonic rat hippocampal neurons*

Initial experiments using **11** were aimed at determining the potential of **11** as a probe for fucose-α(1-2)-galactose binding proteins before using larger amounts to isolate target proteins. Neurons cultured on coverslips (provided by Cristal Gama, Hsieh-Wilson laboratory) were incubated overnight with a 10 mM solution of **11**. The media was removed and the cells were washed with PBS and then irradiated on ice in PBS, using a handheld 18 W long wavelength UV lamp (365 nm). As a control sample, photolysis of **11** in PBS was monitored by UV. After 2 h of irradiation, a decrease in the absorbance at 350 nm indicated a complete photoactivation of the diazirine moiety (figure 4.9). The cells were removed from

the coverslips and lysed in denaturing sample buffer. Cell lysates were resolved by SDS-PAGE and transferred to PVDF membrane. The membrane was then incubated with strepavidin conjugated to HRP followed by chemiluminescent detection of the photolabeled proteins. Results indicated a potential fucose-α(1-2)-galactose binding protein at approximately 68 kDa (figure 4.9). As a control, cultured hippocampal neurons on coverslips were also incubated with methyl ester **20** (figure 4.7) to determine nonspecific binding of proteins to the probe (figure 4.9, lane 2). Two bands appear at a molecular weight slightly less than that seen with probe **11** (figure 4.9, lane 1). No endogenous streptavidin-

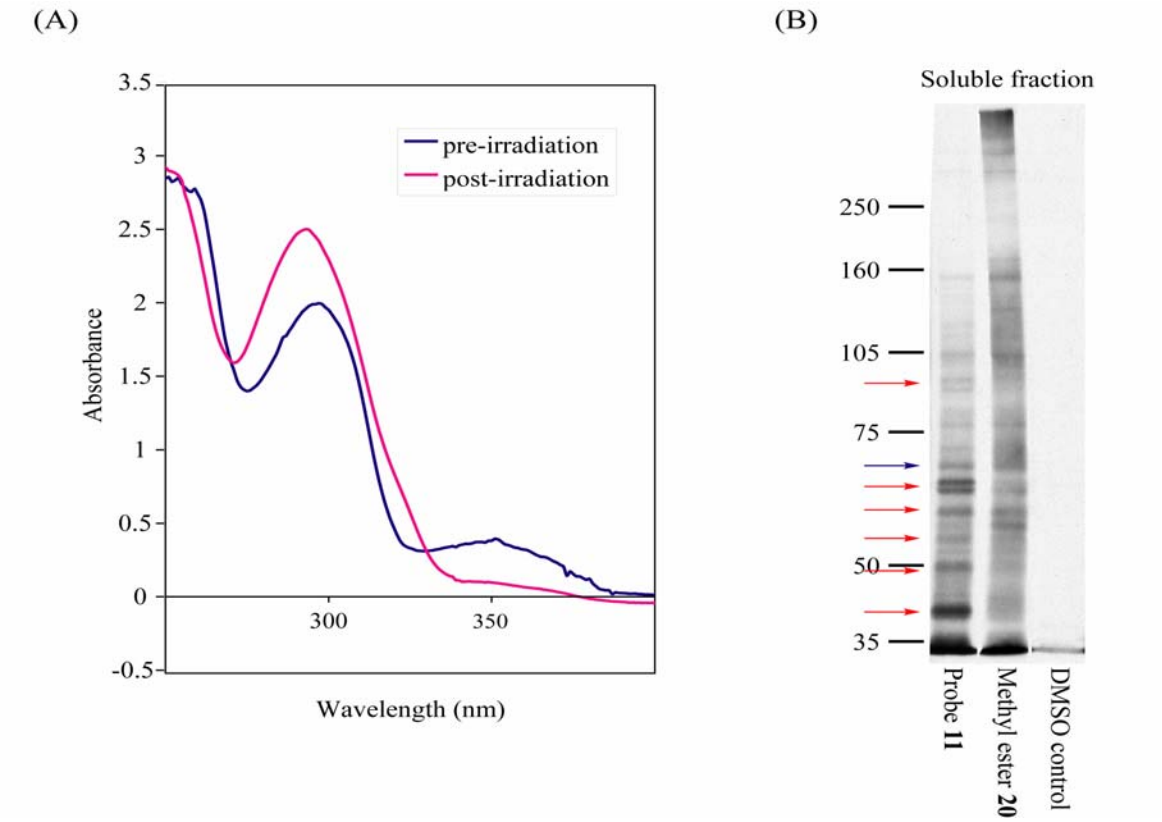

Figure 4.10. A) UV-vis spectrum of probe **11** prior to irradiation and after 4 hours of irradiation. A decrease in absorbance at 350 nm indicates photolyzed product. B) Western blot detection of crosslinked proteins with probe **11** in the soluble fraction of adult rat hippocampal lysates. The blue arrow indicates protein band that was also detected in cultured embryonic rat hippocampal neurons. Note: the exposure time of the methyl ester **20** control lane was 15 s whereas the probe **11** lane and the DMSO control lane have an exposure time of 15 min.

binding proteins were detected from neurons incubated with DMSO (figure 4.9, lane 3). Probing neuons with **11** appears to be sufficient to selectively crosslink to potential proteins of interest with a bit of nonspecific binding as seen probing with compound **20**.

*4.3.4.3 Binding potential of probe **11** to fucose-α(1-2)-galactose binding proteins in adult rat hippocampal neurons*

We also examined whether probe **11** could capture proteins from adult rat hippocampal lysates. Using adult rat hippocampal lysates offers the advantage of a greater amount of total protein over cultured rat embryonic neurons. Briefly, the soluble (S2) protein fraction derived from adult rat hippocampal lysates was incubated with 1 mM of **11** and then irradiated on ice with UV light (365 nm). Again, the photolysis of **11** was monitored by UV, which indicated complete photoactivation after 4 h of irradiation. The samples were then resolved by SDS-PAGE, transferred to PVDF membrane, and probed with streptavidin-HRP. Similar controls were done with methyl ester **20** and DMSO to detect nonspecific binding proteins. Results showed a similar molecular weight band at ~68 kDa to that seen with cultured embryonic hippocampal neurons (figure 4.10, indicated by blue arrow). Additionally, several other protein bands at ~38 kDa, 50 kDa, 58 kDa, 63 kDa, 65 kDa, and 85 kDa (figure 4.10, red arrows) were detected. Comparison with the methyl ester **20** shows that the capture probe has captured proteins of molecular weights that are not seen with the methyl ester. As previously observed, the DMSO control had no detectable levels of endogenous streptavidin-binding proteins. As compared to probing experiments done with cultured neurons on coverslips, there were a greater number of detected proteins in the rat hippocampal lysates. Interestingly, the methyl ester also detected/crosslinked more proteins

in the adult rat hippocampal lysates than in the case of cultured embryonic hippocampal neurons.

*4.3.4.4 Isolation of fucose-α(1-2)-galactose binding proteins in adult rat hippocampal lysates using Probe **11***

Following initial crosslinking experiments, we attempted to isolate the probe-protein complexes using streptavidin-agarose (UltraLink, Pierce, Rockford, IL). As in previous experiments, the soluble protein fraction from adult rat hippocampal lysates was incubated with probe **11** and then irradiated for 4 h. The irradiated lysates were incubated with streptavidin-agarose beads and then the beads were washed to remove unbound proteins. The bound proteins were then eluted by boiling under denaturing conditions, resolved by SDS-PAGE, and subjected to Western blot analysis. Several attempts to remove proteins from the streptavidin-agarose were unsuccessful (data not shown). It is likely that boiling under denaturing conditions was not sufficient to disrupt the high binding affinity between biotin and streptavidin ($K_a \cong 10^{15}$ M). Therefore, attempts to pull down "captured" proteins were carried out using avidin-agarose. The release of biotinylated substrates from avidin-agarose (Sigma, St. Louis, MO) by boiling under denaturing conditions has been well precedented in the literature.[48] Furthermore, UltraLink strepavidin-agarose contains twice the number of biotin-binding sites which may result in a stronger binding affinity due to multivalency. Elution conditions were also modified such that the bound proteins were eluted by boiling under denaturing conditions in the presence of 1000-fold excess of free biotin. If high temperature is not sufficent to completely disrupt biotin-avidin through denaturation, the free biotin would compete for avidin-binding with the photolabeled

proteins—thus, fewer photolysed proteins would return to a bound state on the avidin-agarose.

The soluble protein fraction from adult rat hippocampal lysates was incubated with probe **11**, irradiated for 4 h, and then incubated with avidin-agarose. The beads were then washed to remove unbound proteins. Subsequently, bound proteins were eluted using the modified eluction conditions, resolved by SDS-PAGE, and subjected to Western blot analysis. Western blot analysis of the eluted proteins indicated a faint band at around 58 kDa, which is also seen in the irradiated samples that were not isolated by avidin-agarose purification (figure 4.11, Lane 3, 7). A control with DMSO detected few endogenous avidin-binding proteins (figure 4.11, Lane 8). To ensure the elution conditions were capable of eluting bound proteins from the avidin-agarose, the pull-down experiment was also done with biotinylated bovine serum albumin (BSA). Similar to the irradiated lysates, biotinylated BSA was incubated with avidin-agarose. The beads were washed and bound proteins were eluted using the modified elution conditions, resolved by SDS-PAGE, followed by Western blot analysis. Results from the pull down of biotinylated BSA indicated that the elution conditions were sufficient to disrupt the biotin-avidin affinity and remove bound proteins (figure 4.11, Lane 5, 6).

In addition to pull-down experiments using probe **11**, boiled lysates were also incubated with probe **11** to compare them to unboiled lysates incubated with **11**. Lysates were boiled for 10 min to denature the proteins and then cooled back to room temperature. Subsequently, the boiled proteins were incubated with probe **11**, irradiated for 4 h, and then subjected to Western blot analysis. Similarly, unboiled lysates were treated with probe **11.** DMSO controls were also done with boiled and unboiled lysates. Unboiled lysates incubated

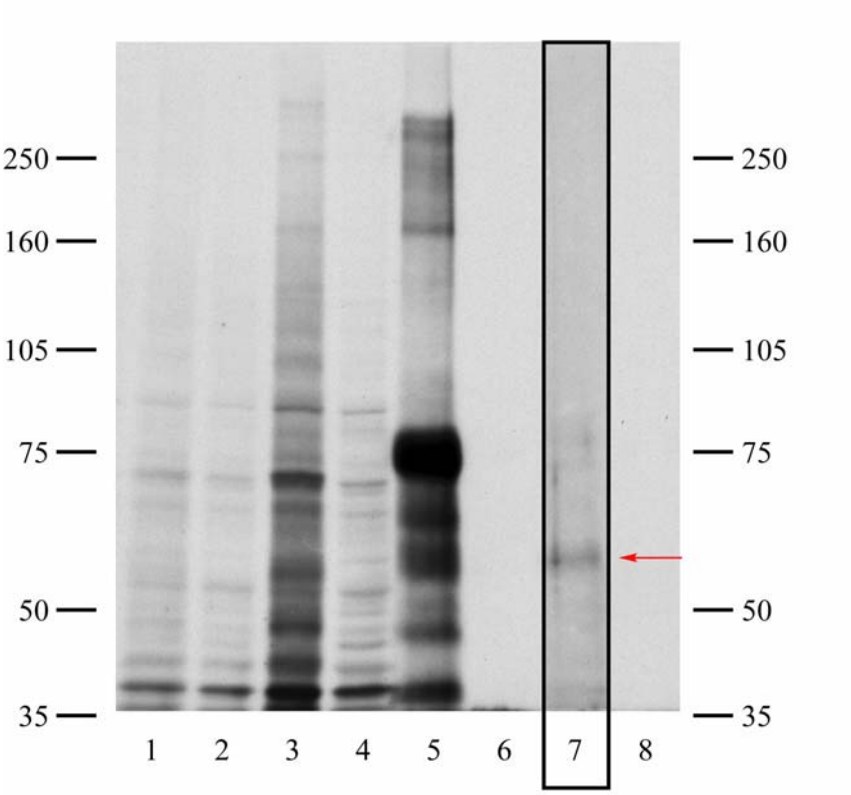

Figure 4.11. Western blot analysis of crosslinked proteins using probe **11** from adult rat hippocampal lysates. Lane 1: 75 μg of boiled adult rat hippocampal lysates with probe **11**; Lane 2: 75 μg of boiled adult rat hippocampal lysates with DMSO; Lane 3: 75 μg of unboiled adult rat hippocampal lysates with probe **11**; Lane 4: 75 μg of unboiled adult rat hippocampal lysates with DMSO; Lane 5: isolated biotinylated BSA using avidin-agarose; Lane 6: avidin-agarose in absence of biotinylated BSA; Lane 7: crosslinked protein complexes with probe **11** from adult rat hippocampal lysates isolated using avidin-agarose; Lane 8: adult rat hippocampal lysates incubated with avidin-agarose. Note: the exposure time for Lane 7 is 12 h while Lanes 1-6, 8 have an exposure time of 1 h.

with probe **11** resulted in bands at similar molecular weights seen in previous experiments (figure 4.11, Lane 3). The boiled lysates treated with probe **11** showed very few bands and are similar to both DMSO controls (figure 4.12, Lane 1, 2, 4). It is likely that the boiling process denatured the proteins, thereby causing loss of function. The observation that binding ability to the fucose-α(1-2)-galactose epitope in probe **11** is lost upon denturing the proteins strongly suggests that the binding to fucose-α(1-2)-galactose is specific. It is

expected then that the results of the boiled lysates incubated with probe **11** would be similar to the DMSO controls. These results were exciting because it demonstrated a loss of function of fucose-galactose binding proteins under denaturing conditions. The presence of bands in the DMSO controls suggests that avidin-agarose is less efficient at removing endogenous streptavidin/avidin-binding proteins, than streptavidin-agarose (which was used to preclear lysates in previous experiments). As a result, future experiments were done using lysates precleared with streptavidin-agarose.

*4.3.4.5 Competition experiments of probe **11** with O-ethyl-fucose-α(1-2)-galactose in adult rat hippocampal lysates*

To further confirm that binding of proteins to probe **11** was due to specificity with the disaccharide moiety, the *O*-ethyl-fucose-α(1-2)-galactose **23** was synthesized. Competition experiments using 1000-fold excess of **23** compared to probe **11** should allow us to determine which proteins are specifically binding to the fucose-α(1-2)-galactose moiety on the probe. Compound **23** was synthesized from the peracetylated thioglycoside **22** (figure 4.12) by treatment of **7** with *N*-iodosuccinimide and silver triflate.[57] Deacetylation of **22** using sodium methoxide in methanol afforded the desired compound **23** in a 1:2 (α:β) ratio. Only the

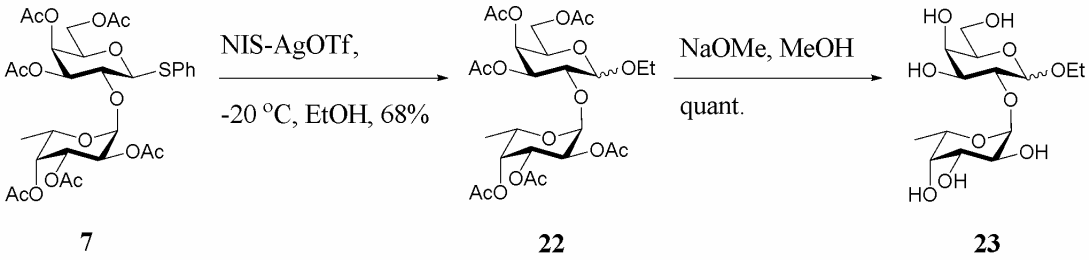

Figure 4.12. Synthesis of *O*-ethyl fucose-α(1-2)-galactose.

β–product was used for the competition experiments. With **23** in hand, the preliminary competition experiments were performed. The soluble protein fraction from adult rat hippocampal lysates was preincubated for 4 h with 1000-fold excess (compared to amount of **11** added later) of **23**. Probe **11** was then added to the mixture and incubated for 8 h, and irradiated. The lysates were then resolved by SDS-PAGE and subjected to Western blot analysis. The same amount of total lysate used in the competition experiment was also incubated with probe **11** to allow for a direct comparison of the intensities for each protein band. A DMSO control was also done with the same amount of total lysate. Results from a preliminary competition experiment showed a decrease in signal upon incubation with the competitor compound **23** (figure 4.13). Specifically, a decrease in intensity was seen with proteins of an approximate molecular weight of 38 kDa, 50 kDa, 65 kDa, and 68 kDa. This suggested that binding of probe **11** to the proteins of interest was due to the fucose-α(1-2)-galactose moiety.

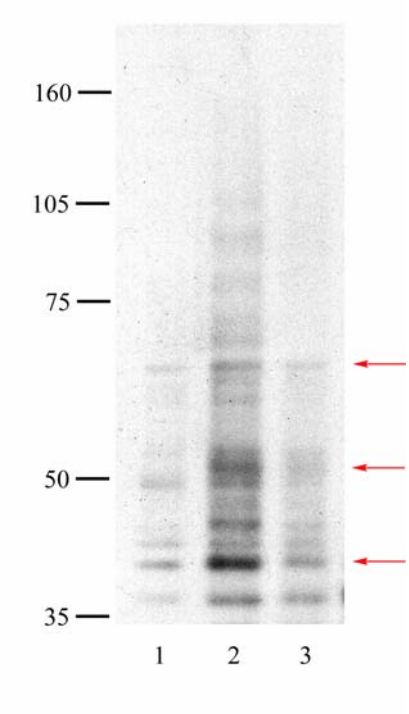

Figure 4.13. Western blot analysis of competition experiments using 1000-fold excess of **23** using the soluble fraction of adult rat hippocampal lysates. Lane 1: adult rat hippocampal lysates with DMSO; Lane 2: adult rat hippocampal lysates with probe **11**; Lane 3: adult rat hippocampal lysates with probe **11** and 1000-fold excess of **23**.

4.3.5 Efforts toward Identification of fucose-α(1-2)-galactose Glycoproteins

In addition to studying fucose-α(1-2)-galactose lectins, we validated the existence of fucose-α(1-2)-galactosyl glycoproteins in the brain using molecular techniques. These

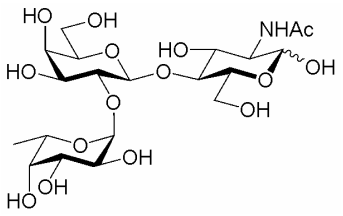

Figure 4.14. Structure of the blood group antigen H type 2, fucose-α(1-2)-galactose-β(1-4)-GlcNAc, which is recognized by the A46-B/B10 antibody.

proteins could be detected by Western blotting with an antibody (A46-B/B10) specific to the blood group antigen H type 2**,** Fucα(1-2)Galβ(1-4)GlcNAc (figure 4.14).[23] Hybridomas were obtained through the generous gift of Dr. Uwe Karsten (Max-Delbruck Centre for Molecular Medicine). Although A46-B/B10 was developed against the trisaccharide, binding studies demonstrated that stringency for selectivity was in the fucose-α(1-2)-galactose moiety, and less so for the trisaccharide.[23] Antibodies were generated (Cocalico) and purified across an IgM antibody purification kit (Pierce, Rockford, IL). Western blotting of adult rat hippocampal lysates indicated the presence of fucose-α(1-2)-galactose bearing proteins of 70 kDa and 80 kDa. Immunoprecipitation of these proteins using immobilized A46-B/B10 antibody was attempted, but was unsuccessful (data not shown). Work towards isolating and identifying the fucose-α(1-2)-galactosyl expressing proteins in the brain is now being continued by Monica Luo (Hsieh-Wilson lab).

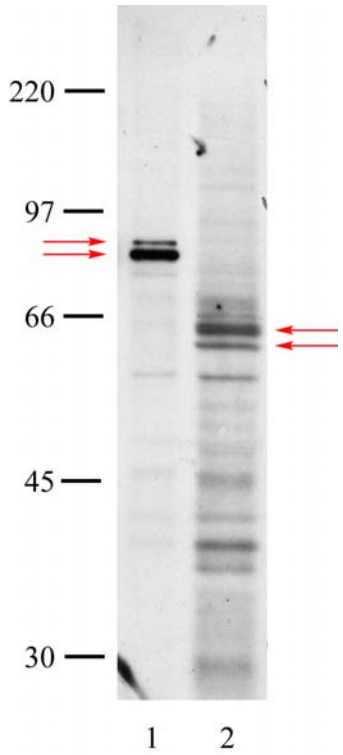

Figure 4.15. Western blot analysis of adult rat hippocampal lysates and cultured embryonic rat hippocampal lysates using A46-B/B-10 antibody. Lane 1: adult rat hippocampal lysates; Lane 2: cultured embryonic (E18) rat hippocampal lysates.

Because carbohydrates are often expressed at different levels during various stages of development, the presence of fucose-α(1-2)-galactose glycoproteins in cultured embryonic hippocampal cells were examined.

Interestingly, Western blotting of cultured embryonic hippocampal cell lysates using the A46-B/B10 antibody detected glycoproteins of different molecular weights than that of adult rat hippocampal tissue (figure 4.15). Probing of adult rat hippocampal lysates revealed fucosylated proteins of 80 kDa and 70 kDa, whereas embryonic lysates have fucosylated proteins of 63 kDa and 61 kDa**.** These results suggest that expression of fucose-α(1-2)-galactose glycoproteins is developmentally regulated. Further studies directed toward identifying the fucose-α(1-2)-galactose glycoproteins, their subcellular localization, and their roles in development are being carried out by Cristal Gama (Hsieh-Wilson laboratory).

4.4 Discussion

4.4.1 General

A growing body of evidence suggests a critical role for carbohydrates in a vast number of neurological processes such as learning and memory. Previous work had strongly suggested a role for fucose-α(1-2)-galactose in learning and memory; however, at the time when this research was undertaken, no fucose-α(1-2)-galactose binding proteins had been identified, nor had there been identification of any fucose-α(1-2)-galactose bearing glycoproteins. Therefore, the herein research was aimed at identifying these proteins through chemical and molecular means. We aimed to use chemical probes to study proteins that bound to fucose-α(1-2)-galactose epitodes. The availability of antibodies specific to fucose-α(1-2)-galactose epitopes afforded us the ability to use molecular means to study fucose-α(1-2)-galactose bearing glycoproteins.

4.4.2 Study of fucose-α(1-2)-galactose binding proteins with chemical probes

Probe **10** was designed and synthesized as an initial probe to examine the presence of fucose-α(1-2)-galactose binding proteins in the brain. It contains a fucose-α(1-2)-galactose epitode tethered to a biotin moiety via a PEG linker. Incubation of **10** with cultured embryonic rat hippocampal neurons followed by imaging using confocal microscopy strongly suggested the presence of fucose-α(1-2)-galactose binding proteins. Incubation of the neurons with biotin attached to a PEG linker, with no fucose-α(1-2)-galactose epitope, resulted in no binding as determined by confocal microscopy. This established the specificity of the binding was via fucose-α(1-2)-galactose epitopes. Furthermore, the fluorescence imaging of the neurons using **10** validated the design of probe **10**—establishing that the disaccharide is sufficient for binding and that the length of the linker arm is compatible with protein binding.

Probe **11** was designed and synthesized to isolate via photoreactive crosslinking fucose-α(1-2)-galactose binding proteins in neurons with lower binding affinities that often hamper "pull-down" experiments. Probe **11** was synthesized in a relatively straightforward fashion with a modular design such that modifications, such as linker length, could be made with relative ease. Initial experiments using **11** were aimed at establishing the ability of **11** to selectively crosslink to proteins of interest in both cultured embryonic rat hippocampal neurons as well as adult rat hippocampal lysates.

Neurons or lysates were incubated with probe **11** or with the corresponding methyl ester **20**. Compound **20** was used as a control to validate the specificity of binding to the fucose-α(1-2)-galactose epitope and not other moieties of **11**. Crosslinking experiments with the cultured embryonic rat hippocampal and adult rat hippocampal lysates both showed

distinct proteins bands, although crosslinking experiments probing the cultured neurons detected fewer proteins than that of the adult lysates (figure 4.9A, 10A). Nonetheless, the results of these experiments were very promising because they suggested that probe **11** is able to selectively capture potential proteins.

In experiments probing cultured embryonic rat hippocampal neurons, protein bands were detected in the negative control using methyl ester **20** (figure 4.9B). The two protein bands seen in the control with the methyl ester **20** may be due to a variety of reasons. It is possible that the increased hydrophobicity of **20** compared to capture probe **11** causes nonspecific hydrophobic interactions between proteins and **20**. It is also possible that some proteins are binding specifically to the aryl ester moiety on **20**. Both possibilities lead to the capture of proteins that may not be specific to the fucose-α(1-2)-galactose epitope.

Interestingly, probing adult rat hippocampal lysates yielded more detected proteins than those found in cultured neurons. These results were very exciting because they indicated that there were potentially more fucose-α(1-2)-galactose binding proteins in the brain than just the single protein initially observed from the cultured neurons experiments. The difference in the proteins seen may be a result of different expression levels of fucose-α(1-2)-galactose binding proteins during different stages of development. These results would support a hypothesis that expression of fucose-α(1-2)-galactose binding proteins is developmentally regulated. Similar to the capture probe, the methyl ester also captures more proteins in the adult rat hippocampal lysates than in the case of cultured embryonic hippocampal neurons. This potentially could be due to nonspecific hydrophobic interactions between the protein and the methyl ester. If this is the case, it is possible that the methyl ester is capturing the most abundant proteins in the lysates. Again, it should be noted that the

protein expression levels are likely to be varied during development, resulting in the capture of different proteins from embryonic hippocampal neurons to adult hippocampal neurons.

Once the binding of compound **11** was established we utilized the biotin handle of **11** to determine if **11** could be used to isolate proteins captured during crosslinking, using avidin-agarose or streptavidin-agarose (figure 4.11). The results of the pull-down experiments were promising because they suggested that fucose-α(1-2)-galactose binding proteins can be isolated through crosslinking with probe **11**, followed by incubation with avidin-agarose. While the results of the pull down experiments using biotinylated BSA indicate that the elution conditions are sufficient for recovery of the bound proteins, the faint appearance of the 58 kDa band in the lysates suggests that the efficiency of pull down experiments needs to be optimized. Future experiments with probe **11** will be aimed at improving the pull-down conditions, possibly through increasing the amount of avidin-agarose used coupled with increasing the incubation time.

We further validated the specificity of the probe towards fucose-α(1-2)-galactose binding proteins with competition experiments using *O*-ethyl-fucose-α(1-2)-galactose **23**. Incubation with 1000-fold excess of **23** over **11** resulted in decreased crosslinking of **11** to fucose-α(1-2)-galactose binding proteins, presumably due to competitive binding of **23** to these proteins (figure 4.13). These results indicated that binding of probe **11** to the proteins of interest was due to the fucose-α(1-2)-galactose moiety. Future experiments aimed at the isolation and identification of fucose-α(1-2)-galactose binding proteins will include additional competition experiments to confirm preliminary results, as well as optimization of pull-down conditions using avidin-agarose.

4.4.3 Study of fucose-α(1-2)-galactose bearing glycoproteins using molecular techniques

To study fucose-α(1-2)-galactose bearing glycoproteins, we utilized the A46-B/B10 antibody that recognizes fucose-α(1-2)-galactose to probe cultured embryonic rat hippocampal neurons and adult hippocampal lysates (Figure 4.15). Our preliminary results demonstrated the presence of fucose-α(1-2)-galactose glycoproteins in both sources of neurons. Interestingly, the fucose-α(1-2)-galactose glycoproteins detected in the cultured embryonic neurons differed in molecular weight from those in the adult lysates. These results suggest that expression of fucose-α(1-2)-galactose glycoproteins is developmentally regulated. Further studies directed toward identifying the fucose-α(1-2)-galactose glycoproteins, their subcellular localization, and their roles in development are being carried out by Cristal Y. Gama (Hsieh-Wilson laboratory).

4.5 Conclusions

In summary, the data strongly suggest the presence of fucose-α(1-2)-galactose binding proteins and fucose-α(1-2)-galactose glycoproteins in the brain. Chemical probes **10** and **11** were synthesized and used to study fucose-α(1-2)-galactose binding proteins. Using probe **10** and confocal fluorescence microscopy, we demonstrated the existence of fucose-α(1-2)-galactose binding proteins in hippocampal neurons. Probe **11** was synthesized to capture fucose-α(1-2)-galactose binding proteins by means of chemical crosslinking. Initial results from experiments with probe **11** were very exciting because they suggest that the design of our probe is sufficient to isolate fucose-α(1-2)-galactose binding proteins from the brain. Furthermore, we were able to use antibodies specific to fucose-α(1-2)-galactose epitopes to examine fucose-α(1-2)-galactose bearing glycoproteins in the brain. Overall, the

described research further demonstrates the power of chemical probes in biological studies. Additionally, the data from both studies utilizing chemical probes and molecular probes strongly suggest that the modifications of proteins with fucose-α(1-2)-galactose epitopes and the expression of fucose-α(1-2)-galactose binding proteins are developmentally regulated. Future studies will be directed at isolating fucose-α(1-2)-galactose binding proteins and identifying these proteins using MALDI-MS. Identification of fucose-α(1-2)-galactose binding proteins and their binding partners at the synapse should provide a greater understanding of the molecular underpinnings of memory formation, through a detailed study of their molecular interactions.

4.6 Experimental methods and materials

4.6.1 General synthetic information.

Unless otherwise stated, all reactions were performed in flame-dried glassware under an atmosphere of nitrogen gas or argon gas. Reagents were obtained from commercial sources and used as received. Thin-layer chromatography (TLC) was performed using E. Merck silica gel 60 F254 precoated plates (0.25 mm). Visualization of the developed chromatogram was performed by fluorescence quenching, cerium ammonium molybdate stain, ninhydrin stain, or *p*-dimethylaminocinnamaldehyde stain (for detection of biotin). Chromatography (flash) was performed using ICN Silica gel (0.032-0.063 mm) or Fluka alumina oxide type 507 C neutral (0.05-0.15 mm). ^{1}H-NMR and ^{13}C-NMR were recorded on a Varian Mercury 300 (300 MHz for ^{1}H-NMR and 74.5 MHz for ^{13}C-NMR). Infrared (IR) spectra were obtained using a Perkin Elmer Paragon spectrometer and are reported in terms of frequency of absorption (cm^{-1}). UV (vis) spectra were recorded on a Unikon Spectrophotometer 930 and are reported in terms of wavelength of maximum absorbance (λ_{max}). Mass spectra were obtained from the Protein/Peptide MicroAnalytical Laboratory at the California Institute of Technology, Pasadena, California.

4.6.2.1 Synthesis of methyl α-L-fucopyranoside

L-fucose (50 g, 0.304 mol) and the acid catalyst Dowex 50W-X8 (Acros) were combined in methanol (500 mL) and refluxed for 48 h. The reaction mixture was cooled, filtered and concentrated under vacuum. The residue solidified and was crystallized from EtOAc. The filtrate, after crystallization, was concentrated and methanol (500 mL) added and the reflux and isolation process was repeated twice to yield methyl α-L-fucopyranoside (45.5 g, 84 %):

^{1}H-NMR (300 MHz, D_2O) δ 1.21 (d, 3H, *J* = 6.6Hz, C*H*$_3$), 3.38 (s, 3H, OC*H*$_3$), 3.77 to 3.90 (m, 3H, H-2, H-3, H-4), 4.04 (m, 1H, *J* = 6.6Hz, H-5**)**, 4.76 (d, 1H, *J* = 3.3Hz, H-1) MS (EI^+) *m/z* 201.0 $[M+Na]^+$.

4.6.2.2 Synthesis of Methyl–2, 3, 4-tri-O-benzyl-α-L-fucopyranoside.

Benzylation of **1** was done as described by Zhang *et al*[53]. To a solution of **1** (25 g, 0.140 mol) in DMF (1.22 L) was added NaH (57%-63% oil dispersion, 11.79 g, 0.280 mol) in portions. After the mixture was stirred for 15 min, benzyl bromide (47.89 g, 0.280 mol) was then added dropwise through an addition funnel at 0 °C. The reaction was stirred for 8 h at room temperature. Methanol (209.48 mL) was then added to the mixture. The reaction mixture was poured to ice water and extracted with EtOAc. The organic layer extract was dried over Na_2SO_4 and filtered. The filtrate was concentrated *in vacuo* to afford an oily residue. Column chromatography on silica gel afforded a colorless oil (59.53 g, 94.8%): ^{1}H-NMR (300 MHz, $CDCl_3$) δ 1.12 (d, 3H, *J* = 6.6Hz, C*H*$_3$), 3.37 (s, 3H, OC*H*$_3$), 3.65 (dd, 1H, *J* < 1, H-4), 3.84 (m, 1H, *J* = 6.6Hz, H-5), 3.94 (dd, 1H, *J* = 10.2Hz, *J* = 3.3Hz, *J* = 2.7Hz, H-3), 4.05 (dd, 1H, *J* = 9.9Hz, *J* = 3.9Hz, H-2), 4.65-5.02 (m, 6H, C*H*$_2$Ph), 4.66 (d, 1H, *J* = 3.9Hz, H-1), 7.26-7.41 (m, 15H, *Ph*); ^{13}C-NMR (74.5MHz, $CDCl_3$) δ17.02, 55.64, 66.37, 73.67, 73.79, 75.10, 76.60, 78.09, 79.71, 99.05, 127.70, 127.79, 127.87, 128.31, 128.39, 128.53, 128.59, 128.65, 138.74, 138.78, 139.14; MS (EI^+) *m/z* 471.2 [M+Na]+, 487.2 [M+K]+; MS (EI^-) *m/z* 483.4 [M+Cl']-.

*4.6.2.3 Synthesis of 2, 3, 4-tri-O-benzyl-α-L-fucopyranoside (**2**)*

Synthesis of 2, 3, 4-tri-O-benzyl-α-L-fucopyranoside was done according to Dejter-Juszynski, M. and Flowers, H. M..[55] A solution of methyl–2, 3, 4-tri-O-benzyl-α-L-fucopyranoside (5.0 g, 11.15 mmol) in 80% acetic acid (80 mL) and 1 N HCl (25 mL) was heated between 95-100 °C for 2 h. After cooling, the reaction mixture was extracted with chloroform. The chloroform solution was washed with a cold saturated solution of $NaHCO_3$, followed by a wash with water. The organic layer was then dried with calcium chloride, filtered, and concentrated *in vacuo*. The solid was crystallized from ether-hexane to yield **2** (3.84 g, 79.2%): ^{1}H-NMR (300 MHz, $CDCl_3$) δ 1.14 (d, 3H, *J* = 6.6Hz, C*H*$_3$), 3.89 (dd, 1H, *J* = 2.7, *J* = 9.9), 3.67 (d, 1H, *J* = 1.8, H-4), 3.89 (dd, 1H, *J* = 2.7, *J* = 9.9, H-3), 4.05 (dd, 1H, *J* = 3.9, *J* = 9.9, H-2), 4.10 (q, 1H, *J* = 6.6Hz, H-5), 4.65-5.00 (m, 6H, C*H*$_2$), 5.27 (s, 1H, H-1); MS (EI$^+$) *m/z* 457.2 [M+Na]+, 473.2 [M+K]+.

*4.6.2.4 Synthesis of 1, 6-Anhydro-3, 4-O-isopropylidene-2-O-(2, 3, 4-tri-O-benzyl-α-L-fucopyranosyl)- β-D-galactopyranose (**4**)*

To a solution of **2** (2.5 g, 5.75 mmol) in CH_2Cl_2 (39.68 mL) was added potassium carbonate (3.04 g, 21.99 mmol) and freshly distilled trichloroacetonitrile (3.17 mL, 4.56 g, 31.61 mmol). The reaction mixture was stirred vigorously for 1 h under argon. Sodium hydride (261.07 g of 57%-63% oil dispersion, 6.2 mmol) was added portion-wise and the reaction mixture was allowed to stir for 5 h at room temperature. The reaction mixed was then cooled on ice and poured into ice-cold saturated aqueous $NaHCO_3$ and extracted with CH_2Cl_2 (x 3). The organic layer was dried with Na_2SO_4, filtered and concentrated *in vacuo* to afford a dark orange oil. Attempts to purify the crude material across silica gel were unsuccessful so the O-(2, 3, 4-tri-O-benzyl-α-L-fucopyranoside)trichloroacetimidate was

taken directly to the next step with no purification. The crude imidate was lyophilized for at least 5 h to remove any residual moisture before the synthesis of **4**. To a solution of crude imidate and **3** in dry ether (500 mL), was added trimethylsilyl triflate (5.99 mmol) at room temperature. The reaction was stirred at room temperature until thin layer chromatography (1:1 pet ether: EtOAc) showed one major product. $NaHCO_3$ (39.94 g) was added and the mixture was stirred for 15 min., filtered, and extracted with ether. The extract was washed with saturated aqueous NaCl, dried over $MgSO_4$. Column chromatography (1:1 pet ether: EtOAc) of the residue gave **4** (3.10 g, 87.25% yield overall for both steps): ^{1}H-NMR (300 MHz, $CDCl_3$) δ 1.12 (d, 3H, *J* = 6.6Hz, C*H*$_3$), 1.31 (s, 3H, C*H*$_3$), 1.53 (s, 3H, C*H*$_3$), 3.56 (dd, 1H, *J* = 7.2Hz, *J* = 5.4Hz, H-5), 3.70 (s, 2H, H-2, H-4′), 3.93 (dd, 1H, *J* = 9.9Hz, *J* = 2.7Hz, H-3′), 3.98 (q, 1H, H-5′), 4.04 (dd, 1H, *J* = 9.6Hz, *J* = 3.9Hz, H-2′), 4.09 (d, 1H, *J* = 7.2Hz, H-6), 4.24 (d, 1H, *J* = 7.2 Hz, H-3), 4.40-4.50 (m, 2H, H-4,6), 4.60-5.00 (m, 7H, 3PhC*H*$_2$, and including at 4.91, H-1′, d, *J* = 3.6Hz), 5.42 (s, 1H, H-1), 7.25-7.45 (m, 15H, 3Ph); ^{13}C-NMR (74.5 MHz, $CDCl_3$) δ 17.0, 24.8, 26.2, 63.5, 67.2, 69.4, 72.5, 73.4, 73.8, 74.8, 75.2, 76.5, 77.6, 79.5, 99.3, 100.6, 108.8, 127.6, 127.7, 127.8, 127.9, 128.0, 128.4, 128.6, 128.6, 138.6, 138.8, 139.0; MS (EI^+) *m/z* 641.4 [M+Na]+, 657.2 [M+K]+.

4.6.2.5 Synthesis of 1, 6-Anhydro-2-O-(2, 3, 4-tri-O-benzyl-α-L-fucopyranosyl)- β-D-galactopyranose

Compound **4** (8 g, 12.93 mmol) was treated with 1 N HCl (18.3 mL) in methanol (91.3 mL) at 40 °C overnight. The reaction was quenched by addition of $NaHCO_3$ at 4 °C (ice bath) until pH was established at approximately 7. The mixture was then filtered through Celite® and concentrated *in vacuo*. Column chromatography on silica gel (1:1 Pet

ether: EtOAc) gave the desired product (4.56 g, 61% yield): ^{1}H-NMR (300 MHz, $CDCl_3$) δ1.10 (d, 1H, *J* = 6.3Hz, C*H*$_3$), 3.58-3.62 (m, 2H), 3.92 (dd, 1H, *J* = 2.7Hz, *J* = 10.2Hz), 3.92 (m, 1H), 3.98-4.05 (m, 3H), 4.20 (d, 1H, *J* = 7.8Hz, H-6), 4.42 (t, 1H, *J* = 3.6Hz), 4.59-4.99 (m, 6H), 4.86 (d, 1H, *J* = 3.00Hz, H-1'), 5.45 (s, 1H, H-1), 7.28-7.38 (m, 15H); ^{13}C-NMR (74.5 MHz, $CDCl_3$) δ 17.0, 30.1, 64.0, 64.6, 67.2, 69.7, 73.4, 73.9, 75.1, 75.2, 76.7.78.5, 79.3, 99.4, 101.2, 127.6, 127.7, 127.8, 127.9, 128.1, 128.4, 128.6, 126.62, 128.64, 138.6, 138.8, 139.0; MS (EI$^+$) *m/z* 601.2 [M+Na]+, 617.4 [M+K]+; MS (EI$^-$) *m/z* 613.4 [M+Cl']-; IR 3446cm^{-1}.

*4.6.2.6 Synthesis of 3,4-Di-O-acetyl-1,6-anhydro-2-O-(2, 3, 4-tri-O-benzyl-α-L-fucopyranosyl)- β-D-galactopyranose (**5**)*

To a solution of 1, 6-Anhydro-2-O-(2, 3, 4-tri-O-benzyl-α-L-fucopyranosyl)- β-D-galactopyranose (4 g, 6.91 mmol) in dry pyridine (88.89 mL) was added 0.2 equivalents of DMAP and the reaction was allowed to stir at room temperature for 10 min. Dry acetic anhydride (44.44 mL) was then added slowly and the reaction was stirred until starting material was consumed as monitored by thin layer chromatography. The mixture was concentrated and repeatedly evaporated with toluene to remove residual pyridine to afford an orange oil. Column chromatography in (2:1 pet ether: EtOAc) yielded **5** in 77% yield; ^{1}H-NMR (300 MHz, $CDCl_3$) δ 1.10 (d, 3H, *J* = 6.6Hz), 2.05 (s, 3H), 2.12 (s, 3H), 3.56 (s, 1H, H-2), 3.67-3.71 (m, 2H, H-4'. H-6), 3.94 (dd, 1H *J* = 3.0Hz, *J* = 10.2Hz, H-3'), 3.98 (m, 1H, H-5'), 4.03 (dd, 1H, *J* = 3.3Hz, *J* = 10.5Hz, H-2'), 4.31 (d, 1H, *J* = 7.5Hz, H-6), 4.47 (m, 1H, *J* = 3.9Hz, *J* = 4.2Hz, H-5), 4.62-5.00 (m, 6H, C*H*$_2$), 4.94 (d, 1H, *J* = 3.9Hz, H-1'), 5.27 (dd, 1H, *J* < 1Hz, *J* = 5.0Hz, H-4), 5.30 (dd, 1H, *J* < 1Hz, *J* = 5.0Hz, H-3), 5.42 (s, 1H, H-1),

7.26-7.40 (m, 15H); MS (EI^+) *m/z* 685.2 [M+Na]+, 701.2 [M+K]+; MS (EI^-) *m/z* 697.6 [M+Cl']-.

*4.6.2.7 Synthesis of 3,4-Di-O-acetyl-1,6-anhydro-2-O-(2,3,4-tri-O-acetyl-α-L-fucopyranosyl)- β-D-galactopyranose (**6**)*

To a solution of **5** (3 g, 4.53 mmol) in degased EtOAc (62.2 mL) and dry methanol (62.2 mL) was added 10% Pd/C (0.78 g). The reaction mixture was pressurized to 1.3 atm of H_2 gas and allowed to stir for 6 h. Reaction was determined to have proceeded to completion by H-NMR. Solvents were evaporated, and the debenzylated compound was stirred with dry pyridine (77.72 mL) and 0.2 equivalents of DMAP for ten minutes. Dry acetic anhydride (31.09 mL) was added slowly, and the mixture was allowed to stir at room temperature overnight. Solvents were evaporated, and the remaining pyridine was removed by repeated evaporation with toluene. Column chromatography (1:2 = EtOAc:hexanes) afforded **6** (1.97 g, 84 % yield) : ^{1}H-NMR (300 MHz, $CDCl_3$) δ 1.13 (d, 3H, *J* = 6.6Hz), 1.99 (s, 3H), 2.04 (s, 3H), 2.09 (s, 3H), 2.13 (s, 3H), 2.15 (s, 3H), 3.61 (s, 1H, H-2), 3.72 (dd, 1H, *J* = 5.2Hz, *J* = 6.8Hz, H-6), 4.28 (q, 1H, *J* = 6.6Hz, H-5'), 4.31 (d, 1H, *J* = 7.8Hz, H-6), 4.46 (t, 1H, *J* = 4.5Hz, H-5), 5.08 (dd, 1H, *J* = 1.2Hz, *J* = 5.4Hz, H-4), 5.14 (dd, 1H, *J* = 1.2Hz, *J* = 5.4Hz, H-3), 5.19 (t, 1H, *J* = 4.5Hz), 5.24 (d, 1H, *J* = 3.9Hz, H-1'), 5.30-5.34 (m, 2H), 5.42 (s, 1H, H-1); ^{13}C-NMR (74.5 MHz, $CDCl_3$ w/TMS) δ 16.2, 20.9, 20.97, 20.98, 21.0, 21.2, 64.7, 65.4, 65.4, 67.7, 68.2, 68.3, 71.1, 72.3, 77.0, 97.3, 100.5, 169.2, 169.8, 170.1, 170.6, 170.7; MS (EI^+) *m/z* 541.2 [M+Na]+; MS (EI^-) *m/z* 553.2 [M+Cl']-.

4.6.2.8 Synthesis of 5-(acetyl-4,5-diacetyloxy-6-methylperhydro-2H-pyran-2-yloxy)-4-acetyloxy-2-(hydroxymethyl)-6-phenylthioperhydro-2H-pyran-3-yl acetate

A mixture of **6** (1.75 g, 3.38 mmol), (phenylthio)trimethylsilane (1.96 mL, 10.37 mmol), and zinc iodide (3.33 g, 10.44 mmol) in CH_2Cl_2 (19.6 mL) was stirred at room temperature for 21 h. The mixture was diluted with EtOAc (120.23 mL) and washed successively with sat. aq. $NaHCO_3$ (150.15 mL), water (3 x 56.15 mL), and brine (18.77 mL) and dried with sodium sulfate. The organic layer was filtered to remove the sodium sulfate, and then concentrated *in vacuo*. The residue was dissolved in dry THF (15.02 mL) and to that was added 1 M tetrabutylammonium fluoride (TBAF) in THF (6.62 mL). The reaction mixture was allowed to stir for an additional 20 min. The solvent was evaporated and the residue was dissolved in EtOAc (60.03 mL) and washed with water (3 x 30.1 mL), sat. aq. $NaHCO_3$ (30.1 mL), and brine (30.1 mL) and dried over sodium sulfate, filtered and concentrated to afford an oil. Column chromatography (2.5:1= hexanes:EtOAc) afforded the β-thioglycoside (1.61 g, 76%): In future synthesis, this material is taken directly onto next step with no purification.

4.6.2.9 Synthesis of 5-(acetyl-4,5-diacetyloxy-6-methylperhydro-2H-pyran-2-yloxy)-4-acetyloxy-2-(acetyloxymethyl)-6-phenylthioperhydro-2H-pyran-3-yl acetate (7)

To a solution of 5-(acetyl-4,5-diacetyloxy-6-methylperhydro-2H-pyran-2-yloxy)-4-acetyloxy-2-(hydroxymethyl)-6-phenylthioperhydro-2H-pyran-3-yl acetate (312.7 mg, 0.499 mmol) in dry pyridine (6.42 mL) was added acetic anhydride (3.21 mL). The reaction was allowed to stir at room temperature overnight. The solvent was evaporated and residual pyridine was removed by repeated evaporation with toluene. Column chromatography (2.5:1

hexanes:EtOAc) on silica gel afforded **7** (333.69 mg) in quantitative yield: ^{1}H-NMR (300 MHz, $CDCl_3$) δ 0.97 (d, 1H, *J* = 6.6Hz), 1.92 (s, 3H), 1.96 (s, 6H), 2.00 (s, 3H), 2.10 (s, 3H), 2.11 (s, 3H), 4.03 (d, 2H, *J* = 6.3Hz, H-6), 4.25 (dd, 1H, *J* = 6Hz, *J* = 10.5Hz, H-2), 4.33 (q, 1H, *J* = 6.6Hz, H-5'), 4.70 (t, 1H, *J* = 6.3Hz, H-5), 4.99 (dd, 1H, *J* = 3.7, *J* = 10.4Hz, H-2'), 5.18 (dd, 1H, *J* = 3.3, *J* = 10.2Hz, H-3), 5.27-5.31 (m, 3H, H-1', H-4', H-3), 5.41 (dd, 1H, , *J* = 1.2, *J* = 3.3Hz, H-4), 5.66 (d, 1H, *J* = 5.4Hz, H-1), 7.24-7.5 (m, 5H); MS (EI^+) *m/z* 693.2 [M+Na]+, 709.2 [M+K]+.

*4.6.2.10 Synthesis of 5-(acetyl-4,5-diacetyloxy-6-methylperhydro-2H-pyran-2-yloxy)-4-acetyloxy-2-(acetyloxymethyl)-6-{2-[2-)2,2,2-trifluoroacetylamino)ethoxy]ethoxy}perhydro-2H-pyran-3-yl acetate (**9**)*

Compound **7** (793 mg, 1.19 mmol) and **8** (225 mg, 1.12 mmol) were evaporated repeatly with toluene to remove excess water and then placed under argon gas. **7** and **8** were dissolved in CH_2Cl_2 (8.4 mL) and mol sieves (4 Å). *N*-iodosuccinimide (NIS) (289 mg, 1.28 mmol) was added and the mixture was cooled to -20 °C. Silver triflate (316 mg, 1.23 mmol) was added portionwise at -20 °C. The reaction occurred almost instantly upon addition of silver triflate. The reaction was diluted with CH_2Cl_2 and filtered. The organic layer was washed with 10% aq. sodium thiosulfate, followed by sat. sodium bicarbonate and then brine. The organic layer was dried with sodium sulfate, filtered and concentrated to afford a yellow oil. Column chromatography (2:1 hexanes:EtOAc) on silica gel obtained **9** (810 mg, 95% yield): ^{1}H-NMR (300 MHz, $CDCl_3$) δ1.10 (d, 3H, *J* = 6.0Hz), 1.99 (s, 3H), 2.00 (s, 3H), 2.01 (s, 3H), 2.04 (s, 3H), 2.13 (s, 3H), 2.15 (s, 3H), 3.40 (q, 1H, *J* = 6.6Hz), 3.55-3.78 (m, 6H), 3.88 (t, 1H, *J* = 6.5Hz), 3.97 (dd, 1H, *J* = 7.8Hz, *J* = 10.2Hz), 4.06 (dd, 1H, *J* = 6.6Hz, *J* =

9.3Hz), 4.14 (dd, 1H, *J* = 6.6Hz, *J* = 14.4Hz), 4.187 (m, 1H), 4.50 (d, 1H, *J* = 7.8Hz, H-1**β**, confirmed by decoupling experiments), 4.76 (q, 1H, *J* = 6.6Hz), 5.00 (dd, 1H, *J* = 3.3Hz, *J* = 10.2Hz), 5.02 (dd, 1H, *J* = 3.3Hz, *J* = 10.2Hz), 5.25-5.31 (m, 3H), 5.42 (d, 1H, *J* = 3.6Hz), 7.49 (bs, 1H, N-H); MS (EI^+) *m/z* 784.6 [M+Na]+, 800.4 [M+K]+

4.6.2.11 Synthesis of 5-((2S)-6,8-diazo-7-oxo-3-thiabicyclo[3.3.0]oct-2-yl)-N-(2-{2-[4,5-dihydroxy-6-(hydroxymethyl)-3-(3,4,5-trihydroxy-6-methylperhydro-2H-pyran-2yloxy) perhydro-2H-pyran-2-yloxy]ethoxy}ethyl)pentanamide (10)

Compound **9** (361.2 mg, 0.474 mmol) was dissolved in 50.07 mL of 7% potassium carbonate in methanol/water (2:5) and allowed to stir until complete deprotection has occurred as detected by drop in R_f in thin layer chromatography and appearance of amine as seen by ninhydrin staining. The solvent was removed *in vacuo* and the deprotected product was extracted from the residue with methanol. The extraction was concentrated and the resulting residue was dissolved in DMF (11.73mL). The pH of the mixture was adjusted to 10 using triethylamine (TEA). NHS-biotin is added and the reaction is allowed to stir overnight. The reaction mixture is concentrated to afford an off-white syrup. Purification by HPLC yields **(10)** in 60% yield: ^{1}H-NMR (300 MHz, D_2O) δ 1.05 (d, 3H, *J* = 6.6Hz), 1.23-1.31 (m, 2H), 1.41-1.60 (m, 4H), 2.12 (t, 2H, *J* = 7.0Hz), 2.62 (d, 1H, *J* = 13.2Hz), 2.84 (dd, 1H, *J* = 4.8Hz, *J* = 12.6Hz), 3.17 (dd, 1H, *J* = 4.8Hz, *J* = 9.3Hz), 3.23 (dd, 1H, *J* = 4.8Hz, *J* = 8.7Hz), 3.42-3.75 (m, 11H), 3.90 (dt, 1H, *J* = 4.2Hz, *J* = 11.7Hz), 4.19 (q, 1H, *J* = 6.6Hz), 4.27 (dd, 1H, *J* = 4.7Hz, *J* = 7.8Hz), 4.35 (d, 1H, *J* = 8.4, H-1**β**), 4.46 (dd, 1H, *J* = 4.8Hz, *J* = 8.1Hz), 5.08 (d, 1H, *J* = 6Hz); MS (EI^+) *m/z* 662.2 [M+Na]+, 678.2 [M+K]+.

4.6.2.12 Synthesis of NHS-biotin

Biotin (2.0 g, 8.19 mmol) was dissolved in DMF (24.8 mL) with gentle heating (40 °C). To the reaction mixture was added *N*-hydroxysuccinimide (1.23 g, 10.65 mmol) and dicyclohexylcarbodiimide (DCC) (1.69 g, 8.19 mmol). The reaction was allowed to stir for 24 hours at room temperature. The reaction was then filtered to remove the dicyclohexylurea (DCU) and the filtrate was partially concentrated. The desired product was precipitated from diethyl ether and washed with diethyl ether followed by a wash with isopropanol to afford a white solid (2.43 g, 87%).

4.6.2.13 Synthesis of N-trifluoroacetylpiperidine

Trifluoroacetic anhydride (59.2 g, 0.282 mol) was slowly added to piperidine (20.0 g, 0.235 mol) at 0 °C with vigorous stirring. The reaction was allowed to stir overnight at room temperature. The reaction was concentrated *in vacuo* to remove any trifluoroacetic acid, which afforded the product (42.0 g, 99 %): ^{1}H-NMR (300 MHz, $CDCl_3$) δ 1.58-1.76 (m, 6H), 3.57 (dt, 4H); MS (EI^+) *m/z* 182.2 $[M+H]^+$.

4.6.2.14 Synthesis of tert-butyl hypochlorite

In a 500 mL flask was placed commercial household bleach (250mL, Clorox®). The flask was placed in an ice bath and vigorously stirred until the temperature dropped below 10 °C. At this point the lights in the vicinity were turned off to protect the reaction from light. A solution of *tert*-butanol (18.5 mL, 0.195 mol) and glacial acetic acid (12.25 mL, 0.215 mol) was added in a single portion to the bleach solution with rapid stirring. The reaction was stirred for about 3 minutes. After stirring, the entire reaction was poured into a

separatory funnel and the lower aqueous layer was discarded while the oily organic layer was washed with 10 % aqueous $NaHCO_3$ (25 mL) and then water (25 mL). The product was dried over $CaCl_2$ (0.5 g) and filtered. The product was used as is in the subsequent reactions and stored over $CaCl_2$.

4.6.2.15 Synthesis of (tert-butoxy)-N-[2-(2-hydroxyethoxy)ethyl]carboxamide

2-(2-aminoethoxy)ethanol (10.0 g, 95.11 mmol) was dissolved in CH_3CN (634 mL). Boc-anhydride (24.3 g, 95.11 mmol) and 1 N NaOH (79.3 mL) was added to the solution and the reaction mixture was stirred for 3 h at room temperature. The reaction mixture was evaporated to dryness and the residue was dissolved in EtOAc. This solution was dried over $MgSO_4$ and filtered. The solvent was removed *in vacuo* and chromatography afforded a yellow oil (17.96 g, 92%): ^{1}H-NMR (300 MHz, $CDCl_3$) δ1.33 (s, 9H), 3.34 (dd, 2H, *J* = 5.4Hz, *J* = 5.7Hz, *J* = 10.4Hz), 3.56 (t, 2H, *J* = 6.1Hz), 3.58 (t, 2H, *J* = 5.1Hz, *J* = 5.4Hz), 3.75 (t, 2H, *J* = 6.0Hz); MS (EI^+) *m/z* 206.3 [M+H]+ 228.3 [M+Na]+.

*4.6.2.16 Synthesis of (tert-butoxy)-N-[2-(2-bromoethoxy)ethyl]carboxamide. **(18)***

(tert-butoxy)-N-[2-(2-hydroxyethoxy)ethyl]carboxamide (5.0 g, 24.36 mmol), carbon tetrabromide (10.11 g, 30.45 mmol), K_2CO_3 (5.12 g, 36.54 mmol) and CH_2Cl_2 (60.9 mL) were placed in a flask. To the mixture was added triphenylphosphine (9.62 g, 36.54 mmol) in CH_2Cl_2 (60.9 mL) over 15 min at room temperature. After stirring for 13 h at room temperature, the reaction mixture is filtered and the filtrate is concentrated. The residue was treated with a mixture of EtOAc:hexanes (1:1, 121.8 mL) by filtration and the filtrate was concentrated. Chromatography of the residue on silica gel afforded the bromide (3.46 g, 53

%): ^{1}H-NMR (300 MHz, $CDCl_3$) δ1.33 (s, 9H), 3.20 (dd, 2H, *J* = 5.4Hz, *J* = 5.7Hz, *J* = 10.4Hz), 3.36 (t, 2H, *J* = 6.0Hz), 3.45 (t, 2H, *J* = 5.1Hz, *J* = 5.4Hz), 3.67 (t, 2H, *J* = 6.0Hz), 5.02 (bs, 1H); ^{13}C-NMR (74.5MHz, $CDCl_3$ w/TMS) δ 28.4, 30.5, 40.3, 60.3, 70.0, 70.7, 155.8; MS (EI^+) *m/z* 291.2 [M+Na]+.

4.6.2.17 Synthesis of 2,2,2-Trifluoro-1-(3-methyoxyphenyl)ethanone ***(12)***

Magnesium turnings (3.22 g), 3-bromoanisole (18.7 g, 100 mmol), and anhydrous THF (100 mL) were placed in a round bottom flask fitted with a condenser. The mixture was cautiously heated with a heating mantle until a vigorous reaction took place. The reaction was removed from heat and the reaction was allowed to proceed until almost all the Mg turnings were dissolved. The reaction was cooled in an ice bath. A solution of *N*-trifluoroacetylpiperidine (14.6 g, 80 mmol) in anhydrous THF (20 mL) was added to the Grignard reagent dropwise with stirring at 0 °C. After the addition, the reaction was stirred at room temperature for 2 h, then quenched with the addition of saturated aqueous NH_4Cl (10 mL). The precipitates were removed by filtration and the filtrate dried over $MgSO_4$. The filtrate was concentrated to afford a dark amber oil. Vacuum distillation of the residual oil afforded a colorless oil (9.34 g, 57%): ^{1}H-NMR (300 MHz, $CDCl_3$) δ 3.80 (s, 3H), 7.16-7.72 (m, 4H); MS (EI^+) *m/z* 205.2 [M+H]+, 227.2 [M+Na]+.

4.6.2.18 Synthesis of 2,2,2-Trifluoro-1-(3-methoxyphenyl)ethanoneOxime ***(13)***

A solution of **12** (10.0 g, 48.98 mmol) and hydroxylamine hydrochloride (3.51 g, 50.45 mmol) in absolute ethanol (27 mL) and dry pyridine (49 mL) was heated at 60 °C for 12 h. After evaporation of the solvents, the residue was partitioned between water and

diethyl ether. The organic layer was washed with 1 N HCl and dried with $MgSO_4$. After evaporation of the solvent, the crude oxime was purified by column chromatography on silica gel (CH_2Cl_2) to afford **13** (10 g, 93%): ^{1}H-NMR (300 MHz, $CDCl_3$ w/TMS) δ 3.83 (s, 3H), 7.00-7.43 (m, 4H), 8.67 and 8.85 (each bs, total 1H); ^{13}C-NMR (74.5 MHz, $CDCl_3$ w/TMS) δ 55.6, 114.0, 114.4, 116.3, 116.5, 120.9, 129.8, 129.9, 159.5; MS (EI^+) *m/z* 220.2 $[M+H]^+$; MS (EI^-) *m/z* 218 [M-H]-.

*4.6.2.19 Synthesis of 3-(3-methoxyphenyl)-3-(trifluoromethyl)diaziridine (**14**)*

To a solution of oxime **13** (1.32 g, 6.02 mmol), triethylamine (1.54 g, 15.23 mmol), and (*N*, *N*-dimethylamino)pyridine (36.8 mg, 0.301 mmol) in CH_2Cl_2 (10.8 mL) at 0 °C was added *p*-toluenesulfonyl chloride (1.30 g, 6.80 mmol) portionwise with stirring. After addition, the reaction was allowed to stir at room temperature. After 45 minutes of stirring, the reaction was washed with water, and the organic layer is dried with magnesium sulfate and filtered. The solvent was removed to afford a white solid. The crude oxime was then dissolved in CH_2Cl_2 (3.2 mL) and brought to -78 °C (dry ice and acetone bath). Ammonia gas was condensed into the reaction flask with the use of a cold finger until approximately 3-4 mL of liquid ammonia was present. The reaction was allowed to stir for 12 h at room temperature under NH_3 with a cold finger attached to the reaction flask. After 12 h, the excess ammonia was allowed to evaporate off at room temperature. The reaction was partitioned between water and CH_2Cl_2. The organic layer was washed with water, dried over $MgSO_4$, filtered and concentrated. Column chromatography on alumina (diethyl ether) of the crude oil afforded **14** (1.15 g, 89%): ^{1}H-NMR (300 MHz, $CDCl_3$ w/TMS) δ 2.24 (d, 1H, J = 8.1Hz), 2.78 (d, 1H, J = 9Hz), 3.83 (s, 3H), 6.98 (ddd, 1H, J = 1.2Hz, J = 2.2Hz, J = 8.3Hz),

7.15-7.25 (m, 2H), 7.33 (t, 1H, *J* = 7.8Hz, *J* = 8.1Hz); ^{13}C-NMR (74.5 MHz, $CDCl_3$ w/TMS) δ 55.6, 113.7, 115.9, 120.4, 121.7, 125.4, 130.0, 133.1, 159.7; MS (EI^+) *m/z* 219.2 $[M+H]^+$.

Note: The following reaction and reactions thereafter were done amberized glass to protect the product and starting material from light due to its photosensitivity. All precautions were taken to protect the compounds from light sources.

*4.6.2.20 Synthesis of 3-(3-methoxyphenyl)-3-(trifluoromethyl)-3H-diazirine (**15**)*

To a solution of **14** (1.25 g, 5.73 mmol) and triethylamine (2.13 g, 21.03 mmol) in *tert*-butanol (2.88 mL) and absolute ethanol (2.88 mL) at 0 °C, was cautiously added a solution of *tert*-butyl hypochlorite in *tert*-butanol (1.72 mL). The reaction was stirred at room temperature for 2 h. After 2 h of stirring, the reaction was quenched by the addition of 10% aqueous sodium metabisulfite. The reaction mixture was extracted with hexane and the organic layer was dried over $MgSO_4$, filtered and concentrated to afford a crude oil. Column chromatography on silica gel (hexane:CH_2Cl_2 = 2:1) afforded a colorless oil **15** (0.995 g, 80%): ^{1}H-NMR (300 MHz, $CDCl_3$ w/TMS) δ 3.80 (s, 3H), 6.69 (s, 1H), 6.78 (d, 1H, *J* = 7.8Hz), 6.94 (dd, 1H, *J* = 2.1Hz, *J* = 2.7Hz, *J* = 8.4Hz), 7.31 (t, 1H, *J* = 8.1Hz, *J* = 8.4Hz); ^{13}C-NMR (74.5 MHz, $CDCl_3$ w/TMS) δ55.5, 112.4, 115.3, 118.8, 120.4, 124.0, 130.1, 130.6, 159.8; MS (EI^+) *m/z* 517.0 $[M+H]^+$; UV(hex) λ_{max} 365 nm

*4.6.2.21 Thallation of **15** in preparation for the synthesis of **16***

Thallium compounds are known to be very toxic. As a result, thallations were performed in a well-ventilated glove box and all safety precautions were taken to prevent exposure and

contamination. Any glassware and tools that came into direct contact with thallium were disposed of properly. Double gloving and rubber gloves were used.

Diazirine **15** (2.0 g, 9.25 mmol) in trifluoroacetic acid (9.25 mL) was treated with 1.1 equiv of thallium(III) trifluoroacetate (5.50 g, 10.18 mmol) for 24 h at room temperature. The resulting arylthallium ditrifluoroacetates were used in the next step without further purification.

*4.6.2.22 Synthesis of 2-Methoxy-4-[3-(trifluoromethyl)-3H-diazirin-3-yl]benzoic Acid Methyl Ester (**16**)*

After the thallation of **15** (2.0 g, 9.25 mmol) as described above, the solvent trifluoroacetic acid was evaporated *in vacuo*. The residual arylthallium compound was dissolved in dry methanol (59.2 mL) and then added to a solution of palladium(II)chloride (210.39 mg, 1.19 mmol), lithium chloride (1.01 g, 23.84 mmol), and magnesium oxide (953.6 mg, 23.66 mmol) in dry methanol (59.2 mL) under an atmosphere of CO. The reaction mixture was allowed to stir at room temperature under an atmosphere of CO for 48 h. *Reactions involving CO were carried out in a well-ventilated hood*. After stirring the reaction mixture was brought to 0 °C and the pH was adjusted to 2 with 1 N HCl. The reaction mixture was partitioned between diethyl ether and water. The organic layer was washed with 1 N HCl and then dried over $MgSO_4$ and filtered. The filtrate was concentrated and column chromatography of the residue on silica gel (hexane:CH_2Cl_2 = 1:1) afforded a colorless oil (1.57 mg, 62%): ^{1}H-NMR (300 MHz, $CDCl_3$ w/TMS) δ 3.89 (s, 3H), 3.90 (s, 3H), 6.68 (s, 1H), 6.82 (d, 1H, *J* = 8.3Hz), 7.81 (d, 1H, *J* = 7.8Hz); ^{13}C-NMR (74.5 MHz, $CDCl_3$ w/TMS) δ 52.3, 56.1, 109.7, 118.0, 120.0, 121.3, 123.7, 132.1, 134.3, 159.0, 165.6;

MS (EI^+) *m/z* 297.2 $[M+Na]^+$; IR (neat) ν 1735 (CO) cm^{-1}; UV(EtOH) λ_{max} 349 nm; IR 1733 cm^{-1}.

*4.6.2.23 Synthesis of 2-Hydroxy-4-[3-(trifluoromethyl)-3H-diazirin-3-yl]benzoic Acid Methyl Ester (**17**)*

Compound **16** (1.00 g, 3.65 mmol) was dissolved in dry CH_2Cl_2 (7.25 mL) and cooled to 0 °C. To that was slowly added a 1 M solution of boron tribromide in CH_2Cl_2 (6.21 mL, 6.21 mmol). The reaction was allowed to stir at 0 °C for 30 min. Water was added to quench the reaction. The reaction mixture was extracted with diethyl ether, dried over $MgSO_4$, filtered and concentrated to afford a brown residue. The crude residue was used without further purification: crude ^{1}H-NMR (300 MHz, $CDCl_3$ w/TMS) δ 3.97 (s, 3H), 6.65 (d, 1H, *J* = 8.9Hz), 7.84 (d, 1H, *J* = 8.1Hz), 10.83 (s, 1H); MS (EI^+) *m/z* 283.2 [M+Na]+.

*4.6.2.24 Synthesis of **19***

The diazirine **17** (710 mg, 2.73 mmol) was dissolved in DMF (5.0 mL) and to that was added K_2CO_3 (377.3 mg, 2.73 mmol) at 0 °C. **18** (807.1 mg, 3.01 mmol) and tetrabutylammonium iodide (100.8 mg, 0.273 mmol) were added at room temperature. The reaction was refluxed at 60 °C for 19 h with stirring. The reaction was then filtered to remove insoluble material. The solvent was removed *in vacuo* and residue was partitioned between benzene and water. The organic layer was dried with $MgSO_4$, filtered and concentrated under reduced pressure. Chromatography of the residue on silica (hexane:diethyl ether = 1:1) afforded **22** (874.4 mg, 72%): ^{1}H-NMR (300 MHz, $CDCl_3$

w/TMS) δ 1.42 (s, 9H), 3.34 (dd, 2H, *J* = 5.4Hz, *J* = 10.5Hz), 3.64 (t, 2H, *J* = 4.8Hz, *J* = 5.4Hz), 3.87 (dd, 2H, *J* = 4.5Hz, *J* = 9.3Hz), 3.89 (s, 3H), 4.18 (t, 2H, *J* = 4.5Hz, *J* = 5.1Hz), 5.12 (bs, 1H), 6.72 (s, 1H), 6.82 (d, 1H, *J* = 8.7Hz), 7.82 (d, 1H, *J* = 8.4Hz); ^{13}C-NMR (74.5 MHz, $CDCl_3$ w/TMS) δ 28.5, 40.5, 52.4, 53.6, 69.0, 69.1, 70.6, 79.2, 111.5, 118.5, 120.0, 121.8, 123.7, 132.2, 134.3, 158.4, 165.5; MS (EI^+) *m/z* 470.2 $[M+Na]^+$, 486.2 $[M+K]^+$, 442.2 $[M+H]^+$; UV(EtOH) λ_{max} 355 nm.

*4.6.2.25 Synthesis of methyl 2-(2-{2-[5-((2S)-6,8-diaza-7-oxo-3-thiabicyclo[3.3.0]oct-2-yl)pentanoylamino]ethoxy}ethoxy)-4-[3-(trifluoromethyl)(1,2-diazirin-3—yl)]benzoate (**20**)*

Boc-deprotection was performed by treatment of **19** (700 mg, 1.57 mmol) with 50% trifluoroacetic acid in CH_2Cl_2 (3.14 mL) for 3 h at 0 °C with stirring. After 3 h of stirring, the reaction mixture was concentrated. The residue was dissolved in DMF (1.57 mL) and brought to 0 °C. To that, was added triethylamine (544 μL) followed by a solution of NHS-biotin (535.97 mg, 1.57 mmol) in DMF (9.42 mL). The reaction mixture was allowed to stir overnight at room temperature. The solvent was removed *in vacuo* and the residue was partitioned between CH_2Cl_2 and water. The organic layer was dried with $MgSO_4$ and concentrated. Chromatography on silica ($CHCl_3$:ethanol = 6:1) afforded **20** (649 mg, 72%): ^{1}H-NMR (300 MHz, $CDCl_3$ w/TMS) δ 1.41 (m, 2H), 1.66 (m, 4H), 2.23 (t, 1H, *J* = 7.2Hz, *J* = 7.8Hz), 2.71 (d, 1H, *J* = 13.2Hz), 2.88 (dd, 1H, *J* = 4.8Hz, *J* =5.1Hz, *J* = 12.8Hz,), 3.12 (m=dd, 1H, *J* = 7.2Hz, *J* = 7.8Hz, *J* = 11.7Hz), 3.47 (dd, 2H, *J* = 5.1Hz, *J* = 5.7Hz, *J* = 10.2Hz), 3.87 (t, 1H, *J* =4.8Hz, *J* = 5.1Hz), 3.87 (t, 2H, *J* = 5.1Hz), 3.88 (s, 3H), 4.18 (t, 2H, *J* =4.5Hz), 4.28 (dd, 1H, *J* = 4.5Hz, *J* = 7.8Hz), 4.47 (dd, 1H, *J* = 4.8Hz, *J* = 7.2Hz), 5.36 (bs,

1H), 6.15 (bs, 1H), 6.70 (s, 1H), 6.72 (bs, 1H), 7.83 (d, 1H, J = 8.1Hz); MS (EI^+) *m/z* 574.2 $[M+H]^+$, 596.2 $[M+Na]^+$, 612.2 $[M+K]^+$; UV(EtOH) λ_{max} 364 nm.

4.6.2.26 Synthesis of 2-(2-{2-[5-((2S)-6,8-diaza-7-oxo-3-thiabicyclo[3.3.0]oct-2-yl)pentanoylamino]ethoxy}ethoxy)-4-[3-(trifluoromethyl)(1,2-diazirin-3—yl)]benzoic acid

Compound **20** (9.4 mg, 0.0164 mmol) was dissolved in methanol (307 μL) and cooled to 0 °C. 1 N aqueous NaOH (82 μL) was added at 0 °C and the reaction was allowed to stir overnight at room temperature. After evaporation of the methanol, the residue was dissolved in water and acidified with 1 N aqueous HCl. The crude acid was purified by reprecipitation in chloroform-hexane to yield the desired product (7.5 mg, 82%): The product was used as is in next step; MS (EI^+) *m/z* 582.0 [M+Na]+, 560.2 [M+H]+.

*4.6.2.27 Synthesis of 2,5-dioxopyrrolidiny 2-(2-{2-[5-((2S)-6,8-diaza-7-oxo-3-thiabicyclo[3.3.0]oct-2-yl)pentanoylamino]ethoxy}ethoxy)-4-[3-(trifluoromethyl)(1,2-diazirin-3—yl)]benzoate. (**21**)*

Compound 2-(2-{2-[5-((2S)-6,8-diaza-7-oxo-3-thiabicyclo[3.3.0]oct-2-yl)pentanoylamino]ethoxy}ethoxy)-4-[3-(trifluoromethyl)(1,2-diazirin-3—yl)]benzoic acid (100 mg, 0.179 mmol) was dissolved THF/CH_3CN (1:1, 4 mL) and *N*-hydroxysuccinimide (21.41 mg, 0.186 mmol) was added. To the reaction mixture was added a solution of N-(3-Dimethylaminopropyl)-N'-ethylcarbodiimide hydrochloride (31.36 mg, 0.202 mmol) in THF (0.8 mL). Triethylamine (20.44 mg, 0.202 mmol) was added to the reaction mixture and the reaction is allowed to stir at room temperature overnight. The reaction was then concentrated and the residue was partitioned between CH_2Cl_2 and water. The organic layer was dried with

$MgSO_4$, filtered and concentrated to afford **21** (85.2 mg, 73%): ^{1}H-NMR (300 MHz, $CDCl_3$ w/TMS): δ 1.34 (m, 2H), 1.61 (m, 4H), 2.14 (t, 2H, *J* = 7.2Hz, *J* = 7.8Hz), 2.85 (m, 1H), 2.91 (s, 4H), 3.10 (dd, 1H, *J* = 7.2Hz, *J* = 7.8Hz, *J* = 9.8Hz), 3.40 (dd, 2H, *J* = 4.8Hz, *J* = 5.4Hz, *J* = 10.2Hz), 3.61 (t, 2H, *J* = 4.8Hz, *J* = 5.1Hz), 3.85 (dd, 2H, *J* = 2.7Hz, *J* = 3.6Hz, *J* = 5.0Hz), 4.20 (t, 2H, *J* = 3.9Hz, *J* = 4.8Hz), 4.26 (dd, 1H, *J* = 4.8Hz, *J* = 5.7Hz, *J* = 7.4Hz), 4.45 (dd, 1H, *J* = 4.8Hz, *J* = 5.1Hz, *J* = 7.7Hz), 5.49 (s, 1H), 6.31 (s, 1H), 6.52 (bs, 1H), 6.72 (s, 1H), 6.88 (d, 1H, *J* = 8.1Hz), 8.03 (d, 1H, *J* = 8.1Hz); ^{13}C-NMR (74.5 MHz, $CDCl_3$ w/TMS) δ 25.7, 25.8, 25.9, 28.2, 28.4, 35.9, 39.3, 40.7, 55.8, 60.3, 61.8, 68.8, 69.1, 70.2, 77.4, 111.1, 115.9, 118.6, 119.8, 123.5, 133.1, 136.8, 159.4, 159.8, 164.1, 169.5, 173.4; MS (EI^+) *m/z* 657.2 $[M+H]^+$, 679.2 $[M+Na]^+$, 695.2 $[M+K]^+$, UV(H_2O) λ_{max} 364 nm.

*4.6.2.28 Synthesis of Probe 5-((2S)-6,8-diazo-7-oxo-3-thiabicylco[3.3.0]oct-2-yl)-N-[2-(2-{2-[N-2-{2-[4,5-dihydroxy-6-(hydroxymethyl)-3-(3,4,5-trihydroxy-6-methylperhydro-2H-pyran-2-yloxy)perhydro-2H-pyran-2-yloxy]ethoxyl}ethyl)carbamoyl]-5[3-(trifluoromethyl)(1,2-diazirin-3-yl)phenoxy}ethoxy)ethyl]pentanamide (**11**)*

8 (62.84 mg, 0.152 mmol) was dissolved in the minimal amount of DMF (15 mL) and the pH was adjusted to approximately 9 using TEA. To that was added **21** (100 mg, 0.152 mmol) and the reaction was allowed to stir at room temperature for 10 h. After 10 h of stirring another 0.2 equiv. of **21** was added and the reaction was stirred for another 5 h. Another 0.2 equiv. of **21** was added every 5 h until staining by ninhydrin showed the disappearance of **8**. The reaction was then concentrated and the crude was purified by HPLC (22% CH_3CN/H_2O on C18 resin) to afford **11** (34.9 mg, 24%): ^{1}H-NMR (300 MHz, $CDCl_3$ w/TMS) δ1.18 (d, 3H, *J* = 6.6Hz), 1.36-1.46 (m, 2H), 1.51-1.77 (m, 4H), 2.19 (d, 2H, *J* =

7.5Hz), 2.69 (d, 1H, *J* = 12.9Hz), 2.91 (dd, 1H, *J* = 4.8Hz, *J* = 12.6Hz), 3.17 (dt, 2H, *J* = 3.6Hz, *J* = 5.7Hz), 3.41 (t, 2H, *J* = 5.5Hz), 3.54-3.65 (m, 8H), 3.67-3.75 (m, 7H), 3.80 (m, 2H), 3.86-3.93 (m, 4H), 4.16 (q, 1H, *J* = 6.6Hz), 4.28 (dd, 2H, *J* = 4.5Hz, *J* = 8.1Hz), 4.33 (d, 1H, *J* = 8.4, H-1**β**), 4.48 (dd, 1H, *J* = 4.5Hz, *J* = 8.1Hz), 5.00 (d, 1H, *J* = 3.9, H-1'**α**), 6.86 (s, 1H), 7.04 (d, 1H, *J* = 8.1Hz), 8.01 (d, 1H, *J* = 8.1Hz); MS (EI^+) *m/z* 955.4 $[M+H]^+$, 977.4 $[M+Na]^+$, 993.4 $[M+K]^+$.

*4.6.2.29 Synthesis of 4,5-diacetyloxy-2-[4,5-diacetyloxy-6-(acetyloxymethyl)-2-ethoxyperhydro-2H-pyran-3-yloxyl]-6-methylperhydro-2H-pyran-3-yl acetate (**22**)*

7 (143.4 mg, 0.214 mmol) is repeatedly evaporated with toluene to remove excess water. **7** is brought up in CH_2Cl_2 (1.53 mL) and dry EtOH (9.88 mg, 0.214 mmol) and mol. sieves (4 Å) are added. The mixture stirred for 10min and then cooled to -20 °C. To that is added NIS (58.5 mg, 0.247 mmol), followed by addition of solver triflate (60.64 mg, 0.236 mmol). The reaction was allowed to warn to room temperature and proceeds almost instantaneously upon addition of silver triflate. After it had gone to completion, the reaction was diluted with CH_2Cl_2 and filtered. The filtrate is washed with sat. aq. sodium thiosulfate, sat. aq. sodium bicarbonate, and brine. The organic layer is dried with sodium sulfate, filtered and concentrated. Column chromatography (3:1 hexanes: EtOAc) affords **22** (84.9 mg, 70%, α:β = 1:3): only β is used: ^{1}H-NMR (300 MHz, $CDCl_3$ w/TMS) δ1.10 (d, 3H, *J* = 6.6Hz), 1.24 (t, 3H, *J* = 7.2Hz), 1.96 (s, 3H), 1.97 (s, 3H), 1.98 (s, 3H), 2.02 (s, 3H), 2.11 (s, 3H), 2.13 (s, 3H), 3.59 (quin., 1H, *J* = 7.2Hz), 3.85 (t, 1H, *J* = 6.6Hz), 3.92 (dd, 1H, *J* = 7.8Hz, *J* = 9.9Hz), 4.00 (dd, 1H, *J* = 6.9Hz, *J* = 9.3Hz), 4.08 (dd, 1H, *J* = 6.6Hz, *J* = 11.7Hz), 4.16 (dd, 1H, *J* = 6.6Hz, *J* = 11.1Hz), 4.46 (d, 1H, *J* = 7.8Hz, H-1**β**), 4.59 (q, 1H, *J* = 6.6Hz),

4.98 (dd, 1H, *J* = 4.5Hz, *J* = 10.2Hz), 5.00 (dd, 1H, *J* = 3.3Hz, *J* = 9.9Hz), 5.27 (m, 2H), 5.33 (dd, 2H, *J* = 3.6Hz, *J* = 8.4Hz); MS (EI^+) *mz* 629.4 $[M+Na]^+$, 645.4 $[M+K]^+$.

4.6.2 Molecular Biology: General

Unless otherwise stated, chemicals and molecular biology reagents were purchased from Fisher (Fairlawn, NJ) and used as is. Protease inhibitors were purchased from Aldrich Chemicals (St. Louis, MO) and Alexis Biochemicals (San Diego, CA).

4.6.2.1 Periodic Acid Treatment of Bovine Serum Albumin (BSA)

Bovine serum albumin (4 g) was dissolved in 0.1 M sodium acetate, pH 4.5 (90 mL). Periodic acid (227.9 mg, 1 mmol) was dissolved in 0.1 M sodium acetate, pH 4.5 (3 mL). The periodic acid solution was added to the solution of BSA and the mixture was stirred for 6 h or until the absorbance at 265 nm exhibited no change. The reaction was quenched by the addition of glycerol (73 uL, 1 mmol). The reaction was dialyzed against 2 changes of phosphate buffered saline (PBS, pH 7.4) and then diluted to a final concentration of 3 g in 100 mL with PBS. HIO_4 treated BSA was reused and stored at 4 °C.

4.6.2.2 Recovery of adult rat hippocampal tissue

100 g male Sprague-Dawley rats were purchased from Charles River Laboratories (Kingston, Mass) and housed at the California Institute of Technology Laboratory Animal Facilities. Rats were anesthetized with carbon dioxide for 2 min and immediately euthanized by decapitation with a guillotine (Kent Scientific Co.) The brain was promptly removed and

placed on ice. The required portion of the brain dissected on ice and placed a glass dounce homogenizer tube for subsequent treatment.

4.6.2.3 Preparation and A46-B/B10 Western Blotting of Adult Rat Hippocampus Brain and Cultured Rat Enbryonic Hippocampus Neurons

The hippocampus from one adult Sprague-Dawley rat (100 g) was removed and to that was added 4 volumes of boiling 1 % SDS supplemented with protease inhibitors (aprotinin, 20 μg/mL; leupeptin, 20 μg/mL; antipain, 20 μg/mL; pepstatin, 5 μg/mL; chymstatin, 5 μg/mL; PMSF, 1 mmol) The tissue was homogenized with 5 strokes of a teflon-glass homogenizer followed by 5 passes through a 25-gauge syringe needle to clarify the tissue solution. The solution was transferred to an eppendorf tube and boiled for ten minutes. The solution was allowed to cool and the protein concentration of the solution was determined using BCA Assay (Pierce). Cultured E18 hippocampus neurons (provided by Cristal I. Gama) were removed from the culture plate and centrifuged at 1000 x g for 5 min. The supernatant was removed and the pellet was washed with PBS. The pellet was resuspended in 200 μL of boiling 1 % SDS supplemented with protease inhibitors and sonicated for 2 times 5 s on ice (10 s interval in between). The sample was then boiled for 10 min and the concentration determined by BCA Assay. Loading dye was added to each sample of desired protein content and each sample was boiled for 5 min and the cooled to room temperature. The samples were then loaded on to a 10% polyacrylamide stacking gel and resolved at 200 V. The proteins were then transferred to a nitrocellulose membrane at 150 mA. The membrane was blocked using periodic acid treated BSA for 1 h at room temperature. The membrane was then washed with (2 x 10 min) followed by an incubation

with A46-B/B10 antibody overnight at 4 °C. The membrane was then washed with TBST (2 x 20 min) and incubated with goat-anti-mouse antibody conjugated to horseradish peroxidase (HRP) for 1 h at room temperature. The membrane was then washed successively with TBST (1 x 10 min, 2 x 30 min, 1 x 20 min) and visualized by enhanced chemiluminescence (Amersham, Pittsburgh, PA) and developed on to film (Kodak, X-OMAT AR).

4.6.2.4 Representative Protocol for detection of fucosyl-galactose binding proteins using Probe 11

Preparation of lysates was done using procedures adapted from previously reported procedures.[48] The hippocampi of six 100 g Sprague-Dawley rats was removed and homogenized in 5 volumes of Buffer A supplemented with protease inhibitors with ten strokes of a Teflon tissue homogenizer. The lysates was passed through a 26 gauge needle five times to clarify, followed by sonication on ice (2 x 5 s). Lysates were then centrifuged at 800 x g for 10 min to remove cell debris and nuclei. The supernatant was removed and centrifuged at 100,000 x g (Beckman Ultima centrifuge) for 1 h. The supernatant, which was considered the soluble protein fraction (S2), was removed and stored at 4 °C. The pellet was then resuspended in Buffer A plus protease inhibitors and centrifuged at 100,000 x g for 1 h. The supernatant was removed and the pellet was resuspended in the minimal amount of Buffer A plus 1 % CHAPSO supplemented with protease inhibitors. Brief sonication on ice was used to facilitate resuspension. The lysate was diluted to 10 mg/mL with Buffer A plus 1 % CHAPSO and incubated with rocking for 1 h at 4 °C. The lysates was then centrifuged at 100,000 x g for 1 h. The supernatant was removed and considered the membrane fraction. The soluble fraction and the membrane fraction were then diluted 10 fold, using Buffer B (50

mM PIPES plus protease inhibitors, to a final total protein concentration of approximately 0.5 μg/mL. The soluble fraction and the membrane fraction were each precleared to remove any endogenous streptavidin-agarose by incubating the protein fractions with streptavidin-agarose (30 μL of slurry/100 μg of protein) with rocking for 1 h at 4 °C. *The next step was done in the dark to prevent the photoactivation of* **11**. Each fraction of protein (membrane and soluble) was incubated in the dark with 1 mM of **11** with rocking for 8 h at 4 °C. After 8 h of incubation, each sample was irradiated with 365 nm light (handheld 18 W UV lamp) at a 2 cm working distance for 4 h at 4 °C. Photolysis of **11** was monitored by UV-vis spectrophotometry. The samples were treated with denaturing sample loading dye (Pierce), boiled for 5 min and allowed to cool. The samples were resolved using electrophoresis under denaturing conditions on a 7% polyacrylamide gel. Proteins were transferred to PVDF membrane and the blot was blocked with HIO_4 treated BSA for 1 h, rinsed quickly with TBST, and incubated with streptavidin conjugated with horseradish peroxidase (streptavidin-HRP) in TBST for 1 h. The blot was then washed with TBST (1 x 10 min, 3 x 20 min) and visualized using enhanced chemiluminescence (Amersham).

4.7 References

1. Helenius, A.; Aebi, M., Intracellular functions of N-linked glycans. *Science* **2001,** 291, (5512), 2364-9.
2. Rudd, P. M.; Elliott, T.; Cresswell, P.; Wilson, I. A.; Dwek, R. A., Glycosylation and the immune system. *Science* **2001,** 291, (5512), 2370-6.
3. Sharon, H.; Lis, H., *Essays Biochem.* **1995,** 30, 59.
4. Lasky, L. A., Selectin-Carbohydrate Interactions and the Initiation of the Inflammatory Response. *Annual Review of Biochemistry* **1995,** 64, 113-139.
5. Mahal, L.; Charter, N. W.; Angata, K.; Fukuda, M.; Koshland, D. E.; Bertozzi, C. R., A small-molecule modulator of poly-alpha2,8-sialic acid expression on cultured neurons and tumor cells. *Science* **2001,** 294, 380-382.
6. Stanojev, D.; Gurd, J. W., Characterization of Fucosyl Oligosaccharides Associated with Synaptic membrane and Synaptic Junctional Glycoproteins. *Journal of Neurochemistry* **1987,** 48, 1604-1611.
7. Muller, D.; Wang, C.; Skibo, G.; Toni, N.; Cremer, H.; Calaora, V.; Rougon, G.; Kiss, J. Z., PSA-NCAM Is Required for Activity-Induced Synaptic Plasticity. *Neuron* **1996,** 17, 413-422.
8. Ong, E.; Nakayma, J.; Angata, K.; Reyes, L., Developmental regulation of polysialic acid synthesis in mouse directed by two polysialyltransferases, PST and STX. *Glycobiology* **1998,** 8, (4), 415-424.
9. Rutishauser, U., Polysialic Acid at the Cell Surface: Biophysics in Service of Cell INteractions and Tissue Plasticity. *Journal of Cellular Biochemistry* **1998,** 70, 304-312.
10. Murakami, S.; Seki, T.; Rutishauser, U.; Arai, Y., Enzymatic removal of Polysialic acid from Neural cell adhesion molecule perturbs the migration route of Leuteinizing Hormone-releasing Hormone Neurons in the Developing Chick forebrain. *The Journal of Comparative Neurology* **2000,** 420, 171-181.
11. Zanetta, J. P., Synaptosomal Plasma Membrane Glycoproteins. II. Isolation of Fucosyl-glycoproteins by Affinity Chromatography on the Ulex Europeus Lectin Specific for L-fucose. *Brain Research* **1977,** 138, 317-328.
12. Matthies, H., *Prog. Neurobiology* **1989,** 32, 277-349.
13. Angenstein, F.; Matthies, H.; Staeck, S., *Neurochemical International* **1992,** 21, 403-408.
14. Popov, N.; Schulzeck, S.; Pohle, W.; Matthies, H., Changes in the incorporation of 3H-fucose into rat hippocampus after acquisition of a brightness discrimination reaction. An electrophoretic study. *Neuroscience* **1981,** 5, 161-167.
15. Popov, N.; Schmidt, S.; Schulzeck, S.; Jork, R.; Lossner, B.; Matthies, H., Changes in activity of fucokinase and fucosyltransferase in rat hippocampus after acquisition and consilidation of a brightness discrimination. *Pharmacol. Biochem. Behav.* **1983,** 19, 43-47.
16. Burgoyne, R. D.; Rose, S. P. R., Subcellular-localization of increased incorporation of [H-3]Fucose Following passive-avoidance Learning in the Chick. *Neuroscience Letters* **1980,** 19, 343-348.
17. Wetzel, W.; Popov, N.; Lossner, B.; Schulzeck, S.; Honza, R.; Matthies, H., Effect of L-fucose on Brain Protein-metabolism and retention of a Learned behvaior in Rats. *Pharmacol. Biochem. Behav.* **1980,** 13, 765-771.

18. Matthies, H.; Staak, S.; Krug, M., Fucose and fucosyllactose Enhance in-vitro Hippocampal Long-term Potentiation. *Brain Research* **1996,** 725, 276-280.
19. Rose, S. P. R.; Jork, R., Long-term Memory Formation in Chicks is blocked by 2-deoxygalactose, a Fucose Analog. *Behavioral and Neural Biology* **1987,** 48, 246-258.
20. Tiunova, A. A.; Anokhin, K. V.; Rose, S. P. R., Two Critical Periods of Protein and Glycoprotein SYnthesis in Memory Consolidation for Visual Categorization Learning in CHicks. *Learning and Memory* **1998,** 4, 401-410.
21. Barber, A. J.; Rose, S. P. R., Amnesia Induced by 2-deoxygalactose in the Day-Old Chick: Lateralization of Effects in Two Different One-Trial Learning Taska. *Behavioral and Neural Biology* **1991,** 56, 77-88.
22. Bullock, S.; Potter, J.; Rose, S. P. R., Effects of the Amnesic Agent 2-deoxygalactose on incorporation of fucose into chick brain glycoproteins. *Journal of Neurochemistry* **1990,** 54, (1), 135-141.
23. Karsten, U.; Pilgrim, G.; Hanisch, F.-G.; Uhlenbruck, G.; Kasper, M.; Stosiek, P.; Papsdorf, G.; Pasternak, G., A new monoclonal antibody (A46-B/B10) highly specific for the blood group H type 2 epitope: Generation, epitope analysis, serological and histological evaluation. *British Journal of Cancer* **1988,** 58, 176-181.
24. Liang, R.; Yan, L.; Loebach, J.; Ge, M.; Uozumi, Y.; Sekanina, K.; Horan, N.; Gildersleeve, J.; Thompson, C.; Smith, A.; Biswas, K.; Still, W. C.; Kahne, D., Parallel synthesis and screening of a solid phase carbohydrate library. *Science* **1996,** 274, (5292), 1520-2.
25. Nicolaou, K. C.; Winssinger, N.; Pastor, J.; DeRoose, F., A general and highly efficient solid phase synthesis of oligosaccharides. Total synthesis of a heptasaccharide phytoalexin elicitor (HPE). *Journal of the American Chemical Society* **1997,** 119, (2), 449-450.
26. Sofia, M. J.; Allanson, N.; Hatzenbuhler, N. T.; Jain, R.; Kakarla, R.; Kogan, N.; Liang, R.; Liu, D.; Silva, D. J.; Wang, H.; Gange, D.; Anderson, J.; Chen, A.; Chi, F.; Dulina, R.; Huang, B.; Kamau, M.; Wang, C.; Baizman, E.; Branstrom, A.; Bristol, N.; Goldman, R.; Han, K.; Longley, C.; Axelrod, H. R.; et al., Discovery of novel disaccharide antibacterial agents using a combinatorial library approach. *J Med Chem* **1999,** 42, (17), 3193-8.
27. Sears, P.; Wong, C. H., Toward automated synthesis of oligosaccharides and glycoproteins. *Science* **2001,** 291, (5512), 2344-50.
28. Seeberger, P. H.; Haase, W. C., Solid-phase oligosaccharide synthesis and combinatorial carbohydrate libraries. *Chem Rev* **2000,** 100, (12), 4349-94.
29. Berecibar, A.; Grandjean, C.; Siriwardena, A., Synthesis and Biological Activity of Natural Aminocyclopentitol Glycosidase Inhibitors: Mannostatins, Trehazolin, Allosamidins, and Their Analogues. *Chem Rev* **1999,** 99, (3), 779-844.
30. Elbein, A. D., Inhibitors of the biosynthesis and processing of N-linked oligosaccharide chains. *Annu Rev Biochem* **1987,** 56, 497-534.
31. Kim, C. U.; Lew, W.; Williams, M. A.; Liu, H.; Zhang, L.; Swaminathan, S.; Bischofberger, N.; Chen, M. S.; Mendel, D. B.; Tai, C. Y.; Laver, W. G.; Stevens, R. C., Influenza neuraminidase inhibitors possessing a novel hydrophobic interaction in the enzyme active site: design, synthesis, and structural analysis of carbocyclic sialic acid analogues with potent anti-influenza activity. *J Am Chem Soc* **1997,** 119, (4), 681-90.

32. Kim, Y. J.; Ichikawa, M.; Ichikawa, Y., A rationally designed inhibitor of alpha-1,3-galactosyltransferase. *Journal of the American Chemical Society* **1999,** 121, (24), 5829-5830.
33. Platt, F. M.; Neises, G. R.; Reinkensmeier, G.; Townsend, M. J.; Perry, V. H.; Proia, R. L.; Winchester, B.; Dwek, R. A.; Butters, T. D., Prevention of lysosomal storage in Tay-Sachs mice treated with N-butyldeoxynojirimycin. *Science* **1997,** 276, (5311), 428-31.
34. von Itzstein, M.; Wu, W. Y.; Kok, G. B.; Pegg, M. S.; Dyason, J. C.; Jin, B.; Van Phan, T.; Smythe, M. L.; White, H. F.; Oliver, S. W.; et al., Rational design of potent sialidase-based inhibitors of influenza virus replication. *Nature* **1993,** 363, (6428), 418-23.
35. Khidekel, N.; Arndt, S.; Lamarre-Vincent, N.; Lippert, A.; Poulin-Kerstien, K. G.; Ramakrishnan, B.; Qasba, P. K.; Hsieh-Wilson, L. C., A chemoenzymatic approach toward the rapid and sensitive detection of O-GlcNAc posttranslational modifications. *J Am Chem Soc* **2003,** 125, (52), 16162-3.
36. Khidekel, N.; Ficarro, S. B.; Peters, E. C.; Hsieh-Wilson, L. C., Exploring the O-GlcNAc proteome: direct identification of O-GlcNAc-modified proteins from the brain. *Proc Natl Acad Sci U S A* **2004,** 101, (36), 13132-7.
37. Kiessling, L. L.; Pohl, N. L., Strength in numbers: non-natural polyvalent carbohydrate derivatives. *Chem Biol* **1996,** 3, (2), 71-7.
38. Roy, R., Syntheses and some applications of chemically defined multivalent glycoconjugates. *Curr Opin Struct Biol* **1996,** 6, (5), 692-702.
39. Crews, C. M.; Splittgerber, U., Chemical genetics: exploring and controlling cellular processes with chemical probes. *TIBS* **1999,** 24, 317-320.
40. Fleming, S. A., Chemical Reagents in Photoaffinity Labeling. *Tetrahedron* **1995,** 51, (46), 12479-12520.
41. Hashimoto, M.; Hatanaka, Y., Identification of Photolabeled Peptides for the Acceptor Substrate Binding Domain of beta-1,4-Galactosyltransferase. *Chemical and Pharmaceutical Bulletin* **1999,** 47, (5), 667-671.
42. Fabry, M.; Brandenburg, D., Detection of a New Hormone Contact Site Within the Insulin Receptor Ectodomain by the Use of a Novel Photoreactive Insulin. *Journal of Biological Chemistry* **1992,** 267, (13), 8950-8956.
43. Ambroise, Y.; LeBlanc, G.; Rousseau, B., Active-Site-Directed Photolabeling of the Melibiose Permease of Escherichia coli. *Biochemistry* **2000,** 39, 1338-1345.
44. Hibert-Kotzyba, F.; Kapfer, I.; Goeldner, M., Recent Trends in Photoaffinity Labeling. *Angewandte Chemie (English Edition)* **1995,** 34, 1296-1312.
45. Drake, J., Richard R.; Haley, B. E., Synthesis and Properties of 5-Azido-UDP-Glucose. *Journal of Biological Chemistry* **1989,** 264, (20), 11925-11933.
46. Evans, R. K.; Haley, B. E., Synthesis and Biological Properties of 5-Azido-2'-deoyuridine 5'-triphosphate, a Photoreactive Nucleotide Suitable for Making Light-sensitive DNA. *Biochemistry* **1987,** 26, 269-276.
47. Toone, E. J., Structure and Energetics of Protein Carbohydrate Complexes. *Current Opinion in Structural Biology* **1994,** 4, 719-728.
48. Li, Y.-M., Photoactivatable gamma-secretase inhibitors directed to the active site covalently label presenilin 1. *Nature* **2000,** 405, 689-694.
49. Koumanov, F., Cell-surface Biotinylation of GLUT4 Using bis-Mannose Photolabels. *Biochemical Journal* **1998,** 330, 1209-1215.
50. Brunner, J., 3-Trifluoromethyl-3-phenyldiazirine. *Journal of Biological Chemistry* **1980,** 255, (8), 3313-3318.

51. Wegmann, B.; Schmidt, R. R., Synthesis of the H-disaccharide (2-O-alpha-L-fucospyranosyl-D-galactose) via the trichloroacetimidate method. *Carbohydrate Research* **1988,** 184, 254-261.
52. Binkley, R. W.; Goewey, G. S.; Johnston, J. C., Regioselective Ring Opening of Selected Benzylidene Acetals. A Photochemically Initiated Reaction for Partial Deprotection of Carbohydrates. *Journal of Organic Chemistry* **1984,** 49, 992-996.
53. Zhang, Z.; Ollmann, I. R.; Ye, X.-S.; Wischnat, R.; Baasov, T.; Wong, C.-H., Programmable One-Pot Oligosaccharide Synthesis. *Journal of the American Chemical Society* **1999,** 121, 734-753.
54. Ye, X.-S.; Wong, C.-H., *Journal of Organic Chemistry* **2000,** 65, 2410-2431.
55. Deijter-Juszynski, M.; Flowers, H. M., Studies on the Koeings-Knorr Reaction. *Carbohydrate Research* **1971,** 18, 219-226.
56. Roush, W. R., *Tetrahedron* **1997,** 53, (26), 8837-8852.
57. Motawia, M. S.; Olsen, C. E.; Moller, B. L.; Marcussen, J., Chemical synthesis and NMR spectra of a protected branched-tetrasaccharide thioglycoside, a useful intermediate for the synthesis of branched oligosaccharides. *Carbohydrate Research* **1994,** 252, 69-84.
58. Kanie, O.; Ito, Y.; Ogawa, T., Orthogonal Glycosylation Strategy in Synthesis of Extended Blood Group B Determinant. *Tetrahedron Letters* **1996,** 37, (26), 4551-4554.
59. Newman, H., Trifluoroacettl as a Protecting Group for 1-Halo Sugars. *Journal of Organic Chemistry* **1965,** 30, 1287-1288.
60. Hatanaka, Y., A Novel Family of Aromatic Diazirines for Photoaffinity Labeling. *Journal of Organic Chemistry* **1994,** 59, 383-387.
61. Hatanaka, Y., A Novel Biotinylated Heterobifunctional Cross-linking Reagent Bearing an Aromatic Diazirine. *Bioorganic and Medicinal Chemistry* **1994,** 2, (12), 1367-1373.
62. Cockburn, W. F.; Bannard, R. A. B., The reaction of acetic acid and trifluoroacetic anhydrides with some substituted gaunidine hydrochlorides. *Canadian Journal of Chemistry* **1957,** 35, 1285-1292.
63. Mintz, M. J.; Walling, C., t-Butyl Hypochlorite. *Organic Syntheses* CV5, 184.